



IntechOpen

Groundwater Contaminant and Resource Management

Edited by Muhammad Salik Javaid



WEB OF SCIENCE™



GROUNDWATER - CONTAMINANT AND RESOURCE MANAGEMENT

Edited by **Muhammad Salik Javaid**

Groundwater - Contaminant and Resource Management

<http://dx.doi.org/10.5772/61696>

Edited by Muhammad Salik Javaid

Contributors

Hsin-Fu Yeh, Chen-Feng Yeh, Jhe-Wei Lee, Cheng-Haw Lee, Anita Etale, Sabelo Mhlanga, Bill X. Hu, Zexuan Xu, Ajay Kumar Vashisht, S K Shakya, Vilim Filipović, Gabriel Ondrasek, Lana Matijević, Zulfiqar Ahmad, Arshad Ashraf, Norma Patricia Lopez-Acosta, José Alfredo Mendoza-Promotor

© The Editor(s) and the Author(s) 2016

The moral rights of the and the author(s) have been asserted.

All rights to the book as a whole are reserved by INTECH. The book as a whole (compilation) cannot be reproduced, distributed or used for commercial or non-commercial purposes without INTECH's written permission.

Enquiries concerning the use of the book should be directed to INTECH rights and permissions department (permissions@intechopen.com).

Violations are liable to prosecution under the governing Copyright Law.



Individual chapters of this publication are distributed under the terms of the Creative Commons Attribution 3.0 Unported License which permits commercial use, distribution and reproduction of the individual chapters, provided the original author(s) and source publication are appropriately acknowledged. If so indicated, certain images may not be included under the Creative Commons license. In such cases users will need to obtain permission from the license holder to reproduce the material. More details and guidelines concerning content reuse and adaptation can be found at <http://www.intechopen.com/copyright-policy.html>.

Notice

Statements and opinions expressed in the chapters are those of the individual contributors and not necessarily those of the editors or publisher. No responsibility is accepted for the accuracy of information contained in the published chapters. The publisher assumes no responsibility for any damage or injury to persons or property arising out of the use of any materials, instructions, methods or ideas contained in the book.

First published in Croatia, 2016 by INTECH d.o.o.

eBook (PDF) Published by IN TECH d.o.o.

Place and year of publication of eBook (PDF): Rijeka, 2019.

IntechOpen is the global imprint of IN TECH d.o.o.

Printed in Croatia

Legal deposit, Croatia: National and University Library in Zagreb

Additional hard and PDF copies can be obtained from orders@intechopen.com

Groundwater - Contaminant and Resource Management

Edited by Muhammad Salik Javaid

p. cm.

Print ISBN 978-953-51-2465-8

Online ISBN 978-953-51-2466-5

eBook (PDF) ISBN 978-953-51-4191-4

We are IntechOpen, the world's leading publisher of Open Access books Built by scientists, for scientists

3,600+

Open access books available

113,000+

International authors and editors

115M+

Downloads

151

Countries delivered to

Our authors are among the
Top 1%

most cited scientists

12.2%

Contributors from top 500 universities



WEB OF SCIENCE™

Selection of our books indexed in the Book Citation Index
in Web of Science™ Core Collection (BKCI)

Interested in publishing with us?
Contact book.department@intechopen.com

Numbers displayed above are based on latest data collected.
For more information visit www.intechopen.com



Meet the editor



Dr. Muhammad Salik Javaid has been working on research, development, planning, execution, management and policy formulation assignments with Corps of Engineers in Pakistan and abroad for over three decades. He has also worked as Chief Consulting Engineer (Water Supply and Drainage Services) with Engineer-in-Chief and Director General Planning for the Earthquake

Reconstruction and Rehabilitation Authority after the 2005 earthquake in Pakistan. He is a graduate of Georgia Tech, Atlanta, USA, where he undertook his Masters and Doctoral studies in the fields of hydraulics and water resources. Presently, he is the Head of Department of Civil Engineering at Abasyn University Islamabad Campus, Pakistan. He has also conducted courses on 'water resources management' and 'river engineering' for civil engineering students at various campuses and universities.

Contents

Preface XI

Section 1 Resource Management 1

Chapter 1 **Appraisal of Groundwater Flow Simulation in the Sub-Himalayan Watershed of Pakistan 3**

Zulfiqar Ahmad, Arshad Ashraf and Mohsin Hafeez

Chapter 2 **Spatiotemporal Analysis of Groundwater Recharge Trends and Variability in Northern Taiwan 27**

Hsin-Fu Yeh, Chen-Feng Yeh, Jhe-Wei Lee and Cheng-Haw Lee

Chapter 3 **Flow through Multiple Well Points System 45**

Ajay K. Vashisht and Shri K. Shakya

Chapter 4 **Mobility and Transformation of Inorganic Contaminants in Mining-impacted Groundwater 69**

Anita Etale and Sabelo Mhlanga

Section 2 Numerical Simulations 89

Chapter 5 **Numerical and Analytical Methods for the Analysis of Flow of Water Through Soils and Earth Structures 91**

Norma Patricia López-Acosta

Chapter 6 **Numerical Simulation of Groundwater Flow and Solute Transport in a Karst Aquifer with Conduits 115**

Bill X. Hu and Zexuan Xu

Chapter 7 **Modelling Water Dynamics, Transport Processes and Biogeochemical Reactions in Soil Vadose Zone 133**

Vilim Filipović, Gabrijel Ondrašek and Lana Filipović

Chapter 8	Study of Unsaturated Soils by Coupled Numerical Analyses of Water Flow-Slope Stability	163
	Norma Patricia López-Acosta and José Alfredo Mendoza-Promotor	

Preface

Groundwater is one of the most precious resources provided by nature for the benefit of humanity. Even though it forms only small portion of the fresh water available on this globe, yet its importance and contribution in the human survival on this planet cannot be fully expounded.

Groundwater is an important part of the hydrological cycle between the processes of percolation (entry into the ground) and extraction (natural or forced exit from the ground). The movement, transportation, geo-biochemical actions and reactions and behavior inside the ground are most fascinating for engineers, researchers, hydrologists, agriculturists, industrialists and general consumers. Aquifer maintenance and management, aquifer conservation and aquifer resource balance between discharge and recharge are the areas for study to avoid and mitigate conflicts among the transboundary stakeholders. Positive contribution by engineers and scientists can not only add towards the development of this resource but also help in just and equitable utilization of it by all.

Whereas the fast pace development of built-up area and communication and habitation infrastructure has grossly reduced the infiltration, percolation and aquifer recharge, on the other hand the extraction has increased manifold. There is thus a dire need to check the depletion rate and work for conservation and enhancement of this precious resource. These aspects can form the goals for future research and investment by all nations of the world. Numerical and computer modelling of groundwater movement and contaminant transport may help identify the gray areas and also suggest solutions in concrete terms.

This book contains eight chapters, which have been grouped into two sections. Section I includes chapters 1–4, which are related to resource development and aquifer management, focusing on the issues of water quantity, water quality, contaminant transport, etc. Section II includes chapters 5–8, which are related to the study and use of numerical simulations and computer modelling in analysis of groundwater flows. Chapters in each section have been grouped having the common focus and theme, thus synergizing the thought and knowledge. Within Section I, the first chapter provides an appraisal of groundwater flow and aquifer recharge in sub-Himalayan watershed. Chapter 2 gives an insight into the groundwater recharge trends and variability in Taiwan. Chapter 3 describes the flow through multiple well point systems, and the final chapter in this section analyses the mobility of inorganic contaminants in mining impacted groundwater. All the four chapters in Section II provide an insight into some particular aspect of numerical modeling and simulation of groundwater flow. Chapter 5 focuses on various methods available for numerical analysis of flow through earth structure. Chapter 6 homes around karst aquifers and conduits and transport of water and solute within these. The next chapter encompasses the study of trans-

port processes in vadose zone, whereas the final chapter is about water mobility and slope stability coupled numerical analysis within unsaturated soils.

This book has a broad-based wider scope due to elaborate coverage on many aspects of groundwater. The book is aimed to serve the needs of graduate students and professionals in groundwater engineering, water resource engineering, hydrogeology, water resource management, environmental sciences and geotechnical engineering.

Many persons contributed directly or indirectly towards the completion of this book project, which is thankfully acknowledged. It would not have been possible to complete this book without the professional contributions of the eminent authors whose names appear with each chapter title; the groundwater scientists and engineers the world over. Guidance, advice and blessings of my professional colleagues and friends and unwavering support of my family members (wife Sultana, daughters Humaira and Sumayyah, and son Hammaad) are fully acknowledged; therefore, I dedicate this book to my family and colleagues in the profession of handling groundwater. Dr. Jamil Ahmad, Vice Chancellor, faculty and staff of Abasyn University, Islamabad, need a mention for providing me working atmosphere, space, time and resources at university's cost. Last but not least I would like to thank Ms. Andrea Koric, the publishing process manager whose patience, guidance and relentless efforts made us all follow and obey the laid out time lines.

Dr. Muhammad Salik Javaid

Abasyn University,
Islamabad, Pakistan

Resource Management

Appraisal of Groundwater Flow Simulation in the Sub-Himalayan Watershed of Pakistan

Zulfiqar Ahmad, Arshad Ashraf and Mohsin Hafeez

Additional information is available at the end of the chapter

<http://dx.doi.org/10.5772/63324>

Abstract

Numerical modeling of an aquifer is increasingly used as a power tool for monitoring and management of groundwater. This paper focuses on conceptualizing hydrogeological condition and establishing numerical simulation model using Visual MODFLOW to simulate the continuous depletion of groundwater in the southwestern part of the Soan watershed in Pakistan. An integrated groundwater modeling and management approach was adopted to provide suitable alternatives for water management in different hydro-environments. Geospatial techniques were employed for spatial database development, integration with a remote sensing (RS), and numerical groundwater flow modeling capabilities to simulate groundwater flow behavior. The calibration results indicated a reasonable agreement between the calculated and observed heads. The calibrated heads were used as initial conditions in the transient-state modeling. The modeling approach facilitated in identifying potential groundwater regime besides providing artificial recharge options for sustainable groundwater development.

Keywords: groundwater flow modeling, aquifer recharge, MODFLOW, geoinformatics, Himalayan watershed

1. Introduction

The growing trend in global warming has resulted in the occurrence of extreme climate events (drought/floods) that impact the hydrological system of the Himalayan region in South Asia. The response of groundwater behavior to environmental changes has been studied worldwide by numerous researchers, for example, see references [1–4]. The changing pattern of precipitation affects the recharge of the groundwater, which controls the behavior of water table

in the system [5,6]. The Indus groundwater system is also facing the temporal as well as spatial impacts of changing environment. A detailed appraisal of the subsurface aquifer system is thus vital in the context of prevailing conditions of drought/flood and the growing demand of water for sustainable development in the region. In recent years, groundwater numerical simulation models have been widely applied to groundwater dynamic simulation and as a management tool. The development and application of a groundwater model is a common practice for the management of groundwater resources [7]. Many scientific efforts have been made to develop more comprehensive and computationally efficient models involving complex hydrogeologic processes [8,9]. In many numerical models of a groundwater aquifer, for example, Feflow and MODFLOW, the continuous domain of groundwater system is replaced by a discretized grid network and the governing groundwater flow equation is solved at the network nodes. The inverse modeling (also called parameter optimization) is capable of assigning approximate values to the hydrological parameters by employing approximate methods to solve the partial differential equation (PDE), which describes the flow in a porous medium.

Pakistan is in the grip of a water crisis. This involves a hydroelectric power shortfall, per capita water availability less than 1100 m³, falling levels of groundwater, and limited water supplies in metropolitan areas, including the twin cities of Rawalpindi and Islamabad. Because pumping exceeds recharge, groundwater reserves are becoming significantly depleted. Groundwater overdraft has caused the groundwater table to decline remarkably and resulted in a series of ecological issues such as deterioration of water quality, soil aridity, deterioration of vegetation, and land desertification [10,11].

In the present study, a three-dimensional numerical groundwater flow modeling using finite-difference Visual MODFLOW coupled with decision support tools of geoinformatics was applied to analyze the spatial and temporal behavior of groundwater in the valley plain of the sub-Himalayan watershed in Pakistan. The multilayered aquifer system of the watershed is recharged mainly by the surrounding dissected land and rocky mountainous terrain. The behavior of the groundwater system was predicted in response to probable hydrogeological stresses.

2. Case study

The growing need of water supplies for both domestic and irrigation purposes has led to the exploitation of surface and groundwater resources in the Soan watershed of Indus basin. In the last drought of 1999–2002, the groundwater abstractions have been increased due to rapid increase in the number of private tube wells for irrigation purpose. Excessive pumpage of groundwater from these wells causes a gradual decline in water table. The decline in groundwater levels in the Rawalpindi area has imposed not only a threat to the livelihood of the residing communities but also a significant influence on the sustainable development of the watershed as a whole. Therefore, understanding and investigation of the groundwater dynamics in the target area have great significance in facilitating the socioeconomic and ecological development, as well as the sustainable development of the water resources. The

watershed contains metropolitan areas of major cities of Islamabad and Rawalpindi, the combined population of which is about 2.8 million, with a density of 880 persons/km². Surface water supplies are maintained from Rawal and Simly reservoirs, which provide 21 million gallons per day (MGD) to Rawalpindi city and 17 MGD to Islamabad city. Groundwater supplies are 24 MGD from about 200 public tube wells in Islamabad, and 27 MGD from about 300 public tube wells in Rawalpindi. The average needs of Islamabad and Rawalpindi are 65 and 175 MGD, respectively, which exceed the capacity of available water resources.

2.1. Description of the study area

The Soan watershed covers an area of about 1684 km² with its longitude 72° 54'–73° 34' E and latitude 33° 26'–33° 56' N in the Pothwar plateau of Pakistan (**Figure 1**). In the north and northeast, it is bounded by the Margalla and Murree hills, which are covered with permanent mixed scrub and coniferous forest. The altitude in the watershed increases gradually from the southwest (<500 m) toward the northeast, near the Murree hills (>2000 m). The area is characterized by gentle to steep slopes. The dominant formations (e.g., the Murree and Kamlial belonging to the Rawalpindi Group of Miocene age) are composed of sandstone, shale, and lenses of conglomerates. The Lei Nullah conglomerates of Quaternary age consist of poorly sorted pebbles and boulders of mostly Eocene limestone strata [12]. The most important aquifers are composed of gravels and boulders in the unconsolidated sediments of Pleistocene and Recent age. Alluvium (the channel-fill deposits) consists of dominantly silt and clay with subordinate amount of gravel and sand. The soils are mainly gravelly, medium to fine textured over calcareous material in the north and northeast and medium to coarse textured over sandstone in the south (**Figure 2**). The main perennial stream in the watershed is the Soan, whose primary tributaries are the Ling, Gumrah Kas, Korang, and Lei Nullah. The Korang and

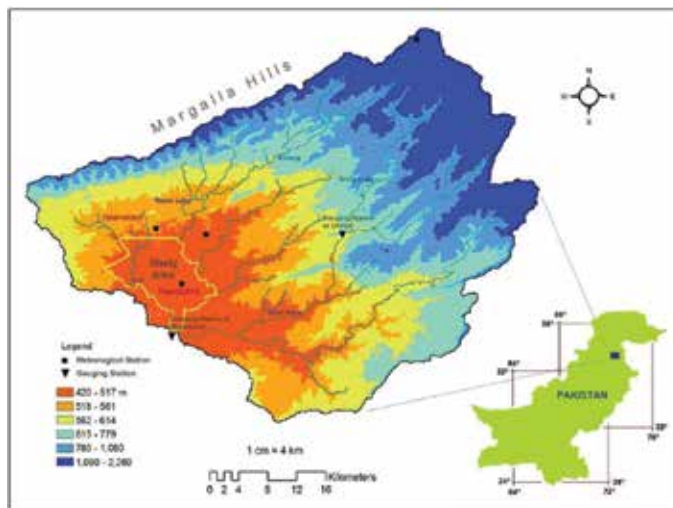


Figure 1. Location of Islamabad watershed and study area.

Soan rivers are dammed at Rawal and Simly reservoirs, respectively. Due to high urban sprawl, a major area has been converted into various degrees of built-up category in the model domain (Figure 3).

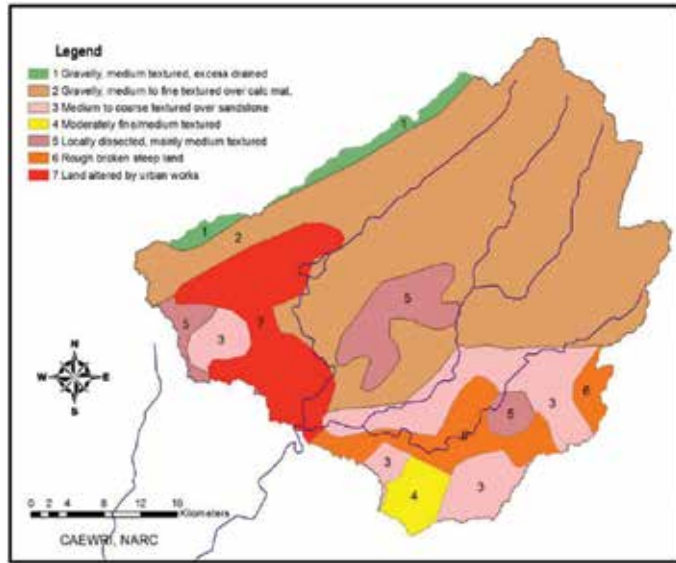


Figure 2. Dominant soil classes in the Soan watershed.

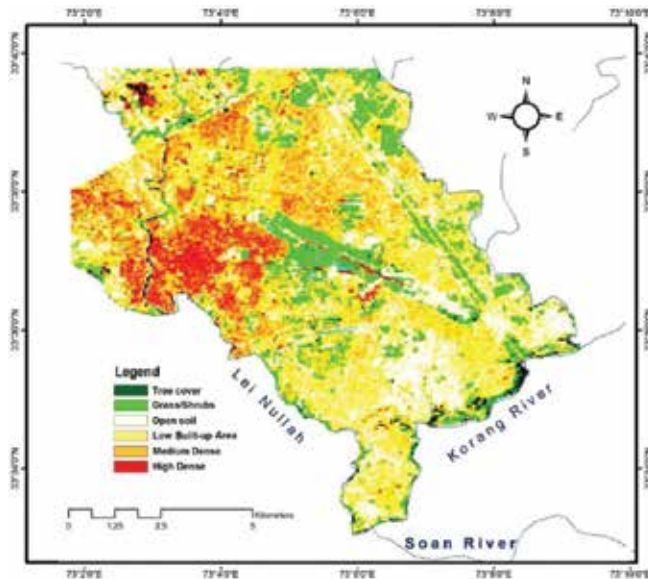


Figure 3. Major land cover/land use in the study area.

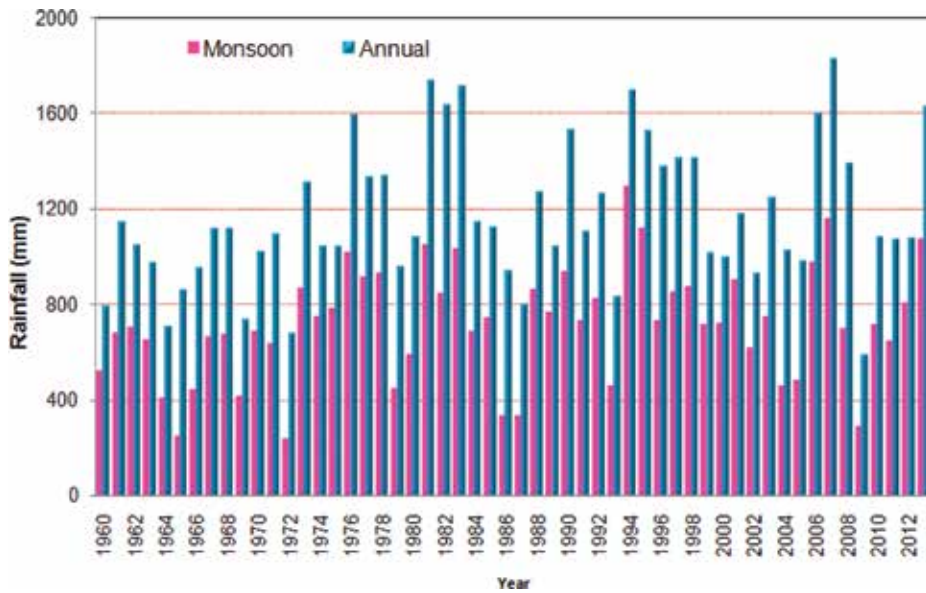


Figure 4a. Trend in annual precipitation at Islamabad Airport (1960–2013).



Figure 4b. The mean monthly precipitation at Islamabad airport.

Lei Nullah extends approximately 30 km from the Margalla hills in the northwest to the Soan River at the southeastern edge. The Lei catchment area is composed of 239.8 km² (169.0 km² in Islamabad and 70.7 km² in Rawalpindi) [13,14]. The total rainfall during the monsoon rainy season is about 60% of the annual average rainfall, that is, about 1169 mm. The annual and mean monthly rainfall trends at Islamabad for 1960–2013 periods are shown in **Figure 4a** and

b, respectively. Floods in the Lei Nullah basin occur during the monsoon season, which usually starts near the end of June with peaks in August and finishes by September. In June, the daily maximum temperature reaches 40 °C, while the daily minimum temperature falls near 0 °C in December and January [15].

2.2. Hydrogeologic framework

Silt and clay dominate the subsurface lithology where gravel deposits are present in discontinuous layers with silty clay. The gravel beds are generally 1–20 m thick and are composed of limestone and sandstone pebbles mixed with sand (**Figure 5**). The thickness of the gravel beds decreases in the south and west. In contrast to the gravels, the bedrock is usually considered to act as an aquitard rather than an aquifer since well yields are much lower than encountered in the gravels. The maximum thickness of the alluvium is more than 200 m, as encountered in the test holes RWP-6 and 8 in Dhok Khabba and Dhok Ratta, respectively. Individual beds range in thickness to 30 m or more. The thickness of alluvium probably exceeds 300 m, as indicated by a deep resistivity survey. They are grayish brown to reddish in color and appear to have been deposited from reworked loess, Siwalik, and Murree rocks. It can become difficult to differentiate rotary cuttings of bedrock formations from the alluvial clays and silts. Sand formations are comparatively rare. Generally, the sand is disseminated within the gravel lenses or constitutes a minor fraction of the clays and silts. The aquifers are composed of seven permeable geological horizons with a total average depth of 137 m. About 300 water wells are being pumped for about 18–22 h per day year round to meet the growing demand of the inhabitants of the city.

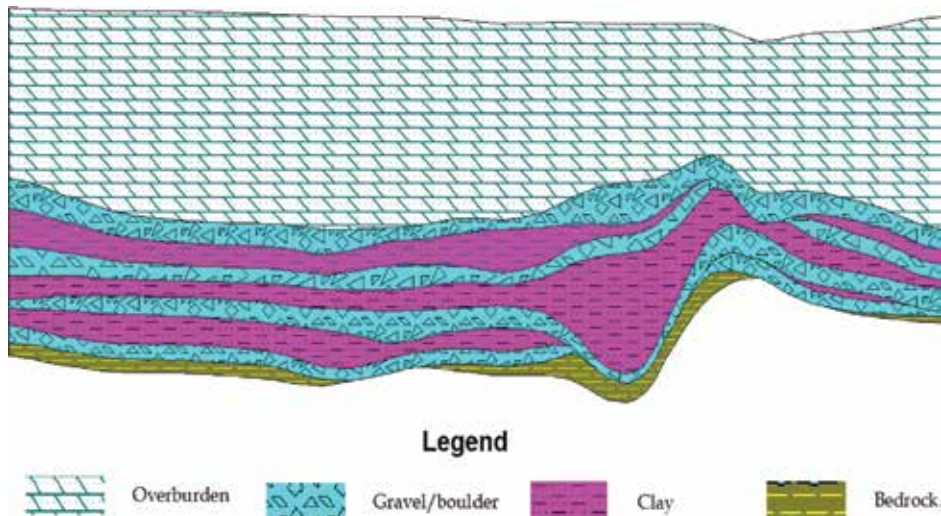


Figure 5. Schematic of lithological section in the study area.

3. Materials and methods

The remote sensing (RS) image data of Landsat-8 were used to analyze the land-cover/land-use status and surface hydrological conditions that were found to be helpful in conceptualizing the recharge/discharge sources of aquifer. Discharge data for the Soan and Korang rivers were obtained from the Water and Power Development Authority (WAPDA) and Surface Water Hydrology Project (SWHP). Both rivers recharge the aquifer system during rainy months and are sustained by base flow at other times. Digital elevation model (DEM) of SRTM 90 m was used to generate the watershed boundary and elevation classes of the watershed area.

The study focuses on conceptualizing hydrogeological condition and establishing numerical simulation model using Visual MODFLOW to simulate the groundwater flow and predict the future response of the aquifer to the growing pumping in Rawal Town (a major part of the Rawalpindi city). The major steps of modeling process include as follows:

- Collection and review of available hydrogeological data.
- Collection and review of details of existing tube wells, including their location, depth, and extraction rates.
- Quantification of discharge rate, with assessment of the rates and periods of extraction.
- Prediction of the effect of increased extraction or changes in usage patterns and location of the sustainable yield and quality of supply.
- Preparation of water balance including the assessment of recharge potential in the existing aquifer.
- Outline recommendation for future exploitation of groundwater aquifer and recharge to groundwater in the study area.

3.1. Modeling groundwater flow

Darcy's law describes the flow of groundwater and is applied to evaluate aquifer and aquifer material hydraulic characteristics. Darcy's experiments show that the flow of water through a column of saturated sand is proportional to the difference in the hydraulic head at the ends of the column. Darcy's law is still used as the basic principle that describes the flow of groundwater (**Figure 6**) and is expressed as Eq. 1 as follows:

$$Q = KiA \quad (1)$$

where

Q = quantity of water discharged, in cfs.

K = hydraulic conductivity (constant factor).

i = hydraulic gradient, in feet.

A = cross-sectional area, in square feet.

The hydraulic gradient (i) determines the direction of groundwater flow following Eq. 2

$$i = \frac{(h_1 - h_2)}{L} \tag{2}$$

where

h = hydraulic head

L = horizontal distance from h_1 to h_2

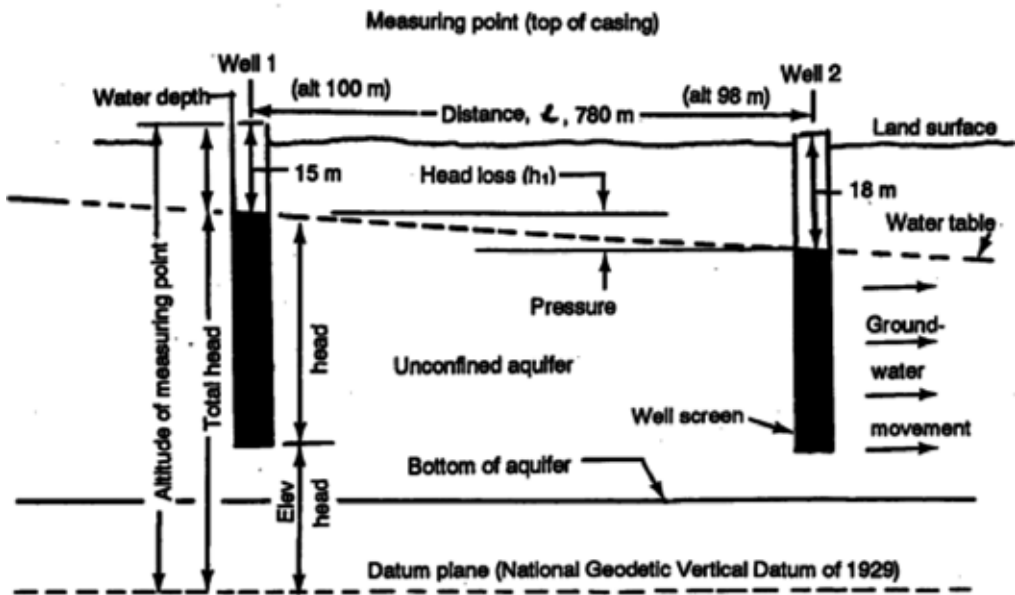


Figure 6. Hydraulic gradient determining the direction of groundwater flow under Darcy's law.

Hydrological models can be classified based on the application of several criteria, for example, according to the degree of conceptualization of the represented processes as physically based (white-box), conceptual (gray-box), and black-box models. Physically based models use PDEs in space and time to accurately represent in a deterministic way all the processes occurring in the physical system. Black-box models often include stochastic components, for example, relating outputs to inputs through a set of empirical functions, such as simple mathematical expressions, time series equations, autoregressive moving average (ARMA) models, and artificial neural networks (ANNs) disregarding any physical insight. Somewhere in between, conceptual models often represent parts of the system as series of tanks that exchange water with one another. Through a quite simplified description, they represent all the relevant parts of hydrological processes.

3.2. Numerical simulation of groundwater flow

The applications of MODFLOW, a modular three-dimensional finite-difference groundwater model of the US Geological Survey, to the description and prediction of the behavior of groundwater systems have increased significantly over the last few years. It has become the worldwide standard groundwater flow model that is used to simulate a wide variety of systems like water supply, containment remediation, and mine dewatering [16]. Several packages are integrated with MODFLOW that deals with a specific feature of the hydrologic system to be simulated, such as wells, recharge, or river. Models or programs can be stand-alone codes or can be integrated with MODFLOW. A stand-alone model or program communicates with MODFLOW through data files, for example, the advective transport model PMPATH [17], the parameter estimation programs PEST [18], and UCODE [19] use this approach.

PMWIN comes with a professional graphical user interface, the supported models and programs, and several other useful modeling tools, for example, Time-Variant Specified-Head (CHD1) [20], Direct Solution (DE45) [21], Density (DEN1) [22], Horizontal-Flow Barrier (HFB1) [23], Interbed-Storage (IBS1) [20], Reservoir (RES1) [24], and Streamflow-Routing (STR1) package [25]. Simulation results include hydraulic heads, drawdowns, cell-by-cell flow terms, compaction, subsidence, Darcy velocities, concentrations, and mass terms. The graphical user interface allows one to create and simulate models and displays temporal development curves of simulation results including hydraulic heads, drawdowns, subsidence, compaction, and concentrations. In many cases, the development of effective and efficient automatic calibration procedures, based on numerical optimization methods, has replaced the calibration of hydrological models conducted manually by "trial-and-error" parameter adjustment. The purpose of PEST and UCODE is to assist in data interpretation and in model calibration. If there are field or laboratory measurements, PEST and UCODE can adjust model parameters and/or excitation data in order that the discrepancies between the pertinent model-generated numbers and the corresponding measurements are reduced to a minimum. Both codes do this by taking control of the model (MODFLOW) and running it as many times as is necessary in order to determine this optimal set of parameters and/or excitations.

The software package Visual MODFLOW [26] has been used for three-dimensional numerical simulations of groundwater flow and drawdown within the study area. A finite-difference rectangular grid was constructed by establishing a network of nodal points. The model computes drawdown, direction of flow with vector lines, and hydraulic heads on each nodal point [27]. The flow model requires a boundary array for each cell. A positive value in that array defines an active cell (the hydraulic head is computed), a negative value defines a fixed-head cell (the hydraulic head is kept constant throughout the simulation), and the zero value defines an inactive cell (no flow takes place within the cell). A fixed-head boundary exists whenever an aquifer is in direct hydraulic contact with a river, a lake, or a reservoir in which the water level is known. Such a boundary provides an inexhaustible supply of water, which in some situations may be unrealistic [4, 28,29]. Visual MODFLOW requires initial hydraulic heads at the beginning of a flow simulation. For steady-state simulations, the initial heads are starting guessed values for the iterative equation solvers. The heads at the fixed-head cells

must be the actual values while all other initial heads can be set arbitrarily. For transient-flow simulations, the initial heads must be the actual values [30–33].

3.3. Model conceptualization and setup

The modeling area is bounded by the Korang River in the southeast and the Lei Nullah in the southwest. The hydrogeological system of the area was modeled as multilayered using Finite-difference Visual MODFLOW. The major steps involved during the modeling process were as follows: (a) expression of field parameters such as piezometric head, hydraulic conductivity; (b) formulation of the groundwater flow equation in an integral form; (c) integration of the integral form of the groundwater equation; (d) assembly of the algebraic matrix equations that result from the integration step into global system of linear equation; (e) time integration; and (f) solution of the global system of linear equations. The data from test holes and wells drilled by WAPDA [34,35] had been used in this study. **Table 1** shows specific yield and retention percentages for various lithologies. Hydraulic characteristics obtained from the analysis of pumping test data are provided in **Table 2**. We visited 278 tube wells in Rawal and Pothwar Towns for water-level measurements, as summarized in **Table 3** and shown in **Figure 7**. The mean water table depth was 28 m.

Material	Porosity	Specific yield	Specific retention
Soil	55	40	15
Clay	50	2	48
Sand	25	22	3
Gravel	20	19	1
Limestone	20	18	2
Sandstone	11	6	5

Table 1. Specific yield and retention percentages (values in percent by volume).

Test hole	Easting	Northing	Transmissivity m ² /s	Permeability coefficient m/s	Storage coefficient	Specific capacity m ³ /day/m
TH-1	3214782	1053687	1.5×10^{-2}	5.6×10^{-4}	7×10^{-2}	607
TH-6	3211368	1048417	3.6×10^{-3}	1.5×10^{-4}	2×10^{-3}	116
TH-8	3212866	1047817	1.4×10^{-3}	6.9×10^{-5}	2×10^{-4}	116
TH-9	3212299	1049052	1.3×10^{-2}	4.6×10^{-4}	5×10^{-2}	840

Table 2. Hydraulic characteristics of the aquifer in the study area.

Category	No. of tube wells	
	East zone	West zone
Water supply tube wells in Rawal Town	120	100
Water supply tube wells in Pothwar Town	24	
New tube wells installed	26	
Private tube wells visited	8	
Total	278	

Table 3. Brief summary of the tube wells used in the modeling study.

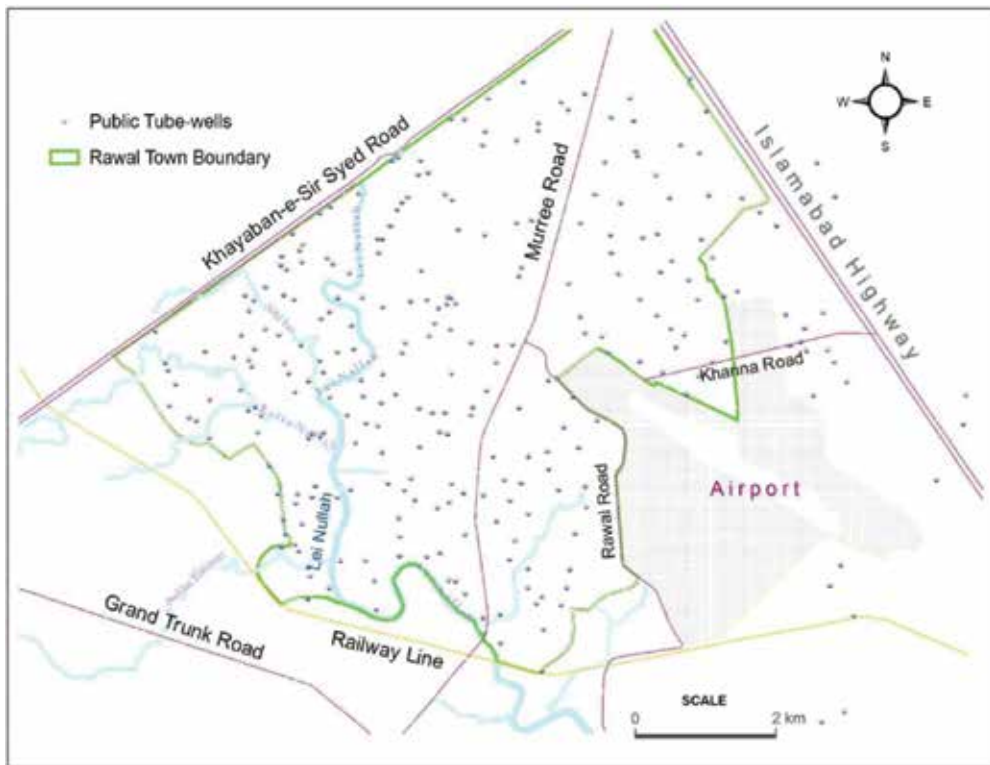


Figure 7. Location of the water supply public tube wells surveyed in the study area.

There are two major sources of recharge to groundwater: precipitation and infiltration from surface streams. Direct infiltration to the water table from precipitation is likely to occur especially in July and August, when rainfall is highest, although evaporation and soil moisture deficit in these months are also high. Recharge is also possible during the winter rains in February and March. We assume that 30% of rainfall is lost through runoff into the Soan and Korang rivers, 40% is lost through evapotranspiration from the surface and soil zone, and 15% is lost through the capillary and deep roots. Therefore, about 15% of rainfall, that is, $5.58 \times$

10^{-9} m/s [36–38], is available to recharge the shallow groundwater. In the Margalla hills, 7–15% of the precipitation tends to recharge the aquifer system through deep fractures of variable sizes in the limestone. Recharge within the urban areas of Islamabad and Rawalpindi is limited by impervious cover. The setting of the flow model is given below:

- Grids 95 columns \times 89 rows. The size of grid is 91.4 m (300 ft) in x and y directions
- The total modeling area is 70.7 km²
- Number of layers = 7
- Layer 1 (25 m) type = unconfined/confined (transmissivity [T] constant)
 - Layer 2 (12 m) type = aquiclude
 - Layer 3 (20 m) type = confined (T constant)
 - Layer 4 (12 m) type = aquiclude
 - Layer 5 (25 m) type = confined (T constant)
 - Layer 6 (4 m) type = aquiclude
 - Layer 7 (22 m) type = confined (T constant)

T -values are used from the results of pumping tests at 35 tube wells. Overall, T is set at 2.8×10^{-3} m²/s for layer 1, 4.6×10^{-4} m²/s for layer 3, 6.85×10^{-4} m²/s for layer 5, and 2.78×10^{-4} m²/s for layer 7. Boundary conditions consider all the cells active with the Korang River as a constant head boundary and the Lei Nullah as a recharge boundary. Horizontal hydraulic conductivity varies depending upon the type of subsurface material in layer 1 and is computed from T . The initial hydraulic heads are set at 28 m from initial guess and observed heads in the field. The top of the layer 1 is set at 426.7 m above the mean sea level (masl), and the bottom of the layer 1 is set at 47 m from the ground surface including 12 m layer of aquiclude. The top of the layer 2 is set at 47 m from the ground surface. The bottom of the layer is set at 106.7 m. Therefore, the thickness of layer 2 (saturated) is considered to be 57.9 m including 12-m layer of aquiclude. The top of the layer 3 is set at 106.7 m from the ground surface. The bottom of the layer is set at 137 m. Therefore, the thickness of layer 3 (saturated) is considered to be 30.4 m including 4-m layer of aquiclude. The specific yield (required for flow-path calculations) is set at 0.06 for layer 1, 0.009 for layer 3, 0.005 for layer 5, and 0.007 for layer 7. The Korang River is considered as the constant head boundary. Lei Nullah was considered to be influent (losing) or effluent (gaining) at places that would automatically adjust the situation during the simulations of different stress period in the steady-state and non-steady state conditions. The River Package was used to assign the following values of hydraulic properties of the rivers to the model cells:

- Hydraulic conductance of the river bed = 1.5×10^{-4} m²/s
- Head in the river = 27 m from the top of the layer = 0.0
- Elevation of the river bed bottom = 27.5 m from the top of the layer = 0.0

Observed hydraulic heads were obtained for 1998 and 2003 from the previous literature review [14], while for 2007 data were collected physically in the field. When data were collected, only

one well was switched off while the others were pumping, as it was not actually possible to shut off all the wells simultaneously. Consequently, spikes were apparent for hydraulic heads measured in 2007. Three-dimensional projections of the hydraulic heads are shown in **Figures 8–10**.

4. Results and discussion

4.1. Simulation of the groundwater flow

First, the model was run for steady-state condition with one time step of 20 years duration. The model was calibrated by comparing observed and computed heads using the UCODE automatic calibration program [19,39]. The hydraulic conductivity and recharge values were estimated during the process of steady-state calibration. Initially, the model was run to achieve

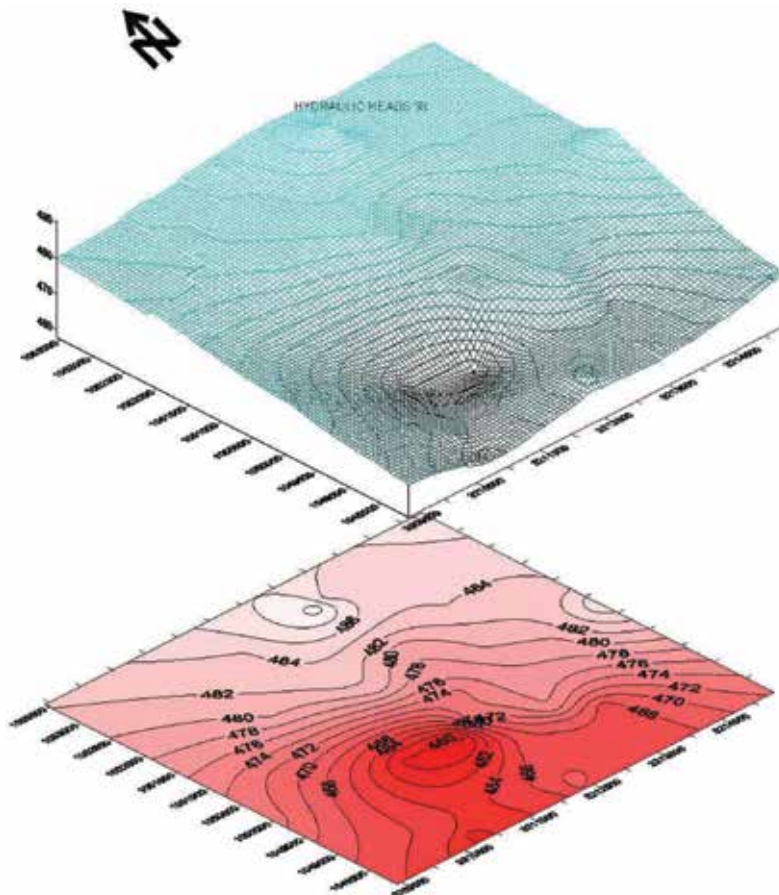


Figure 8. Three-dimensional projection of observed hydraulic heads in non-steady-state condition (1998).

the steady-state condition without pumping the wells and results obtained were calibrated with the available hydraulic head of 1998, as the available heads in 2003 and 2007 were very fluctuating due to the pumping effects. Simulated steady-state hydraulic heads for different aquifer layers are shown in **Figure 11**. Vector plots indicate groundwater flows toward Korang River in the southeast. Mass balance analysis showed a good balance between the inflow and the outflow components during the steady-state condition (**Figure 12**).

For transient-flow simulations, the initial heads were taken from the steady-state model. Withdrawals were set to a realistic range of pumping rates (in the range of 0.0094–0.015 m³/s).

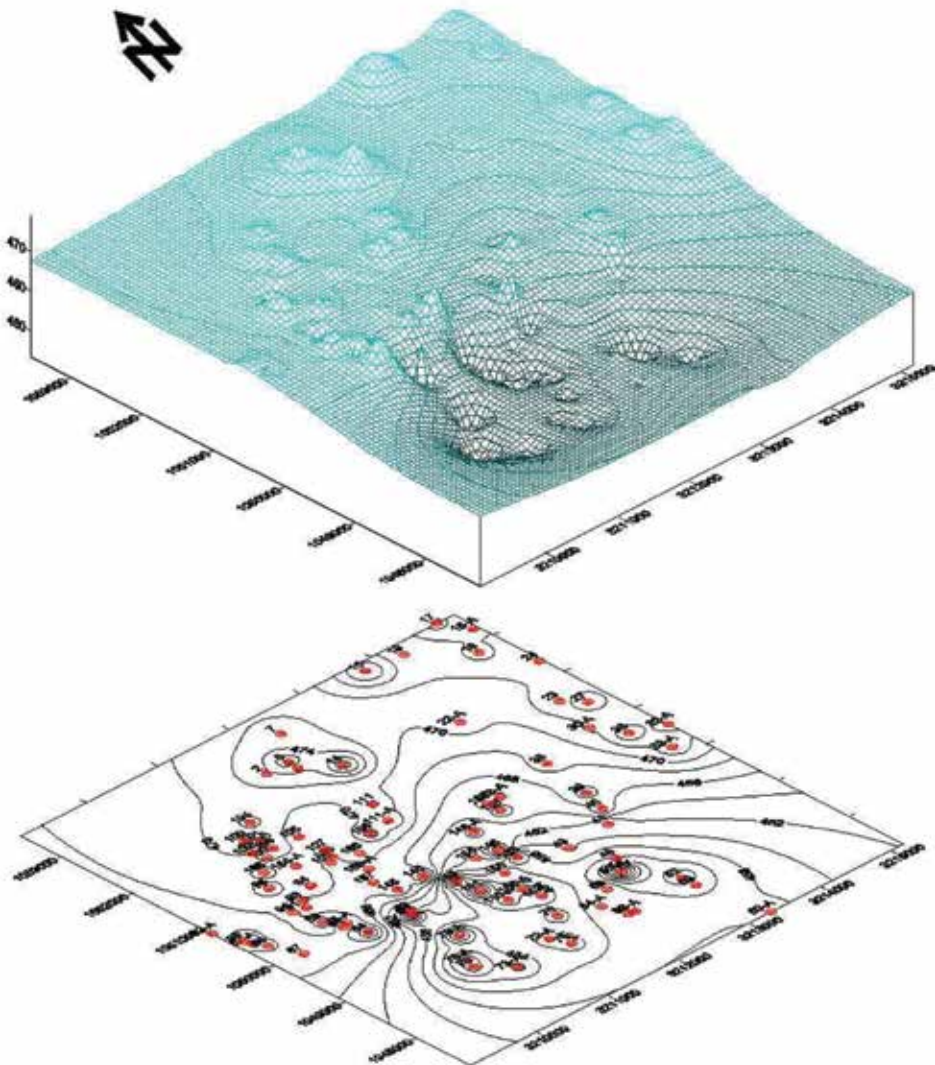


Figure 9. Three-dimensional projection of observed hydraulic heads with reference to water supply tube wells (2003).

The non-steady-state model was run for 1, 3, and 5 years. Transient-state simulations carried out up to year 2012 showed that the flow field had changed in the underlying aquifer layers because of pumping, as indicated by the arrowheads in **Figure 13**. Cone of depressions of layers 1, 3, and 7 for the southwestern area during 2008 are shown in **Figure 14a–c**. In the southwest

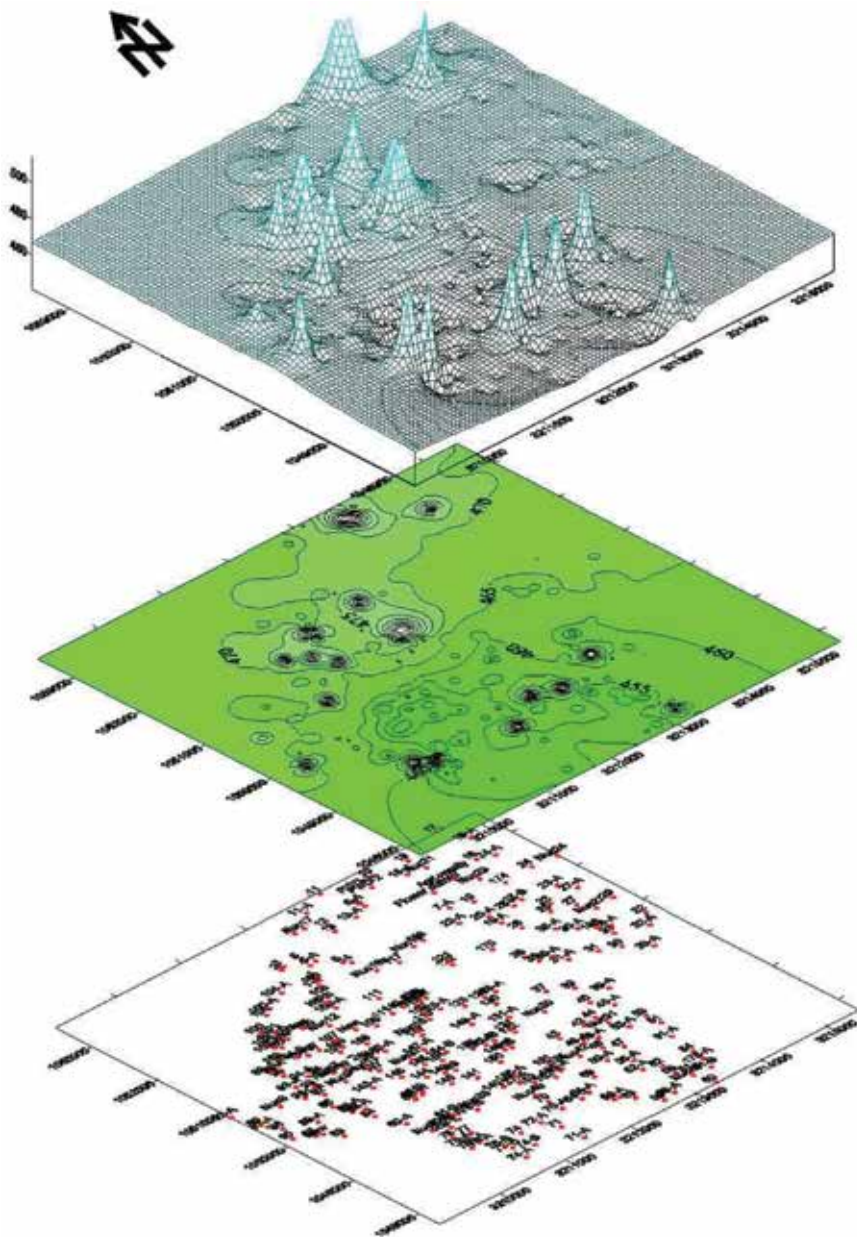


Figure 10. Three-dimensional projection of observed hydraulic heads with reference to water supply tube wells (2007).

(around Rawal Town), the flow is diverted toward a composite depression trough, but the flow in the southeastern area (around Pothwar Town) still moves into the Korang River. In the extreme south, the flow tends to rise where several wells are not pumping. A maximum of 20 m drawdown was observed at the end of a 3-year simulation in 2010. As a result, groundwater in the upper horizon (47 m) has already been depleted and pumping continues in the remaining permeable layer 3 through layer 7.

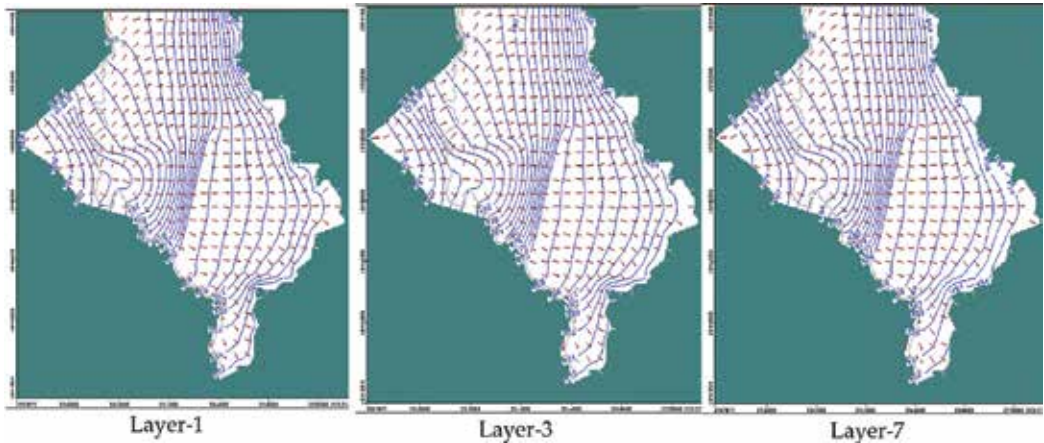


Figure 11. Steady-state hydraulic head in layers 1, 3, and 7 (after 20 years).

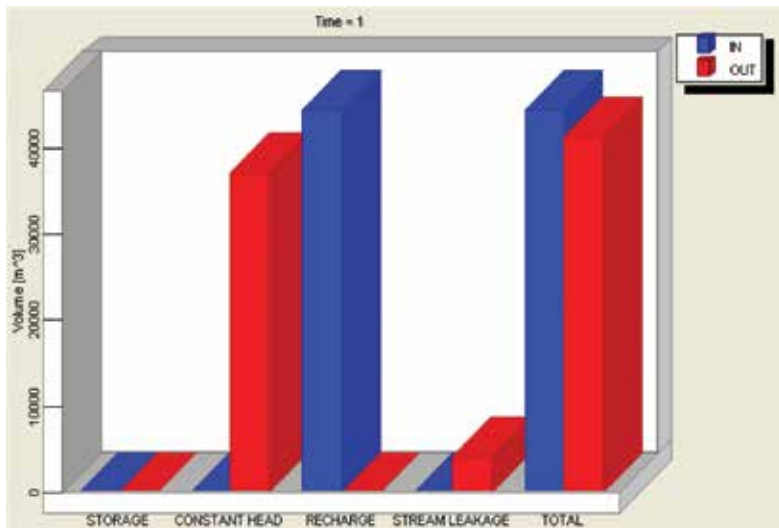


Figure 12. Mass balance during steady-state calibration.

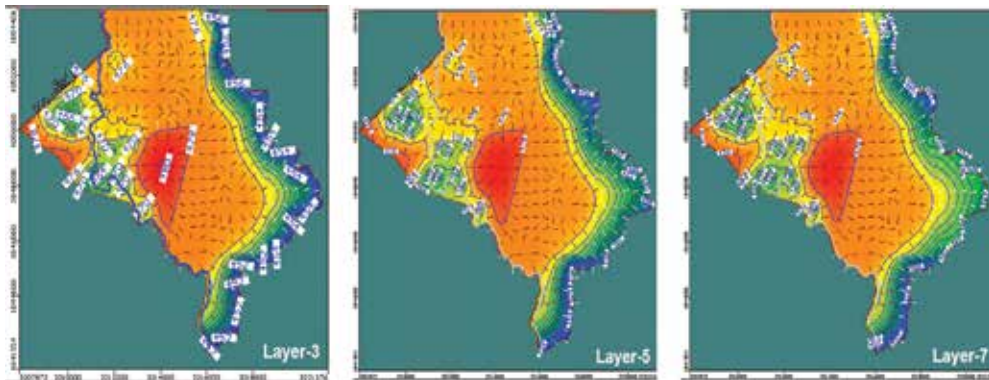


Figure 13. Hydraulic head in layers 3, 5, and 7 during 2010 (non-steady state).

The physical properties of the aquifer were found favorable for the development of groundwater with moderate values of transmissivity and specific yield. There is a continuous drop in hydraulic heads in the vicinity of pumped tube wells in Rawal Town and adjacent areas. Simulations indicated a maximum drawdown of 20 m. Existing tube wells could be safely pumped for a period of 5 years at the existing rate of discharge. However, drawdown could reach as deep as the fifth layer of the aquifer. Velocity vectors indicate that the groundwater in Rawalpindi city moves southeast toward the Korang River. Groundwater flow pattern in the layers 3, 5, and 7 is almost identical, but the velocity of flow is different for different layers.

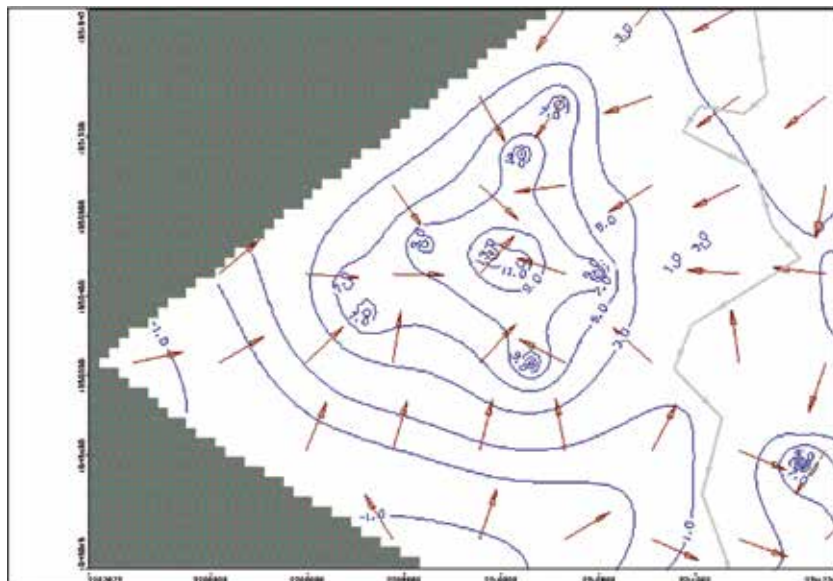


Figure 14a. Cone of depression in layer 3 (1-year simulation in 2008, non-steady state).



Figure 14b. Cone of depression in layer 5 (1-year simulation in 2008, non-steady state).

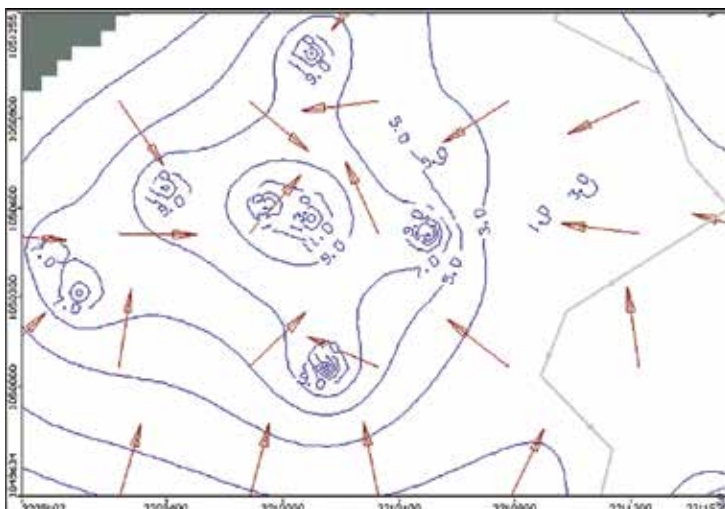


Figure 14c. Cone of depression in layer 7 (1-year simulation in 2008, non-steady state).

4.2. Management options for groundwater development

Under the present water scarcity conditions, there is a need to initiate integrated water resources management programs, with site-specific interventions, especially to harness the available rainwater. This would not only contribute to groundwater recharge in the basin but also supplement the water supplies to meet future water demand for various uses. Surface water drainage system/network (Figure 1) carries rainwater and is a potential source of

recharge to groundwater. The Soan and Korang rivers recharge the aquifer system during rainy months and are sustained by base flow at other times. Therefore, more water wells could be constructed along the Korang River where the underlying aquifer layers have good potential yield. Pumping of water wells in the western part of the study area needs to be monitored strictly in order to enable the groundwater levels to recover. Necessary bye-laws are established to restrict the overexploitation of groundwater and installation of unplanned tube wells. Similarly, bye-laws are established for restricted clearance of vegetation cover for unplanned urban development, as vegetative cover on the free catchment has proven to be an aid to groundwater recharge. The recharging system should be so designed that the amount of recharge during a year is at least equal to the amount of groundwater extracted during the year. Some of the recharging techniques may include as follows:

4.2.1. Dams and pounds

Water-charging pounds in open spaces, dams, and check dams need to be constructed in nullahs and distributaries. Such ponds would serve as water storage for emergency as well as for recharging of the groundwater (**Figure 15**). Main parks and green belts astride main roads of the twin cities and the dissected valleys around the built-up lands are ideal places to harvest rainwater by making water ponds recharging wells, etc.



Figure 15. Water ponds provide potential source not only for storing the surface runoff but also for recharging the groundwater.

4.2.2. Infiltration using wells and boreholes

Water can be infiltrated by injection using wells or boreholes in the areas where low-permeability strata overlies target aquifers as in the parts of watershed containing medium- to fine-textured soils over calcareous material (**Figure 2**). This technique is suitable for deep-seated aquifers that form a source of groundwater for urban areas lying in the valley plains of the watershed. The water-injecting wells have advantage that recharge water can bypass thick impervious layers to be introduced to the most permeable portions of the aquifer [40].

4.2.3. Water spreading

Water is diverted from surface water runoff into infiltration basins, ditches, or low-lying areas where the aquifer to be recharged is at or near to the ground surface as in the areas with flat to gentle topography. The water-spreading method could be practiced in medium- to coarse-textured soils in the gently sloping southeastern and some central parts of the watershed (shown in **Figure 2**). The exposed rocks of limestone and sandstone in the vicinity of the urban areas also provide potential recharge environment for subsurface water (**Figure 16**).



Figure 16. Joints and openings in the rocks facilitate recharge to the subsurface water.

Acknowledgements

The authors gratefully acknowledge the Australian Department of Education, Employment, and Workplace Relations (DEEWR) for providing post-selection support services and funding the research under the Executive Endeavour Award 2010. The Water and Power Sanitation Authority (WASA), Asian Development Bank (ADB), Osmani & Company (Pvt) Ltd, Department of Earth Sciences, Quaid-i-Azam University (QAU), and College of Earth and Environmental Sciences, Punjab University, are acknowledged for providing access to reliable data. Dr. Alan Fryar and Terencen Hamilton from the University of Kentucky, USA, are gratefully acknowledged to review and edit the manuscript.

Author details

Zulfiqar Ahmad^{1*}, Arshad Ashraf² and Mohsin Hafeez³

*Address all correspondence to: fz97@hotmail.com

1 Department of Earth Sciences, Quaid-i-Azam University, Islamabad, Pakistan

2 National Agricultural Research Center, Islamabad, Pakistan

3 Bureau of Meteorology, Brisbane, Australia

References

- [1] Allen DM. Historical trends and future projections of groundwater levels and recharge in coastal British Columbia, Canada, SWIM21 – 21st Salt Water Intrusion Meeting, 21–26 June 2010, Azores, Portugal. 2010: 267–270.
- [2] Crosbie, Russell S, McCallum, James L, Walker, Glen R and Chiew, Francis HS. Episodic recharge and climate change in the Murray-Darling Basin, Australia, *Hydrogeology Journal*. 2012; 20(2): 245–261.
- [3] Okkonen, Jarkko, Jyrkama, Mikko and Kløve, Bjørn. A conceptual approach for assessing the impact of climate change on groundwater and related surface waters in cold regions (Finland), *Hydrogeology Journal*. 2010; 18: 429–439.
- [4] Ashraf A and Ahmad Z. Regional groundwater flow modeling of upper Chaj Doab, Indus Basin, *Geophysical Journal International*. 2008; 173(1): 17–24.
- [5] McCallum JL, Crosbie RS, Walker GR and Dawes WR. Impacts of climate change on groundwater in Australia: a sensitivity analysis of recharge, *Hydrogeology Journal*. 2010; 18: 1625–1638.

- [6] Kumar CP. Impact of Climate Change on Groundwater Resources, Munich, GRIN Verlag, .2014. <http://www.grin.com/en/e-book/281606/impact-of-climate-change-on-groundwater-resources> (Accessed on May 2, 2016)
- [7] Mohammadi Z. Variogram-based approach for selection of grid size in groundwater modeling, *Applied Water Science*. 2013; 3: 597–602.
- [8] Noronha A and Lee J. On the use of information theory to quantify parameter uncertainty in groundwater modeling, *Entropy*. 2013; 15: 2398–2414.
- [9] Dams Jef, Salvadore, Elga and Batelaan, Okke. Predicting impact of climate change on groundwater dependent ecosystems, 2nd International Interdisciplinary Conference on Predictions for Hydrology, Ecology and Water Resources Management: Changes and Hazards caused by Direct Human Interventions and Climate Change, 20–23 September 2010, Prague, Czech Republic.
- [10] Wei XM, Kang SZ, Su XL, et al. Impact of oasis agricultural development on the transforming relationship between surface water and groundwater in the Shiyang River Basin, *Transactions of the Chinese Society of Agricultural Engineering*. 2005; 21(5): 38–41 (in Chinese).
- [11] Ma L, Wei XM. Analysis on aberrance point of annual runoff serials in the downstream of Shiyang River, *Agricultural Research in the Arid Areas*. 2006; 24(2): 174–177 (in Chinese).
- [12] Allchin B. The palaeolithic of the Pothwar plateau Punjab, Pakistan: a fresh approach, *Paléorient*. 1981; 7(1): 123–134. doi:10.3406/paleo.1981.4291. http://www.persee.fr/web/revues/home/prescript/article/paleo_0153-9345_1981_num_7_1_4291
- [13] Bender FK and Raza HA (Eds.). *Geology of Pakistan* Tutte Druckerei, GmbH, Salzwegpassau. 1995.
- [14] JICA. *Compilation of report of Islamabad–Rawalpindi ground water study by the Japan International Cooperation Agency, Capital Development of Authority, Pakistan*. 1988.
- [15] Ahmad B, Kaleem MS, Butt MJ and Dahri ZH. Hydrological modelling and flood hazard mapping of Nullah Lai, *Proceedings of the Pakistan Academy of Sciences*. 2010a; 47(4): 215–226.
- [16] Kumar CP. Numerical modelling of ground water flow using MODFLOW, *Indian Journal of Science*. 2013; 2(4): 86–92.
- [17] Chiang WH and Kinzelbach W. *3D-Groundwater modeling with PMWIN, A simulation system for modeling groundwater flow and pollution*. Springer. ISBN: 978-3-662-05551-9. 2003.
- [18] Doherty J. *PEST ver. 2.04, Watermark computing, Corinda, Australia*. 1995.

- [19] Poeter EP and Hill MC. Documentation of UCODE, a computer code for universal inverse modelling, U.S. Geological Survey, Water-Resources Investigations Report 98-4080. Denver, Colorado. 1998.
- [20] Leake SA and Prudic DE. Documentation of a computer program to simulate aquifer system compaction using the modular finite-difference ground-water flow model. Open-File Report 88-482, U.S. Geological Survey. 1991
- [21] Harbaugh AW. Direct solution package based on alternating diagonal ordering for the U.S. Geological Survey modular finite-difference ground-water flow model: U.S. Geological Survey Open-File Report 95-288; 1995: 46 pp.
- [22] Schaars FW and van Gerven MW. Density package, simulation of density driven flow in MODFLOW. KIWA-report SWS 97.511, ISBN 90-74741-42-8. KIWA Research & Consultancy, Nieuwegein, The Netherlands. 1997.
- [23] Hsieh and Freckleton. Documentation of a computer program to simulate horizontal-flow barriers using the U.S. Geological Survey's modular three-dimensional finite-difference groundwater flow model. U.S. Geological Survey, Open-File Report 92-477. 1993.
- [24] Fenske JP, Leake S A and Prudic DE. Documentation of a computer program (RES1) to simulate leakage from reservoirs using the modular finite-difference ground-water flow model (MODFLOW), U.S. Geological Survey, Open-File Report 96-364. 1996.
- [25] Prudic DE. Documentation of a computer program to simulate stream-aquifer relations using a modular, finite-difference, ground-water flow model, U.S. Geological Survey, Open-File Report 88-729, Carson City, Nevada. 1988.
- [26] Schlumberger Water Services (SWS)., 2010 Waterloo, ON N2L 5J2, www.swstechnology.com/novamatrix (Accessed on May 5, 2016)
- [27] Pollock DW. Semi-analytical computation of path lines for finite difference models, *Ground Water*. 1988; 26(6): 743–750.
- [28] Ahmad Z and Sergio Serrano. Numerical groundwater flow modeling of the Rechna Doab Aquifer, Punjab, Pakistan, Proceeding of International Groundwater Modeling Conference (IGWMC), MODFLOW 2001 and other Modeling Odysseys, Colorado School of Mines and Geophysics, Denver (12–14 September), USA. 2001.
- [29] Ahmad Z and Khawaja AA. Three-dimension flow and solute transport modeling of the Eolian Aquifer in a uniform flow field of a Chemical Plant, *Pakistan Journal of Hydrocarbon Research*. 1999; 11: 59–74.
- [30] McDonald MG and Harbaugh AW. A modular three-dimensional finite difference groundwater flow model. USGS open-file report 83-875: Modeling Techniques, Book 6. 1996.

- [31] Ahmad Z, Ashraf M and Siddiqui RF. Groundwater computer modeling of the National Park area in the vicinity of Rawal Lake, Islamabad, *Journal of Drainage and Water Management*. 1997; 1: 8–21.
- [32] Elci A, Molz FJ and Waldrop WR. Implications of observed and simulated ambient flow in monitoring wells, *Ground Water*. 2001; 39(6): 853–862.
- [33] Ghulam M and Ahmad Z. Management of groundwater resources in Punjab, Pakistan, using a groundwater flow model, *Journal of Environmental Hydrology*. 2007; 15: 1–14.
- [34] WAPDA, Lower Indus Report. Physical Resources, groundwater, suppl.6.1.6, Tubewells and Boreholes. Lahore, Pakistan. 1965.
- [35] WAPDA, Regional groundwater investigations in Islamabad and Rawalpindi areas, suppl.12. Ground water studies. Lahore, Pakistan. 1980.
- [36] Ahmad K. Pakistan: Lei Nullah basin flood problem Islamabad-Rawalpindi cities, WMO/GWP Associated programme on flood management. www.apfm.info/publications/casestudies (Accessed on May 5, 2016)
- [37] Ahmad Z, Kausar R and Ahmad I. Implications of depletion of groundwater levels in three layered aquifers and its management to optimize the supply demand in the urban settlement near Kahota Industrial Triangle area, Islamabad, Pakistan, *Environmental Monitoring and Assessment*. 2010b; 166(1–4): 41–55.
- [38] Ahmad Z, Kausar R and Ahmad I. Highlighting the implications of selenium dispersion from disposal of Kahota industrial triangle area, Islamabad, Pakistan using three-dimension solute transport model, *Environmental Monitoring and Assessment*. 2010c; 167(1–4): 565–579.
- [39] Poeter EP and Hill MC. UCODE, a computer code for universal inverse modelling, *Computers and Geosciences*. 1999; 25: 457–462.
- [40] Gale I, et al. The effectiveness of artificial recharge of groundwater: a review, British Geological Survey, Commercial Report CR/02/108N. 2002.

Spatiotemporal Analysis of Groundwater Recharge Trends and Variability in Northern Taiwan

Hsin-Fu Yeh, Chen-Feng Yeh, Jhe-Wei Lee and Cheng-Haw Lee

Additional information is available at the end of the chapter

<http://dx.doi.org/10.5772/63508>

Abstract

In this study, the base flow estimation method was used to assess long-term changes of groundwater recharge in Northern Taiwan. The Mann-Kendall test was used to examine the characteristics of the trends. This was followed by trend slope calculation and change-point analysis. The annual groundwater recharge was found to exhibit a significant upward trend for the Fushan and Hengxi stations (Tamsui river basin). On the other hand, the Ximen Bridge station (Lanyang river basin) recorded a significant downward trend. Calculations showed that the rate of change for the Fengshan and Touqian river basins was small (less than 10%). However, that for the following stations was greater than 30%: Fushan, Hengxi, Ximen Bridge, and Niudou (also in the Lanyang river basin). The results of the change-point analysis further indicated a significant change-point for the annual recharge at Fushan, Hengxi, and Ximen Bridge stations in 1999, 1983, and 2001, respectively. The findings can be used for regional hydrological studies and as reference for water resource planning.

Keywords: groundwater recharge, base flow, Mann-Kendall test, Northern Taiwan

1. Introduction

The annual average precipitation in Taiwan is 2500 mm, 2.6 times higher than the global average values. In spite of the high precipitation per unit area, the annual precipitation per person is only 1/7 of the global average, due to both small land area and large population [1]. Analysis of environmental sustainability indicators revealed that Taiwan ranked 18th among 146 countries experiencing water shortages, with the average available water per person in

Taiwan being 1740 m³/year [2]. Climate changes and increasing temperature experienced in recent decades caused the precipitation in Taiwan to increase during the rainy season, while decreasing in the dry season, resulting in a drier dry season and a wetter wet season [3]. Consequently, stream flow in both dry and wet seasons varied significantly. Thus, it is urgent to assess and discuss groundwater recharge characteristics, toward effective water resource management in Taiwan.

When analyzing the hydrogeological model and groundwater system of a region, the study on recharging groundwater through precipitation is a very important but complex issue. Meteorological factors (e.g., intensity and delay of precipitation, temperature, humidity, and wind speed), thickness of the soil layer, prevailing groundwater level, topographical conditions on the surface, vegetation cover, and land uses, all have direct relationships with the system and must be considered [4–10]. It is very easy to measure precipitation and run-off amounts when analyzing water balance, but it is very difficult to quantify the recharging process. Its evaluation requires not only precipitation data, but also other factors, such as prevailing climatic conditions, soil type, soil moisture status, vegetation cover, and evapotranspiration conditions [11, 12]. The infiltration of precipitation into the soil leads to the recharging process and is an important factor determining circulation of the groundwater system and its recharge volume.

Groundwater recharge can be quantitatively estimated using two methods. The first is the water balance model [13–16], which is applicable for humid regions; the second is for arid regions and involves the use of tensiometers, tracers, infiltrometers, and other instruments on site to observe the movement of water in the unsaturated zone, before estimating the groundwater recharge for that area [17–19]. However, it is generally more difficult to implement the second method because of high costs and the need for long-term monitoring on site. The existing methods for estimating groundwater recharge at the regional level using the water balance model are further divided into two types: (i) precipitation, infiltration, runoff, evapotranspiration, and groundwater recharge are treated as components of an interrelated system, with the soil moisture status being that of an ever-changing soil water balance model [7, 20, 21]; and (ii) the hydrograph of a stream flow is used to estimate its base flow, with the latter being treated as the groundwater recharge (based on the assumption that the heterogeneous hydrogeological conditions within the catchment area are ignored) [22–26].

In this study, the base flow estimation method was used to determine groundwater recharge and the evapotranspiration from the unsaturated zone was not considered. The calculation method to determine the effective recharge is simple, and it neither requires any complicated hydrogeological models, nor factors such as weather conditions and soil types. In this study, the calculation method was used to assess long-term changes of groundwater recharge in Northern Taiwan, and the findings can serve as reference for the management of water resources.

2. Methodology

2.1. Base flow model

Based on the concept of water balance and the data from stream flow gauging stations in the main river basins of the catchment area, this study employed the stream flow PARTitioning (PART) program (a base flow analysis method) developed by the US Geological Survey [27]. This method utilized the stream flow data to separate the base flow, which is regarded as the groundwater recharge. However, for rainy and humid regions and steep mountainous areas, if the estimation of groundwater recharge is based solely on base flow separation, it will often lead to overestimation of the base flow during the wet season [7, 28]. Therefore, the calculation of a steady base flow separation is required. In this study, a method for steady base flow analysis was adopted for this calculation to subsequently estimate a reasonable groundwater recharge.

Using Grey theory, the steady base flow analysis obtains data trends with reference to the rearrangement and accumulation of data. The steady base flow analysis uses trends for a low-flow period, a steady base flow period, and an overestimated base flow period, as shown in **Figure 1**. These are obtained after the rearrangement and accumulation of the separated base flows, and then, the steady base flow period is linearly extrapolated to achieve the steady base flow.

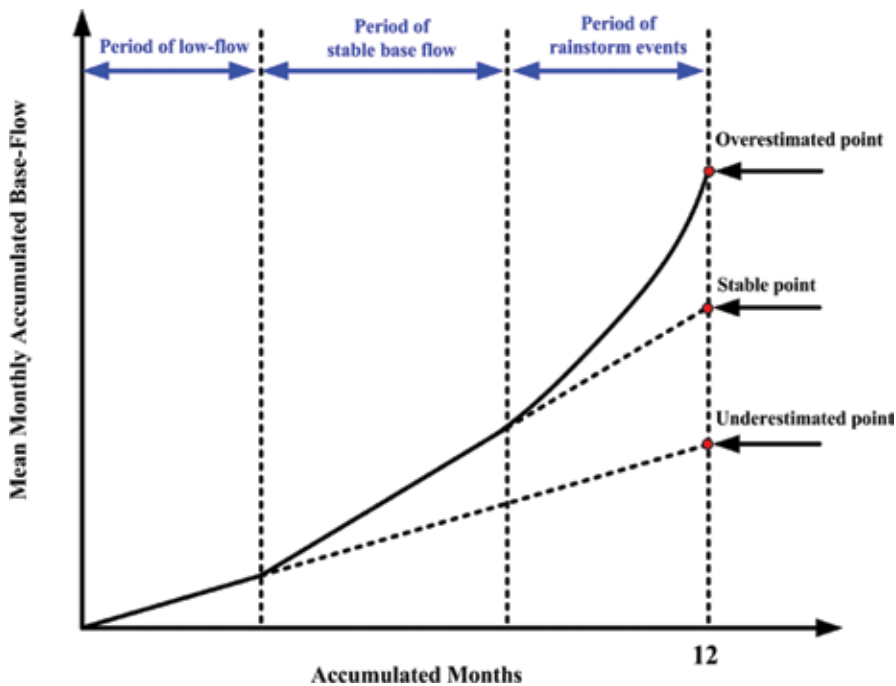


Figure 1. The diagram of the stable base flow analysis.

The steps in the analytical process are as follows:

1. Obtain the base flow of each month by base flow separation.
2. Sum the base flow per month over several years and then average the sum to achieve the long-term mean base flow on a month-by-month basis.
3. Sort the long-term mean base flow of each month in descending order and accumulate them to obtain the base flow accumulated per month and the trend of such base flows.
4. Determine the rising point of the base flow by the trend line of the accumulated base flow and obtain the steady base flow period.
5. Obtain the annual base flow, namely the annual groundwater recharge, by the extrapolation of the linear regression equation.

2.2. Mann-Kendall test

Mann-Kendall (MK) [29, 30] test is a nonparametric method developed from Kendall's tau (τ). It can be used to test the relationship between two sets of data. The advantages of this method is that extreme values and missing data problems will not seriously affect the certification value. The MK test assesses the trend in a series via comparing the value of the series before and after to determine whether the series exhibits a specific degree of trend. The null hypothesis given that if there is not significant trend in the series, test statistic S is defined as follows:

$$Sign(X_j - X_i) = \begin{cases} +1, & X_j - X_i > 0 \\ 0, & X_j - X_i = 0 \\ -1, & X_j - X_i < 0 \end{cases}, \quad S = \sum_{i=1}^{n-1} \sum_{j=i+1}^n Sign(X_j - X_i) \quad (1)$$

where $\{X_1, X_2, X_3, \dots, X_n\}$ is stream flow data which is arranged in accordance with time $\{T_1, T_2, T_3, \dots, T_n\}$. n is the number of data. When n is close to infinity, the probability of the S distribution curve will present as a normal distribution with a mean of 0. In addition, when n is more than 10, the variance of S can be substituted into the following approximate solution:

$$\sigma^2 = \frac{n(n-1)(2n+5)}{18} \quad (2)$$

In this study, long-term stream flow data are likely to be repeated in the data series; thus, Kendall modified the approximated solution Eq. (2) to Eq. (3).

$$\sigma^2 = \frac{1}{18} \left[n(n-1)(2n+5) - \sum_{u=1} u(u-1)(2u+5) \right] \quad (3)$$

where u is the duplicate value number of the data series.

Finally, the normalized statistical test S values becomes the Z value, as follows:

$$Z = \begin{cases} \frac{S-1}{\sigma} & , S > 0 \\ 0 & , S = 0 \\ \frac{S+1}{\sigma} & , S < 0 \end{cases} \quad (4)$$

When Z is a positive value, this indicates that the series is exhibiting an increasing trend; in contrast, when the value is negative, it indicates that the series has decreased. At this time, the obtained Z value should be tested by a significance test to assess whether the series is significant. Assuming a significance level of α , if $|Z| \geq Z_{\alpha}$, the null hypothesis is rejected, which represents that the series has a significant trend, otherwise the series has no significant trend. In the study, the significance level is set as $\alpha=0.05$. When $|Z| \geq 1.96$, the series has a significant trend. When it is below this level, there is no significant trend.

2.3. Theil-Sen slope

The Theil-Sen slope [31] is used to estimate the magnitude of the trend slope. The Theil-Sen slope estimation method is different from the slope values calculated using a linear regression, because it selects the median value, and therefore, the properties are less affected by extreme values. Thus, it is often used with the MK test. Slope β is defined as follows:

$$\beta = \text{Median} \left(\frac{X_j - X_i}{j - i} \right), \text{ for all } i < j \quad (5)$$

$$\begin{aligned} X(t) &= \beta t + C \\ X(t) &= X_1 \sim X_n, t = 1 \sim n \end{aligned} \quad (6)$$

2.4. Mann-Whitney-Pettit test

The Mann-Whitney-Pettit (MWP) test [32] can be used to search for significant change points in a data series. The definition of a change point is when a data series $\{X_1, X_2, \dots, X_n\}$ has a change point X_t . Order $\{X_1, X_2, \dots, X_t\}$ is $F_1(X)$ and $\{X_{t+1}, X_{t+2}, \dots, X_n\}$ is $F_2(X)$, then $F_1(X) \neq F_2(X)$. The definition of is as shown in Eq. (7) shown. If there is not a change point in the data series, $|U_{t,n}|$ on the function of time, t will continue to rise, and there will be no turning point. On the contrary, if there is a change point, $|U_{t,n}|$ on the function of time t , there will be a decreasing turning point. In the same data series, the turning point may occur several times on behalf of this data series, and there may be more than one change point.

$$\text{Sign}(X_i - X_j) = \begin{cases} +1, & X_i - X_j > 0 \\ 0, & X_i - X_j = 0 \\ -1, & X_i - X_j < 0 \end{cases}, \quad U_{t,n} = \sum_{i=1}^t \sum_{j=t+1}^n \text{Sign}(X_i - X_j) \quad (7)$$

$$K_n = \text{Max} |U_{t,n}|, \quad 1 \leq t < n \quad (8)$$

To confirm that change points exist, Eq. (8) is used to calculate the extreme value of $|U_{t,n}|$ that is turning point as K_n . Equation (9) is used to calculate the probability of a change point. In this study, $P = 0.95$ is set the as confidence level, where $P > 0.95$ judges that the time is a significant changing point.

$$P = 1 - \exp\left(\frac{-6K_n^2}{n^2 + n^3}\right) \quad (9)$$

However, in some data series, a change point may not exist by itself; thus, Eq. (10) is used to calculate each year's $P(t)$ value. The $P(t)$ value is identified when it is greater than the confidence level.

$$P(t) = 1 - \exp\left(\frac{-6|U_{t,n}|^2}{n^2 + n^3}\right) \quad (10)$$

3. Study area

The northern region of Taiwan includes several administrative districts, namely Yilan County, Keelung City, New Taipei City, Taipei City, Taoyuan County, and Hsinchu City. There are five types of terrains in this region: plains (mainly distributed in the Taoyuan Alluvial Fan and the Hsinchu Plain in the west, as well as the Yilan River Delta in the east); hills (mainly the Chutung Hill in Keelung); tablelands (the Linkou Plateau); basins (the Taipei Basin); and mountainous areas (the Tatun Mountain range in the north and the Central Mountain range). With these varied topographic features, this region ranges significantly in height from the <100 m above mean sea level (AMSL) plain areas to the <500 m AMSL hilly areas and to the >1000 m AMSL mountainous areas. The main rivers in the region are the Tamsui River, Lanyang River, Fengshan River, and Touqian River, with drainage areas of 2726, 978, 250.1, and 565.9 km², respectively. The annual average overall stream flow in the region is less than 15.1 billion m³, which is less than that of the central, southern, and eastern regions. The data for the past several years indicate that the stream flow of the northern region during the dry season is different from that of the wet season. The total stream flow of the dry season (from November to April) is approximately 5.62 billion m³; while during the wet season (from May to October), it is 9.48 billion m³ [33].

The long-term data on stream flow in Northern Taiwan were collected from the Water Resources Agency, Ministry of Economic Affairs. We selected stream flow stations that are not affected by artificial irrigation facilities and for which recorded data go as far back as 30 years. The eight gauging stations studied were Niudou and Ximen Bridge (Lanyang river basin); Fushan, Gaoyi, and Hengxi (Tamsui river basin); Xinpu (Fengshan river basin); and Neiwan and Shangping (Touqian river basin). Detailed information and geographical location of the various stations are shown in **Table 1** and **Figure 2**, respectively.

Basin	Station	Area (km ²)	X-coordinate (TWD67 ^a)	Y-coordinate (TWD67 ^a)	Record years
Lanyang River	Niu-Dou	446.7	306388.4	2726321	1979-2013
	Ximen Bridge	101.4	324454.8	2739377	1984-2013
Danshui River	Fu-Shan	160.4	298991.3	2742949.3	1953-2012
	Gaoyi	542.0	286029.3	2734394.2	1957-2002
	Hengchi	52.9	289452.4	2758619.3	1958-2012
Fengshan River	Hsin-Pu	208.1	255810.3	2746676	1970-2012
Touqian River	Nei-Wan	139.1	267503.3	2733084	1971-2012
	Shang-Ping	221.7	260738.5	2729330	1971-2012

Note: ^a is Taiwan triangulation points' coordinates.

Table 1. Information on gauging stations in Northern Taiwan.

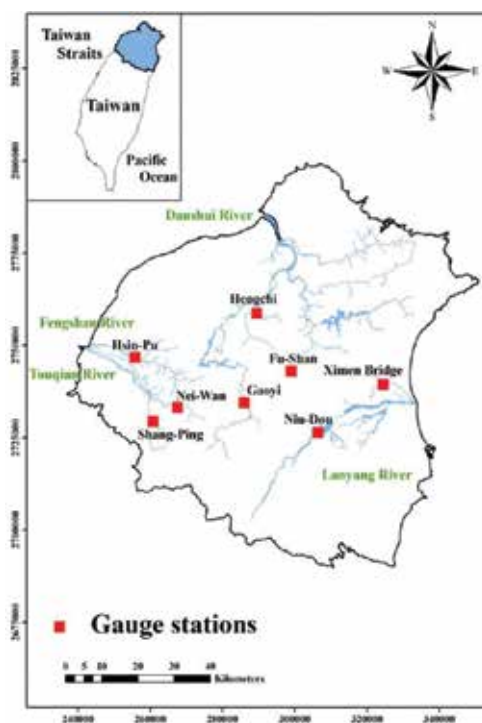


Figure 2. Spatial distribution of gauging stations in Northern Taiwan.

4. Results and discussion

4.1. Results of base flow separation

After collecting the annual stream flow data of the stations, the PART program developed by the United States Geological Survey (USGS) was used for analysis and to calculate the base flow of each station. The results showed that the trends of the base flow and stream flow were consistent, with the former ranging from 60.9 to 284.9 cm/year. Since Taiwan is located in a subtropical humid zone with perennial precipitation, during the steady base flow period, the recharge derived from base flow separation might still be greater than the groundwater recharge and discharge situations reflected by stream flow.

From a short-term perspective, base flow is affected by the amount of precipitation for that year. However, the amount of water discharged from the groundwater system should be a constant value over the long-term. Hence, stable base flow analysis was used to examine and estimate the groundwater recharge. Lee et al. [7] pointed out that the calculated base flow is likely to be overestimated when the base flow estimation method is used to assess stream flow data. This will in turn affect the calculations of the groundwater recharge. After estimating the base flow for all eight stations, evaluation was made using stable base flow analysis. This provided the depth of annual groundwater recharge for each station. The results are shown

in **Table 2**. The depth of annual groundwater recharge for the northern region was 15.6–160.65 cm/year. The maximum and minimum values were recorded at the Fushan and Niudou stations, respectively.

Basin	Station	Record years	Recharge depth (cm/year)
Lanyang River	Niu-Dou	1979-2010	15.60
	Ximen Bridge	1983-2012	142.89
Danshui River	Fu-Shan	1953-2012	160.65
	Gaoyi	1957-2002	144.07
	Hengchi	1958-2012	50.55
Fengshan River	Hsin-Pu	1970-2012	20.56
Touqian River	Nei-Wan	1971-2012	52.23
	Shang-Ping	1971-2012	55.83

Table 2. Results of the depth of annual groundwater recharge in Northern Taiwan.

4.2. Analysis of groundwater recharge

After calculating the depth of groundwater recharge for the respective stations using stable base flow analysis, the results were multiplied by the area of the water catchment. This gave the annual groundwater recharge for each station and the long-term average amount (**Table 3**). Annual groundwater recharge for the northern region worked out to be between 2.67×10^7 and 7.81×10^8 m³/year. Both largest and smallest volumes were found in the Tamsui river basin, at the Gaoyi and Hengxi stations, respectively.

Basin	Station	Record years	area (km ²)	Recharge Depth (cm/year)	annual recharge (m ³ /year)
Lanyang River	Niu-Dou	1979-2010	446.7	15.60	6.97×10^7
	Ximen Bridge	1983-2012	101.4	142.89	1.45×10^8
Danshui River	Fu-Shan	1953-2012	160.4	160.65	2.58×10^8
	Gaoyi	1957-2002	542.0	144.07	7.81×10^8
	Hengchi	1958-2012	52.9	50.55	2.67×10^7
Fengshan River	Hsin-Pu	1970-2012	208.1	20.56	4.28×10^7
Touqian River	Nei-Wan	1971-2012	139.1	52.23	7.26×10^7
	Shang-Ping	1971-2012	221.7	55.83	1.24×10^8

Table 3. Results of annual groundwater recharge in Northern Taiwan.

4.3. Analysis of trends in groundwater recharge

The Mann-Kendall test was used to analyze the characteristics of the long-term annual recharge trends for Northern Taiwan and to examine the distribution of significant trends. The test results are shown in **Table 4**. The significant level $\alpha = 5\%$ was adopted as the standard, meaning that $|Z_{\alpha/2}| = 1.96$ was used to verify that a trend was of significance. Three river flow stations were found to exhibit significant trends, namely Fushan, Hengxi, and Ximen Bridge stations. It was a significant upward trend for the first two stations, but a significant downward trend for the third station (**Table 4**). Overall, among the eight stations within the study area, only two exhibited downward trends: Gaoyi station at upstream Tamsui River and Ximen Bridge at downstream Lanyang River. The spatial distribution of trends for the various stations is shown in **Figure 3**. In addition, the Theil-Sen estimation method was used to calculate the trend slope. An upward and downward trend is indicated by a value larger and smaller than zero, respectively. The trend line can also be calculated using the trend slope values and annual recharge volume for the individual years. **Equation (10)** was then used to calculate the rate of change and the results are shown in **Figure 4**.

Basin	Station	Record years	Mann-Kendall test result	Slope estimator	Relative change
Lanyang River	Niu-Dou	1979-2010	1.768	0.155	30.9%
	Ximen Bridge	1983-2012	-3.604	-5.254	-106.6%
Danshui River	Fu-Shan	1953-2012	2.991	1.198	44.0%
	Gaoyi	1957-2002	-0.095	-0.026	-0.8%
	Hengchi	1958-2012	2.195	0.363	33.7%
Fengshan River	Hsin-Pu	1970-2012	0.415	0.049	10.0%
Touqian River	Nei-Wan	1971-2012	0.398	0.087	7.0%
	Shang-Ping	1971-2012	0.356	0.105	7.9%

Note: * indicates the significant trends. The positive values represent increasing trends, and the negative ones represent decreasing trends.

Table 4. Results of significant trend, slope, and relative change in Northern Taiwan.

It was observed that the rate of change for the annual recharge was small at the Fengshan and Touqian river basins: that for the Xinpu, Neiwan, and Shangping stations was all less than 10%. For the Tamsui river basin, with the exception of Gaoyi, the rate of change for the other stations was greater than 30%. In particular, the increases for Fushan and Hengxi stations were 44.0 and 33.7%, respectively. The rate of change was also greater than 30% for the Niudou and Ximen Bridge stations. However, it was an increase of 30.9% for the former, but a decrease of 106.6% for the latter. The slopes of the significant trends in stream flow are shown in **Figure 4**.

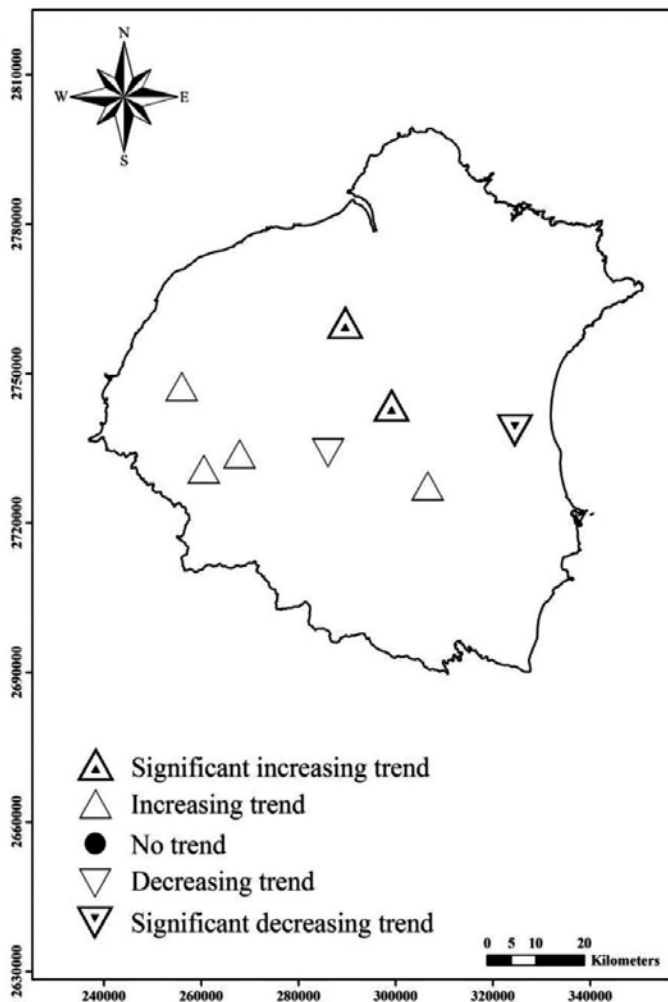


Figure 3. Map showing spatial variation in trends in annual recharge in Northern Taiwan.

The change-point analysis results revealed that change points occurred at three gauging stations: Fushan, Hengxi, and Ximen Bridge (Table 5 and Figure 5). The change point for the Fushan station occurred in 1999. The average annual groundwater recharge before and after the change point was 23.1×10^2 and 35.2×10^7 m³/year, respectively. The amount exhibited an upward trend post-1999, and the rate of increase was 46.9%. For the Hengxi station, the change point occurred in 1983, with the before and after volume being 2.2×10^7 and 3.3×10^7 m³/year, respectively. There was an overall upward trend as well, and the rate of increase was 41.7%. The change point for the Ximen Bridge station occurred in 2001. The before and after volumes there were 19.6×10^7 and 6.7×10^7 m³/year, respectively. The overall trend after the change point declined by as much as 89.4%. Among the three aforementioned gauging stations, the magnitude of change at the Ximen Bridge station was the largest.

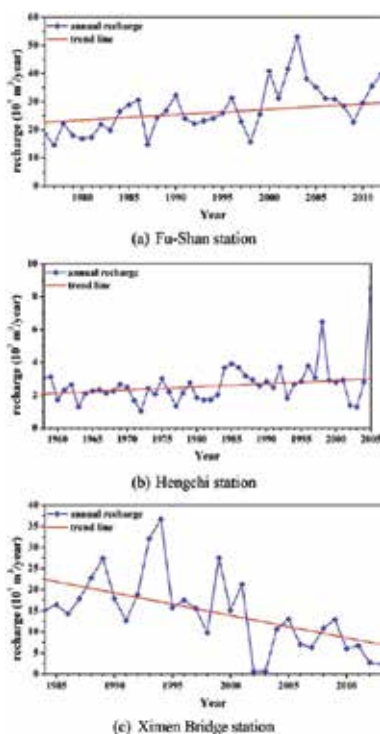
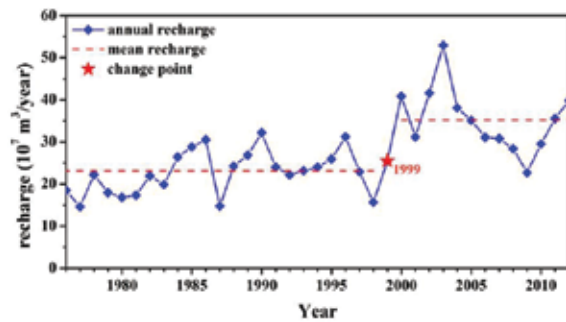


Figure 4. The significant trend line of gauging stations in Northern Taiwan. (a). Fu-Shan station, (b) Hengchi station, (c) Ximen Bridge station

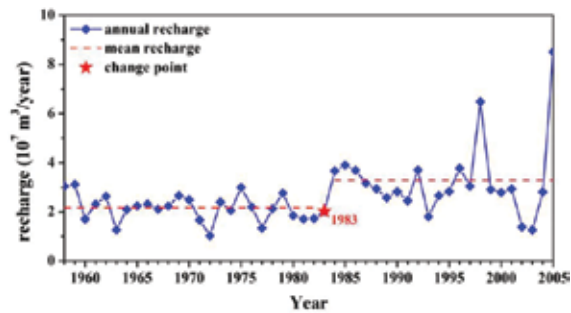
Basin	Station	Change point (year)	P (Mann-Whitney-Pettitt)	Mean recharge (10 ⁷ m ³ /year)		Relative change at the change point
				before change point	after change point	
Lanyang River	Niu-Dou	-	0.8423	-	-	-
	Ximen Bridge	2001	0.9999	19.6	6.7	-89.4%
Danshui River	Fu-Shan	1999	0.9995	23.1	35.2	46.9%
	Gaoyi	-	0.8553	-	-	-
	Hengchi	1983	0.9990	2.2	3.3	41.7%
Fengshan River	Hsin-Pu	-	1.0660	-	-	-
Touqian River	Nei-Wan	-	0.8012	-	-	-
	Shang-Ping	-	0.7013	-	-	-

Note: The number in bold indicates a statistically significant difference.

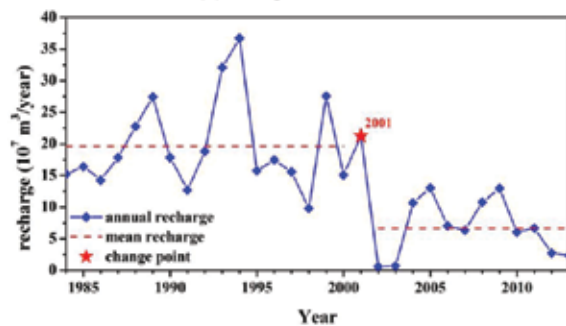
Table 5. Results of change points using cumulative deviations and Mann-Whitney-Pettitt test.



(a) Fu-Shan station



(b) Hengchi station



(c) Ximen Bridge station

Figure 5. The results of change points of significant trend stations. (a)Fu-Shan station, (b) Hengchi station, (c)Ximen Bridge station

5. Conclusions

In this study, the base flow estimation method and stable base flow analysis were used to evaluate the long-term stream flow data of eight stations in Northern Taiwan. The range was between 2.67×10^7 and 7.81×10^8 $m^3/year$ based on the cumulative annual recharge. The characteristics of the trends were examined using the Mann-Kendall test. Further, trend slope calculation and change-point analysis were carried out. The results provided an understanding

of the trends for the eight stations and indicated that only two had downward trends: Gaoyi station at the upstream of the Tamsui River and Ximen Bridge at the downstream of the Lanyang River. The rate of change for the Fengshan and Touqian river basins was relatively small. Separately, the rate of change for the annual groundwater recharge was greater than 30% for all stations in the Lanyang river basin, while Gaoyi station was the only exception in the Tamsui river basin. The results of the change-point analysis showed that the change point for the Fushan, Hengxi, and Ximen Bridge stations occurred in 1999, 1983, and 2001, respectively. The average annual groundwater recharge for the first two stations exhibited an upward trend before and after the change point (46.9 and 41.7%, respectively), while that for the last station decreased by as much as 89.4%. The findings can be used for regional hydrological studies and as reference for water resources planning.

Acknowledgements

The authors are grateful for the support of the Research Project of the Ministry of Science and Technology (MOST 103-2221-E-006-205-MY2).

Author details

Hsin-Fu Yeh^{1*}, Chen-Feng Yeh¹, Jhe-Wei Lee² and Cheng-Haw Lee¹

*Address all correspondence to: hfyeh@mail.ncku.edu.tw

1 Department of Resources Engineering, National Cheng Kung University, Tainan, Taiwan

2 Department of Hydraulic and Ocean Engineering, National Cheng Kung University, Tainan, Taiwan

References

- [1] Chung YD, Kuo CC, Chen CS. The temporal variation of regional rainfall characteristics in Taiwan. *Journal of Chinese Agricultural Engineering*. 2009;55:1–18. (in Chinese)
- [2] Esty D, Srebotnjak T, Goodall M, Andonov B, Campbell K, Gregg K, Kim C, Li Q, Martinez M, Townsend J, Zhang B, Levy M, de Sherbinin A, Anderson B, Saltelli A, Saisana M, Nardo M, Dahl A. *Environmental sustainability index: benchmarking national environmental stewardship*. Yale Center for Environmental Law & Policy: New Haven, USA; 2005.

- [3] Hsu HH, Chen CT, Lu MM, Chen YM, Chou C, Wu YC. Climate change in Taiwan: scientific report 2011; National Science and Technology Center for Disaster Reduction: New Taipei City, Taiwan.
- [4] Scanlon BR, Healy RW, Cook PG. Choosing appropriate techniques for quantifying groundwater recharge. *Hydrogeology Journal*. 2002;10:18–39.
- [5] Keese KE, Scanlon BR, Reedy RC. Assessing controls on diffuse groundwater recharge using unsaturated flow modeling. *Water Resources Research*. 2005;41:W06010.
- [6] Döll P, Fiedler K. Global-scale modeling of groundwater recharge. *Hydrology and Earth System Sciences*. 2008;12:863–885.
- [7] Lee CH, Yeh HF, Chen JF. Estimation of groundwater recharge using soil moisture budget method and base-flow model. *Environmental Geology*. 2008;54:1787–1797.
- [8] Kim JH, Jackson RB. A global analysis of groundwater recharge for vegetation, climate, and soils. *Vadose Zone Journal*. 2012;11:188–222.
- [9] Ibrahim M, Favreau G, Scanlon BR, Seidel JL, Le Coz M, Demarty J, Cappelaere B. Long-term increase in diffuse groundwater recharge following expansion of rainfed cultivation in the Sahel, West Africa. *Hydrogeology Journal*. 2014;22:1293–1305.
- [10] Sanford WE, Nelms DL, Pope JP, Selnick DL. Estimating mean long-term hydrologic budget components for watersheds and counties: an application to the commonwealth of Virginia, USA. *Hydrology Current Research*. 2015;6:191.
- [11] Wang TJ, Istanbuluoglu E, Lenters J, Scott D. On the role of groundwater and soil texture in the regional water balance: an investigation of the Nebraska Sand Hills, USA. *Water Resources Research*. 2009;45:W10413.
- [12] Taylor RG, Scanlon B, Doll P, et al. Ground water and climate change. *Nature Climate Change*. 2013;3:322–329.
- [13] Dripps WR, Bradbury KR. A simple daily soil-water balance model for estimating the spatial and temporal distribution of groundwater recharge in temperate humid areas. *Hydrogeology Journal*. 2007;15:433–444.
- [14] Westenbroek SM, Kelson VA, Dripps WR, Hunt RJ, Bradbury KR. SWB-a modified Thornthwaite-Mather soil-water-balance code for estimating groundwater recharge. U.S. Geological Survey. *Techniques and Methods*. 2010;6–A31.60p.
- [15] Mair A, Hagedorn B, Tillery S, El-Kadi AI, Westenbroek S, Ha K, Koh GW. Temporal and spatial variability of groundwater recharge on Jeju Island, Korea. *Journal of Hydrology*. 2013;501:213–226.
- [16] Beigi E, Tsai FTC. GIS-based water budget framework for high-resolution groundwater recharge estimation of large-scale humid regions. *Journal of Hydrologic Engineering*. 2014;19:05014004.

- [17] Cuthbert MO, Mackay R, Nimmo JR. Linking soil moisture balance and source-responsive models to estimate diffuse and preferential components of groundwater recharge. *Hydrology and Earth System Sciences*. 2013;17:1003–1019.
- [18] Bekele E, Patterson B, Toze S, Furness A, Higginson S, Shackleton M. Aquifer residence times for recycled water estimated using chemical tracers and the propagation of temperature signals at a managed aquifer recharge site in Australia. *Hydrogeology Journal*. 2014;22:1383–1401.
- [19] Vásquez V, Thomsen A, Iversen BV, Jensen R, Ringgaard R, Schelde K. Integrating lysimeter drainage and eddy covariance flux measurements in a groundwater recharge model. *Hydrological Sciences Journal*. 2015;60:1520–1537.
- [20] Bakundukize C, Camp MV, Walraevens K. Estimation of groundwater recharge in Bugesera region (Burundi) using soil moisture budget approach. *Geologica Belgica*. 2011;14:85–102.
- [21] Oke, MO, Martins O, Idowu OA. Determination of rainfall-recharge relationship in River Ona basin using soil moisture balance and water fluctuation methods. *International Journal of Water Resources and Environmental Engineering*. 2014;6:1–11.
- [22] Nathan RJ, McMahon TA. Evaluation of automated techniques for base flow and recession analysis. *Water Resources Research*. 1990;26:1465–1473.
- [23] Rutledge AT, Daniel III CC. Testing an automated method to estimate ground-water recharge from streamflow records. *Ground Water*. 1994;32:180–189.
- [24] Mau DP, Winter TC. Estimating ground-water recharge from streamflow hydrographs for a small mountain watershed in a temperate humid climate, New Hampshire, USA. *Ground Water*. 1997;35:291–304.
- [25] Lee CH, Chen WP, Lee RH. Estimation of groundwater recharge using water balance coupled with base-flow-record estimation and stable-base-flow analysis. *Environmental Geology*. 2006;51:73–82.
- [26] Yeh HF, Lin HI, Lee ST, Chang MH, Hsu KC, Lee CH. GIS and SBF for estimating groundwater recharge of a mountainous basin in Wu River watershed, Taiwan. *Journal of Earth System Science*. 2014;123:503–516.
- [27] Rutledge AT. Computer programs for describing the recession of ground-water discharge and for estimating mean ground-water recharge and discharge from streamflow records-update. U.S. Geological Survey Water-Resources Investigations Report 98-4148;1998. 43p.
- [28] Rutledge AT. Considerations for use of the RORA program to estimate ground-water recharge from streamflow records. U.S. Geological Survey. 2000;Open-File Report 00-156, 44p.
- [29] Mann HB. Non-parametric test against trend. *Econometrica*. 1945;13:245–259.

- [30] Kemdall MG. Rank correlation methods. Charles Griffin, London; 1975.
- [31] Sen PK. Estimates of the regression coefficient based on Kendall's tau. *Journal of the American Statistical Association*. 1968;63:1379–1389.
- [32] Pettit AN. A non-parametric approach to the change point problem. *Applied Statistics*. 1979;28:126–135.
- [33] Water Resources Agency (WRA). Hydrological year book of Taiwan. Ministry of Economic Affairs: Taipei, Taiwan; 2013.

Flow through Multiple Well Points System

Ajay K. Vashisht and Shri K. Shakya

Additional information is available at the end of the chapter

<http://dx.doi.org/10.5772/63347>

Abstract

Under natural geographical settings, there are regions all over the world where the native groundwater quality is brackish. However, recharging from the surface water bodies (i.e., rivers and canals) establishes freshwater lenses in the upper portions of these brackish aquifers. Skimming of these freshwater lenses is a viable technique for sustaining livelihood and agricultural practices in these regions. In the present chapter, various skimming methods have been discussed. In addition, one another type of problem has also been developed in certain pockets of these regions. The non-withdrawal of groundwater and the excess use of easily available surface water resources (i.e., canal water) have created severe water logging conditions. Subsequently, it leads to the creation of salt-affected soils. One of such areas located in the southwestern Punjab (India) was taken under study. Keeping the region's problems in mind and considering the merits and demerits of all the skimming methods, a much efficient and affordable technique named multiple well points system (MWPS) has been proposed. The continuous use of MWPS not only reclaimed the area but also improved the groundwater quality. The system was field tested and modified before recommending to the farmers. Later on, the MWPS's feasibility as a groundwater recharging system was also demonstrated in the field and the results have shown that it is a viable technique for reviving freshwater lenses in the region.

Keywords: brackish/saline aquifers, groundwater recharging, multiple well points system, skimming wells, well hydraulics

1. Introduction

Since ancient times, it is a natural tendency of humankind to settle near the perennial and freshwater resources. But for many millennia, humankind's capability to abstract groundwater was very little compared with the available resources [1]. With time the demand for

freshwater increases due to rapid population growth and expanding economies in many parts of the world [2]. The mechanization advancements in the twentieth century, geological knowledge, well drilling, and pump technology made it more convenient to abstract groundwater from deeper aquifers [3, 4]. Globally, groundwater withdrawal ranges between 600 and 700 km³/y [5]. In the past five-to-six decades, the overexploitation of fresh groundwater beyond sustainability limits has resulted in the widespread and progressive depletion of water level all over the world. As a result, the freshwater resources are becoming scarcer every year. The global warming and climate change is further threatening its security all over the world [6]. Moreover, the heavy withdrawal of freshwater in the regions surrounded by brackish/sea water is responsible for the intrusion of brackish/sea water into the freshwater aquifers [7]. It is not only the anthropogenic reasons that are responsible for the development of brackish aquifers, these may also occur naturally. Under natural geographical settings, there are regions all over the world where the native groundwater quality is brackish [8] and one of the possible reasons is the retention of ions from salt water trapped at the time of ancient marine transgression [9]. The vast stretches in the states of Rajasthan, Punjab, and Haryana of India and Indus basin of Pakistan are having brackish aquifers. Since the groundwater quality is not fit for domestic and agricultural purposes, alternate sources of freshwater were generated to fulfill the demand for potable supply in these regions. Keeping in mind the agricultural productivities of the regions, the governments of both the countries make lots of efforts to lay dense canal network by constructing hydroelectric projects and/or barrages on major rivers and their tributaries. It is a well-known fact that under all practical situations a huge quanti-



Figure 1. Photograph showing the water table at the ground surface (snapped in early 1980s).

ty of water is lost through seepage from the canal network (either lined or unlined) before reaching the destination. According to Wachyan and Rushton [10], a well-maintained canal with a 99% perfect lining reduces seepage to about 30–40%, but seepage cannot be controlled completely. By the time water reaches the field, around 45% of the actual volume of water supplied from the canal head seeps out [11]. In Indian conditions, the loss of water through seepage from unlined canals generally varies from 0.3 to 7.0 m³/s per 10⁶ m² wetted surface; which depends on the permeability of soil through which the canal passes, location of water table, distance of drainage, bed width, side slope, and water depth inside the canal [12]. Because of the excess seepage from the dense canal network (lined and unlined), deep percolation losses from surface irrigation practices, and in the absence of adequate drainage facilities, the water table has started rising in these regions. Consequently, the water table has risen from 3.65 m in 1930s to less than 1.20 m in 1980s in most of the lower Indus basin [13]. The situation was worse in certain pockets of Indus basin of India where the water table has virtually reached the land surface (**Figure 1**). As a result, the soils become severely alkaline (i.e., alkaline) in nature (**Figure 2**). These conditions have debarred the agricultural practices in the region.



Figure 2. Photograph showing the alkaline soils in the region (snapped in early 1980s).

Under these circumstances, the major challenges in front of the water resource managers were

- a. to decline the water table and to improve the condition of soil in the areas where water is virtually standing on the surface (is termed as the *first type of problem*), and

- b. to arrest the further rise of water table in the areas where water table is near to create water logging conditions (is termed as the *second type of problem*).

First type of problem: The reclamation process for this type of problem is comparatively difficult and takes longer period of time than the second type of problem. The main reason of high water table in the area is more inflow than the outflow. In general, the aquifers in these areas are very thin (i.e., near about 10 m). High water table conditions are further responsible for the creation of alkaline soils. It is a well-known fact that the presence of high sodium content in alkaline soils makes clay particles to remain in suspension and appear in the form of slurry. It makes the construction of trenches and installation of pipe drainage system difficult at the desired depth and suspects its workability. Therefore, the first requirement for reclaiming such areas was to decline the water table and to improve the soil conditions. In these conditions, only vertical drainage was possible as it was the only way by which the clay particles would be trapped in the upper part of the aquifer. The main advantage of the vertical drainage is that it lowers the water table to any desired depth which is not possible in the case of subsurface and pipe drainage system. Further, the increase in outflow from the aquifer creates space for the storage of seeped-out freshwater from the nearby canal.

Second type of problem: The sustenance of cultivation practices in these regions was vest in the condition that the existing groundwater could be used which will eventually lower the water table. This decision was based on the existence of those freshwater lenses which had established in varied thicknesses over the native brackish water due to the seepage from surface water bodies. Since the aquifer contains water of different densities in two layers, therefore, pumping the aquifer by merely placing the screen of a partially penetrating well in the freshwater zone will not serve the purpose as the development of discharge head in the aquifer may cause up-coning of fresh-brackish water interface to effective pumping zone of the well [14]. This phenomenon can be better explained by the Ghyben-Herzberg principle. Both the researchers have independently recognized the flotation of a steady-state, fresh groundwater lens on top of sea water [15, 16]. If h_f is the freshwater head above sea level and h_s is the depth to the sharp interface (i.e., considering immiscible fluids) below sea level, then for a system in static equilibrium the pressure at the interface due to the overlying column of freshwater must be equivalent to that due to the column of salt water (**Figure 3**). Considering ρ_f is the density of freshwater and ρ_s as that of saltwater, static equilibrium as shown in **Figure 3** can be expressed mathematically as

$$h_s \rho_s = (h_s + h_f) \rho_f \quad (1)$$

Rearranging the terms, Eq. (1) changes to

$$h_s = \left(\frac{\rho_f}{\rho_s - \rho_f} \right) h_f \quad (2)$$

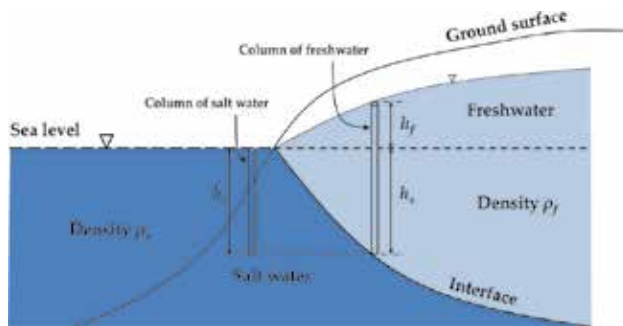


Figure 3. Schematic sketch explaining the Ghyben–Herzberg principle.

According to Eq. (2), the up-coning of the interface depends on the density difference between the fresh and brackish water. For any operational discharge head value, decrease in density difference between freshwater and brackish/saline water leads the interface to rise higher [8], and which is synonymous to Wang's [17] results. Reclamation of such lands for sustaining livelihood is a major challenge for the scientists of India and Pakistan. Researchers from all over the world have also shown keen interest in the reclamation of such areas. Based upon the hydrogeological conditions of the areas, various water management techniques have been proposed. More specifically, the stress has been given to skim the available freshwater from the fresh–brackish/saline aquifers. In the subsequent sections, various types of skimming techniques are discussed.

1.1. Skimming tube well(s)

During the pumping of freshwater from fresh–brackish/saline aquifer, the pressure head in the vicinity of well is lowered which ultimately leads to the rise of brackish/saline water. This phenomenon is known as up-coning and is responsible for the increase in salt content of the pumped water. Obviously, the purpose is to pump the freshwater without much disturbing the brackish/saline zone. Therefore, the term “*skimming tube well*” may be defined as the *tube well to extract freshwater from the fresh–brackish–saline aquifer by specifying the extraction rate so as to limit the rise of fresh–brackish/saline interface to reach effective pumping zone of the well (Figure 4a)*. The performance of a skimming tube well depends upon the factors, viz., (i) relative thickness of the freshwater lens with respect to the brackish/saline water zone at the point of extraction, (ii) densities of freshwater and brackish-/saline water, (iii) screen length penetrating the freshwater zone, (iv) distance of skimming well from the recharging source (i.e., canal/river), (v) diameter of the well, (vi) spacing between the adjoining skimming wells, and (vii) the aquifer parameters. Studies show that the single-bore skimming tube well technique is successful only in aquifer with the freshwater zone having thickness more than 30 m [18]. In the regions where the thicknesses of the freshwater zones are less than 30 m, the farmers' have to compromise either with the discharge rate or with the pumped water quality if they abstract groundwater through single-bore well. In such situations, a more practicable technique is to abstract water through a number of smaller capacity tube wells which are installed arbitrarily in circular array and are joined with a single pumping unit (Figure 4b). The complete pumping

setup may be termed much appropriately as “*skimming tube wells system.*” Field experience shows that the number of tube wells in such type of system may vary from 2 to more than 16 [18]. However, based upon the performance studies on skimming tube wells system with reference to quantity and quality of pumped freshwater it was found that the double-strainer skimming well is most efficient [19]. Its basic reason is explained in Section 1.6.

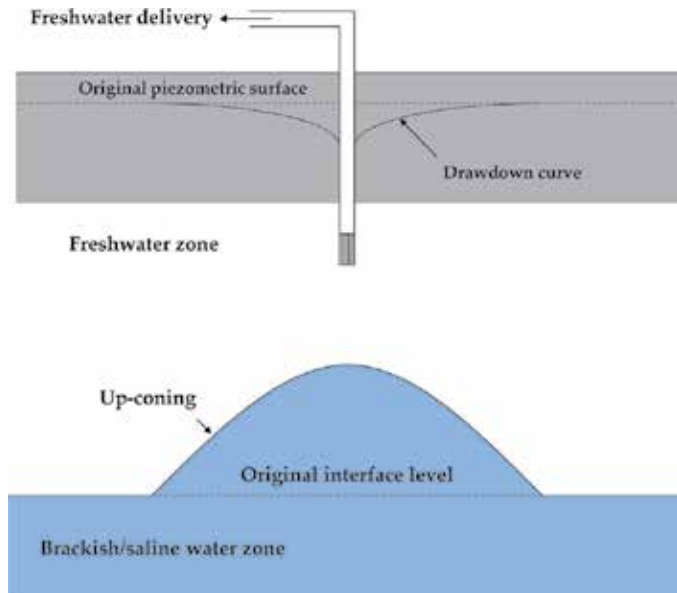


Figure 4a. Schematic sketch showing a skimming tube well.

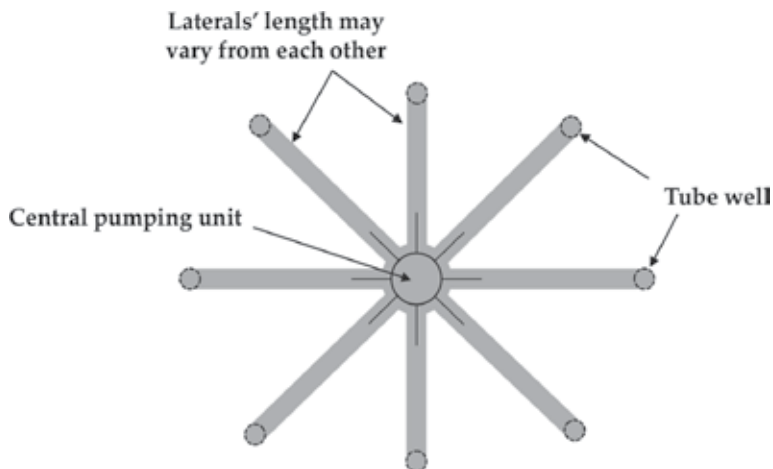


Figure 4b. Schematic sketch showing skimming tube wells system in which smaller capacity tube wells are installed arbitrarily in circular array and are joined with a single pumping unit.

1.2. Scavenger well system

To restrict the rise of fresh-brackish/saline interface to reach the effective pumping zone of the well, the adoption of scavenger well system is one of the possible solutions in which pumping from the production well is accompanied by brackish/salt water pumping from a scavenger well in the vicinity [20, 21]. In a scavenger well system, two wells (i.e., production well and scavenger well) are installed either in a single-bore hole (**Figure 5a**) or side-by-side bore holes (**Figure 5b**). The production well screens the freshwater zone whereas scavenger well taps the brackish/saline water zone. The development of discharge heads due to simultaneous pumping of these wells restricts the mixing of freshwater with brackish/saline water. The discharge rates of the two wells are adjusted in such a way that the up-coning caused by pumping from the production well could be countered by the down-coning of the interface caused by pumping from the scavenger well [20]. The resultant level of interface at any radial distance from the well can be evaluated from the difference of hydraulic heads of both production and scavenger wells considering both are working independently (**Figure 5a** and **b**). Ideally, this difference should be zero for keeping the interface at original level. Considering its pumped water quality, around 400 scavenger wells were installed in the lower Indus basin of Pakistan [13]. However, the concerns such as the mobilization of deep salts, disposal of pumped saline water, and the long-term negative environmental impacts due to seepage of saline water during its disposal were the major limitations on the sustainability of scavenger wells [13].

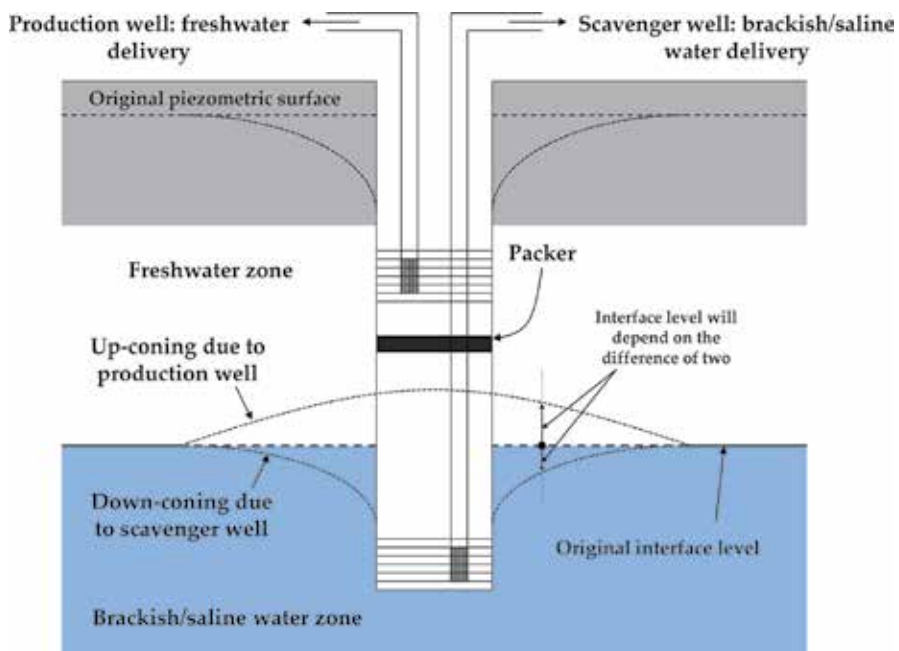


Figure 5a. Schematic sketch showing scavenger well system installed in a single-bore hole.

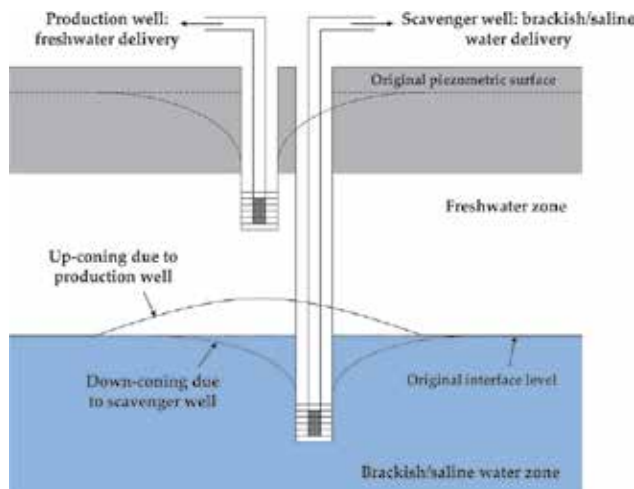


Figure 5b. Schematic sketch showing scavenger well system installed in side-by-side bore holes.

No doubt, the answer to these major limitations was given days back in 1965 by Jacob who proposed and patented a doublet well system (Figure 6) which was different from the present day scavenger well system in the sense that the scavenging discharge is pumped back to deeper formation [22], but its acceptability was restricted to thick aquifers only. From the above discussion it is clear that the adaption of scavenger well system for inlands depends upon the safe disposal of pumped brackish water. On the other hand, scavenger well system may prove to be best fresh-saline aquifer management practice in the coastal regions as the disposal of pumped saline water is comparatively easy by constructing reasonably long seepage-proof conveyance channels.

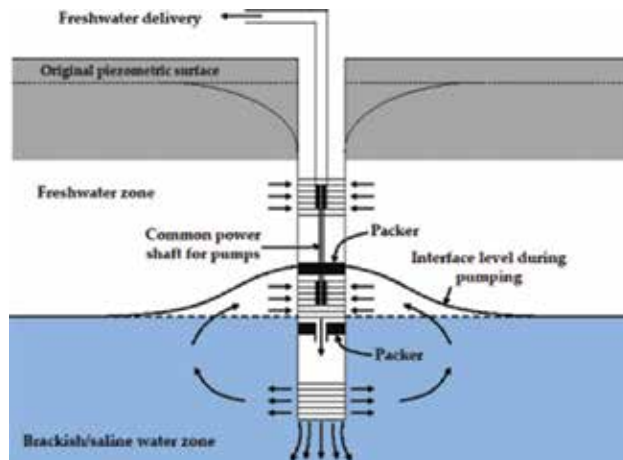


Figure 6. Schematic sketch showing the doublet well.

1.3. Recirculation well

The design of a recirculation well is somewhat similar to scavenger well (**Figure 7**). Unlike scavenger well, its lower screen is also kept in the freshwater zone. A part of the freshwater pumped from the upper screen is recirculated under gravity pressure into the lower screened chamber of the well which is separated from the upper through a packer. The injection of recirculated freshwater into the aquifer counters the up-coning of brackish/saline water mound beneath the well. Depending upon the position of lower screen with respect to interface, intermixing of injected freshwater may occur with the saline water. The establishment of flow pattern from the lower to upper screen takes this mixed quality water to freshwater zone, thus deteriorates the pumped water quality. Though the technique has been used in the petroleum industry [23], but the recirculation well's performance results in the water industry are not yet available [19].

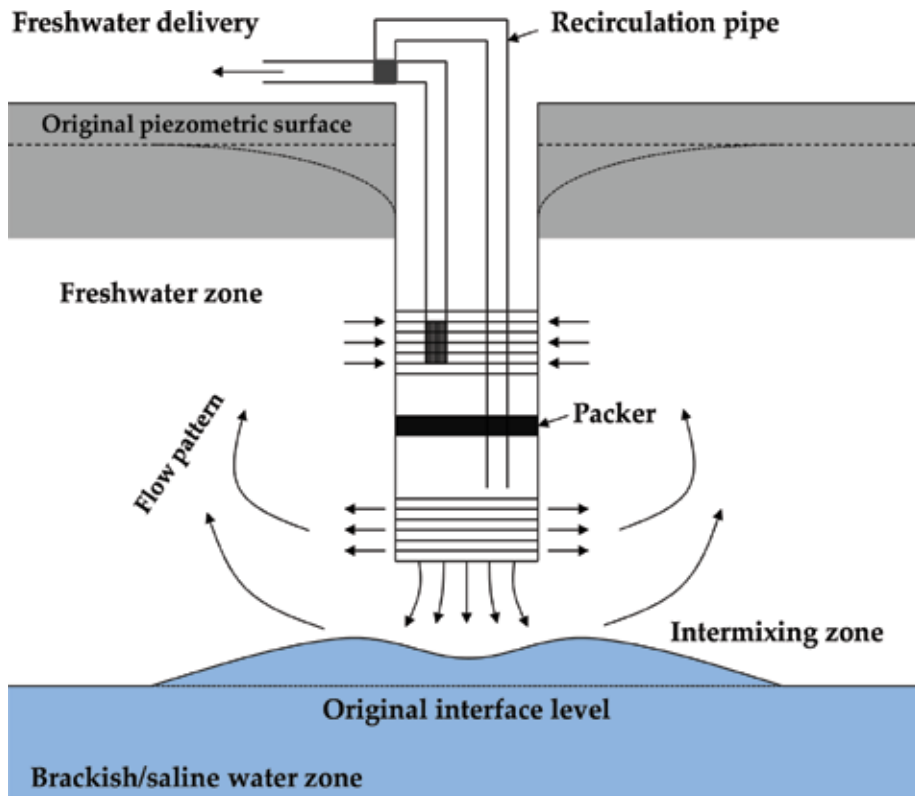


Figure 7. Schematic sketch showing recirculation well and its probable behavior while pumping.

1.4. Horizontal wells

To control the rise of interface to reach the effective pumping zone of the abstraction well, the only feasible option is to limit its discharge head [8]. For the purpose, horizontal wells can be

used to abstract groundwater. Previously, the horizontal well is introduced for the remediation of contaminated groundwater [24] as in comparison to vertical well, horizontal well can influence a large planar area during remediation [25]. However, now these wells are gaining popularity for use in water supply and drainage fields. Rushton and Brassington [26] have grouped the horizontal wells into two configurations. The first one is the radial collector well in which a number of horizontal perforated pipes are connected to a shaft or caisson. The second configuration consist of a single perforated pipe which is placed in shallow unconfined aquifer with a suction pump located either toward the center or at one end of the horizontal well [27]. The horizontal wells can be differentiated from the fully penetrating vertical wells on the basis of the flow components around the wells [28]. The vertical flow components are more dominant near a horizontal well whereas flow patterns around a fully penetrating vertical well are horizontal (or two dimensional). No doubt, in case of partially penetrating or partially screened wells, the flow in the near vicinity of pumping/recharging well is strictly three dimensional in nature [29]. From the above discussion, it can be envisaged that the radial collector wells may be the suitable option in the regions under study. But, its installation is difficult and requires extreme precision. Field experiences show that the construction of shaft, particularly in alkaline soils is a very hard task [30].

1.5. Dug wells

The areas where freshwater zones are very thin (less than 5 m) and where soils are not alkaline in nature, dug well can be constructed for skimming freshwater. Sometimes, these are also referred as shallow hand-dug wells [31]. Though the yield of these wells is very less, even then the available water can be efficiently utilized by opting well-recognized pressurized irrigation systems. The yield of a dug well can be increased by increasing its diameter and penetration. Large diameter of well facilitates water storage and its construction. However, the well penetration is limited by the fresh-brackish/saline interface.

1.6. Multiple well points system

In Sections 1.1–1.5, various skimming techniques are discussed. The performance of any skimming technique depends on the persisting hydrogeological conditions of area and every technique may not be suitable under all set of conditions. The major drawbacks in all the above-mentioned techniques are stated below:

- a. Skimming tube well (i.e., single-bore well) is not feasible in aquifer having very thin freshwater zone.
- b. In skimming tube wells system, various studies have concluded that the groundwater procured with fewer number of bore holes is of better quality in comparison to more number of bore holes [19, 32]. With the increase in the number of skimming wells, various types of geometrical patterns are possible in which these wells can be installed in the field. All the patterns create different flow conditions in the aquifer and hence affect the freshwater skimming. However, the adoption of a particular configuration without considering the resultant flow pattern toward the wells becomes responsible for the

deterioration of pumped water quality. It is explained schematically in **Figure 8**. It is a well-known fact that during pumping, the adjoining portion of the well screen is recuperated by the aquifer formation under influence. It is obvious that during the pumping of the system the recuperation of the aquifer formation with freshwater in the enclosed portions (as shown in **Figure 8b–d**) is minimal as the major portion of the freshwater moving toward the system is trapped by the wells before reaching the enclosed portions. Moreover, the interference of wells causes the drawdown to increase to maximum extent in the enclosed portion which in turn raises the interface to effective pumping zone of the wells. Combined effect of both these factors which comes into action with the start of pumping is responsible for the up-coning of brackish/saline water. On the other hand, in case of two and in-line tube wells system (**Figure 8a and e**), recuperation rate of freshwater is much higher than the other enclosed patterns and thus the procured groundwater quality is noticeably better than the other patterns.

- c. The major limitations on the sustainability of the scavenger wells are the mobilization of deep salts, disposal of pumped saline water, and seepage of saline water from its disposal system. The acceptability of the doublet well system is also restricted to thick aquifers only.
- d. Though the recirculation wells are more efficient than scavenger wells, the intermixing of brackish/saline water with the injected freshwater and the rising of this mixed quality water to freshwater zone are few undesirable features.
- e. Extreme precision is required in the installation of horizontal wells. Moreover, its construction (specifically in alkaline soils) is a very hard task.
- f. The low-yield of the dug wells restricts its adaption in surface irrigation practices. The available water's utilization is limited to well-recognized pressurized irrigation systems only.

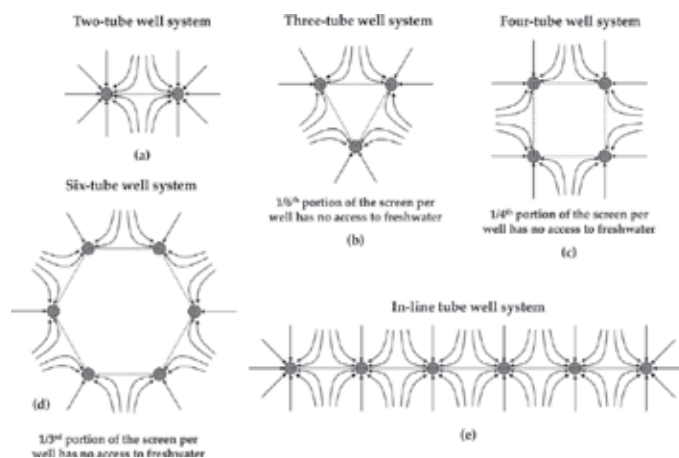


Figure 8. Schematic sketches showing general geometrical patterns in which skimming wells can be installed.

Keeping the region's problems in mind and considering the merits and demerits of all the above-mentioned skimming techniques, Shakya et al. [33] proposed the skimming of thin freshwater layers by a much efficient and affordable technique named multiple well points system (MWPS). The proposed system was capable to reclaim both types of problems (as mentioned in Section 1) persisted in the region. No doubt, skimming of freshwater was the basic objective but in comparison to other drainage technologies it can drain water logged soils by lowering the water table in wide spread region without disturbing much the deeper brackish water zone. The proposed MWPS was different from the skimming tube wells system [34] as mentioned in Section 1.2. In skimming tube wells system, different wells are installed almost in a circular array and are attached to the central pumping unit with separate lateral pipes of varied lengths (**Figure 4b**); whereas, MWPS constitutes several smaller capacities well points partially penetrating the aquifer and are arranged in a line connected to each other below the ground surface through single lateral and pumped centrally (**Figure 9**).

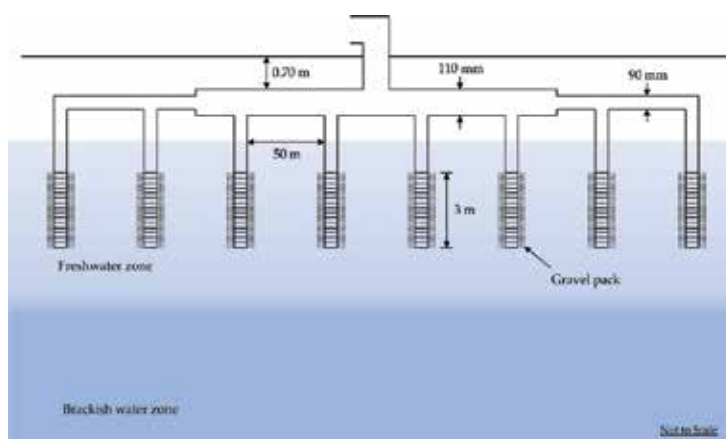


Figure 9. Schematic sketch showing multiple well points system with eight bores.

2. Study area

To examine the performance of conceived MWPS, an area which was out of cultivation was considered (as shown in **Figures 1** and **2**). The area is situated at a distance of 15 km from Ferozepur city on Ferozepur-Faridkot state highway No. 15 (**Figure 10**). The land of the project area belongs to three villages namely Golewala, Chak Kalan Tola, and Jhariwala (District Faridkot, Punjab, India). Project area falls in the arid zone having the minimum and maximum temperatures of 10 and 46°C during the months of January and June, respectively. The average values of the minimum and maximum relative humidity are 37 and 65%, respectively. The mean annual rainfall received in the region is about 400 mm. The topography of the area is leveled in general.

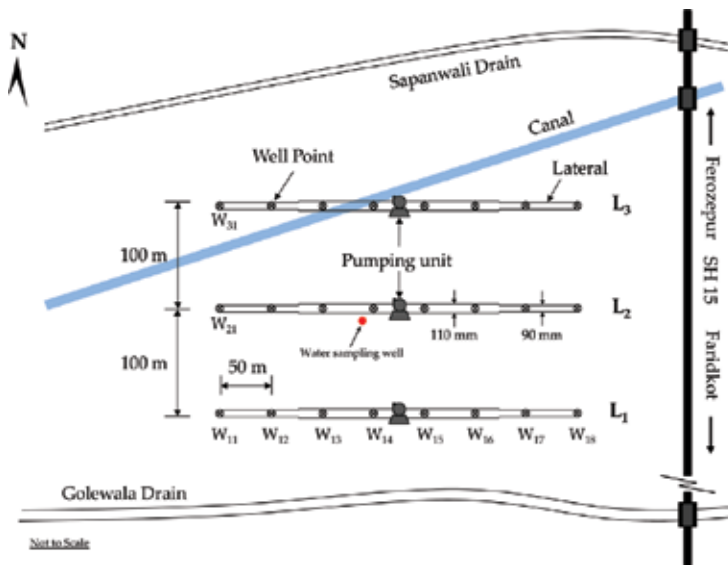


Figure 10. Schematic sketch showing the study area.

3. Characterization of underground water

Before the installation of MWPS, depth-wise analysis of the groundwater quality was performed. In **Figure 11** the change in electrical conductivity (EC) and residual sodium carbonate (RSC) with depth is shown. Perusal of **Figure 11** shows that the groundwater quality deteriorates with depth. Water can be considered fit for irrigation only if EC and RSC are less than 2 dS/m and 2.5 me/l, respectively. Though the salinity is within range but because of higher RSC,

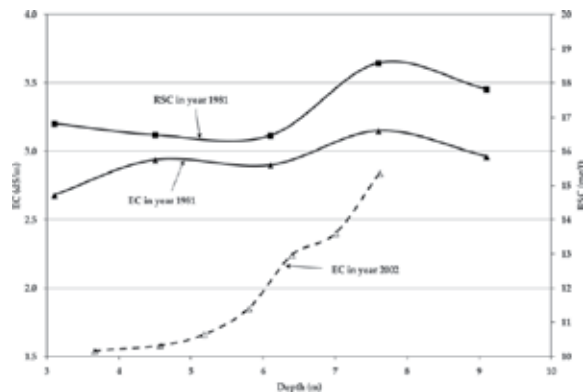


Figure 11. Change in EC and RSC of the groundwater with depth.

groundwater of the study area was not fit for irrigation. Hence, the project area was under the first type of problem.

4. Pumping test of the aquifer

A pumping test was conducted in a farmer's well which was existing in the project area. From the well log data, it was found that the depth of the soil at the location was 2.5 m and the aquifer was 10 m thick. Diameter of the well was 7.5 cm and it was installed in the said aquifer at a total depth of 10.5 m out of which 4.5 m was blind pipe of galvanized iron (GI). The well had a coir strainer of length 6 m. At a radial distance of 28.8 m from this well, another irrigation well of certain specifications was available which was used as a piezometer. Other than this available tube well, two more piezometers each of 9.0 m deep were installed at radial distances of 60 and 90 m from the test well, respectively. During the pumping test, the well was pumped at the rate of 10.82 l/s and drawdowns were recorded in all the three piezometers with respect to time. The change in drawdowns with respect to time at the three piezometric locations is presented in **Figure 12**. The recorded data were analyzed by the Walton method [35]. From the pumping test data, the average values of transmissivity T , hydraulic resistance c , and storage coefficient S were evaluated equal to 570 m²/d, 17.04 d, and 0.0142, respectively [30]. The hydraulic conductivity of the overlying soil layers ranged from 1.4 to 2.0 cm/d.

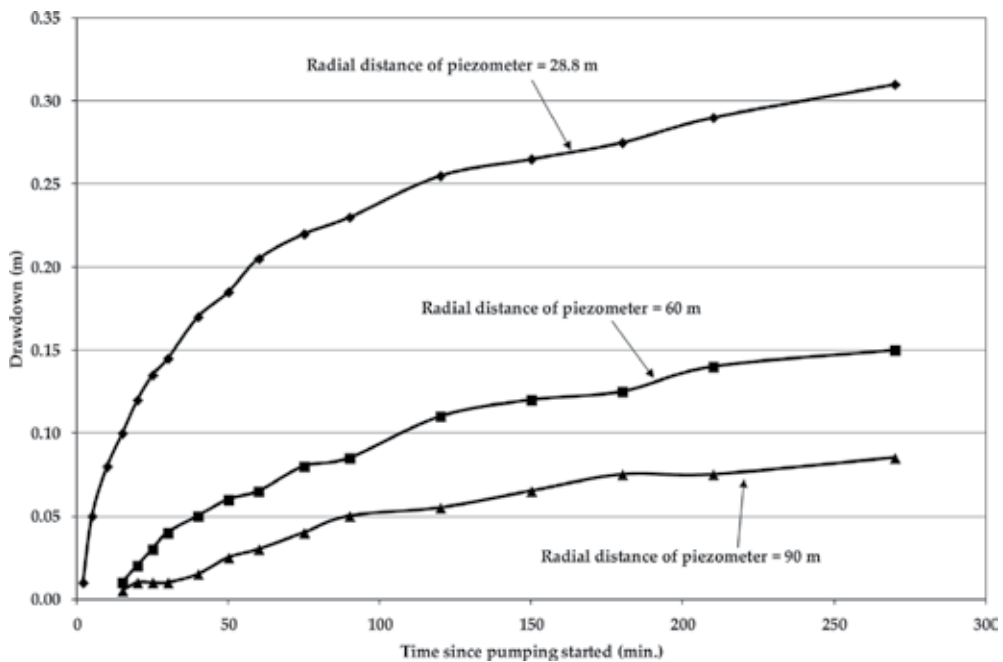


Figure 12. Change in drawdown with time at three piezometric locations while performing pumping test.

5. Installation of multiple well points system

It was proposed to install a battery of 24 wells constituting three laterals L_1 , L_2 , and L_3 spaced 100 m apart. The well spacing along the laterals was considered to be 50 m with 8 wells on each lateral (**Figure 9**). The wells were installed by the local drillers. These wells were connected to each other at about 70 cm below the ground surface using 90 and 110 mm diameter PVC pipes by digging trenches. The screen of each well point had an effective perforated area of about 16% which is surrounded by pea size, clean, river bed, well rounded gravel pack of 30 mm thickness. In the middle of each 350 m long lateral, a T-section was provided which was raised to the ground surface such that it remained in level with the ground after placement of reflux valve. The centrifugal pumps were connected with the aforesaid outlet points of three laterals. In order to prime the lateral, a reciprocating pump was placed over the delivery of each centrifugal pump. Initially, the air from the lateral was removed through the reciprocating pump and when there was an adequate flow of water, centrifugal pump was started. Whenever, there was disruption of flow, reciprocating pump was operated and was stopped when there was continuity in flow. Before covering the laterals with soil, the complete system was tested for any leakage. From the desired discharge rate and available head values, the power requirement to operate the system was evaluated equal to ~ 4 hp (considering the working efficiencies of both centrifugal pump and diesel engine equal to 80% each). Therefore, three diesel engine operated pumps of capacity 5 hp each (nearest available higher size in the market) were installed on each lateral.

6. Behavior of multiple well points system and its applicability

For monitoring the drawdown distribution in an aquifer while pumping through MWPS, piezometers were installed close to each well point and at the midpoint of the well spacing along the laterals. Each piezometer was of diameter 40 mm and was installed at a depth of 6 m. The piezometers installed near to well points were given names in accordance with their nearness to the respective well points. The symbol W_{LN} indicates the Nth well point on the Lth lateral. The piezometers adjoining to the respective well points are named as P_{LN} . For example, P_{23} indicates the piezometer near to the third well point on the second lateral (i.e., W_{LN}). The piezometers installed at the midpoint of two adjacent well points along the lateral are named as $P_{LN-L(N+1)}$. For example, P_{23-24} represents the piezometer installed midway between the well points W_{23} and W_{24} . The lateral L_1 was discharging at a rate of 3110.4 m³/d whereas the laterals L_2 and L_3 were delivering at a rate of 2419.2 m³/d each. The available drawdown data were plotted and is presented in **Figure 13**. It is evident from **Figure 13** that the lowering of the water table is minimal at the four locations (i.e., in the center of the laterals at the outer boundary of the system). On the other hand, maximum lowering has been noticed around the central well points of middle lateral. Considering a section along the lateral lines L_1 or L_3 for the water table profiles, it is evident that the difference between the maximum water level at the midway between the wells and that of inside the wells was varied from 0.5 m at outer well to 0.72 m

for central wells. These variations for L_2 lateral were found to vary from 0.47 m at outer well to 0.87 m for central wells.

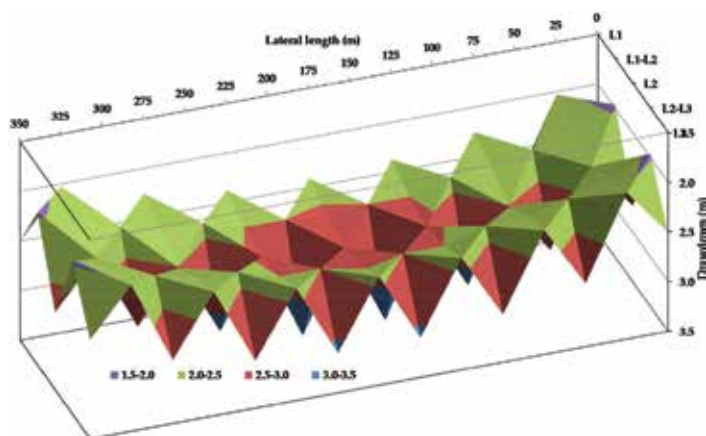


Figure 13. Behavior of multiple well points system while pumping.

Since the first type of problem was persisting in the project area, there was a need to control the water table first. Therefore, the pumping test was done with a schedule of 8 h of pumping and 16 h of recovery in a day for a week to observe the water table behavior in aquifer and soil. A residual drawdown of 17 cm in aquifer and 24 cm in soil was observed. It was also observed that the rise of water table in the soil during recovery is delayed with the passage of time. It could be explained as, once the water from soil is drained, rise would take place only after the pores of the soil are filled with water. It has imparted the delayed effect in rise of water tables in the soil. These encouraging results motivated us and long duration pumping of the aquifer was performed. Eventually, with the lowering of water table agricultural practices were started with the cultivation of paddy. Marginal quality water was used for irrigating the paddy which was achieved by mixing pumped water supply (through MWPS) with canal water. Studies show that the irrigation with marginal quality water does not affect the yield of paddy to much extent [30]. The motive was to continue pumping from the aquifer. In due course, groundwater quality in the upper portion of the aquifer started improving. In year 2002, groundwater samples were again analyzed for EC depth-wise and are presented in **Figure 11**. Perusal of the comparison clearly indicates that there is a drastic improvement in the groundwater quality in the upper portion of the aquifer. The excellent performance by the MWPS has proven that it is a viable technology for the region and needs promotion.

7. Recommendation based on experimental results

In order to propagate the use of MWPS in the region, a smaller system with four-well points spaced at 6 m in a line connected horizontally at about 1 m below the land surface, pumped centrally was found to give technically satisfactory performance (i.e., no mixing of floating

good quality water with the underlying poor quality groundwater) and economically viable results. Each well point has a screen length of 3 m which has 16% effective perforation and surrounded by pea size, well rounded clean river bed gravel envelope. Blind pipe may be adjusted according to the depth of aquifer. The details are shown in **Figure 14**. After watching the enthusiastic results of the project area, farmers of the region have adopted the recommended MWPS with four-well points on a large scale. As per the survey of Faridkot district in year 2000–2001, around 1400 MWPSs have already been installed [36]. From the analysis of water quality samples taken from some selected MWPSs, it was found that these are withdrawing good quality water that is fit for irrigation. Farmers themselves have admitted that they are using MWPS from last 10 years and have not noticed any deterioration in pumped water quality. Moreover, the adoption of MWPS has also lowered the water table in the region.

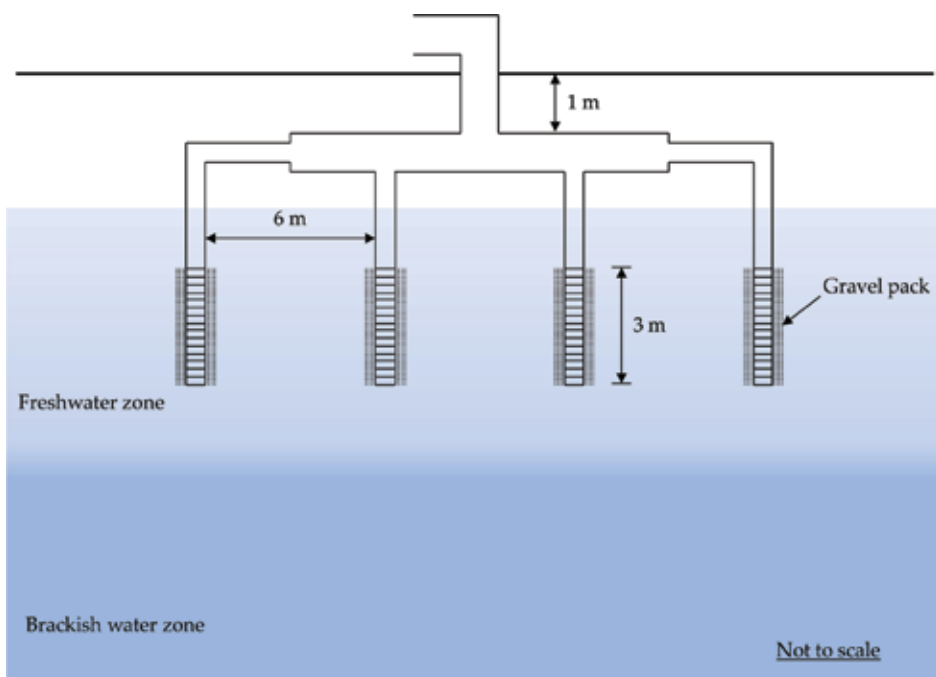


Figure 14. Multiple well points system with four bore holes.

8. Groundwater recharging through MWPS under constant head conditions

It is already mentioned in Section 7 that farmers of the region have adopted the MWPS in big way and their dependency on canal water has declined considerably. It is also true that these freshwater lenses are very limited and are now under stress. For long-term sustainability of these limited freshwater lenses, enhancement in freshwater recharging rate is required. Therefore, we have conceived an idea to recharge the freshwater zones with surplus canal

water when available during the monsoon season through the existing MWPSs in the region [37]. Aquifer storage recovery (ASR) is worldwide recognized technique for managing brackish/saline aquifers [38] in which freshwater when available is stored in the aquifer and later on recovered for use. However, our proposal was little different from this basic technique. In the ASR technique, recharging of the brackish/saline aquifer is generally performed with the fully penetrating well of high capacity in which the injected freshwater displaces the saline water. As a result, considerable portion of the stored freshwater gets salinized before its recovery. The native groundwater movement and the buoyancy effect are the two factors which are responsible for the irrecoverable portion of stored freshwater. With the use of multiple partially penetrating wells in a single bore hole, the freshwater losses can be reduced considerably [39]. In this modified ASR technique, freshwater is injected in the deeper portion of the aquifer whereas its recovery is made from the shallow well. On the other hand, as the MWPS operates under limited head conditions and it penetrates only the upper portion of the freshwater zone of the aquifer through smaller capacity wells, it causes minimum disturbance to the denser native brackish water which is flowing in the lower portion of the aquifer [8]. The recharged water gets an opportunity to store in the wide-spread portion of the aquifer. Hydraulic head distribution in the aquifer while recharging through MWPS is shown in **Figure 15**. While evaluating this, we have considered the recharging rates through individual laterals equal to the pumping rates as mentioned in Section 6. Perusal of **Figure 15** indicates that the freshwater got an opportunity to store in the upper portion of the aquifer and it causes minimum disturbance to deeper brackish water zone.

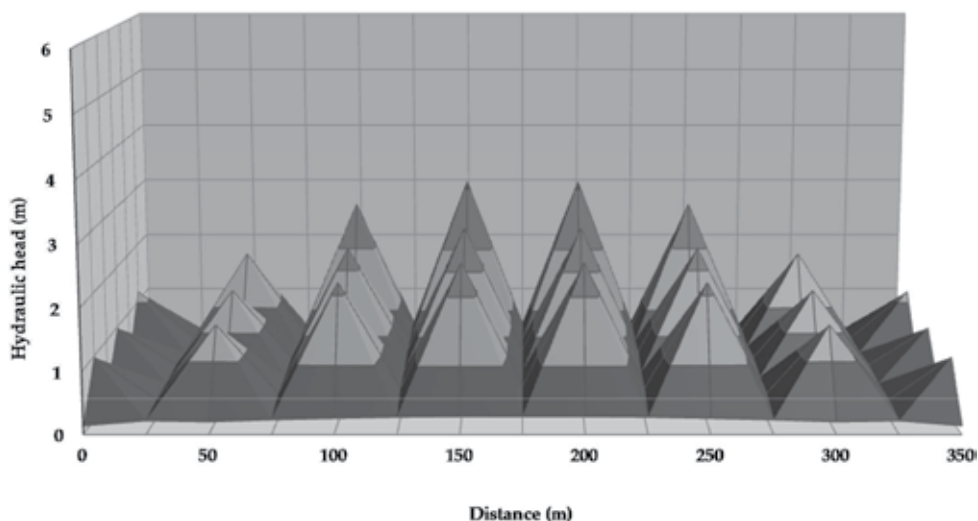


Figure 15. Hydraulic head distribution in the aquifer while recharging through MWPS.

Other than the theoretical investigations, field study was also conducted to monitor the change in quality of aquifer while recharging with freshwater. In the field study, canal water was

allowed to recharge the aquifer through MWPS under constant head conditions. Radial flow filter was used for removing turbidity from the canal water (**Figure 16**).

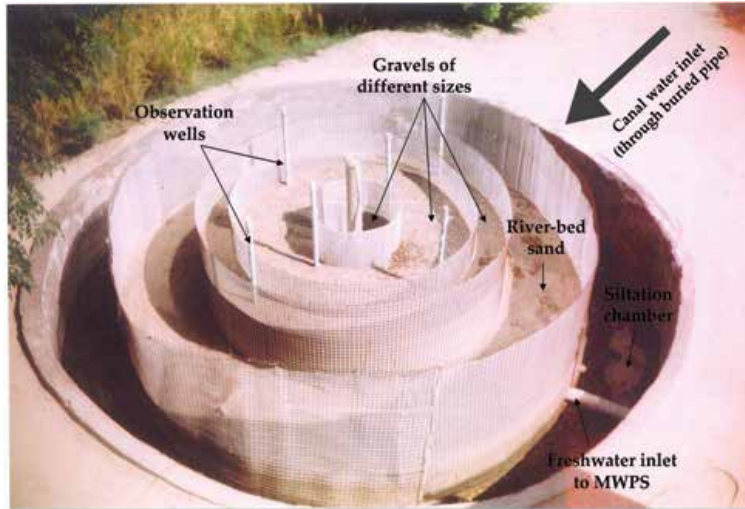


Figure 16. Radial flow filter for removing turbidity of canal water before recharging through MWPS.

For monitoring the change in quality of groundwater due to recharging, a water sampling well of length 9.144 m having diameter 10.16 cm was installed at a radial distance of 3.27 m from the well point W_{24} (**Figure 10**). The perforated length of the observation well was 6 m. For critically analyzing the effect of recharging on the quality of brackish water, it was necessary to collect water samples depth-wise with minimum disturbance. For this purpose, a specialized water sampler was fabricated. In spite of this, for achieving accuracy, considerable time was given between consecutive samplings. Before starting the recharging operation, groundwater samples from various depths were collected and analyzed for EC and pH. The recharging operation was continued for net 65 days and on its completion, water samples were collected from the same depths and were again analyzed for EC and pH. Comparison of the change in groundwater quality due to freshwater recharging is shown in **Figures 17 and 18**. Perusal of both the figures indicates that the recharging of freshwater in fresh-brackish aquifer through MWPS is a viable technique for reviving freshwater lenses in the region. However, for planning any recharging project through MWPS, theoretical investigations are required *a priori*. Realizing this need, Vashisht and Shakya [8] have proposed a semianalytical solution for evaluating hydraulic head distribution and recharging rate in a single leaky aquifer while recharging freshwater under constant head conditions through MWPS. The proposed solution was based on the introduction of a new relation termed as “position-oriented *opportunistic proportion*.” The most important advantage of recharging through MWPS is that it covers the wide-spread region of the aquifer without disturbing much the native brackish water. The developed hydraulics for MWPS may be considered as the backbone for planning and execution of policies for managing brackish groundwater aquifers in the region.

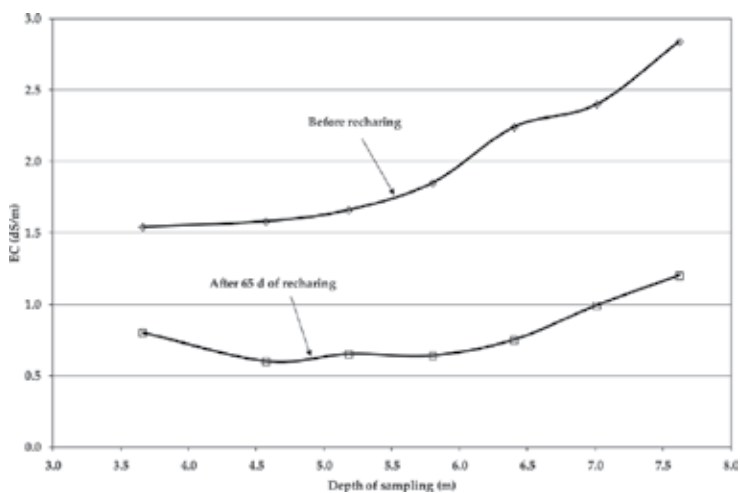


Figure 17. Change in EC of groundwater depth-wise after recharging canal water through MWPS.

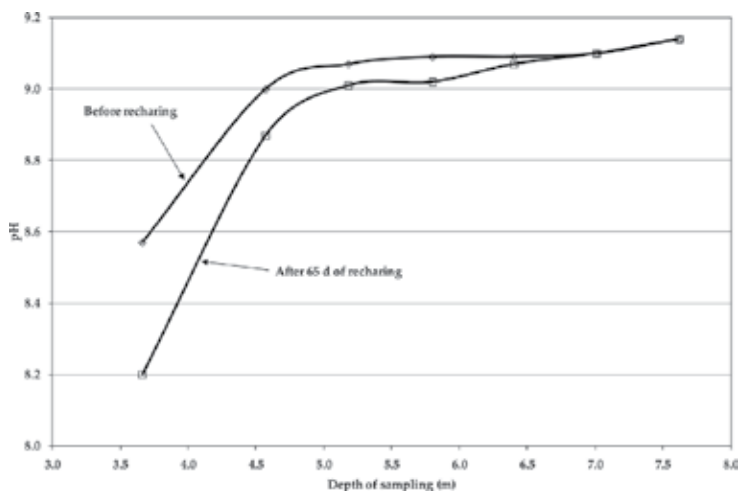


Figure 18. Change in pH of groundwater depth-wise after recharging canal water through MWPS.

9. Conclusion

Long-term field investigations were made on the MWPS for checking its performance as a drainage system, a skimming system, and a recharging system. On the basis of the field results and theoretical investigations, it is concluded that MWPS is a viable technique for managing brackish aquifers of a region.

Acknowledgements

The authors are grateful to the All India Coordinated Research Project on Agricultural Drainage under Actual Farming Conditions on Watershed Basis (Sponsored by Indian Council of Agricultural Research, New Delhi), Department of Soil and Water Engineering, Punjab Agricultural University, Ludhiana, Punjab, India for providing the relevant data related to MWPS for completing this chapter.

Author details

Ajay K. Vashisht^{1*} and Shri K. Shakya²

*Address all correspondence to: akvashisht74@yahoo.com

1 Department of Soil and Water Engineering, College of Agricultural Engineering and Post-Harvest Technology, Central Agricultural University, Ranipool, Sikkim, India

2 Department of Soil and Water Engineering, College of Agricultural Engineering and Technology, Punjab Agricultural University, Ludhiana, Punjab, India

References

- [1] Foster SSD, Chilton PJ. Groundwater: the processes and global significance of aquifer degradation. *Philosophical Transactions of the Royal Society of London B: Biological Sciences*. 2003; 358(1440): 1957–1972.
- [2] Shaffer DL, Yip NY, Gilron J, Elimelech M. Seawater desalination for agriculture by integrated forward and reverse osmosis: improved product water quality for potentially less energy. *Journal of Membrane Science*. 2012; 415: 1–8.
- [3] Foster SSD, Chilton PJ, Moench M, Cardy WF, Schiffler M. Groundwater in rural development: facing the challenges of supply and resource sustainability. *World Bank Technical Paper 463*; 2000.
- [4] Vashisht AK. Will the flow end? Artesian wells of Uttarakhand's Tarai. *Economic and Political Weekly*. 2014; 49(6): Web exclusives.
- [5] Zektser IS, Lorne E. Groundwater resources of the world and their use. In: *IHP Series on Groundwater*, No. 6, UNESCO; 2004.
- [6] Vörösmaty CJV, Green P, Salisbury J, Lammers RB. Global water resources: vulnerability from climate change and population growth. *Science*. 2000; 289(5477): 284–288.

- [7] Michaeli A. Brackish water resources in Israel. In: Proceedings of the Ninth Israel Symposium on Desalination, Israel; 1972. pp. 25–33.
- [8] Vashisht AK, Shakya SK. Development of semi-analytical solution for recharging through multiple well points system under constant head conditions. *ISH Journal of Hydraulic Engineering*. 2016; 22(1): 50–58.
- [9] Hahn J. Aspects of groundwater salinization in the Wittmund (East Friesland) coastal area. In: *Hydrogeology of Salt Water Intrusion—A Selection of SWIM Papers*, Hannover; 1991. pp. 251–269.
- [10] Wachyan E, Rushton KR. Water losses from irrigation canals. *Journal of Hydrology*. 1987; 92(3–4): 275–288.
- [11] Sharma HD, Chawla AS. Manual on canal lining. Technical Report No. 14. Central Board of Irrigation and Power, India; 1975.
- [12] Indian Bureau of Standards. Measurement of seepage losses from canals—code of practice. IS 9452 (part 1); 1993. pp. 1–6.
- [13] Ali G, Asghar MN, Latif M, Hussain Z. Optimizing operational strategies of scavenger wells in lower Indus basin of Pakistan. *Agricultural Water Management*. 2004; 66: 239–249.
- [14] Reilly TE, Goodman AS. Analysis of saltwater upconing beneath a pumping well. *Journal of Hydrology*. 1987; 89(3–4): 169–204.
- [15] Badon-Ghyben W. Nota in verband met de voorgenomen putboring nabij Amsterdam (Notes on the probable results of well drilling near Amsterdam). *Tijdschrift van het Koninklijk Instituut van Ingenieurs*, The Hague. 1888; 9: 8–22.
- [16] Herzberg A. Die Wasserversorgung einiger Nordseebäder (The water supply on parts of the North Sea coast in Germany). *Journal für Gasbeleuchtung und verwandte Beleuchtungsarten, sowie für Wasserversorg.* 1901; 44: 815–819.
- [17] Wang EC. Approximate theory of skimming well formation in the Indus Plain of West Pakistan. *Journal of Geophysical Research*. 1965; 70(20): 5055–5063.
- [18] Saeed MM, Asghar MN, Bruen M. Options for skimming fresh groundwater in the Indus basin of Pakistan: a review. *Journal of Groundwater Hydrology (Japanese Association of Groundwater Hydrology)*. 2003; 11(3): 1–13.
- [19] Sufi AB, Latif M, Skogerboe GV. Simulating skimming well techniques for sustainable exploitation of groundwater. *Irrigation and Drainage Systems*. 1998; 12: 203–226.
- [20] Saravanan K, Kashyap D, Sharma A. Model assisted design of scavenger well system. *Journal of Hydrology*. 2014; 510: 313–324.

- [21] Jones CRC, van Wonderen JJ. Exploitation of fresh groundwater lenses: implementation of scavenger wells in Pakistan. In: Proceedings of the International Conference on Groundwater – Drought, Pollution and Management. Brighton, UK; 1994.
- [22] Wickersham G. Review of C.E. Jacob's doublet well. *Groundwater*. 1977; 15(5): 344–347.
- [23] Smith CR, Pirson SJ. Water coning control in oil wells by fluid injection. *Society of Petroleum Engineers Journal*. 1963; 3(04): 314–326.
- [24] Cleveland TG. Recovery performance for vertical and horizontal wells using semianalytical simulation. *Groundwater*. 1994; 32(1): 103–107.
- [25] Sawyer CS, Lieualen-Dulam KK. Productivity comparison of horizontal and vertical groundwater remediation well scenarios. *Groundwater*. 1998; 26(1): 98–103.
- [26] Rushton KR, Brassington FC. Hydraulic behaviour and regional impact of a horizontal well in a shallow aquifer: example from Sefton coast, northwest England (UK). *Hydrogeology Journal*. 2013; 21: 1117–1128.
- [27] Brassington FC, Preene M. The design, construction and testing of a horizontal well point in a dune sands aquifer as a water source. *Quarterly Journal of Engineering Geology and Hydrogeology*. 2003; 36: 355–366.
- [28] Langseth DE, Smyth AH, May J. A method for evaluating horizontal well pumping tests. *Groundwater*. 2004; 42(5): 689–699.
- [29] Vashisht AK, Shakya SK. Hydraulics of a drainage well fully penetrating a leaky aquifer through a multisection screen. *Journal of Hydraulic Engineering (ASCE)*. 2013; 139(12): 1258–1264.
- [30] Shakya SK. Agricultural drainage under actual farming conditions on watershed basis. Department of Soil and Water Engineering. Punjab Agricultural University, Ludhiana, India; 2002. p 108.
- [31] Mace RE. Estimation of hydraulic conductivity in large-diameter, hand-dug wells using slug-test methods. *Journal of Hydrology*. 1999; 219: 34–45.
- [32] Hafeez A, Piracha ZA, Ahmad N. Multi-strainer tubewells for skimming top layer of freshwater underlain by saline aquifer. Mona Reclamation Experimental Project, Water and Power Development Authority (WAPDA), Bhalwal, Pakistan; 1986. Publication No. 152. p. 50
- [33] Shakya SK, Singh SR, Panda SN, Gupta PK. Drainage by multiple well point system for land and aquifer management. In: Proceedings of the National Symposium on Drainage and Reclamation of Salt Affected Waterlogged Land, CSSRI Karnal; India; 1986.
- [34] Saeed MM, Ashraf M. Feasible design and operational guidelines for skimming wells in the Indus basin, Pakistan. *Agricultural Water Management*. 2005; 74: 165–188.

- [35] Kruseman GP, De Ridder MA. Analysis and evaluation of pumping test data. Institute for land reclamation and improvement, Wageningen, The Netherlands; 1970. Publication No. 11.
- [36] Vashisht AK, Shakya SK. Managing saline/sodic soils and brackish water aquifers using multiple well point system. Success Story—II. Agricultural Engineering Today. 2005; 29(3–4): 67–72.
- [37] Vashisht AK. Modeling brackish water management by recharging through multiple well points. Ph.D. Thesis. Punjab Agricultural University, Ludhiana, Punjab, India; 2004.
- [38] Bakker M. Radial Dupuit interface flow to assess the aquifer storage and recovery potential of saltwater aquifers. Hydrogeology Journal. 2010; 18(1); 107–115.
- [39] Zuurbier KG, Zaadnoordijk WJ, Stuyfzand PJ. How multiple partially penetrating wells improve the freshwater recovery of coastal aquifer storage and recovery (ASR) systems: a field and modeling study. Journal of Hydrology. 2014; 509: 430–441.

Mobility and Transformation of Inorganic Contaminants in Mining-impacted Groundwater

Anita Etale and Sabelo Mhlanga

Additional information is available at the end of the chapter

<http://dx.doi.org/10.5772/63092>

Abstract

Mining often results in the contamination of groundwater by metal, sulphate and radionuclide ions following their percolation from tailings impoundments. This chapter discusses the processes by which elements within tailings are transformed and translocated to groundwater and the role of aquifer characteristics and colloids in these processes. The prevention and remediation of contaminated groundwater is also discussed, with particular attention given to the use of permeable reactive barriers and sulphate reducing bacteria.

Keywords: colloidal transport, acid mine drainage, inorganic contaminants, groundwater remediation, permeable reactive barriers, sulphate reducing bacteria

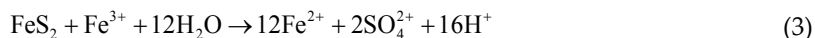
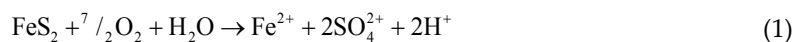
1. Introduction

Mining has been the mainstay of many economies across the globe for centuries. There is evidence, for example, of copper mining in Cyprus from as early as 4000 BC and from the Rio Tinto deposits in Spain from 1200–1500 BC [1]. However, along with the economic growth spurred by mining came unprecedented environmental pollution. The contamination of water resources by high concentrations of metals, non-metals and radionuclide elements has been reported from Spain and Portugal [2], to Australia [3] and South Africa [4]. Groundwater may be contaminated by direct infiltration of leachate from mine tailings and other mine wastes or following underground disposal of mine wastes [5]. Contaminated groundwater then recharges surface water with acidic metal-laden water (acid mine drainage) (**Figure 1**).



Figure 1. A river in the west of Johannesburg, South Africa, contaminated by acid mine drainage from disused underground mines. Note the orange colour which is due to deposition of iron flocs on the river bed.

Acid mine drainage (AMD) is formed via a cascade of reactions (Equations 1–4) when sulphide minerals are exposed to oxygen by mining [6]. The process begins when oxygenated water percolates through the finely divided tailings and pyrite is oxidised to ferrous iron (Equation 1) and then to ferric iron (Equation 2). Ferric iron which is soluble at pH below 3.5 then acts as an additional oxidising agent for pyrite (Equation 3). Above pH 3.5, ferric iron precipitates as $\text{Fe}(\text{OH})_3$ (Equation 4); a reaction that is able to buffer the pH of AMD at pH 2.5–3.5 [7].



This sustained acidity leads to the dissolution of other sulphide ores hence the presence of ions including Ag, Au, Cd, Co, Mn, Ni, Hg, Mo, Se, U, Th and Zn in mine drainage [4] and metal-laden water percolates through the tailings heaps to recharge groundwater. A conceptual model of this process was supplied by Tutu et al. [4] (**Figure 2**). In this model, ingress through the dump by oxygenated water results in the oxidation of tailings and the dissolution of elements followed by a downward movement of these dissolved ions into groundwater. This chapter focuses on the transformation and mobility in groundwater, of inorganic contaminants originating from mining activity. Here, groundwater encompasses water in aquifers below tailings dumps as well as that in pores within tailings (pore water).

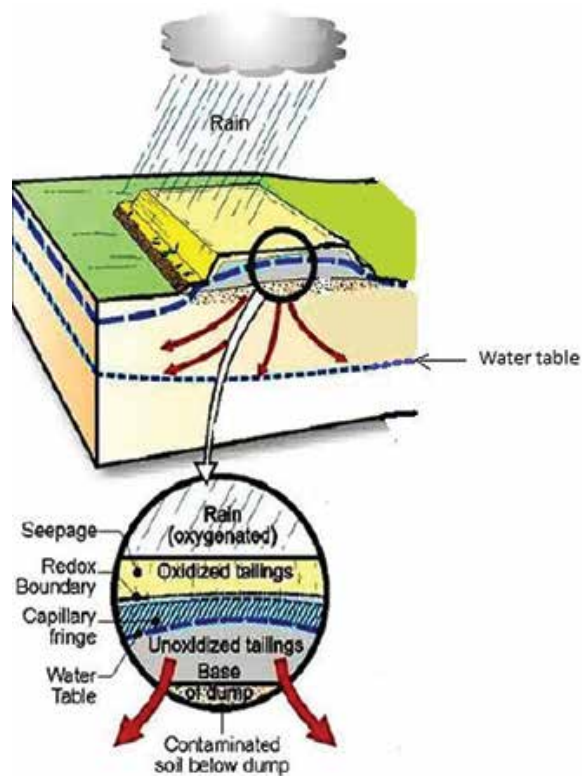


Figure 2. A conceptual model of the downward movement of elements through tailings dumps into groundwater (After [4]).

2. Transformation of inorganic contaminants in groundwater

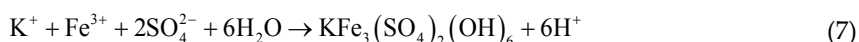
The transformation of inorganic contaminants in groundwater is influenced by a number of chemical and physical characteristics of aquifers such as pH, redox potential (Eh) and organic matter [8]. These properties have an influence over contaminant transformation reactions

including precipitation/co-precipitation-dissolution, oxidation-reduction and acid–base/sorption–desorption [9].

2.1. Precipitation/dissolution

Precipitation/co-precipitation and dissolution reactions play an important role in determining elemental concentrations in groundwater. Jean and Bancroft [10] showed, using pyrite (FeS), sphalerite (ZnS), galena (PbS) and pyrrhotite (Fe_{1-x}S), that sulphide minerals are excellent scavengers for dissolved Hg²⁺, Pb²⁺, Zn²⁺ and Cd²⁺ ions, acting as adsorbents for these metals. However, Özverdi et al. [11] reported that under acidic conditions (< pH 3), metal removal by pyrite was by precipitation of metal sulphides due to the presence of H₂S. In contrast, metal hydroxides were precipitated under basic conditions. These observations were supported by the field studies of Muller et al. [12] in the Kristineberg mines in Sweden and Al et al. [13] in the Kidd Creek tailings impoundment in Ontario, Canada, which that both adsorption and precipitation reactions were responsible for metal attenuation.

Ferric iron is ubiquitous in AMD-contaminated environments. Its precipitation via various pathways (Equations 5–7) is a significant process in the attenuation of metal on concentrations in mine drainage via co-precipitation reactions [14]. Indeed, Fe- and Al-compounds are commonly used for the chemical precipitation of As(III) and As(V) in water treatment plants [15].



Ferrous iron, on the other hand, is controlled by the precipitation of siderite (FeCO₃) (Equation 8), a reaction occurring mainly in shallow tailings.



Elemental concentrations are also controlled by simple precipitation reactions in response to solution pH through the formation of insoluble hydroxides such as Pb(OH)₂ and Cu(OH)₂ or following reaction with sulphides and carbonates to form insoluble compounds [11].

With respect to dissolution, McGregor et al. [16] found that Ca and Mg concentrations in the Copper Cliff tailings in Ontario, Canada, were controlled by the dissolution of carbonate and aluminosilicate minerals during pH buffering reactions. Similarly, Mn was derived from the dissolution of pyroxene, chlorite, amphibole or carbonates, Al and Si from weathering of

biotite, orthopyroxene and feldspars and Ni and Zn concentrations from the oxidation and dissolution of pentlandite ((Fe,Ni)₉S₈) and sphalerite (ZnS). K and Na on the other hand were controlled by dissolution of aluminosilicate minerals although their concentrations were limited by equilibrium with respect to jarosite (KFe₃(SO₄)₂(OH)₆) and natrojarosite (NaFe₃(SO₄)₂(OH)₆). Dissolution may also be microbially-driven. Cummings et al. [17] reported the release of arsenate following the dissolution of scorodite (FeAsO₄·2H₂O) by an iron-reducing bacterium, *Shewanella alga*.

2.2. Oxidation–reduction

Oxidation–reduction reactions may be chemically- or biologically-driven [18]. Selenate (SeO₄²⁻) may be reduced to elemental selenium (Se⁰) by ferrous hydroxide [19] and zero-valent iron (ZVI) has been used for the reductive precipitation of As from contaminated water [20]. Microbial oxidation-reduction in some cases can be many times faster than abiotic reactions [21]. The oxidation of As(III) to As(V) by a *Thermus* species, for example, was found to be approximately 100 times faster than abiotic rates [22].

Redox states of As have environmental implications because of their effect on As speciation. As(V), the predominant form in aerobic environments, is more strongly sorbed to mineral surfaces and thus less mobile than As(III) which sorbs less strongly and is thus more mobile [23]. Routh et al. [24] conducted microcosm experiments to investigate As behaviour in mine tailings near the Adak mine in northern Sweden. They found that microbial reduction of As(V) to As(III) increased the concentrations of the latter in aqueous media and as such, enhanced As remobilisation from sediments. In contrast, As(V) concentrations increased in sediments and aqueous media of control experiments treated with formaldehyde and HgCl₂.

Treatments applied to mine tailings may also have an effect on microbial activity and As behaviour in mining-impacted environments. Macur et al. [25] reported that the addition of lime (CaO), a common treatment applied to mine tailings to immobilise metal ions, stimulated As-reducing microorganisms (*Caulobacter*-, *Sphingomonas*- and *Rhizobium*-like populations) and in turn, enhanced As(V) reduction and mobilisation in tailings.

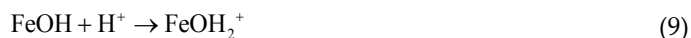
Fe, an important variable in mining-impacted environments, also influences As mobilisation. Han et al. [26] reported that Fe(II) significantly inhibited the removal of As(III) by MnO₂ in acidic environments (pH 3). They postulated that ferric iron compounds formed a coating on MnO₂ surfaces which inhibited access of As(III) ions to oxidation sites on MnO₂. The inhibition was however dependent on how Fe(II) ions were introduced into the system. Where the MnO₂ was pre-treated with Fe(II), As(III) diffused through the schwertmannite coatings that formed on the MnO₂ and its oxidation to As(V) was possible. However, where Fe(II) and As(III) were introduced simultaneously, competitive oxidation of the two ions prevented the complete oxidation of As(III) due to the formation of FeOHAs or FeAsO₄ coatings on the MnO₂ surface.

Cr exists mainly as Cr(III) and Cr(VI). Cr(VI) is highly soluble and therefore more mobile while Cr(III), tends to precipitate as amorphous hydroxides e.g. Cr(OH)₃ and ((Fe,Cr)OH)₃ in slightly acidic and alkaline environments. Cr(III) is commonly oxidised to Cr(VI) by manganese oxides.

In fact, manganese oxides are the only naturally-occurring inorganic phases capable of this reaction [27, 28] which Weaver and co-workers [29] found proceeded in multiple stages. However, Eary and Rai [28] reported that Cr(III) oxidation by pyrolusite ($\beta\text{-MnO}_2$) was slow in both acidic and slightly acidic solutions. In an acidic solution, slow oxidation was likely the result of the strong sorption of the oxidation product, Cr(VI), to the pyrolusite surface. Such sorption limited contact of unoxidised species with the pyrolusite surface, inhibiting additional oxidation [30]. In slightly acidic to basic media, slow oxidation was the result of the low solubility of $\text{Cr}(\text{OH})_3$. Clearly, the equilibrium favoured the trivalent ion. Nevertheless, as with As, a suite of reducing microorganisms exist for reduction of Cr(VI) to Cr(III). Native isolates of *Acinetobacter sp.* from the Sukinda Valley in Jaipur, India were able to reduce initial Cr(VI) concentrations of 5 mg L^{-1} by 80% in 7 hours [31]. Similar results were reported by Dhal et al. [32] using a *Bacillus sp.* bacterium from chromite mine soils in Boula-Nuasahi mine in Orissa, India. The strain reduced > 90% of 100 mg L^{-1} Cr(VI) in 144 hours at pH 7 and 35°C .

2.3. Acid–base/sorption–desorption

Variable charge/amphoteric minerals such as crystalline and short-range ordered Fe-, Al-, and Mn- significantly influence the concentrations of elements in groundwater through adsorption/ion exchange reactions. This is because of (i) their large surface areas (ii) the acid–base surface hydroxyl groups resulting from the dissociative chemisorption of water molecules on their surfaces [33, 34]. Surface functional groups on mineral oxides undergo protonation (Equation 9) and deprotonation (Equation 10) reactions depending on solution pH [35]. As such, oxide surfaces are positively charged and primed for anion adsorption at lower pH values and negatively charged and primed for cation sorption at higher pH values [35, 36].



Adsorption of ions from solution (**Figure 3**) is therefore a bid to maintain electric neutrality both on the oxide surface as well as in the solution (ion exchange) [36].

The adsorption of divalent ions to oxide surfaces including goethite, hydrous iron and manganese oxides has been reported in several studies. Borah and Senapati [37] investigated the factors influencing the adsorption of Cd^{2+} to natural pyrite. They found that metal uptake increased with decreased pyrite particle size and was maximal at 30°C and pH 6. At this pH, Cd^{2+} ions were the main ions in solution and metal uptake was thus an exchange between the H^+ and Cd^{2+} ions on the pyrite surface. Similar findings were reported by Forbes et al. [38] in the adsorption of Cd^{2+} , Co^{2+} , Pb^{2+} , and Zn^{2+} on goethite and by Gadde and Laitinen [39] in the adsorption of Pb^{2+} , Cd^{2+} , Zn^{2+} and Tl^+ onto hydrous iron and manganese oxides. Ion exchange may also occur with fixed charge minerals such as zeolites where contaminated water comes into contact with clay minerals [40–42]. Adsorption is not always accompanied by proton loss. In the adsorption of arsenate to goethite, for example, $\text{FeAsO}_4\text{H}_2^0$ and FeAsO_4H^- were the

dominant species at pH < 5 and pH 5–8 respectively, in reactions that were not accompanied by the loss of protons from the goethite surface [35].

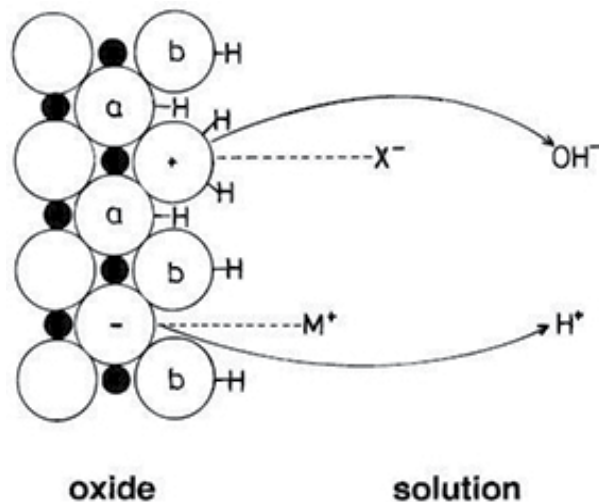


Figure 3. Acid and base hydroxyl sites on metal oxide surfaces and ion exchange reactions at the oxide-solution interface: ●=metal ions, ○=oxide ions, a=acid hydroxyl sites and b=base hydroxyl sites [36].

Determining the mode of contaminant binding is essential to predicting their behaviour in groundwater. Contaminants may be sorbed by electrostatic, hydrogen or covalent bonds. Electrostatic bonds are formed between charged hydrated species and oppositely charged mineral surfaces forming weak outer-sphere complexes. Contaminants sorbed in this way are easily desorbed by perturbations in solution parameters e.g. pH, ionic strength. Hydrogen bonds have intermediate strength while covalent bonding results in strong sorption of contaminants. Contaminants sorbed this way are harder to desorb and colloidal transport may play an important role in their transport through groundwater.

3. Mobility of inorganic contaminants in groundwater

The mobility of contaminants in groundwater has been the subject of many investigations. Early models of contaminant mobility divided contaminants between only two phases: the dissolved phase (mobile) and a sorbed phase (immobile). However, after contaminants were detected at distances further than was predicted by this model, a third phase, the mobile colloidal phase, was applied (**Figure 4**) [16, 33, 43–47]. Buddemeier and Hunt [48] found that colloids were responsible for the transport of Mn, Co, Ce and Eu from the Nevada ammunitions test site to a location 300 m away from the disposal site. Similar findings were made by Kersting et al. [47] for the transport of Pu from the same site and by Hochella et al. [49] for the transfer of As, Cu, Pb and Zn from the largest Superfund site in the USA.

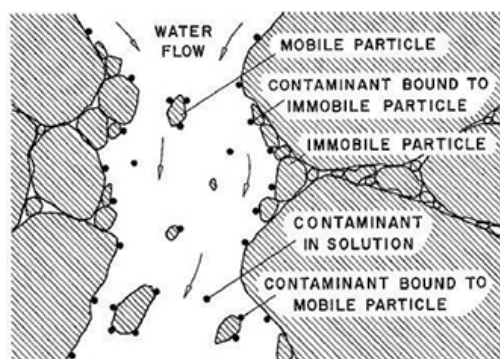


Figure 4. Schematic representation of colloid facilitated transport in a subsurface water-saturated medium. Contaminants (●) are either dissolved in solution, adsorbed to mobile phases (colloids) or to stationary phases [50].

For colloid-facilitated contaminant transport to be efficient, three criteria must be met: (i) colloids must be generated, (ii) a strong association must be formed between contaminants and the colloids, (iii) the colloid-contaminant composites must be transported through groundwater [50, 51]. Colloids are particles in the 1 nm to 1 μm size range [52]. They may be organic e.g. humic acids and microbes or inorganic e.g. metal oxy(hydr)oxides, carbonates, silicates and phosphates [52–54]. Inorganic colloids are particularly important in mining-contaminated groundwater. In these environments, colloids may be formed biogenically, as a result of ore processing or by precipitation from supersaturated solutions [53, 55]. Webster et al. [54] suggested that colloids formed in AMD were more effective sorbents than pure minerals due to the presence of sulphates and the influence of bacterial activity on their synthesis. Colloids may also be mobilised by perturbations to groundwater properties including pH, ionic strength and flow velocity (e.g. flow through fractures or variable infiltration following rainfall events). pH shifts are especially important in AMD-impacted environments as pH influences the formation of Fe and Al colloids [53, 56]. It also influences colloidal surface charges, the affinity of contaminants for colloid surfaces and the suspension or precipitation of colloids.

Solution ionic strength also influences colloid mobilisation due to its effect on the electric double layer of ions as put forward in the DVLO (Derjaguin-Landau-Verwey-Overbeek) theory. According to this theory, colloid mobilisation increases with decreasing ionic strength because the electrostatic double layer around colloids expands resulting in greater repulsion between like-charged colloids. Thus, ^{137}Cs by kaolinite through quartz found that transport was substantially increased at low ionic strengths because kaolinite colloids were more mobile and bound more ^{137}Cs . [57]. Increases in ionic strength on the other hand, lead to compression of the double layers, hence a decrease in repulsive forces and colloid aggregation/coalescence [58, 59]. Thus, contaminant transport may be retarded due to colloidal sedimentation. Kimball et al. [56] found that while Fe colloids aided the transport of As, Cd, Cu, Mn, Pb and Zn from mining flows, the colloidal load decreased by half after the first 50 km due to aggregation and sedimentation of colloids in the stream bed. Retardation may also be due to colloidal plugging/blockage of pores [60] within transport matrices.

4. Prevention and remediation of groundwater contamination by AMD

Conventional methods of AMD treatment involve the hydroxide precipitation using quicklime (CaO), hydrated lime (Ca(OH)₂), caustic soda (NaOH) or soda ash (Na₂CO₃) [9] or sulphide precipitation agents such as NaS, NaHS, BaS, FeS or H₂S [61]. This latter approach is superior because metal sulphides are generally less soluble than hydroxide counterparts, and as such, allows more complete precipitation (although the objectionable odour and toxicity of H₂S has to be considered).

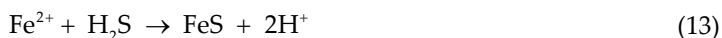
Iron, in its reduced form, either as ferrous salts or zero valent form, has also been used for the chemical treatment of contaminated water. The primary advantages associated with ZVI use include low cost, simplicity in handling and the formation of strong complexes between contaminants and the iron oxides [62]. Farrell et al. [20] and Melitas et al. [63] applied ZVI for the removal of arsenate ions from solution. Adsorption was resolved as the removal mechanism because no As(III) was detected in solution. ZVI was also effective for the removal of CrO₄²⁻, TcO₄⁻, MoO₄²⁻ and UO₂²⁺ ions by reductive precipitation [26, 62, 64–67]. The rate of removal followed the order CrO₄²⁻ > TcO₄⁻ > UO₂²⁺ >> MoO₄²⁻ with CrO₄²⁻ concentrations decreasing from 10,000 µg L⁻¹ to < 5 µg L⁻¹ in 1 hour [65]. Cationic contaminants e.g. Ag⁺ and Hg⁺ may also be reduced to their zero valent metallic forms [68]. The use of ZVI exploits redox reactions and the strong reducing properties of iron to convert contaminants into less soluble immobile forms [63]. In this process, ZVI is first oxidised by water to Fe(II) which then acts as an electron donor for the reduction of dissolved ions (Equation 11) [20, 69].



With the advent of nanotechnology, nanoscale ZVI (nZVI) use has also been attempted in laboratory and field studies [70, 71]. Li et al. [72] reported that for Cr(IV) degradation, reaction rates for nZVI were at least 25–30 times faster and the sorption capacity was much higher compared with granular iron. In another study, 25% of As(V) was reduced to As(III) after 90 days [73]. Despite this, the environmental and human health risks associated with nanoparticles have meant that larger scale application of these materials has been approached with caution. Tratnyek and Johnson [74], however, pointed out that the mobility of nanoscale ZVI was less than a few metres under almost all relevant environmental conditions and thus, human exposure was likely to be minimal.

Sulphate reducing bacteria (SRB) have been increasingly investigated for mine drainage remediation since Tuttle et al. [75] documented sulphate reduction in an AMD-contaminated stream. Samuel et al. [31] reported the remediation of Cr(VI) by indigenous isolates of *Bacillus*, *Acinetobacter* and *Escherichia* spp. from chromite mines in the Sukinda Valley of Orissa, India. SRB utilize organic carbon or hydrogen to reduce sulphates to sulphides (Equation 12) which then facilitate the precipitation of metal sulphides (Equation 13). This reaction also increases the alkalinity and pH of solutions, further promoting metal precipitation [76]. As such, the use

of SRB for AMD treatment reduces sulphate concentrations, precipitates metal ions from solution and raises solution pH.



Cardenas et al. [77] reported the biological in situ remediation of uranium contaminated groundwater. The growth of denitrifying, Fe(III)-reducing and SRB including *Desulfovibrio*, *Geobacter*, *Anaero-myxobacter*, *Desulfosporosinus*, *Acidovorax*, *Ferribacterium* and *Geothrix spp* through weekly injections of ethanol into the subsurface. After 2 years, U concentrations were reduced from 60 mg L⁻¹ to < 30 µg L⁻¹. Sulphate concentrations also decreased when ethanol was injected and rebounded when injection stopped, indicating SRB activity in the subsurface.

Such in situ approaches for the treatment of mine drainage contamination have attracted much attention in recent times. Designed to intercept contaminants in the subsurface with reactive materials, in situ treatment has the advantage of treating contaminated groundwater prior to the oxidation of Fe²⁺ (Reaction 2), thus preventing the generation of additional acidity and mobilisation of additional metal ions [64]. Sulphate reduction is also optimised in the near-neutral pH characteristic of many aquifers and the process is less costly because the volumes of water to be treated are lower than in pump-and-treat systems [78]. Two possible approaches exist for *in situ* remediation. The first involves injecting reactants into the subsurface to form a reactive treatment zone in which reactants are adsorbed onto aquifer materials (**Figure 5a**). The procedure by Cardenas et al. [77] described above falls in this category. Alternatively, permeable reactive barriers may be keyed in to underlying bedrock in the flow path of contaminants (**Figure 5b**).

A number of studies have documented the use of PRBs for the remediation of AMD-contaminated groundwater [64, 78, 79]. The reactive materials within PRBs may be chemical or biological [80]. Baker et al. [81] used a mixture containing 50 wt% silica sand, 45 wt% crushed limestone and 5 wt% metal oxide for the removal of phosphates while ZVI, FeCO₃, FeS were investigated for Cr(VI) removal [82]. Biologically-driven PRBs (biobarriers) mostly comprise of SRB [61, 83] and require (i) an anaerobic environment (redox potential of ~200 mV), (ii) pH values greater than 5, (iii) a sulphate species to be reduced and (iv) an energy source (electron donor), mostly short chain organic substrates e.g. ethanol although a variety of natural substrates including leaf mulch, vegetal compost and sawdust [84] have been tested. Benner et al. [85] installed a PRB 20 m long, 4 m thick and 3.5 m tall into the Nickel Rim aquifer downstream of a tailings impoundment. They recorded, after 22 months, dramatic changes in the concentrations of several contaminants. Concentrations of sulphates, Fe and Ni decreased by 2000–3000 mg L⁻¹, 270–1300 mg L⁻¹ and 30 mg L⁻¹, respectively. In addition, alkalinity increased by 800–2700 mg L⁻¹ and the populations of SRB were 10,000 times greater than before the installation of the PRB. Column experiments by Waybrant et al. [86] showed similar results: iron concentrations decreased from 300–1200 mg/L to <0.01–220 mg/L while Zn and Ni

decreased from 0.6–1.2 mg L⁻¹ to 0.01–0.15 mg L⁻¹ and 0.8–12.8 mg L⁻¹ to <0.01 mg L⁻¹, respectively. The pH increased slightly from 5.5–6.0 to 6.5–7.0 and alkalinity from <50 mg/L to 300–1300 mg L⁻¹. Biobarriers are also effective for the attenuation of Cr(VI) [87] radionuclide ions [88] and sulphates [89]. Sulphate concentrations were decreased from 1800 to <250 mg L⁻¹ and the mine waters neutralised using only bacterially-mediated alkalinity. Natural treatment as

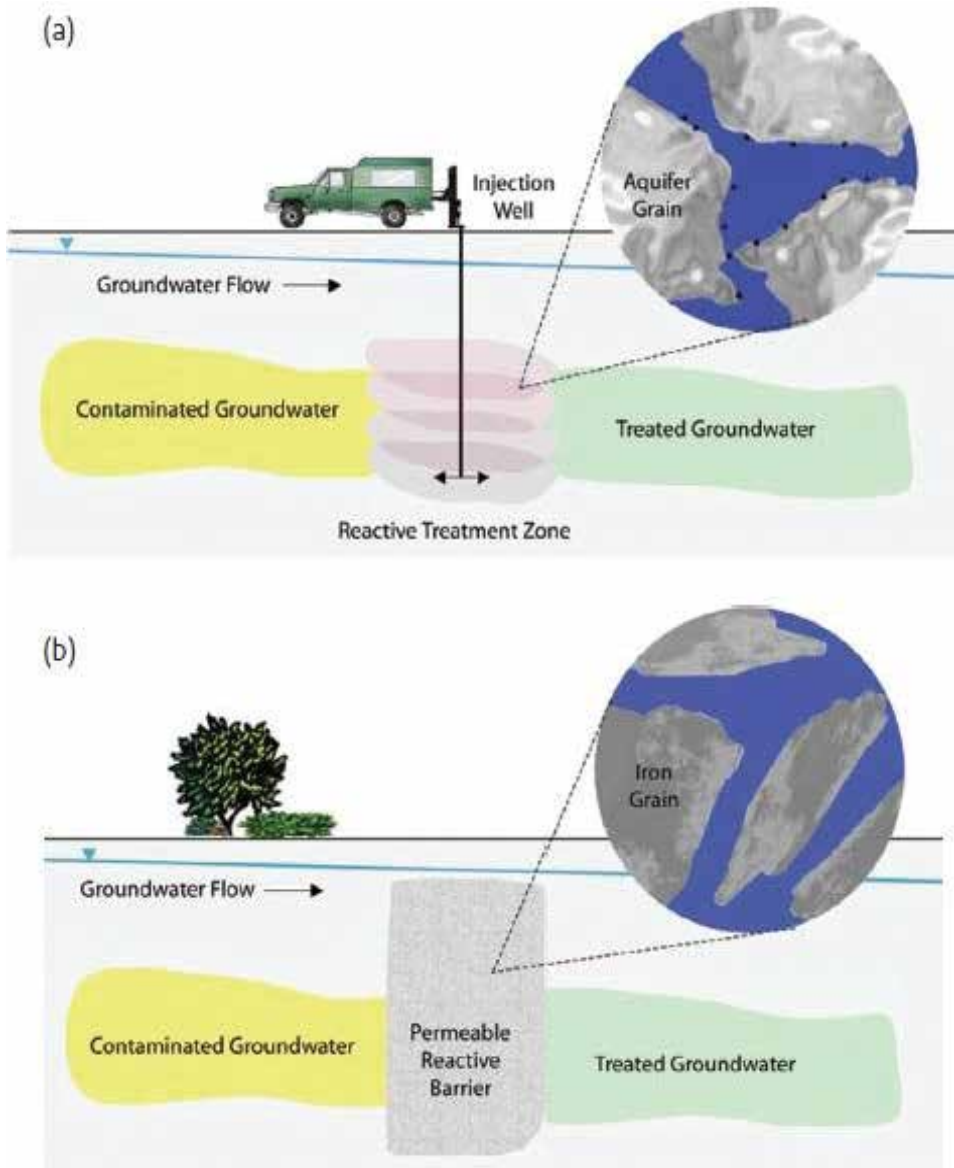


Figure 5. In situ treatment of groundwater may be by a reactive treatment zone (a) or a permeable reactive barrier (b) (After [74]).

well as permeable reactive barriers therefore both hold promise for the treatment of groundwater contamination. Future research should look into the incorporation of nanomaterials e.g. embedded in polymers, into PRBs to facilitate faster reaction times and more efficient removal of contaminants.

5. Conclusions and recommendations

This chapter explored the behaviour of inorganic contaminants from mining activity, in groundwater. The processes influencing their transformation i.e. acid/base, redox and (co)precipitation/dissolution reactions have been discussed in detail. The factors influencing their mobility, specifically, the role of colloids as well as the prevention and remediation of contamination have also been reviewed. Because of their low costs and preclusion of the need for pumping out aquifers, PRBs remain a viable option for the prevention and treatment of contaminated groundwater. Future research should look into the use of nanomaterials in PRBs. With their large surface areas and faster reaction rates, the use of nanomaterials in PRBs will likely result in greater treatment efficacy. Although the current high cost of some nanomaterials may hinder their application, this will be achievable as production technologies improve and prices decrease. On the other hand, the use of SRB in PRBs may provide a more natural alternative devoid of the environmental concerns associated with the introduction of engineered nanomaterials to the environment. It also has the double advantages of removing both metal and sulphate ions. Research into the use of SRB in PRBs will involve identification and isolation of bacterial strains suited for each contaminated site as studies have shown bacteria to be site specific and not transferable.

Author details

Anita Etale* and Sabelo Mhlanga

*Address all correspondence to: aetale@gmail.com

Nanotechnology and Water Sustainability Research Unit, College of Engineering, Science and Technology, University of South Africa, Florida Campus, Johannesburg, South Africa

References

- [1] Leblanc M. 4,500-year-old mining pollution in southwestern Spain: Long-term implications for modern mining pollution. *Econ. Geol.* 2000;95:655–662.
- [2] Nieto JM, Sarmiento AM, Olías M, Canovas CR, Riba I, Kalman J, Delvalls TA. Acid mine drainage pollution in the Tinto and Odiel rivers (Iberian Pyrite Belt, SW Spain)

- and bioavailability of the transported metals to the Huelva Estuary. *Environ. Int.* 2007;33:445–455.
- [3] Hogsden KL, Harding JS. Anthropogenic and natural sources of acidity and metals and their influence on the structure of stream food webs. *Environ. Pollut.* 2012;162:466–474.
- [4] Tutu H, McCarthy TS, Cukrowska E. The chemical characteristics of acid mine drainage with particular reference to sources, distribution and remediation: The Witwatersrand Basin, South Africa as a case study. *Appl. Geochemistry.* Elsevier Ltd; 2008 Dec; 23:3666–3684.
- [5] Roychoudhury AN, Petersen J. Geochemical evaluation of soils and groundwater affected by infiltrating effluent from evaporation ponds of a heavy mineral processing facility, West Coast, South Africa. *J. Geochemical Explor.* 2014;144:478–491.
- [6] Singer PC, Stumm W. Acidic mine drainage: The rate-determining step. *Science.* 1970;167:1121–1123.
- [7] España JS, Pamo EL, Santofimia E, Aduvire O, Reyes J, Baretino D. Acid mine drainage in the Iberian Pyrite Belt (Odiel river watershed, Huelva, SW Spain): Geochemistry, mineralogy and environmental implications. *Appl. Geochemistry.* 2005;20:1320–1356.
- [8] Roy SB, Dzombak DA. Chemical factors influencing colloid-facilitated transport of contaminants in porous media. *Environ. Sci. Technol.* 1997;31:656–664.
- [9] Evanko CR, Dzombak DA. Remediation of Metals-Contaminated Soils and Groundwater. 1997;1–61.
- [10] Jean GE, Bancroft GM. Heavy metal adsorption by sulphide mineral surfaces. *Geochim. Cosmochim. Acta.* 1986;50:1455–1463.
- [11] Özverdi A, Erdem M. Cu^{2+} , Cd^{2+} and Pb^{2+} adsorption from aqueous solutions by pyrite and synthetic iron sulphide. *J. Hazard. Mater.* 2006;137:626–632.
- [12] Muller B, Axelsson MD, Öhlander B. Analyses of trace elements on quartz surfaces in sulfidic mine tailings from Kristineberg (Sweden) a few years after remediation. *Environ. Geol.* 2003;45:98–105.
- [13] Al TA, Blowes DW, Martin CJ, Cabri LJ, Jambor JL. Aqueous geochemistry and analysis of pyrite surfaces in sulfide-rich mine tailings. *Geochim. Cosmochim. Acta.* 1997;61:2353–2366.
- [14] Banks D, Younger PL, Egil RA, Sheila RI. Mine-water chemistry: The good, the bad and the ugly. *Environ. Geol.* 1997;32:157–174.
- [15] Manceau A, Charlet L, Boisset MC, Didier B, Spadini L. Sorption and speciation of heavy metals on hydrous Fe and Mn oxides. From microscopic to macroscopic. *Appl. Clay Sci.* 1992;7:201–223.

- [16] McGregor R, Blowes D, Jambor J, Robertson W. The solid-phase controls on the mobility of heavy metals at the Copper Cliff tailings area, Sudbury, Ontario, Canada. *J. Contam. Hydrol.* 1998; 33:247–271.
- [17] Cummings DE, Caccavo F, Fendorf S, Rosenzweig RF. Arsenic mobilization by the dissimilatory Fe(III)-reducing bacterium *Shewanella alga* BrY. *Environ. Sci. Technol.* 1999;33:723–729.
- [18] Dhal B, Thatoi HN, Das NN, Pandey BD. Chemical and microbial remediation of hexavalent chromium from contaminated soil and mining/metallurgical solid waste: A review. *J. Hazard. Mater.* 2013;250–251:272–291.
- [19] Murphy AP. Removal of selenate from water by chemical reduction. *Ind. Eng. Chem. Res.* 1988;27:187–191.
- [20] Farrell J, Wang J, O'Day P, Conklin M. Electrochemical and spectroscopic study of arsenate removal from water using zero-valent iron media. *Environ. Sci. Technol.* 2001;35:2026–2032.
- [21] Jones CA, Langner HW, Anderson KT, McDermott R, Inskeep WP. Rates of microbially mediated arsenate reduction and solubilization. *Soil Sci. Soc. Am. J.* 1999;64:600–608.
- [22] Gihring TM, Banfield JF. Arsenite oxidation and arsenate respiration by a new *Thermus* isolate. *FEMS Microbiol. Lett.* 2001;204:335–340.
- [23] Oremland RS, Stolz JF. The Ecology of Arsenic. *Science.* 2003;300:939–944.
- [24] Routh J, Bhattacharya A, Saraswathy A, Jacks G, Bhattacharya P. Arsenic remobilization from sediments contaminated with mine tailings near the Adak mine in Västerbotten district (northern Sweden). *J. Geochemical Explor.* 2007;92:43–54.
- [25] Macur RE, Wheeler JT, McDermott TR, Inskeep WP. Microbial populations associated with the reduction and enhanced mobilization of arsenic in mine tailings. *Environ. Sci. Technol.* 2001;35:3676–3682.
- [26] Han X, Li YL, Gu JD. Oxidation of As(III) by MnO_2 in the absence and presence of Fe(II) under acidic conditions. *Geochim. Cosmochim. Acta.* 2011;75:368–379.
- [27] Rai D, Eary LE, Zachara JM. Environmental chemistry of chromium. *Sci. Total Environ.* 1989;86:15–23.
- [28] Eary LE, Rai D. Kinetics of Chromium(III) oxidation to Chromium(VI) by reaction with manganese dioxide. *Environ. Sci. Technol.* 1987;21:1187–1193.
- [29] Weaver RM, Hochella MF, Ilton ES. Dynamic processes occurring at the $\text{Cr}^{\text{III}}_{\text{aq}}$ -manganite (MnOOH) interface: Simultaneous adsorption, microprecipitation, oxidation/reduction, and dissolution. *Geochim. Cosmochim. Acta.* 2002;66:4119–4132.
- [30] Fendorf SE, Fendorf M, Sparks DL, Gronsky R. Inhibitory mechanisms of Cr(III) oxidation by $\delta\text{-MnO}_2$. *J. Colloid Interface Sci.* 1992;153:37–54.

- [31] Samuel J, Paul ML, Pulimi M, Nirmala MJ, Chandrasekaran N, Mukherjee A. Hexavalent chromium bioremoval through adaptation and consortia development from Sukinda chromite mine isolates. *Ind. Eng. Chem. Res.* 2012;51:3740–3749.
- [32] Dhal B, Thatoi H, Das N, Pandey BD. Reduction of hexavalent chromium by *Bacillus sp.* isolated from chromite mine soils and characterization of reduced product. *J. Chem. Technol. Biotechnol.* 2010;85:1471–1479.
- [33] Brown Jr GE, Parks GA. Sorption of trace elements on mineral surfaces: Modern perspectives from spectroscopic studies, and comments on sorption in the marine environment. *Int. Geol. Rev.* 2001;43:963–1073.
- [34] Kinniburgh DG, Jackson ML, Syers JK. Adsorption of alkaline earth, transition, and heavy metal cations by hydrous oxide gels of iron and aluminum. *Soil Sci. Soc. Am. J.* 1976;40:796–799.
- [35] Gao Y, Mucci A. Acid base reactions, phosphate and arsenate complexation, and their competitive adsorption at the surface of goethite in 0.7 M NaCl solution. *Geochim. Cosmochim. Acta.* 2001;65:2361–2378.
- [36] Tamura H, Katayama N, Furuichi R. Modeling of ion-exchange reactions on metal oxides with the frumkin isotherm. 1. acid–base and charge characteristics of MnO₂, TiO₂, Fe₃O₄ and Al₂O₃ surfaces and adsorption affinity of alkali metal ions. *Environ. Sci. Technol.* 1996;30:1198–1204.
- [37] Borah D, Senapati K. Adsorption of Cd(II) from aqueous solution onto pyrite. *Fuel.* 2006;85:1929–1934.
- [38] Forbes EA, Posner AM, Quirk JP. The specific adsorption of divalent Cd, Co, Cu, Pb, and Zn on goethite. *J. Soil Sci.* 1976;27:154–166.
- [39] Gadde RR, Laitinen HA. Studies of heavy metal adsorption by hydrous iron and manganese oxides. *Anal. Chem.* 1974;46:2022–2026.
- [40] Nagy NM, József Kónya, Urbán Z. The competitive exchange of hydrogen and cobalt ions on calcium-montmorillonite. *Colloids and Surfaces A Physicochem. Eng. Asp.* 1997;121:117–124.
- [41] Nagy NM, Kónya J. The exchange of Mn and Ca ions on montmorillonite. *React. Polym.* 1992;17:9–13.
- [42] Das NC, Bandyopadhyay M. Removal of copper using vermiculite. *Water Environ. Res.* 1992;64:852–857.
- [43] Cauwet G, Dai M, Martin J. The significant role of colloids in the transport and transformation of organic carbon and associated trace metals (Cd, Cu and Ni) in the Rhone delta (France). *Mar. Chem.* 1995;51:159–175.
- [44] Kaplan DI, Bertsch PM, Adriano DC. Facilitated transport of contaminant metals through an aquifer. *Groundwater.* 1995;33:708–717.

- [45] McCarthy JF, Zachara JM. Subsurface transport of contaminants. *Environ. Sci. Technol.* 1989;23:496–502.
- [46] Kaplan DI, Hunter DB, Bertsch PM, Bajt S, Adriano DC. Application of synchrotron X-ray fluorescence spectroscopy and energy dispersive X-ray analysis to identify contaminant metals on groundwater colloids. *Environ. Sci. Technol.* 1994;28:6–9.
- [47] Kersting AB, Smith DK. Migration of plutonium in ground water at the Nevada Test Site. *Nature.* 1999;397:56–59.
- [48] Buddemeier RW, Hunt JR. Transport of colloidal contaminants in groundwater: Radionuclide migration at the Nevada Test Site. *Appl. Geochemistry.* 1988;3:535–548.
- [49] Hochella Jr MF, Kasama T, Putnis A, Putnis C V., Moore JN. Environmentally important, poorly crystalline Fe/Mn hydrous oxides: Ferrihydrite and a possibly new vernadite-like mineral from the Clark Fork River Superfund Complex. *Am. Mineralog.* 2005;90:718–724.
- [50] Grolimund D, Borkovec M, Barmettler K, Sticher H. Colloid-facilitated transport of strongly sorbing contaminants in natural porous media: A laboratory column study. *Environ. Sci. Technol.* 1996;30:3118–3123.
- [51] Ryan JN, Elimelech M. Colloid mobilization and transport in groundwater. *Colloids Surfaces A Physicochem. Eng. Asp.* 1996;107:1–56.
- [52] Hasselov M, von der Kammer F. Iron Oxides as Geochemical Nanovectors for Metal Transport in Soil-River Systems. *Elements.* 2008;4:401–406.
- [53] Schemel LE, Kimball BA, Bencala KE. Colloid formation and metal transport through two mixing zones affected by acid mine drainage near Silverton, Colorado. *Appl. Geochemistry.* 2000;15:1003–1018.
- [54] Webster JG, Swedlund PJ, Webster KS. Trace metal adsorption onto an acid mine drainage Iron(III) oxy hydroxy sulfate. *Environ. Sci. Technol.* 1998;32:1361–1368.
- [55] Chapman BM, Jones DR, Jung RF. Processes controlling metal ion attenuation in acid mine drainage streams. *Geochim. Cosmochim. Acta.* 1983;47:1957–1973.
- [56] Kimball A, Axtmann V. Effects of colloids on metal transport in a river receiving acid mine drainage, Upper Arkansas River, Colorado, USA. 1995;10:285–306.
- [57] Saiers JE, Hornberger GM. The influence of ionic strength on the facilitated transport of Cesium by kaolinite colloids. *Water Resour. Res.* 1999;35:1713–1727.
- [58] Kanti Sen T, Khilar KC. Review on subsurface colloids and colloid-associated contaminant transport in saturated porous media. *Adv. Colloid Interface Sci.* 2006;119:71–96.
- [59] Nightingale HI, Bianchi WC. Groundwater turbidity resulting from artificial recharge. *Groundwater.* 1977;15:146–152.

- [60] Torkzaban S, Bradford SA, Vanderzalm JL, Patterson BM, Harris B, Prommer H. Colloid release and clogging in porous media: Effects of solution ionic strength and flow velocity. *J. Contam. Hydrol.* 2015;181:161–171.
- [61] Hammack RW, Edenborn HM, Dvorak DH. Treatment of water from an open-pit copper mine using biogenic sulfide and limestone: A feasibility study. *Water Res.* 1994;28:2321–2329.
- [62] Manning BA, Hunt ML, Amrhein C, Yarmoff JA. Arsenic(III) and arsenic(V) reactions with zerovalent iron corrosion products. *Environ. Sci. Technol.* 2002;36:5455–5461.
- [63] Melitas N, Wang J, Conklin M, O'Day P, Farrell J. Understanding soluble arsenate removal kinetics by zerovalent iron media. *Environ. Sci. Technol.* 2002;36:2074–2081.
- [64] Blowes DW, Ptacek CJ, Jambor JL. In-situ remediation of Cr(VI)-contaminated groundwater using permeable reactive walls: Laboratory studies. *Environ. Sci. Technol.* 1997;31:3348–3357.
- [65] Cantrell KJ, Kaplan DI, Wietsma TW. Zero-valent iron for the in situ remediation of selected metals in groundwater. *J. Hazard. Mater.* 1995;42:201–212.
- [66] Gu B, Liang L, Dickey MJ, Yin X, Dai S. Reductive precipitation of uranium(VI) by zero-valent iron. *Environ. Sci. Technol.* 1998;32:3366–3373.
- [67] Su C, Puls RW. Arsenate and arsenite removal by zerovalent iron: Kinetics, redox transformation, and implications for in situ groundwater remediation. *Environ. Sci. Technol.* 2001;35:1487–1492.
- [68] Gould JP, Masingale MY, Miller M. Recovery of silver and mercury from COD samples by iron cementation. *J. Water Pollut. Control Fed.* 1984;56:280–286.
- [69] Kanel SR, Manning B, Charlet L, Choi H. Removal of arsenic (III) from groundwater by nanoscale zero-valent iron. *Environ. Sci. Technol.* 2005;39:1291–1298.
- [70] Nowack B. Pollution prevention and treatment using nanotechnology. In: Krug H, editor. *Nanotechnology*. Weinheim: WILEY-VCH Verlag GmbH & Co. KGaA, Weinheim; 2010. 1–15.
- [71] Crane RA, Scott TB. Nanoscale zero-valent iron: Future prospects for an emerging water treatment technology. *J. Hazard. Mater.* 2012;211–212:112–125.
- [72] Li X, Elliott DW, Zhang W. Zero-valent iron nanoparticles for abatement of environmental pollutants: Materials and engineering aspects. *Crit. Rev. Solid State Mater. Sci.* 2006;31:111–122.
- [73] Kanel SR, Greneche JM, Choi H. Arsenic(V) removal from groundwater using nano scale zero-valent iron as a colloidal reactive barrier material. *Environ. Sci. Technol.* 2006;40:2045–2050.

- [74] Tratnyek PG, Johnson RL. Nanotechnologies for environmental cleanup. *Nano Today*. 2006;1:44–48.
- [75] Tuttle JH, Dugan PR, Randles CI. Microbial sulfate reduction and its potential utility as an acid mine water pollution abatement procedure. *Appl. Microbiol.* 1969;17:297–302.
- [76] Christensen B, Laake M, Lien T. Treatment of acid mine water by sulfate-reducing bacteria; Results from a bench scale experiment. *Water Res.* 1996;30:1617–1624.
- [77] Cardenas E, Wu WM, Leigh MB, Carley J, Carroll S, Gentry T, Luo J, Watson D, Gu B, Ginder-Vogel M, Kitanidis PK, Jardine PM, Zhou J, Criddle CS, Marsh TL, Tiedje JM. Microbial communities in contaminated sediments, associated with bioremediation of uranium to submicromolar levels. *Appl. Environ. Microbiol.* 2008;74:3718–3729.
- [78] Benner SG, Blowes DW, Ptacek CJ. A full-scale porous reactive wall for prevention of acid mine drainage. *Gr. Water Monit. Remediat.* 1997. 99–107.
- [79] Fruchter J. In Situ Treatment of chromium contaminated groundwater. *Environ. Sci. Technol.* 2002;36:464A – 472A.
- [80] Scherer MM, Richter S, Valentine RL, Alvarez PJJ. Chemistry and microbiology of permeable reactive barriers for in situ groundwater clean up. *Crit. Rev. Microbiol.* 2000;26:221–264.
- [81] Baker MJ, Blowes DW, Ptacek CJ. Phosphorous adsorption and precipitation in a permeable reactive wall: Applications for wastewater disposal systems. *L. Contam. Reclam.* 1997;5:189–193.
- [82] Puls RW, Paul CJ, Powell RM. The application of in situ permeable reactive (zero-valent iron) barrier technology for the remediation of chromate-contaminated groundwater: A field test. *Appl. Geochemistry.* 1999;14:989–1000.
- [83] Gibert O, de Pablo J, Cortina JL, Ayora C. Treatment of acid mine drainage by sulphate-reducing bacteria using permeable reactive barriers: A review from laboratory to full-scale experiments. *Rev. Environ. Sci. Biotechnol.* 2002;1:327–333.
- [84] Waybrant KR, Blowes DW, Ptacek CJ. Selection of reactive mixtures for use in permeable reactive walls for treatment of mine drainage. *Environ. Sci. Technol.* 1998;32:1972–1979.
- [85] Benner SG, Blowes DW, Gould WD, Herbert RB, Ptacek CJ. Geochemistry of a permeable reactive barrier for metals and acid mine drainage. *Environ. Sci. Technol.* 1999;33:2793–2799.
- [86] Waybrant KR, Ptacek CJ, Blowes DW. Treatment of mine drainage using permeable reactive barriers: Column experiments. *Environ. Sci. Technol.* 2002;36:1349–1356.

- [87] Jeyasingh J, Somasundaram V, Philip L, Bhallamudi SM. Pilot scale studies on the remediation of chromium contaminated aquifer using bio-barrier and reactive zone technologies. *Chem. Eng. J.* 2011;167:206–214.
- [88] Michalsen MM, Peacock AD, Smithgal AN, White DC, Spain AM, Sanchez-Rosario Y, Krumholz LR, Kelly SD, Kemner KM, McKinley J, Heald SM, Bogle MA, Watson DB, Istok JD. Treatment of nitric acid-, U(VI)-, and Tc(VII)-contaminated groundwater in intermediate-scale physical models of an in situ biobarrier. *Environ. Sci. Technol.* 2009;43:1952–1961.
- [89] Hammack RW, de Vegt AL, Schoeneman AL. The removal of sulfate and metals from mine waters using bacterial sulfate reduction: Pilot plant results. *Mine Water Environ.* 1998;17:8–27.

Numerical Simulations

Numerical and Analytical Methods for the Analysis of Flow of Water Through Soils and Earth Structures

Norma Patricia López-Acosta

Additional information is available at the end of the chapter

<http://dx.doi.org/10.5772/63706>

Abstract

This chapter presents a compendium of the primary methods that are used to perform water flow analyses with a focus on computational approximation methods. Some of the current algorithms for carrying out this type of analysis are summarized. In addition, general guidelines are provided for using the methodologies for specific types of analysis, such as transient-state flow caused by water drawdown and flow in unsaturated media. Emphasis is placed on the need for stochastic analysis of water flow. Lastly, conclusions and general recommendations are given for performing numerical groundwater seepage analyses in soils.

Keywords: flow of water, groundwater seepage, soils and earth structures, numerical and analytical methods, transient flow, unsaturated soils, stochastic analyses

1. Theoretical foundations

1.1. General considerations

Flow through saturated or unsaturated soils is governed by Darcy's Law, which was originally proposed for saturated media. Research has demonstrated that this law is also applicable to the flow of water in unsaturated soils [1]. The main difference between these flows is that the hydraulic conductivity for saturated media is a constant value, but it varies as a function of the volumetric water content and also indirectly with changes in pore water pressure in unsaturated soils (**Figure 1**) [2, 3]. Darcy's Law [4] is often written as follows:

$$v = k i \tag{1}$$

where v = Darcy’s velocity, k = hydraulic conductivity, and i = total hydraulic head gradient.

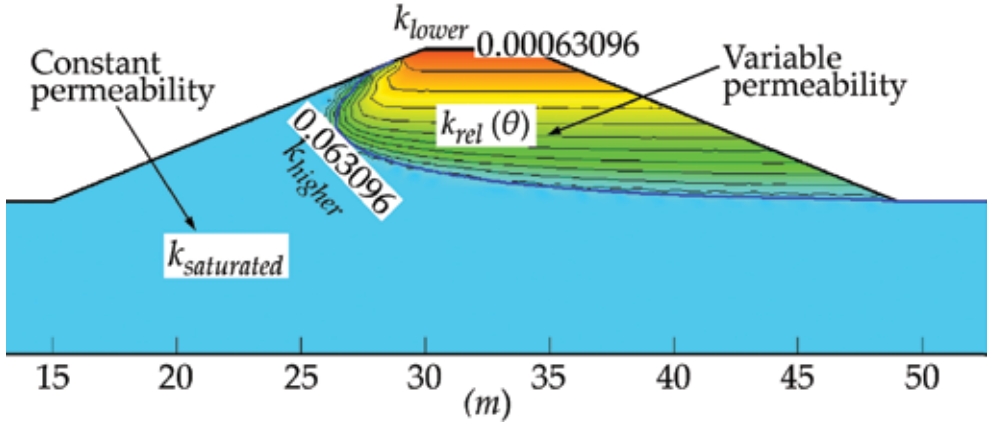


Figure 1. Change in the permeability of a partially saturated medium [5].

The average velocity at which the water moves through a mass of soil is linear and is equal to the Darcy’s velocity divided by the porosity of the soil. In an unsaturated soil, the average velocity is equal to the Darcy’s velocity divided by the volumetric water content of the soil. The majority of analytical and numerical methods that are currently employed for solving water flow problems consider only the Darcy’s velocity.

1.2. Equation for steady-state flow (saturated porous media)

The equation that describes steady-state flow in a porous medium is based on Darcy’s Law [4] and on the principle of flow continuity (which states that the amount of water that enters the medium is equal to the amount that exits) and is known as the Laplace’s equation (for a homogeneous and isotropic medium with $k_x = k_y = k_z$):

$$\frac{\partial^2 h}{\partial x^2} + \frac{\partial^2 h}{\partial y^2} + \frac{\partial^2 h}{\partial z^2} = 0 \tag{2}$$

where h = total hydraulic head, and k_x , k_y , and k_z = hydraulic conductivities in the x -, y -, and z -directions, respectively.

The Laplace’s equation is satisfied under the following conditions: (a) the flow is steady-state, (b) the soil is saturated, (c) the water and the solid particles are incompressible, (d) the flow does not modify the soil structure, and (e) there are no sources (via injection or extraction of water).

1.3. Equation for transient flow (saturated or unsaturated porous media)

In transient flow, the water levels vary as a function of time, and thus, water is either stored in or discharged from the medium. In these cases:

$$\text{Flow that exits} = \text{flow that enters} - \text{flow discharged during a time interval } \Delta t \quad (3)$$

or:

$$\text{Flow that exits} = \text{flow that enters} + \text{flow stored during a time interval } \Delta t \quad (4)$$

Equation (3) refers to the case of water drawdown, and Eq. (4) refers to the case of water filling. All the previous assumptions lead to the general mass balance equation:

$$\frac{\partial}{\partial x} \left(k_x \frac{\partial h}{\partial x} \right) + \frac{\partial}{\partial y} \left(k_y \frac{\partial h}{\partial y} \right) + Q = \frac{\partial \theta}{\partial t} \quad (5)$$

where h = total hydraulic head, k_x = hydraulic conductivity in the x -direction, k_y = hydraulic conductivity in the y -direction, Q = source term (applied boundary flux: injection or extraction), θ = volumetric water content, and t = time.

Equation (5) is the so-called Richards's equation, and it describes transient flow in unsaturated soils. The term on the right ($\partial\theta/\partial t$, the rate of change of the volumetric water content with respect to time) is related to the change in the water level with time. When there is no variation with time ($\partial\theta/\partial t = 0$) and no source term ($Q = 0$), Eq. (5) becomes the Laplace's equation, which is used for steady-state flow in saturated soils. The Richards's equation, or any of its modified forms, has constituted the basis for the development of most numerical models to calculate infiltration through unsaturated porous media under transient-state flow conditions [6].

2. Methods of water flow analysis

2.1. Analytical solutions

2.1.1. Exact solution

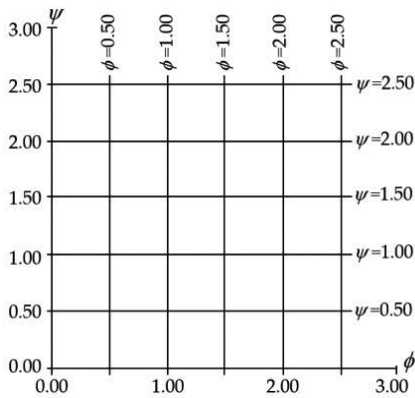
An exact analytical solution is generally only possible to obtain when the geometry of the flux domain and the hydraulic and boundary conditions are simple (isotropic and homogeneous media). However, soil is a heterogeneous, anisotropic, and discontinuous medium that has different characteristics at each point. Thus, exact solutions are difficult and impractical to

obtain in the case of the most complex flow problems, such as those in practical geotechnical engineering. In consequence, approximate solutions are usually sought.

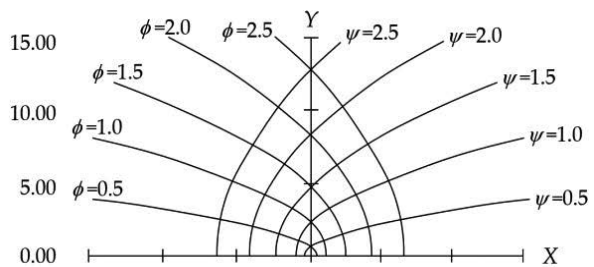
2.1.2. Conformal transformation or mapping

One of the approximate analytical solutions that is used to solve two-dimensional water flow problems involves obtaining a function that can transform the problem from the complex geometric domain into a problem whose solution is known [7]. These functions transform geometric shapes from a complex plane ω into shapes in another complex plane ζ . Thus, the mapping procedure defines the correspondence of the points of one shape in a plane ω to the points of the respective figure in the plane ζ . A transformation or mapping function is called conformal (conformal mapping) when it does not change the angles of intersection or the approximate geometric shapes between the two planes of interest [8]. Based on this concept, the Laplace differential equation can be solved for a domain G (**Figure 2b**) if the transformation or conformal mapping of this domain with a simpler domain G_1 (**Figure 2a**) is known [8–10]. The transformation is carried out by means of the analytical function of a complex variable. One of the best known functions that transform a system of uniform flux in the ω plane (**Figure 2a**) into a system of flux with confocal parabolas in the ζ plane (**Figure 2b**) is as follows (representing the well-known Kozeny’s solution for unconfined flow through dams, **Figure 3**):

$$\zeta = \omega^2 \tag{6}$$



a) Domain G_1 : functions ψ and ϕ in the plane ω



b) Domain G : functions ψ and ϕ in the plane ζ

Figure 2. Conformal mapping [7].

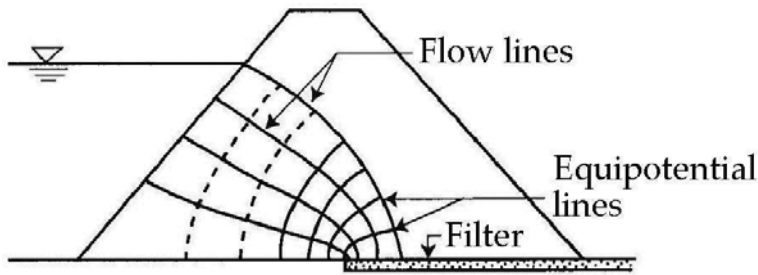


Figure 3. Kozeny's solution for water flow through an earth dam with a horizontal filter [7].

2.1.3. Method of fragments

The method of fragments is an approximate analytical method of solution for confined flow domains of finite depth. The fundamental assumption is that equipotential lines at different parts of the flow region can be approximated by straight vertical lines that divide the flow region into sections or fragments (Figure 4) [8, 11]. This method requires a form factor Φ that is obtained by solving definite integrals set up for each fragment of the flow region. Tables of expressions for different form factors for typical confined flow problems have been developed [8, 11]. The equation for calculating the discharge q through all fragments using this method is as follows:

$$q = k \frac{\sum \Delta h_n}{\sum \Phi_n} = \frac{k \cdot \Delta h}{\sum_{n=1}^m \Phi_n} \quad (7)$$

where k = hydraulic conductivity of the homogeneous and isotropic medium, Δh_n = loss of hydraulic head through fragment n , Δh = total loss of hydraulic head, and Φ_n = dimensionless form factor in fragment n .

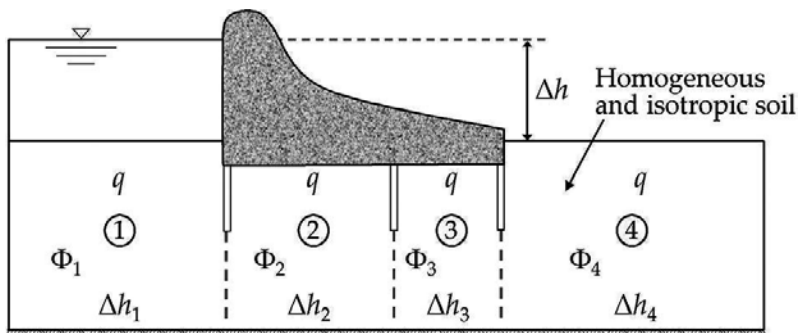


Figure 4. Schematic representation of the method of fragments.

The method of fragments was originally proposed to study confined flow in homogeneous and isotropic media, but at present, it has been implemented in anisotropic media [12]. In combination with conformal mapping and the Kozeny's parabola, it has also been applied to solve problems of unconfined flow through homogeneous levees with horizontal filters [13].

2.2. Graphical solutions

2.2.1. Confined flow

The most popular approximation technique for solving water flow problems is known as the flow net. It is a graphical method that sets up two functions that satisfy the Laplace's equation and that geometrically constitute two families of orthogonal curves: (a) equipotential lines (constant potential ϕ) and (b) flow lines or streamlines (constant values of the stream function ψ). The graphical representation of these lines is the so-called flow net. A drawing that satisfies the boundary and orthogonality conditions allows water flow problems with homogeneous and isotropic soil to be solved simply and graphically. The expression that calculates the discharge or rate of seepage q using a flow net is as follows:

$$q = k \Delta h \left(\frac{n_f}{n_e} \right) = k \Delta h S \quad (8)$$

where k = hydraulic conductivity of the homogeneous and isotropic medium, Δh = total loss of hydraulic head, $S = n_f/n_e$ is the form factor, n_f = number of flow intervals or flow channels, and n_e = number of equipotential intervals.

Flow nets are typically drawn on paper. However, nowadays, it is possible to draw flow nets by computer using several numerical techniques based on finite element method (FEM) or finite difference equations [14], such as successive over-relaxation (SOR) [15]. Examples of flow nets that were drawn using these techniques in confined homogeneous and stratified domains are shown in **Figures 5(a and b)–7**.

2.2.2. Unconfined flow

Free surface problems involve boundary value problems in which a portion of the boundary, the free surface, is unknown and must be determined as part of the solution. The presence of the free surface or water table makes the analysis methods more difficult. Dupuit's parabola [16] and Kozeny's parabola [17] are rigorous solutions for drawing the upper flow line and are only applicable for homogenous and isotropic media with specific geometries, such as vertical walls (Dupuit) or with filters (Kozeny). Other approximated methods, such as the *tangent* [18, 19] and *sine* methods [20], allow mainly calculate the discharge point of the upper flow line. Currently, this can be determined using numerical methods such as finite element method (FEM) and finite differences (FD), among others. The Baiocchi's method [21] and the extended pressure technique [22] are two variants of the successive over-relaxation (SOR) method (based on algebraic finite difference equations) that can be used to determine the position of the upper

flow line in homogeneous media or media composed of materials with different permeability values, respectively.

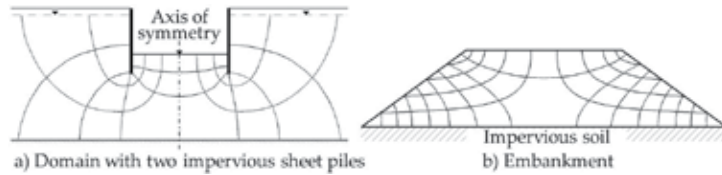


Figure 5. Flow nets in homogeneous and isotropic media obtained using the method of successive over-relaxations (SOR) [23].

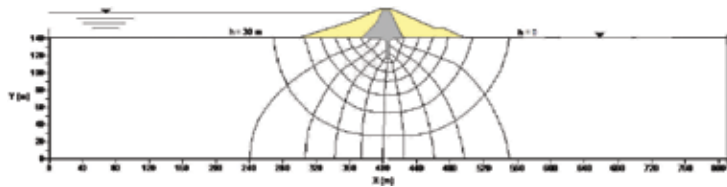


Figure 6. Flow net in a homogeneous and isotropic medium obtained using the finite element method (FEM) [24].

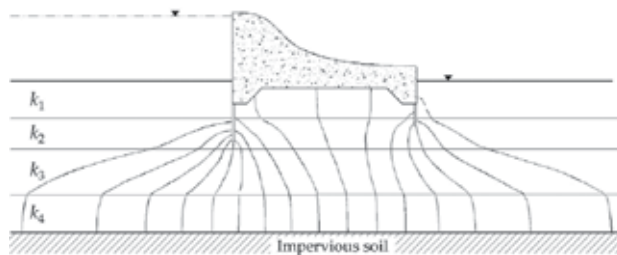


Figure 7. Flow net in a stratified soil under an impermeable dam obtained using the method of successive over-relaxations (SOR) [23].

A simple graphical procedure to draw the Kozeny's parabola or any parabolic upper flow line in a homogeneous and isotropic medium is as follows (**Figure 8a**): (a) The distance a_0 is calculated with the formula $a_0 = y_0/2 = [(d^2 + h^2)^{1/2} - d]/2$; (b) Draw a vertical line through O and also a horizontal line through M ; (c) Divide the OB segment in a number of equal parts, and the MB segment must also be divided into the same number of equal parts; (d) Draw straight lines joining the point O with the divisions made in the MB segment; (e) Draw horizontal lines passing through the divisions made in the OB segment; (f) The intersections of the previous lines are the points of the parabola sought. **Figures 8(b)** and **9** show upper flow lines obtained using this graphical procedure and other numerical methods. Additionally, **Figures 10** and **11** show flow nets that were numerically calculated in these types of free surface problems.

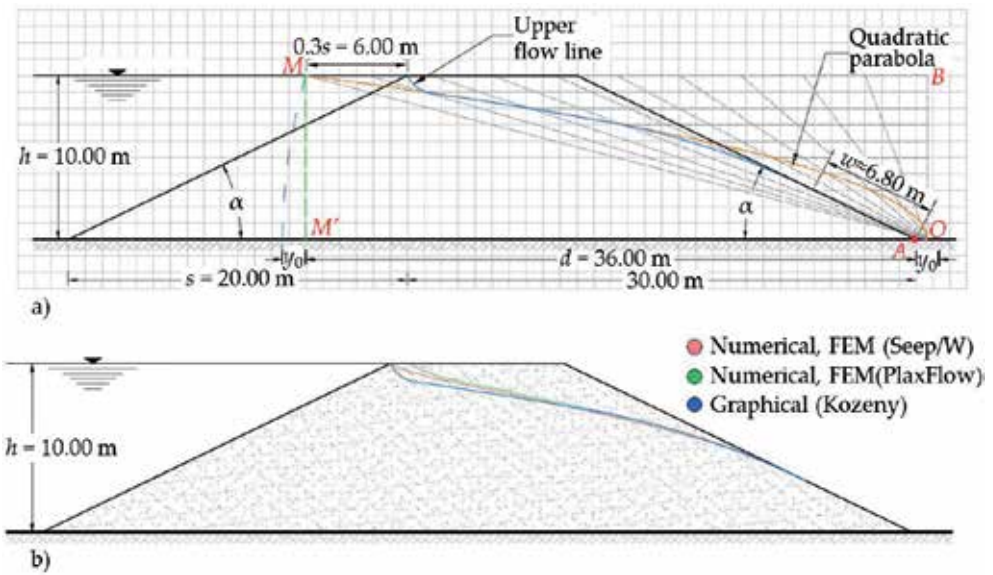


Figure 8. Homogeneous and isotropic embankment: (a) graphical procedure to draw the upper flow line, (b) comparison of the upper flow lines obtained using different methods [14].

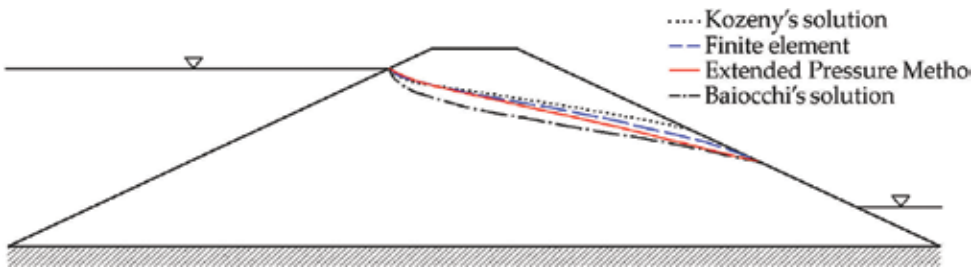


Figure 9. Comparison of the upper flow lines in a homogeneous and isotropic embankment, obtained using different methods [14].

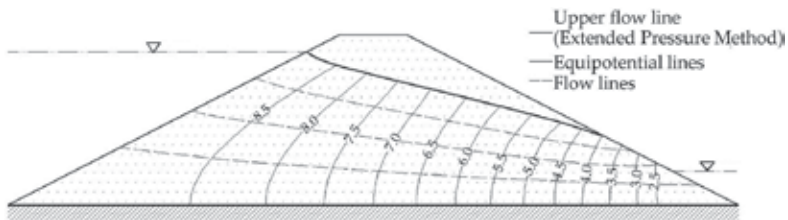


Figure 10. Flow net in a homogeneous and isotropic embankment numerically calculated using the extended pressure technique [14].

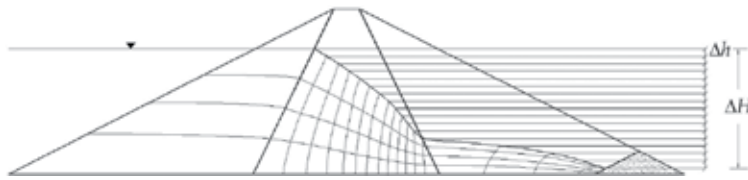


Figure 11. Flow net in a dam with graded materials obtained using the extended pressure technique [23].

2.3. Numerical solutions (approximate solutions)

2.3.1. Finite elements

The finite element method (FEM) is a numerical technique that provides approximate solutions to partial differential equations to solve a problem of a particular field. It is more versatile than other methods because it can consider anisotropy, heterogeneity, and multiple boundary conditions. The 2D finite elements that are generally used in water flow problems are triangles [25] or a combination of triangles and squares [26] whose nodes coincide with their vertices; in addition, triangles (2D) and tetrahedra (3D) can be used [27]. The hydraulic head is assumed to vary linearly within each finite element, and the Laplace's equation can be solved using a variational approach. Thus, the solution to this equation in a domain is found by obtaining the minimum of a function that is related to the equation and is defined for this domain. Based on these assumptions and after several mathematical manipulations, the following systems of homogeneous linear equations are set up:

$$[S]\{h_r\} = 0 \quad (9)$$

$$[S]\{\psi_r\} = 0 \quad (10)$$

The solution to Eq. (9) using a known method, such as Gaussian elimination, helps to determine the hydraulic head h at the nodes in the mesh of finite elements where it is unknown. Similarly, the solution to Eq. (10) provides nodal values of the stream function ψ . The flow net of the problem can be obtained by drawing the isovalue curves for this pair of families. Likewise, once the hydraulic heads h are calculated with Eq. (9), other results for the water flow problem can be obtained, such as the hydraulic gradients, flow velocities, pore pressure, degree of saturation, and flow rate, among others.

2.3.2. Finite differences

The Laplace's equation can be solved using finite difference equations, which are the same as those developed via truncated Taylor series or directly from Darcy's Law [4]. Several methods can be used to evaluate water flow problems that utilize finite differences, including: (a) the

classical method of relaxations, (b) the method of successive over-relaxations, and (c) random walks.

2.3.2.1. Classical method of relaxations

The classical relaxation method is an iterative process in which solutions for water flow through porous media can be obtained by simply knowing the domain geometry and hydraulic boundary conditions. This method can solve Laplace's equation for a point (node) relative to its surrounding points using an algebraic finite difference equation. For this procedure, a square mesh with dimensions of $\delta_x = \delta_y$ is drawn in the flow zone if the medium is homogenous and isotropic (similar to those in **Figure 11a** and **b**), and a rectangular mesh with dimensions of $\delta_x \neq \delta_y$ is drawn if the medium is anisotropic. The intersections of the squares or rectangles constitute the nodes of the mesh. For these nodes, approximate values of the hydraulic head or potential h (points where h requires to be calculated) must be assigned while respecting the known values of h in the flow boundaries. These values usually correspond to the upper and lower water levels or the upstream water level and downstream water level of the problem at hand. The values assigned in the nodes are arbitrary and can be zero or the result of a reasonable estimation. However, although there are several techniques that can be used to ensure that the value of the potential imposed on the nodes where h is not known is as accurate as possible (Young, 1950), it is important to verify the precision of the assigned data manually by calculating the residue in each node [28]. For example, the difference between the hydraulic potential of the four surrounding nodes is calculated with regard to the central or interior node and so on. Therefore, the relaxation procedure involves the systematic refinement of this residue throughout the grid until the residue in all mesh nodes of interest is zero or practically zero. This value indicates that the Laplace's equation in the study domain has been fulfilled, and therefore, the flow problem has been solved for a certain water flow problem. A disadvantage of the method of relaxations is that it is based on assigning arbitrary values to the nodes in the study mesh, which makes it difficult for the residuals to equal zero at an early stage of calculation. As a result, additional steps of reassigning values are generally necessary, which makes the method long and laborious in practice.

2.3.2.2. Technique of successive over-relaxation

The technique of successive over-relaxation (SOR) [15] is a modification of the classical method of relaxations in which the process of residual refinement at the nodes is automatic because it utilizes the Gauss-Seidel iterative method (**Figure 12**); this makes it possible to obtain residuals of zero or nearly zero at all the nodes, which allows water flow problems to be solved relatively quickly and easily [29, 30]. An additional significant advantage of the SOR method is that it can solve the so-called free surface problems (or unconfined flow problems), in which the position of the free (or phreatic) surface must be determined to solve the problem. Other improvements to the SOR method have been developed for this type of problem, including (a) the Baiocchi's solution [21] and (b) the extended pressure method [31, 22]. The former method helps to determine the position of the phreatic surface (upper flow line for steady-state flow)

in a homogeneous medium (**Figure 10**), and the latter method helps to determine this line in both homogeneous and heterogeneous media (**Figure 11**) [14].

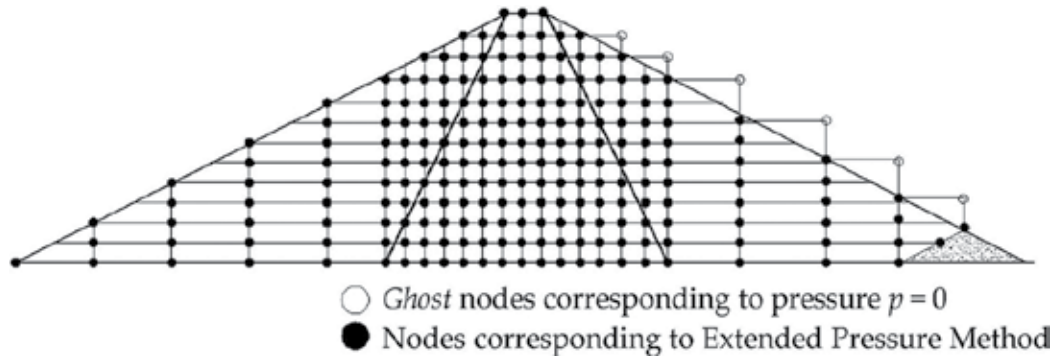


Figure 12. Schematic arrangement of nodes in the dam of graded materials in **Figure 11** using the extended pressure method [23].

2.3.3. Random walks

The random walk method (RWM) consists of studying the movements of a particle that travels in a random way over the nodes of a mesh of a flow domain (**Figure 13a and b**), which allows the hydraulic head to be determined at points of interest by numerical solution of the Laplace’s equation in terms of finite differences. This method relies on the so-called Monte Carlo techniques [32, 33], which are an alternative to the usual methods of water flow analysis. Specifically, the method generates a series of random trajectories (via random numbers) that start from node p_0 in the mesh. Thus, the particle moves randomly through the interior nodes of the mesh and stops when it reaches a boundary node, which is called an absorbent node, because the value of the hydraulic head at that node is known (imposed boundary condition). A complete trajectory is made up of a sequence of nodes, and the last node is an absorbent node. The hydraulic head is then determined by counting the number of trajectories that end at different boundaries, multiplying them by the value of the hydraulic head at the respective boundary and dividing the result by the total number of trajectories. This procedure is repeated several times, and the results are an unbiased measure of the hydraulic head at the node of interest:

$$h_0 = \frac{n_1 f_1 + n_2 f_2}{n_1 + n_2} \tag{11}$$

where h_0 = hydraulic head calculated at point p_0 (**Figure 13b**), f_1 and f_2 = boundaries with known hydraulic heads, and n_1 and n_2 = number of trajectories that reach boundaries 1 and 2, respectively.

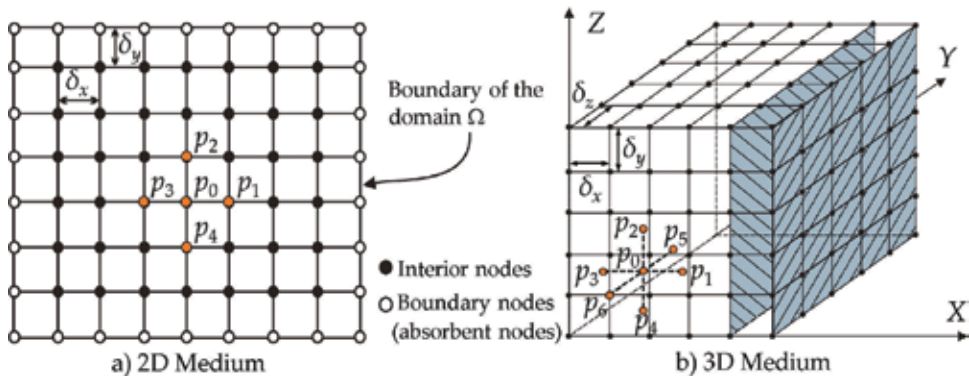


Figure 13. 2D and 3D meshes with which the homogeneous and isotropic flow regions are modelled by the random walk method [24].

The RWM has been utilized to solve confined water flow problems [33] and also to calculate the equivalent permeability $k_{equivalent}$ in simulated heterogeneous media (Figure 14) [24]:

- 1D water flow analysis → $k_{equivalent}$ is the harmonic mean
- 2D water flow analysis → $k_{equivalent}$ is the geometric mean
- 3D water flow analysis → $k_{equivalent}$ tends to the arithmetic mean

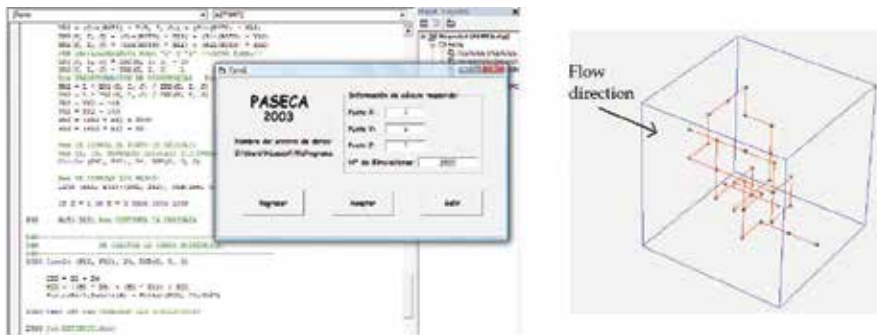


Figure 14. Example of a random walk with the PASECA-2003 algorithm [24].

2.4. Stochastic solutions

The uncertainty due to the spatial variation of permeability is the most important factor that must be taken into account in the analysis of water flow through soils. Figure 15 summarizes the main techniques that are used to evaluate the propagation of this uncertainty. It is common to utilize probabilistic techniques in combination with numerical methods, such as finite elements (FEM), finite differences (FDM), integral equations (BEM), and random walks (RWM). A stochastic analysis permits a more realistic evaluation of water flow problems and can be useful in defining zones of uncertainty, which can be used to identify the parts of the

flow region that are prone to significant variations in properties such as the hydraulic head and hydraulic gradient, as is illustrated in **Figures 16 and 17**, respectively, [24]

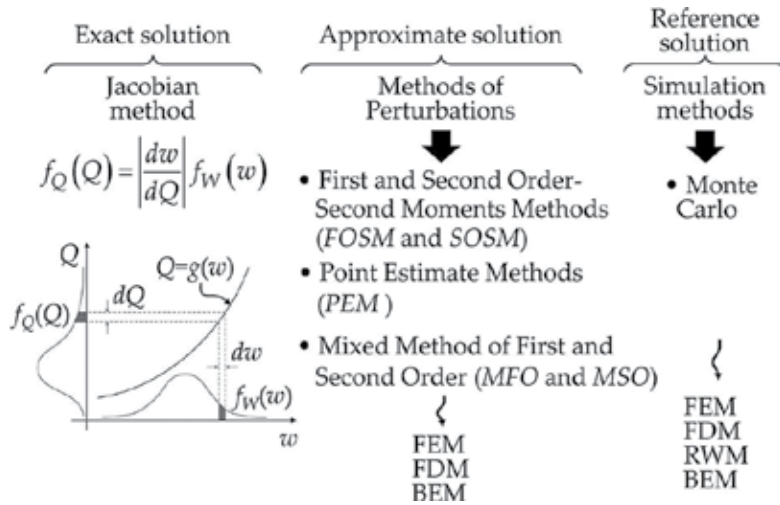


Figure 15. A summary of the main techniques that are used to evaluate uncertainty in water flow analyses [24].

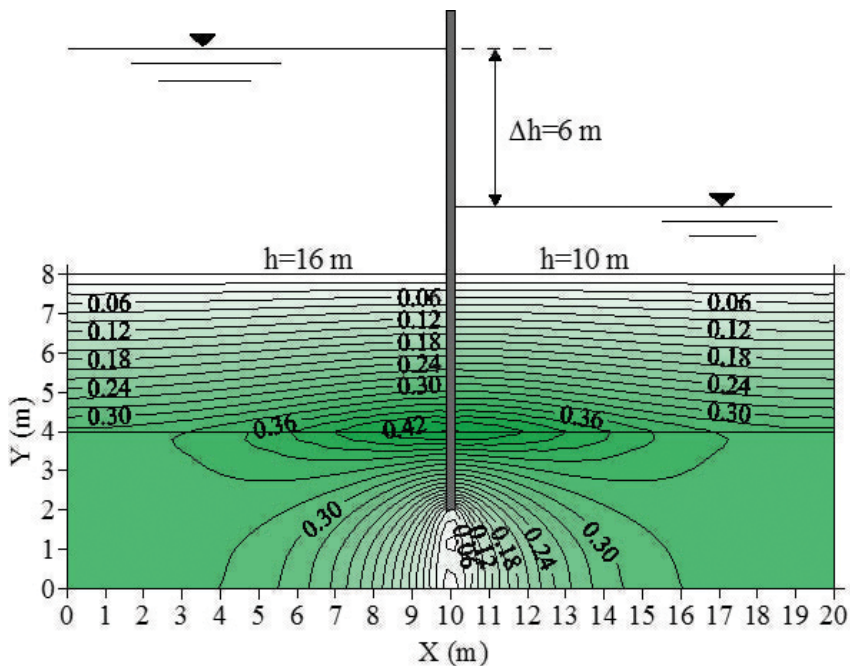


Figure 16. Standard deviation of the hydraulic head (m) under a sheet pile in a medium of two stratified isotropic materials [24].

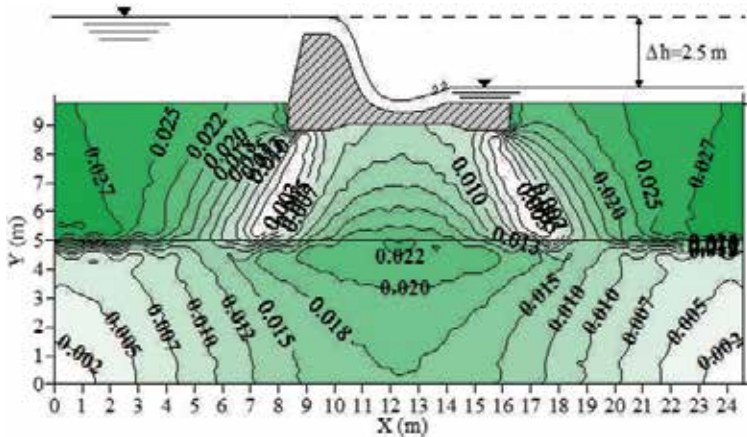


Figure 17. Standard deviation of the (dimensionless) hydraulic gradient under a spillway structure in a medium of two stratified isotropic materials [24].

3. Computer programs and general recommendations for different types of analysis

Numerical techniques are currently preferred because of their ability to solve complex problems in which Eqs. (2) and (5) can be generalized to heterogeneous media with anisotropic materials and boundary conditions of variable complexity [34, 35]. The general methodology for performing a steady- or transient-state water flow analysis is illustrated in **Figure 18**, which shows that some of the most important data for performing water flow analysis are the hydraulic parameters of the materials, which must be obtained from field or laboratory tests that unfortunately are not always carried out because of time or cost. In addition, some tests require specialized personnel and equipment, such as the tests to determine the hydraulic parameters of unsaturated materials, including the soil–water characteristic curve (SWCC). The necessary hydraulic functions of the soil for analyzing unsaturated soils are as follows:

- *The water retention curve (Figure 27)* is also known as the *soil–water characteristic curve (SWCC)* depending on whether the suction is expressed in terms of the degree of saturation or the volumetric water content, respectively. The SWCC is broadly defined as the relationship between the amount of water in the soil and soil suction.
- *The hydraulic conductivity function (Figure 28)* represents the suction as a function of the permeability.

Figures 19 and **20** show several general considerations for different types of water flow analyses, which can be performed relatively easily and rapidly using any of the existing specialized algorithms. **Figure 21** summarizes some of the most popular programs that are used to numerically solve water flow problems. One benefit of computer programs is their

ability to facilitate the study of transient flow and unsaturated soil conditions, which are difficult and laborious to solve analytically.

Several programs for water flow analysis consider soil classification systems that are different from the Unified Soil Classification System (USCS, which is commonly used in geology, soil mechanics, and geotechnical engineering) because they involve parameters that are used to study unsaturated soils, such as:

- HYPRES database = Hydraulic Properties of European Soils
- USDA = United States Department of Agriculture
- STARING = Dutch 'Winand Staring Soil Series'

These systems imply that it is not advisable to use only the standard parameters that the computer programs include for certain types of materials (e.g., sand, clay, silt) because of the variations in the characteristics of soils (European, USA, or Dutch). It is preferable to assign the necessary hydraulic parameters based on the type of analysis and use values that are obtained from laboratory or field tests of the materials of the earth structure or soil that is being studied. In recent years, a comprehensive database that contains the hydraulic parameters of different types of soils from around the world has been developed [36]. Additionally, some algorithms [27] use granulometric curves as well as the index properties of the materials in the flow region and various mathematical expressions to estimate the hydraulic functions that are needed for the analyses (**Figures 27** and **28**). Some of the main mathematical models that are used to obtain the soil hydraulic functions are as follows[37]:

- For the *soil–water characteristic curve* (SWCC)—Brooks and Corey model, Van Genuchten model, Fredlund and Xing model, Aubertin et al. model (modified from Kovacs model) [38–42].
- For the *hydraulic conductivity function*—Brooks and Corey model, Van Genuchten model, Fredlund and Xing model [38–40].

Figures 25–31 show a case of the analysis of water flow through a cofferdam for *La Yesca* dam in Mexico composed of graduated materials assuming that the soil in one part of the cofferdam is partially saturated [37].

The PLAXFLOW algorithm [25] solves transient-state flow problems using the finite element method (FEM) by means of an approximate solution to Eq. (5) and by representing the flow in unsaturated soils with the *Van Genuchten* model. This algorithm performs analyses of transient-state flow in two different ways (**Figure 22**): (a) with step-wise conditions, in which each phase is defined by constant boundary conditions; that is, each time period is associated with a certain water level and (b) with time-dependent conditions, in which the continuous variation of the water level is explicitly considered as a function of time, which can be represented by linear functions, harmonic functions, or data in tables.

Figures 23 and **24** show the results of water drawdown analyses that were carried out using the SEEP/W [26] and PLAXFLOW [25] algorithms, respectively [35, 43].

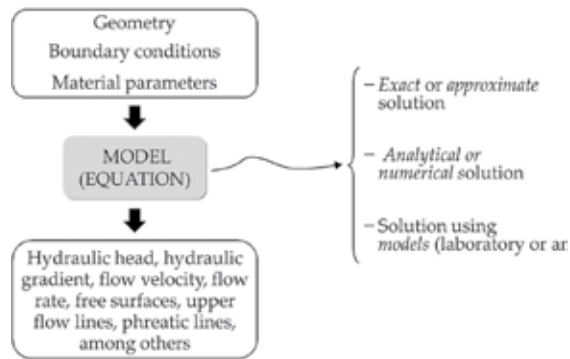


Figure 18. General methodology for steady- or transient-state flow analyses.

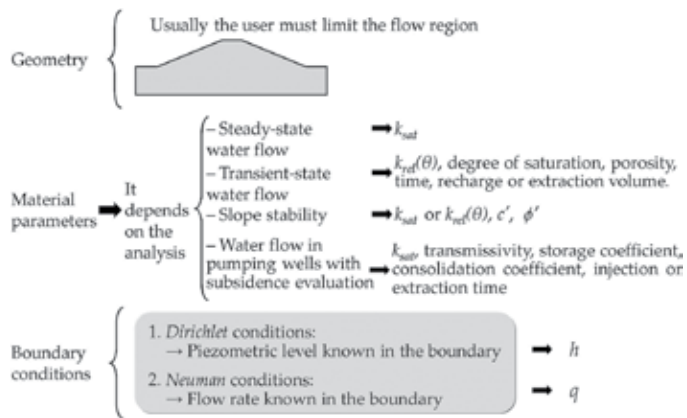


Figure 19. Data for water analyses.

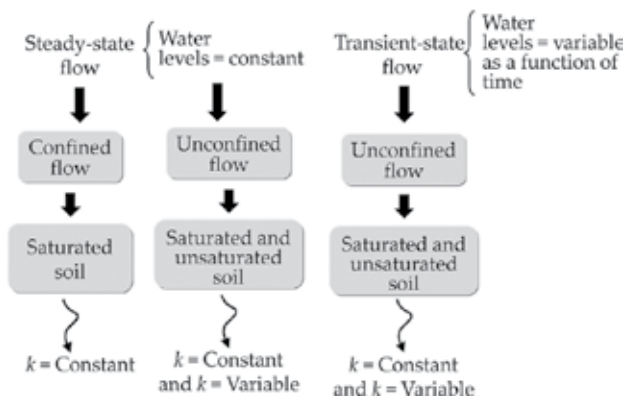


Figure 20. General considerations for different types of water flow analyses.

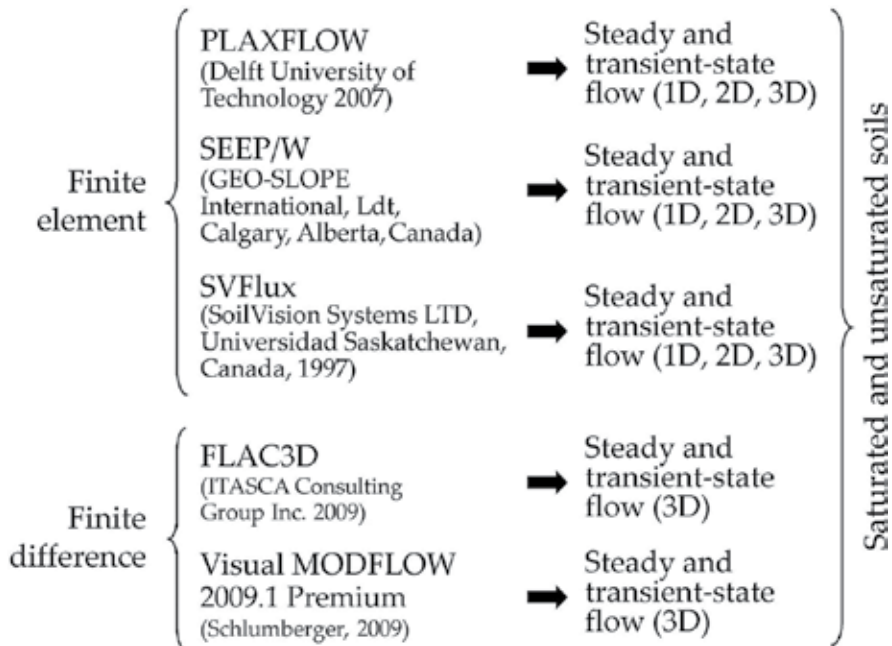


Figure 21. Some algorithms for the numerical modelling of groundwater flow.

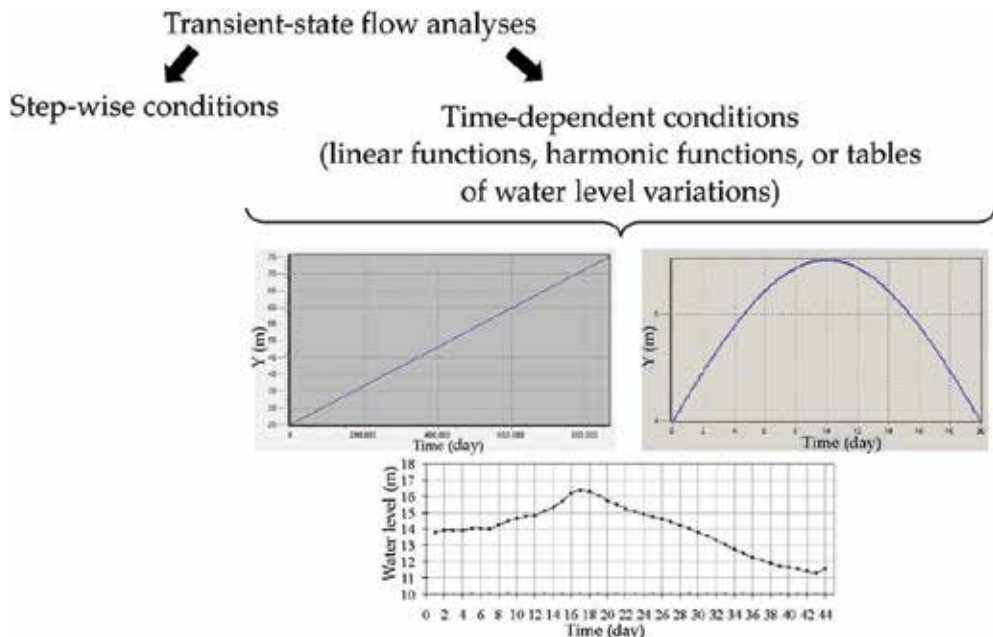


Figure 22. Types of transient flow analyses with the PLAXFLOW algorithm [25].

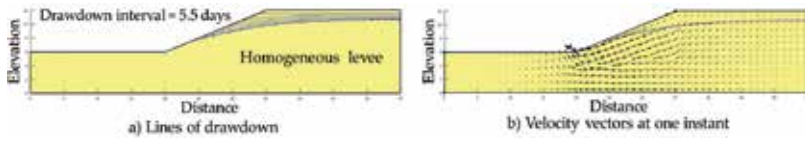


Figure 23. Results of a drawdown analysis [43] using the SEEP/W algorithm [26].

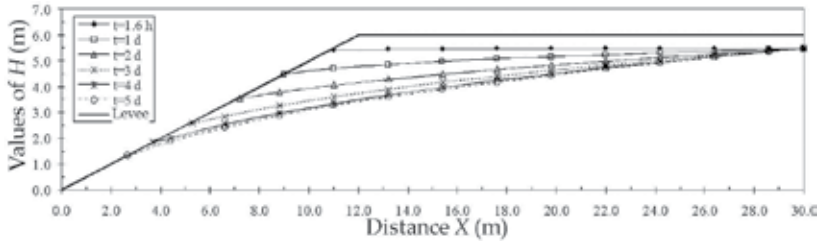


Figure 24. Lines of drawdown at different times during a water drawdown [35] obtained using the PLAXFLOW algorithm [25].

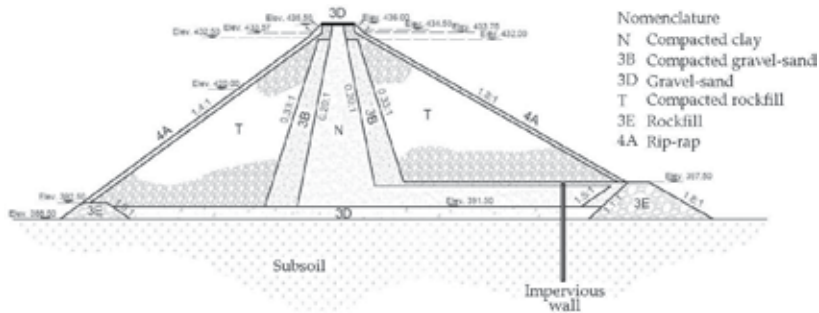


Figure 25. Geometry and materials of a cofferdam for La Yesca Dam in Mexico [37].

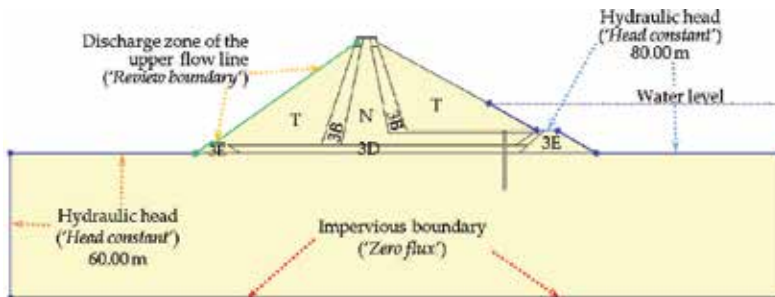


Figure 26. Boundary conditions for numerical analysis of the cofferdam for La Yesca dam in Mexico [37].

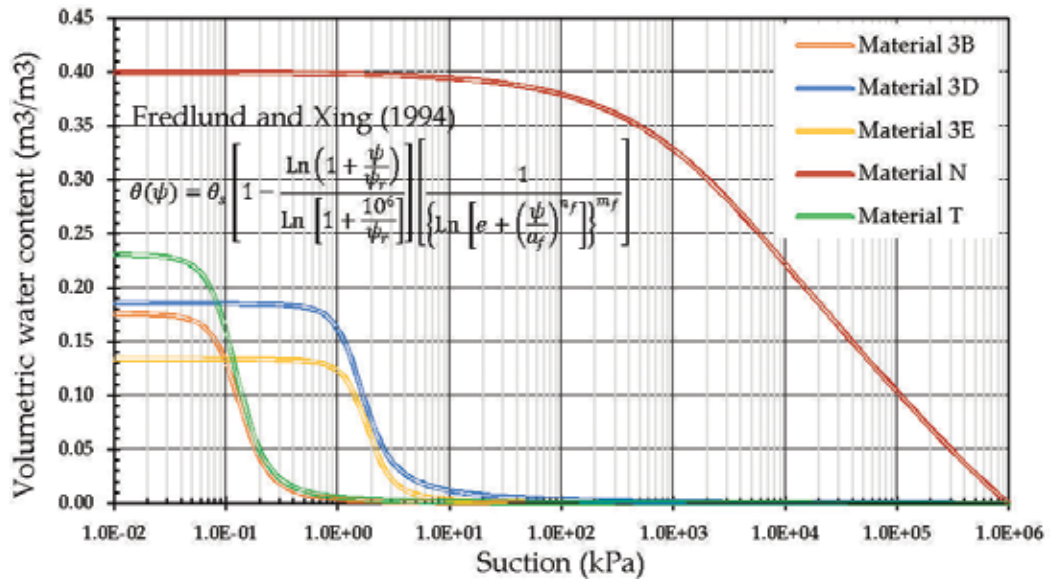


Figure 27. Characteristic curves for materials from the cofferdam for La Yesca Dam in Mexico, used in this analysis [37].

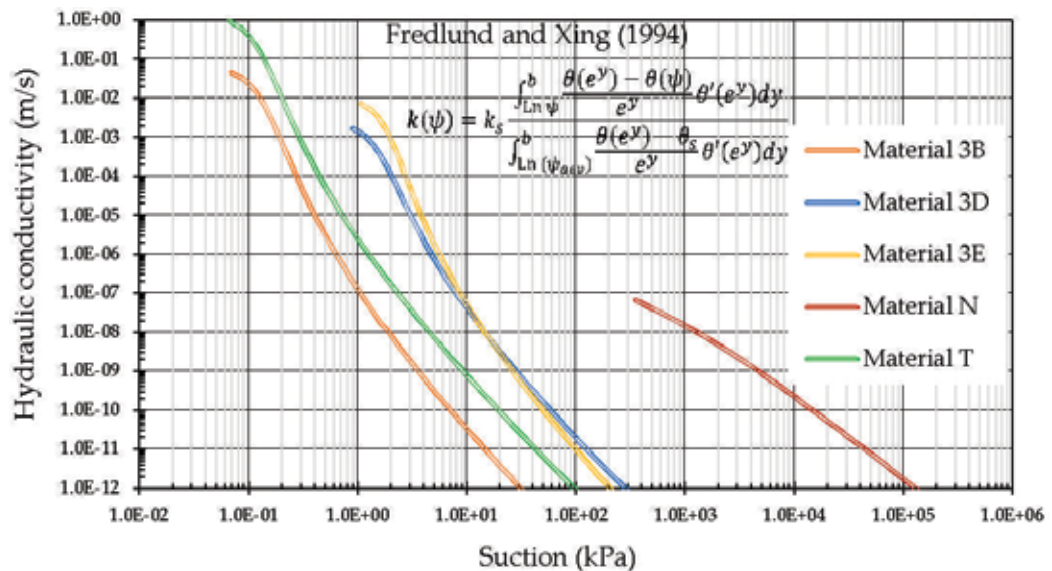


Figure 28. Hydraulic conductivity functions utilized in the numerical model of the cofferdam for La Yesca Dam in Mexico [37].

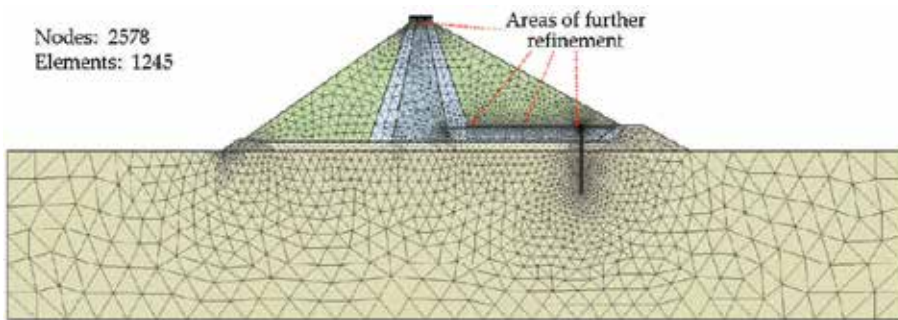


Figure 29. Finite element mesh [37] generated with the SVFlux algorithm [27].

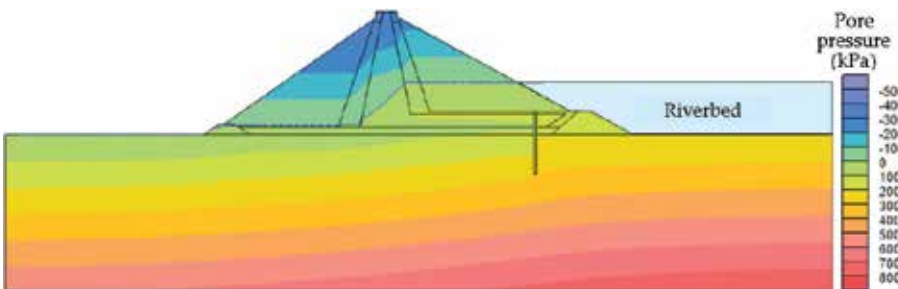


Figure 30. Distribution of the pore water pressure [37] calculated using the SVFlux algorithm 27.

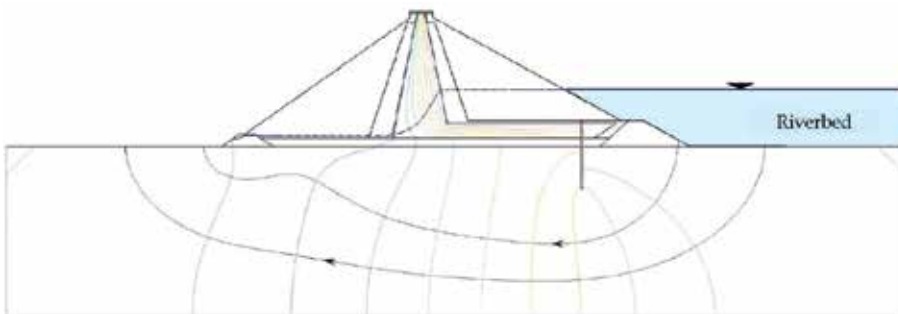


Figure 31. Flow net [37] obtained using the SVFlux algorithm [27].

4. Conclusions

An exact analytical solution of a water flow problem is generally only possible to obtain when the geometry of the flux domain and the hydraulic and boundary conditions are simple

(isotropic and homogeneous media). Exact solutions are difficult and impractical to obtain in the case of the most complex flow problems, such as those in practical geotechnical engineering. In consequence, approximate solutions are usually sought. Numerical techniques are currently preferred over other methods due to their ability to solve complex problems in which the equations for water flow analyses can be generalized to heterogeneous media with anisotropic materials and boundary conditions of varying complexity. However, more sophisticated analyses require the use of a greater number of material parameters, which involves laboratory and field testing that require specialized knowledge and personnel. A series of mathematical models is available to approximate these material parameters. However, the results of numerical analysis should be compared to measurements from monitoring (field instrumentation) of the structures being studied.

Some important comments about the numerical analyses of water flow are as follows:

- In 3D groundwater flow analyses, the use of finite difference equations requires less computational time than the 3D finite element method.
- Computer programs facilitate analyses of transient flow and unsaturated soil conditions, which are difficult and laborious to solve analytically.
- Computer programs cannot replace the good judgment of an engineer.

Author details

Norma Patricia López-Acosta

Address all correspondence to: nlopeza@iingen.unam.mx

Institute of Engineering, Nacional University of Mexico (UNAM), Mexico City, Mexico

References

- [1] Richards L. A. Capillary conduction of liquids through porous medium. *Journal of Physics*. 1931;1:318–333.
- [2] Fredlund D. G, Morgenstern N. R. Constitutive relations for volume change in unsaturated soils. *Canadian Geotechnical Journal*. 1976;13:261–276.
- [3] Fredlund D. G, Morgenstern N. R. Stress state variables for unsaturated soils. *ASCE*. 1977;103:447–464.
- [4] Darcy H. *Les fontaines publiques de la ville de Dijon*. 1st ed. Paris: Victor Dalmont; 1856. 647 p.

- [5] López-Acosta N. P, Auvinet G. Manual design of civil works (chapter B.2.4: behaviour of unsaturated soils and applications). 1st ed. México, DF: Federal Commission of Electricity (Mexico); 2012. 257 p. (in Spanish).
- [6] Espinoza R. D. Numerical analysis of unsaturated flow [dissertation]. Indiana, USA: Faculty of Purdue University; 1993.
- [7] Flores R. Water flow through soils. 4th ed. Mexico DF: Mexican Association of Hydraulics and Mexican Institute of Water Technology; 2000. 256p. (in Spanish).
- [8] Harr M. E. Groundwater and seepage. 1st ed. School of Civil Engineering, Purdue University: Dover publication, Inc; Mineola, New York, 1962. 321 p.
- [9] Panov D. J. Formulas for the numerical solution of partial differential equations by the method of differences. 1st ed. New York: Frederick Ungar Publishing Co; 1963. 133 p.
- [10] Spiegel M. R. Theory of problems of complex variables with an introduction of conformal mapping and its applications. New York: Schaum Publishing Co; 1964.
- [11] Polubarinova-Kochina P. Y. A. Theory of the motion of groundwater. 1st ed. New Jersey: Princeton University Press; 1962. 640 p.
- [12] Shehata A. K. Design of downstream blanket for overflow spillway founded on complex formations. *Journal of Applied Sciences Research*. 2006;2(12):1217–1227.
- [13] Mishra G. C, Singh A. K. Seepage through a levee, technical notes. *International Journal of Geomechanics, ASCE*. 2005;5:74–79.
- [14] López-Acosta N. P, González, J. L. Study of water flow in dams using successive overrelaxations. *Water Technology and Sciences (Tecnología y Ciencias del Agua)*. 2015;6(5):43–58.
- [15] Young D. Iterative methods for solving partial difference equations of elliptic type [dissertation]. Massachusetts: Harvard University; 1950. 74 p.
- [16] Dupuit, J. Etudes théoriques et pratiques sur le mouvement des eaux dans les canaux découverts et à travers les terrains perméables (Theoretical and practical studies of the movement of water in open channels through permeable media). 1st ed. Paris: Dunod; 1863. 304 p.
- [17] Kozeny J. Grundwasserbewegung bei freiem Spiegel, Fluss-und Kanalversickerung-Nasserkraft und Wasserwirtschaft (Groundwater movement with free surface in channels and hydroelectric energy by seepage in channels). *Wasserkraft und Wasserwirtschaft*. 1931;3:28–31.
- [18] Schaffernak F. Uber die Standsicherheit durchlaessiger geschuetteter Dämme (Regarding the stability of permeable draining dams). *Allgemeine Bauzeitung*. 1917;82:S.73.
- [19] Van Iterson F F Th. Eenige Theoretische Beschouwingen over Kwel (Some theoretical considerations about seepage). *De Ingenieur*. 1916,1917;3:629–633.

- [20] Casagrande L. Naeherungsmethoden zur Bestimmung von Art und Menge der Sickerung durch geschuettete Dämme (Approximate methods to determine the seepage through spillway dams) [dissertation]. Vienna: Institute of Technology; 1932.
- [21] Baiocchi C. Sur un problème a frontière libre traduisant le filtrage de liquides à travers des milieux poreux. C. R. Academie des Sciences. Paris. 1971;273:1215–1217.
- [22] Bardet J. P, Tobita T. A practical method for solving free-surface seepage problems. Computers and Geotechnics. 2002;29:451–475.
- [23] González J. L, López-Acosta N. P. Application of the successive over-relaxation technique to confined and unconfined water flow problems. In: Mexican Society for Geotechnical Engineering, editor. Proceedings of the 27th National Meeting on Geotechnical Engineering; November 20–21th; Puerto Vallarta, Jalisco. Mexico: Mexican Society for Geotechnical Engineering; 2014 (in Spanish).
- [24] López-Acosta N. P. Uncertainty in analyses of water flow in soils [dissertation]. Mexico DF: Faculty of Engineering, National University of Mexico (UNAM); 2010. 311 p. (in Spanish).
- [25] Delft University of Technology and Plaxis bv. PLAXFLOW Version 1.6. Scientific Manual. 1st ed. The Netherlands: Plaxis bv; 2008. 20 p.
- [26] SEEP/W-2007. Scientific Manual: Seepage modeling with SEEP/W 2007. 3rd ed. Calgary: GEO-SLOPE International; 2008. 317 p.
- [27] Thode R, Gitirana G. Theory manual of saturated/unsaturated finite element. 2D/3D seepage modeling. 1st ed. Saskatoon: SVFlux, SoilVision Systems Ltd; 2014. 217 p.
- [28] Juárez-Badillo E, Rico A. Water flow in soils. Soil mechanics volume 3 ed. Mexico DF: Limusa; 1972. 414 p. (in Spanish).
- [29] Allen N. de G. Relaxation methods in engineering and science. 1st ed. United States: Mc. Graw Hill Inc; New York, 1954. 257 p.
- [30] Finnemore E. J, Perry B. Seepage through an earth dam computed by the relaxation technique. Water Resources Research. 1968;4:1059–1067.
- [31] Brezis H, Kinderlehrer D, Stampacchia G. Sur une nouvelle formulation du problème de l'écoulement à travers une digue. C. R. Academie des Sciences Paris. 1979;287:711–714.
- [32] Marsal R. J, Reséndiz D. Chapter 6 of the book Fundamentals of design and construction of earth and rockfill dams. 1st ed. Mexico DF: Instituto de Ingeniería (UNAM); 1968. 57 p. (in Spanish).
- [33] Auvinet G. Chapter 6: Monte Carlo techniques. In: Marsal, R. J, editors. Earth and rockfill dams. 1st ed. México DF: Limusa; 1975. 123–131 pp. (in Spanish).

- [34] Lam L, Fredlund D. G, Barbour S. L. Transient seepage model for saturated/unsaturated soil systems: a geotechnical engineering approach. *Canadian Geotechnical Journal*. 1987;24:565–580.
- [35] Auvinet G, López-Acosta N. P. Rapid drawdown condition in submerged slopes. In: Mexican Society for Geotechnical Engineering (SMIG) and Institute of Engineering (UNAM), editors. 15 Presentations of Friends and Colleagues in the Tribute to Jesús Alberro. 1st ed. Mexico DF: Mexican Society for Geotechnical Engineering (SMIG); 2010. 167–189 pp. (in Spanish).
- [36] Fredlund M. Theory manual: a knowledge-based databases system for saturated/unsaturated soil properties. 1st ed. Saskatoon, Saskatchewan, Canada: SoilVision Systems Ltd; 2011. 217 p.
- [37] Mendoza-Promotor J. A. Contribution to the analyses of water flow in unsaturated soils [thesis]. Mexico, D.F: School of Engineering and Architecture (IPN); 2014. 172 p. (in Spanish).
- [38] Brooks R. H, Corey A. T. Hydraulic properties of porous media. *Hydrology Papers*. 1964;3:1–36.
- [39] Van Genuchten M. Th. A closed form-equation for predicting the hydraulic conductivity of unsaturated soils. *Journal of Soil Science Society of America*. 1980;44:892–898.
- [40] Fredlund D. G, Xing A. Equations for the soil-water characteristic curve. *Canadian Geotechnical Journal*. 1994;31(3):521–532.
- [41] Aubertin M, Mbonimpa M, Bussi re B, Chapuis R. P. A model to predict the water retention curve from basic geotechnical properties. *Canadian Geotechnical Journal*. 2003;40(6):1104–1122.
- [42] Kovacs G. Seepage hydraulics (developments in water science). 1st ed. House of the Hungarian Academy of Sciences, Budapest, Hungary: Elsevier Scientific Publishing Company; 1981. 729 p.
- [43] S nchez-Sol s M. A. Hydrogeomechanical behaviour of levees under transient-state flow conditions [thesis]. Mexico DF: Faculty of Engineering, National University of Mexico (UNAM); 2013. 153 p. (in Spanish).

Numerical Simulation of Groundwater Flow and Solute Transport in a Karst Aquifer with Conduits

Bill X. Hu and Zexuan Xu

Additional information is available at the end of the chapter

<http://dx.doi.org/10.5772/63766>

Abstract

Numerical simulation of groundwater flow and solute transport in a dual-permeability karst aquifer is a challenging issue, since groundwater flow in karst conduit network can become non-darcian even turbulent flow. The discrete-continuum model is a relatively new modeling method, which accounts for turbulent and laminar flow in karst aquifer. MODFLOW-CFP (Conduit Flow Process) is compared to the MODFLOW, a numerical code based on Darcy law, to evaluate the accuracy in a sub-regional scale karst aquifer. MODFLOW-CFP is more accurate than the MODFLOW when comparing the head simulation results with field measurements. After that, the CFPv2 and UMT3D numerical models are applied in the WKP to establish a sub-regional scale model to simulate chloride transport processes in the last four decades, and to predict contamination development. Numerical simulation results indicate sprayfields are the major chloride source in the study region. Conduit networks significantly control solute transport and contaminant distribution in the study region. Chloride transports through conduits rapidly and spread to several large contamination plumes in a short period. Chloride concentration started to increase in 1980s due to the operation of sparyfield. Solute transport simulation results by discrete-continuum models are more accurate because of the precise description of conduit network.

Keywords: karst aquifer, numerical modeling, discrete-continuum numerical model, conduit flow process, Solute Transport

1. Introduction

Karst aquifer systems underlie approximately 10–20% of the Earth's landmass and supply potable water to nearly 25% of the world's population [1]. In the United States, karst carbo-

nate aquifers supply almost 52% of all bedrock aquifer withdrawals on a yearly basis [2, 3]. Karst aquifers are typically characterized by relatively large void spaces and loose porous media, which make the karst aquifers to be the most productive aquifer systems in the world, for example, the Floridan aquifer in the USA [4]. The open and porous nature of karst aquifers, combined with the dissolution of joints and fractures within carbonates over time, generate complex subsurface conduit systems and dual-permeability flow regimes [5]. Groundwater flow and solute transport processes in conduit networks are generally more rapid than that in the surrounding carbonate porous media due to significantly higher hydraulic conductivity and porosity in the conduit system [6, 7]. As a result, the water and solute interchanges between the conduit and matrix are particularly important in a dual-permeability karst aquifer system. Karst aquifers are particularly vulnerable when one considers the problems of groundwater contamination [8]. During high-flow events, contaminants in the conduit system can be rapidly transported through the aquifer or actively pushed into the carbonate matrix when the water pressure is high in the conduit system. The process is reversed during low-flow events, and contaminants are slowly released from the surrounding matrix into the conduit system [9]. Therefore, groundwater contamination and seawater intrusion in a karst aquifer can persist for a long time because of the retention and release effect between the conduits and matrix domains [10, 11].

Laboratory experiments using physical models with artificial gypsum or sandbox analog were taken to simulate karst groundwater flow and solute transport [12]. Li [13] evaluated the solute transport and retention in a karst aquifer using two categories of laboratory experiments. Faulkner et al. [14] designed a sandbox laboratory experiment to simulate the interaction between conduit and porous medium domain. In addition to laboratory studies, many numerical models have been developed to study groundwater flow and solute transport in dual-permeability systems, as well as chemical reaction and carbonate dissolution in karst aquifers [15]. For example, a limestone dissolution continuum model coupled with conduit flow was proposed to simulate groundwater flow and karst evolution [16]. Lauritzen et al. [17] coupled laminar flow and carbonate dissolution in two-dimensional (2D) pipe networks to study groundwater flow and karst development in a limestone aquifer. Groves and Howard [18] used 2D pipe networks to simulate conduit development processes under laminar flow conditions at field scales, and the simulation method was later extended to turbulent flow by Howard and Groves [19]. Kaufmann and Braun [20] coupled a pipe network with a continuum system to study karst development and indicated that early karstification might be enhanced by the presence of a diffuse flow system.

The coupling of nonlinear or turbulent flow within the conduit network and Darcian laminar flow in the porous medium is a challenging issue in numerical simulation of a dual-permeability karst aquifer [5, 21, 22]. Darcy equation of continuum groundwater flow is applicable for laminar flow in the porous medium that is linear to hydraulic gradient but is not accurate for nonlaminar or turbulent flow in the conduit. Some hybrid discrete-continuum numerical models were developed to couple Darcian flow in the porous medium with nonlaminar channel flow in the conduit, such as carbonate aquifer void evolution (CAVE) [23, 24],

MODFLOW-CFPM1 [21] and CFPv2 [25, 26]. Those discrete-continuum models were also applied and evaluated in a number of studies [22, 27–30].

The solute transport simulation in the discrete-continuum model involves the coupling of 1D solute transport within the conduit network and the 2D/3D solute transport in the porous medium domain. MT3DMS is a widely used modular 3D model to simulate solute transport in a porous medium, which is based on the solution of groundwater flow from MODFLOW simulation [31]. Therefore, MT3DMS is only applicable for solute transport in porous medium aquifer [31]. Spiessl [32] and Spiessl et al. [33] modified the source code of MT3DMS and developed the reactive hybrid transport RUMT3D model. RUMT3D was coupled with CAVE to calculate groundwater flow in the conduits and then solve solute transport equations in the conduit and porous medium domains of a karst aquifer. Reimann et al. [34] enabled MODFLOW-CFP simulation of unsaturated flow in conduits and water exchange between matrix and variably filled conduits. Furthermore, conduit-associated drainable storage (CADS) was added in MODFLOW-CFPM1 and fixed head-limited flow boundary condition in Reimann et al. [25]. Based on those studies, a research version of CFPv2 has been recently developed by Reimann et al. [26] and used in Xu et al. [29] to simulate the flow of laminar and nonlaminar, as well as nitrate-N transport in conduits and matrix with an updated UMT3D. The CFPv2 and UMT3D models were combined to calculate solute advective exchange between conduit and medium, as well as transport process within a porous medium by advection and dispersion.

2. Study site and model setup

The Woodville Karst Plain (WKP) is a geographic area in the south of Tallahassee, Florida, characterized by prominent karst features such as sinking streams, sink holes, submerged caves systems and springs (**Figure 1**). The upper Floridan aquifer is the primary aquifer, which is composed of the Oldsmar to Chattahoochee/St. Marks formations, with the Clayton formation on the bottom and Hawthorn group acting as the confining unit on the top. Groundwater flow is generally from north to south in the Floridan aquifer. The impermeable Hawthorn group is thin or even absent in the Woodville Karst Plain. Rainwater is able to infiltrate easily and quickly, dissolve the limestone structure and then form substantial networks of karst conduits and sinkholes with a substantial amount of water flows. There are enormous springs existed within the WKP, and the three primary spring discharge points for the cave networks are Wakulla Spring, Spring Creek Springs Group and St Marks Spring. **Figure 1** shows the study area and the hydraulic head contours based on field measurements.

A subregional scale MODFLOW-2000 and MT3DMS models of the Woodville Karst Plain is created by Davis et al. [35], which simulated long-term groundwater flow and nitrate transport in the Woodville Karst Plain. The MODFLOW-2000 model by Davis et al. [35] was created based on a previous regional-scale model, which includes the entire north-central Florida and southeast Georgia by Davis and Katz [36]. In the study by Davis et al. [35], large hydraulic conductivity cells are used in the cells of “cave network” to account for flow in submerged

conduits within the Woodville Karst Plain. The simulated heads, flow and transport within the Woodville Karst Plain by Davis et al. [35] match with the observations very well.

In Gallegos et al. [22], the CFPM1 model of the Woodville Karst Plain is based on the MODFLOW-2000 model by Davis et al. [35] and thus very similar from a conceptual standpoint (**Figure 2**). The conceptual model is divided into two layers, which represent the upper Floridan aquifer. Below the two layers are low permeability sediments, which act as a no-flow boundary. The north boundary and south boundary are set as specified head and constant head boundary, respectively. On the other hand, the southeastern boundary acts as a no-flow boundary. The formation of sinkholes, conduits and caves in the Floridan aquifer is due to the dissolution of limestone with water flowing through these karst features. Sand and clay are observed to cover the upper portion of the aquifer (layer 1) as a low hydraulic conductivity unit. The lower portion of the aquifer (layer 2) has relatively higher hydraulic conductivities with little to no infilling. Therefore, most of the karst conduit networks are located in layer 2. In this study, the Floridan aquifer is simulated as a confined aquifer. Discharge is only simulated at outlets of conduit networks as springs, and at the south boundary that represents the shoreline of Gulf of Mexico. Only the discharges of three springs are simulated in the numerical model: Wakulla Spring, Spring Creek Springs Group and St Marks Spring.

There are 288 rows and 258 columns in the discretization of grid of the subregional CFPM1 model. Model cells are 500 by 500 ft horizontally. The top and bottom of numerical mode are determined from the regional-scale model by Davis and Katz [36]. There are two layers in the CFPM1 model, according to the conceptual model. The upper portion of the upper Floridan aquifer in layer 1 has relatively low hydraulic conductivities. The lower portion of the upper Floridan aquifer in layer 2 has relatively large hydraulic conductivities. The lateral boundaries were set as specified head boundaries in both two layers, except the southeastern portion of the model is set as no-flow boundary. The bottom of lower layer is also considered as a no-flow boundary. Drain package is used to simulate the rivers [37]. Hydraulic conductivity values for the matrix were originally based on the calibrated values from Davis et al. [35]. There are five sources of recharge in the model, including the inflow across lateral boundaries of the model, net precipitation, creek flow into sinkholes, irrigation at sprayfields and discharges from onsite sewage disposal systems (e.g., septic tanks).

In Davis et al. [35], grid cells of submerged conduits and caves are simulated as large values of hydraulic conductivity. The actual mapped caves were only small portions of the high conductivity cells in the model. The remaining very high conductivity cells were placed in their respective locations based on inference from field observations that indicated probable cave locations, which are indicated by tracer tests and the presence of numerous sinkholes due to heavy dissolution in the subsurface. The high tannic flows at lost Creek Sink resulting in flows of dark water at Spring Creek Springs Group also indicate indicating a hydraulic connection between Wakulla Springs and the Spring Creek Springs Group [35, 38, 39]. Cave diver observations found that the water was flowing southward at the southernmost tip of the explored Wakulla caves system.

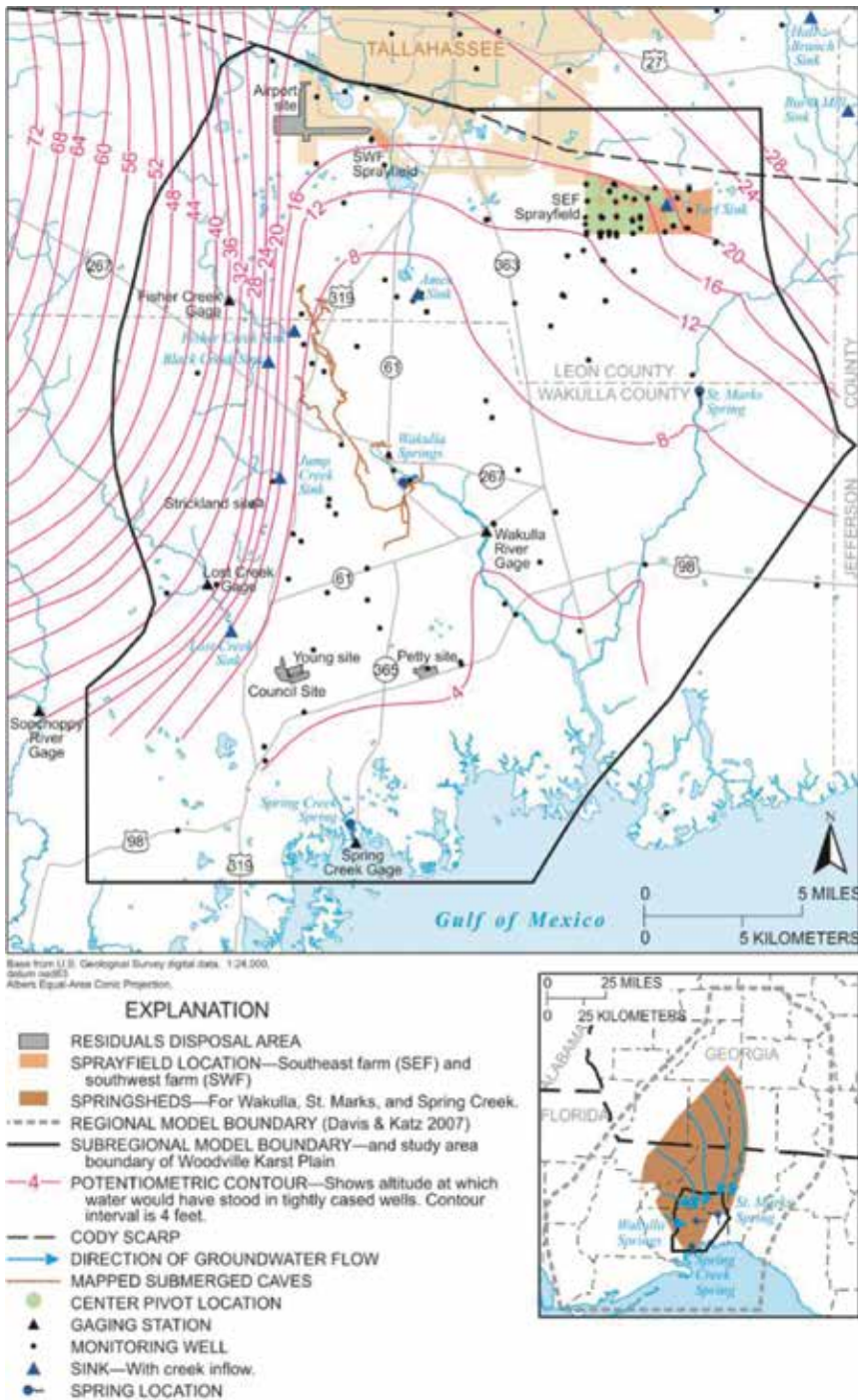


Figure 1. Subregional model boundary of the Woodville Karst Plain. Modified from Davis et al. [35].

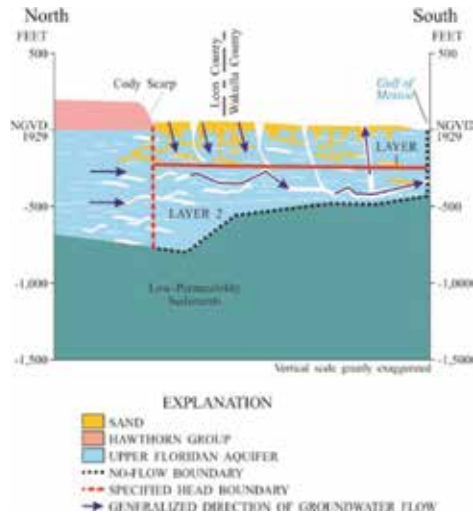


Figure 2. Conceptual model of the Woodville Karst Plain subregional model. Modified from Davis et al. [35].

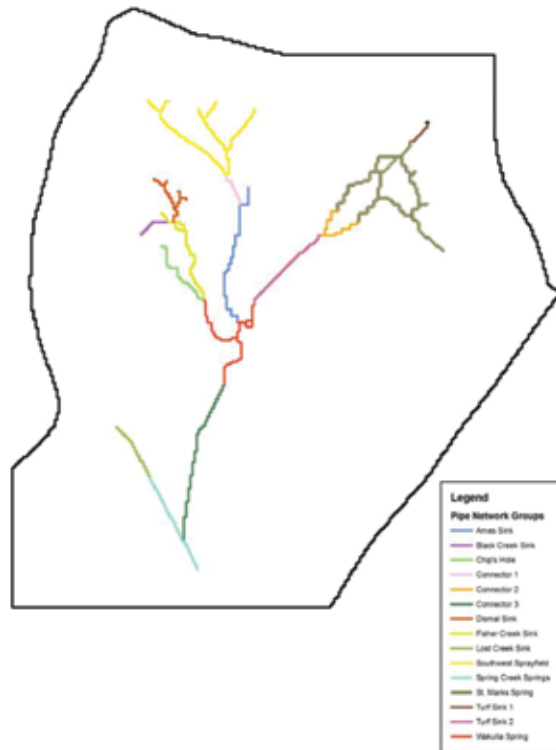


Figure 3. Pipe network in the CFPM1 subregional model of the Woodville Karst Plain. Modified from Gallegos et al. [22].

There are 37 miles explored and mapped conduit networks by cave divers that connect to Wakulla spring [35, 38], which is shown as the brown lines in **Figure 1**. However, the conduit network distribution in the WKP is extended and connected with numerous springs and sinks, including Wakulla Spring, Spring Creeks Springs, Lost Sink, etc. In Gallegos et al. [22], a pipe network showing in **Figure 3** was created using CFPM1 to replace the very high hydraulic conductivity cells from the study of Davis et al. [35]. For the sake of comparison between the CFPM1 and MODFLOW-2000 models, the discrete pipes and nodes of conduit were placed in the exact same cells in layer 2 as the cells with large hydraulic conductivity values in the original MODFLOW-2000 model. In CFPM1 model, conductivity values of the high hydraulic conductivity cells were assigned to be the same as the surrounding hydraulic conductivity cells. There are 1083 pipe nodes and 1087 pipe segments of the conduit network system in the numerical model. In the discrete model, the conduits were subdivided into discrete pipe network groups, based on the locations of recharge or discharge points such as sinks or springs. Discrete conduit network were assumed to be located at the horizontal and vertical center of the model cells; therefore, pipe nodes were assigned to the center of the cells. Cave divers measured the actual diameters of conduit network within the Wakulla Cave System; however, all other diameters for pipes were estimated during calibration or estimated based on the available field data. Tortuosity was calculated for each major cave segment mapped by the cave divers. The mean height of the pipe wall microtopography (i.e., wall roughness) was assumed to be 0.10. Three major springs, including Wakulla Spring, Spring Creek Springs Group and St. Marks Spring, are set as three pipe nodes of constant head in layer 1.

In the study of Xu et al. [29], effective porosity governs solute advection and dispersion transport simulation. In groundwater flow simulation, MODFLOW calculates groundwater velocity within model cell and assumes that groundwater fills the entire cells. However, groundwater velocity is calculated at a more realistic rate by introducing the effective porosity, which restricts the groundwater movement to the percentage of the cell. Effective porosity is difficult to assess accurately, especially in karst terrains. The simulated effective porosity for layer 1 is set as uniformly 0.01. An effective porosity of 0.003 in the area was used in entire model cells in layer 2. However, effective porosity is set as 0.03 in area close to the SEF sprayfield, because aquifers there are quite loose and small conduits are so complicated that we cannot only assume the conduit nodes and tubes using several big tubes by discrete pipes to calculate groundwater flow and solute transport.

3. Numerical simulation of groundwater flow in a karst aquifer

3.1. Governing equations of groundwater flow

According to Darcy equation and mass conservation, the 3D continuum equation for groundwater flow in a porous medium including source/sink term is described as follows:

$$\frac{\partial}{\partial x}\left(K_{xx}\frac{\partial h}{\partial x}\right) + \frac{\partial}{\partial y}\left(K_{yy}\frac{\partial h}{\partial y}\right) + \frac{\partial}{\partial z}\left(K_{zz}\frac{\partial h}{\partial z}\right) \pm W = S_s\left(\frac{\partial h}{\partial t}\right) \quad (1)$$

where K_{xx} , K_{yy} and K_{zz} are values for hydraulic conductivity [LT^{-1}] along the x , y , z axis, respectively; h is the hydraulic head [L]; W is the volumetric flux per unit volume [T^{-1}] as sink/source term; S_s is the specific storage [L^{-1}].

Darcy equation is only appropriate for laminar flow with Reynolds number less than 10 but not for nonlaminar or turbulent flow in the conduit [40]. Therefore, Darcy-Weisbach equation is used to simulate groundwater flow in the high permeable karst conduit networks in which a conduit is conceptualized as a pipe,

$$\Delta h = h_L = f \frac{\Delta l V^2}{d 2g} \quad (2)$$

where Δh or h_L is the head loss [L] measured along the pipe length Δl [L]; f is the friction factor [dimensionless]; d is the pipe diameter [L]; V is the mean velocity [LT^{-1}]; g is the gravitational acceleration constant [LT^{-2}].

Darcy-Weisbach equation can be reformulated to solve for volumetric flow rate in the conduit networks by MODFLOW-CFP [21] and CFPv2 [26]. MODFLOW-CFP and CFPv2 are able to solve nonsaturated pipe flow but not applied in this study, because all layers are assumed as confined aquifers and conduits are fully saturated. Caves and conduits are defined as a discrete pipe network consisting of cylindrical tubes and nodes within the cells of grid defined in the model. The advective exchanges between porous media and conduit nodes are assumed to be linear with head difference as follows:

$$Q_{ex} = \alpha_{j,i,k} (h_n - h_{j,i,k}) \quad (3)$$

where Q_{ex} is the volumetric flow exchange rate [L^3T^{-1}]; $\alpha_{j,i,k}$ is the pipe conductance at MODFLOW cell j, i, k [L^2T^{-1}]; h_n is the head [L] at pipe node n located at the center of the MODFLOW cell; and $h_{j,i,k}$ is the head [L] in the encompassing MODFLOW cell j, i, k .

3.2. Flow modeling application

The discharges into sinkholes were turned off in the simulation of 1991. The pipe nodes of Wakulla Spring, Spring Creek Springs Group and St Marks Spring are set as constant 5, 0 and 9 ft, respectively. The yearly averaged head values are used for the three springs, respectively. In the 2006 simulation, all discharges into sinkholes were turned on. The pipe node for Wakulla Spring, Spring Creek Springs Group and St Marks Spring were set as constant 5, 9.5 and 9 ft, respectively. After 2006, the flow condition of Spring Creek changed, where freshwater

discharges stopped and water began flowing northward from Spring Creek to Wakulla Spring. Therefore, the head at Spring Creek Springs Group was increased to 9.5 ft as calculated equivalent freshwater head.

The simulated and observed water levels for both the 1991 and 2006 hydraulic head data sets are presented in **Figure 4**. With the exception of two points, simulated hydraulic heads were within the calibration criterion of ± 5 ft. One point of the 1991 data falls outside the calibration criterion limits. This is caused by problematic well that is located in an area where the hydraulic gradient is very steep. The simulated heads also did not fit well within the calibration criterion in Davis et al. [35]. The point of 2006 data falls outside the calibration criterion is located in the sprayfield in the northeast corner of the model, which may have large uncertainty because of the regional flow from north boundary. The residual mean was 1.03 ft with a residual standard deviation of 3.84 ft for the 1991 hydraulic head data set. On the other hand, the residual mean was 0.09 ft with a residual standard deviation of 2.32 ft for the 2006 data set. Generally speaking, simulation results are able to match reasonably well with the observed heads in monitoring wells.

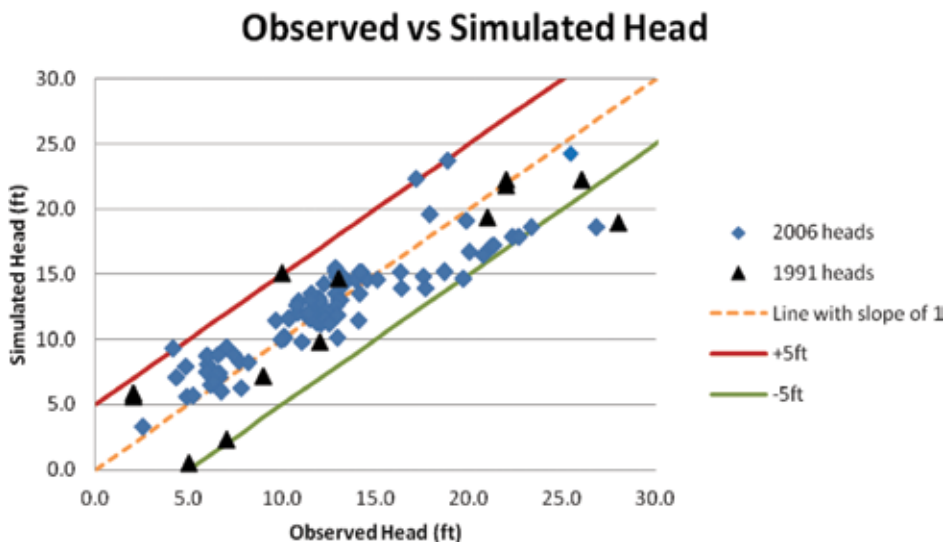


Figure 4. Observed versus simulated heads for the calibrated subregional flow model.

4. Numerical simulation of solute transport in karst aquifer

4.1. Governing equations of solute transport

Solute transport modeling in a porous medium needs to solve groundwater flow advection, molecular diffusion and mechanical dispersion. The second-order partial differential transport

equation that applied in MT3DMS [31, 41] and UMT3D [33] has been simplified as 2D transport equation in this study as follows:

$$\frac{\partial(\theta C)}{\partial t} = \frac{\partial}{\partial x_i} \left(\theta D_{ij} \frac{\partial C}{\partial x_j} \right) - \frac{\partial}{\partial x_i} (\theta v_i C) + q_s C_s \quad (4)$$

where θ is the porosity of the porous medium [dimensionless]; v_i is the seepage or linear pore water velocity [LT^{-1}], which is related to the specific discharge or Darcian flux through the relationship, $v_i = q_i / \theta$; C is the solute concentration [ML^{-3}]; D_{ij} is the hydrodynamic dispersion coefficient tensor [L^2T^{-1}]; C_s is the solute concentration of water entering from sources or flowing out from sinks [ML^{-3}]; q_s is the volumetric flow rate per unit volume of aquifer representing fluid source (positive) and sink (negative) [T^{-1}].

Solute transport in the conduit is describe by the 1D advection equation as well, while mechanic dispersion within the conduit is ignored in the VDFST-CFP model,

$$\frac{\partial C_l}{\partial t} = -q_l \frac{\partial C_l}{\partial x} \quad (5)$$

where C_l is the solute concentration in conduit tube l [ML^{-3}]; q_l is the conduit flow velocity in conduit tube l [LT^{-1}], which could be calculated by volumetric flow rate Q from the Darcy-Weisbach equation [L^3T^{-1}]. It is noted that there are no sink/source terms in the conduit transport equation, because the sink/source terms and exchanges with the surrounding porous media are computed at the conduit nodes only.

Advective exchange rates between a conduit node and the surrounding porous medium cells are determined by the following:

$$K_{ex} = \begin{cases} \frac{Q_{n,ex}^+ C_{i,k}}{V_{i,k}}, Q_{n,ex}^+ > 0 \\ \frac{Q_{n,ex}^+ C_n}{V_{i,k}}, Q_{n,ex}^+ < 0 \end{cases} \quad (6)$$

where $K_{ex,n}$ is the advective exchange rate between a conduit node n and respective matrix cell i, k [$ML^{-3} T^{-1}$]; $Q_{n,ex}^+$ is the exchange flow rate [L^3T^{-1}] at conduit node n ($Q_{n,ex}^+ > 0$, flow direction is from matrix to conduit node; $Q_{n,ex}^+ < 0$, flow direction is from conduit node to matrix); $C_{i,k}$ is the solute concentration of respective cell i, k in the porous medium at conduit node n [ML^{-3}]; C_n is the nodal concentration at conduit node n [ML^{-3}]; $V_{i,k}$ is the volume of respective cell i, k of the porous medium at conduit node n [L^3].

Spiessl et al. [33] pointed out that mass transport within a conduit networks is determined by the flow velocity within the conduits, exchange coefficients between the conduit nodes and porous matrix, the magnitude of conduit sink/source terms and the lengths of conduit tubes. Mathematically, a weighted arithmetic mean of the nodal concentration value C_n [ML⁻³] at conduit node n can be expressed as follows [33]:

$$C_n = \frac{\sum_f^2 Q_{n,l}^{f+} C_{n,l}^f + Q_{n,ex}^+ C_{i,k} + \sum_s Q_{n,s}^+ C_{n,s}}{\sum_f^2 Q_{n,l}^{f+} + Q_{n,ex}^+ + \sum_s Q_{n,s}^+} \quad (7)$$

where superscript f indicates either forward or backward direction of the pipe connected to node n ; $C_{n,l}^f$ is the concentration of tube l connected to face f of the conduit node n [ML⁻³]; $C_{n,s}$ is the concentration of the source or sink term to the conduit node n [ML⁻³]. The superscript + represents the inflow terms at conduit node n , which means that only inflow terms are used to compute the nodal concentration; $Q_{n,l}^{f+}$ is the discharge of tube l connected to face f into the respective conduit node n [L³T⁻¹]; $Q_{n,s}^+$ is the volumetric flow rate of a source term at conduit node n [L³T⁻¹].

4.2. Chloride transport modeling at the WKP

A long-term (1968–2018) chloride transport process is simulated using the coupled CFPv2 and UMT3D models, based on the MODFLOW-2000 numerical simulation in the previous studies. Both the simulated chloride concentrations in some monitoring wells and the extents of chloride plume in the WKP are presented as follows.

Chloride level is significantly affected by the application of sprayfields near the City of Tallahassee. Simulation results and water quality measurements at two monitoring wells near the sprayfields are compared. Chloride concentrations also began to increase from background level of less than 5 mg/L after several months of the west part of SEF sprayfield became operational in 1980 for SE-22 and in 1986 for SE-21 when the east part of SEF sprayfield became operational. The most severe chloride contaminations at wells SE-22 (**Figure 5**, right) can be higher than 35 mg/L in 2000, and chloride concentrations at wells SE-21 (**Figure 5**, left) were also as high as 20 mg/L. Chloride levels continued to increase ever since. Chloride concentrations by simulation in those monitoring wells seem to be stabilized at high concentrations after 2005 to now, and also estimate to keep at this value till 2018. Input from the west boundary is a major chloride source, which also indicates very important groundwater inflow from the west.

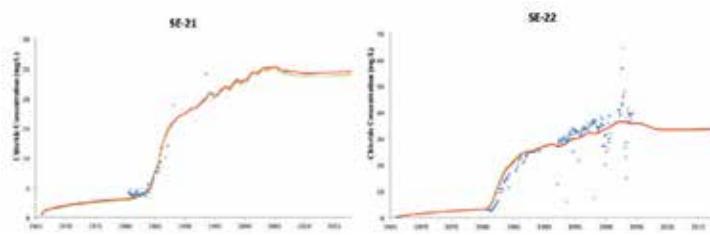


Figure 5. Chloride simulation results at SE-21 and SE-22 monitoring wells near the Tallahassee SEF sprayfield (the concentration scales are different).

Simulated results of chloride concentration distribution in the WKP by the CFPv2 and UMT3D solute transport numerical model at the ends of the years 1967, 1986 and 2004 are discussed in this study. The concentration distributions at end of the model in 2018 as prediction are also included. At the end of 1967, the background chloride level of layer 1 in mainly part of the study site was about 2 mg/L and can be over 10 mg/L in northwest boundary of the study region. In layer 2, high concentration region at northwest and west boundary was much larger than layer 1, but chloride background level is lower than 1 mg/L in most of the region (**Figure 6**, left). Chloride concentration in the area close to SWF sprayfield significantly increased to higher than 5 mg/L in layer 1, which represented the effect of chloride leak from the SWF sprayfield facility and biosolids disposal site (**Figure 6**, right).

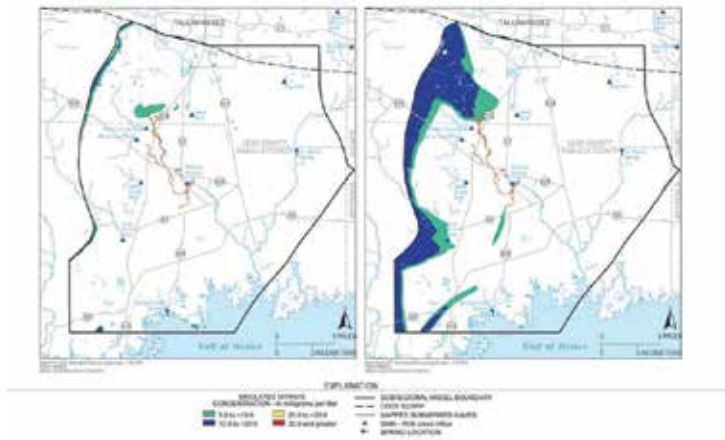


Figure 6. Chloride concentration from the simulation by CFPv2 and UMT3D at the end of 1967 (left: layer 1; right: layer 2).

At the end of 1986, in addition to high chloride level inflow from the northwest boundary, the highest chloride concentration in layer 1 could be about 30 mg/L, had been observed at the SEF sprayfield (**Figure 7**, left). The chloride plumes with concentration higher 5mg/L can be found close to Lost Creek Sink, Wakulla Spring, Jump Creek Sink and Fisher Creek Sink. In layer 2, concentration near the west boundary could be as high as 15 mg/L, decreased to 6 mg/L

L near Wakulla Spring and lower than 3 mg/L at the east boundary (**Figure 7**, right). In the central of the study region, chloride plume area from the sprayfield also increased comparing with 1967 results.

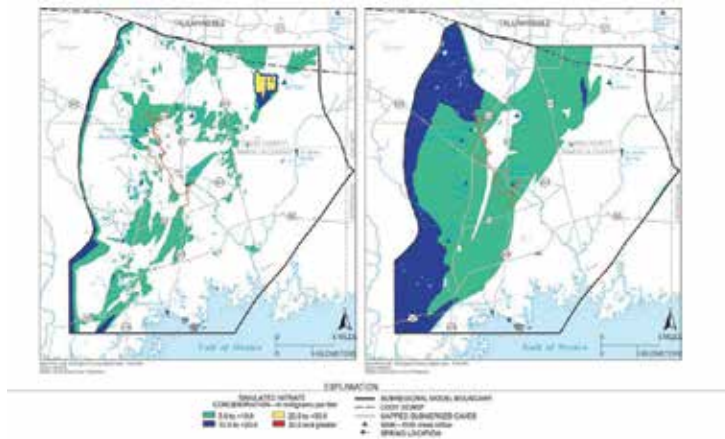


Figure 7. Chloride concentration from the simulation by CFPv2 and UMT3D at the end of 1986 (left: layer 1; right: layer 2).

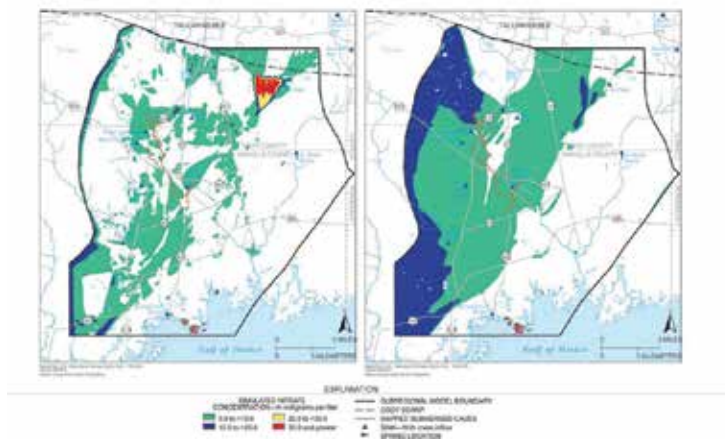


Figure 8. Chloride concentration from the simulation by CFPv2 and UMT3D at the end of 2004 (left: layer 1; right: layer 2).

At the end of 2004, simulated chloride level at the SEF sprayfield decreased to about 12 mg/L, which was much lower than the peak value (**Figure 8**, left). Concentration at the SWF sprayfield was about 5 mg/L due to the sprayfield shutdown. Chloride distribution in 2004 did not change much comparing with the 1986 distribution in the study region, indicated a relatively stable status. In layer 2, chloride plume at the SEF sprayfield was larger than that in 1986 and became

an isolated high concentration zone (**Figure 8**, right). In other parts of the study region, chloride level also decreased from highest at the west boundary to lowest at east, which was similar to the distribution in 1986.

At the end of 2018 as a prediction of future, chloride levels in layer 1 at the SEF and SWF sprayfields keep decreasing since 2004 but are still about 10 mg/L and still higher than surrounding area (**Figure 9**, left). Chloride concentration at Spring Creek Springs is still the highest in the whole study region. In layer 2, chloride concentration in the north of the SWF sprayfield decreases below 5 mg/L because of the flushing effect (**Figure 9**, right). The west part of study region still has higher chloride concentration than the east part.

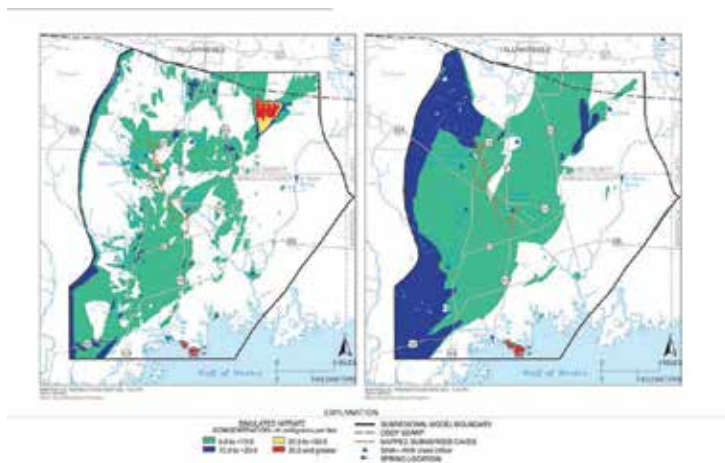


Figure 9. Chloride concentration from the simulation by CFPv2 and UMT3D at the end of 2018 (left: layer 1; right: layer 2).

5. Discussion and conclusion

Groundwater flow in a well-developed karst aquifer is mainly dominated within the fractures, conduits and caves formed and/or enlarged by carbonate dissolution. In general, most groundwater-modeling methods, such as MODFLOW-2000, apply Darcy equation to simulate groundwater flow, in which groundwater flow is laminar in the primary porosity (i.e., matrix porosity) of the aquifer. However, Darcian principle is not applicable in a well-developed karst aquifer due to the dual permeability properties present in the aquifer. Therefore, advanced methodologies, such as the discrete-continuum model, should be used to model groundwater flow in karst aquifers.

The physically based discrete-continuum numerical models are widely applied to simulate groundwater flow and solute transport in a karst aquifer with conduit networks. The CFPM1 is able to accurately simulate groundwater flow in karst aquifers. The major hypothesis of this

study was that CFPM1 would more accurately simulate flow in karst aquifers than MODFLOW-2000 because CFPM1 accounts for turbulent flow, as well as pipe parameters such as pipe diameter, tortuosity, etc. In Gallegos et al. [22], a CFPM1 model of the Woodville Karst Plain was developed based on a previous MODFLOW-2000 model by Davis et al. [35]. Both the CFPM1 and MODFLOW-2000 models are created to run a transient simulation of an actual storm event. The simulated monitoring wells match well with the observations.

The coupled CFPv2 and UMT3D models are able to simulate solute transport in a karst aquifer. Chloride concentration plumes are originated from the sprayfields and extended southward to Wakulla Springs. Sprayfields in the south of Tallahassee and septic tanks in the rural area are the major source of chloride contamination in the WKP. From the monitoring wells observation, chloride concentration started to increased, especially after the SEF sprayfield went into service in 1980s and remained a high value in future prediction. Chloride contamination transported through the conduit network and formed extended plumes far away from the sprayfield. The transport method modified the flow and solute transport within conduits and considered the exchange between conduits and matrix, generated more accurate simulation results due to more precise description of conduits in the model.

Author details

Bill X. Hu^{1,2*} and Zexuan Xu²

*Address all correspondence to: bill.x.hu@gmail.com

1 Department of Ecology, Jinan University, Guangzhou, China

2 Department of Earth, Ocean and Atmospheric Science, Florida State University, Tallahassee, FL, USA

References

- [1] Ford, D.C. and P.W. Williams, *Karst geomorphology and hydrology*. Vol. 601. 1989: Unwin Hyman, London.
- [2] Covington, M.D., et al., *Research in karst: a model for future directions in hydrologic science?* From the Section President, 2011: p. 18.
- [3] Maupin, M.A. and N.L. Barber, *Estimated withdrawals from principal aquifers in the United States, 2000*. 2005: USGS, Reston, Virginia.
- [4] Bush, P.W. and R. Johnson, *Ground-water hydraulics, regional flow, and ground-water development of the Floridan aquifer system in Florida and in parts of Georgia, South Carolina*. 1988: USGS, Denver, Colorado.

- [5] Davis, J.H., *Hydraulic investigation and simulation of ground-water flow in the Upper Floridan aquifer of north central Florida and southwestern Georgia and delineation of contributing areas for selected City of Tallahassee, Florida, Water-Supply Wells*. 1996: U.S. Geological Survey: Tallahassee, Florida. p. 55.
- [6] Ritter, D.F., C.R. Kochel, and J.R. Miller, *Process geomorphology*. 2002: McGraw-Hill. p. 576.
- [7] Scanlon, B.R., et al., *Can we simulate regional groundwater flow in a karst system using equivalent porous media models? Case study, Barton Springs Edwards aquifer, USA*. Journal of Hydrology, 2003. 276(1): pp. 137–158.
- [8] Kuniansky, E.L., *U.S. geological survey karst interest group proceedings, bowling green, Kentucky*. 2008: U.S. Geological Survey Bowling Green, Kentucky. p. 142.
- [9] Martin, J.B. and R.W. Dean, Temperature as a natural tracer of short residence times for groundwater in karst aquifers. In: *Karst modeling*, edited by Arthur N. Palmer, Margaret V. Palmer and Ira D. Sasowsky, 1999: Karst Waters Institute Special Publication, Charlottesville, Virginia. 5: pp. 236–242.
- [10] Green, R.T., et al., *Groundwater contamination in karst terranes*. Water, Air, & Soil Pollution: Focus, 2006. 6(1): pp. 157–170.
- [11] Katz, B.G., A.R. Chelette, and T.R. Pratt, *Use of chemical and isotopic tracers to assess nitrate contamination and ground-water age, Woodville Karst Plain, USA*. Journal of Hydrology, 2004. 289(1): pp. 36–61.
- [12] Ford, D., S. Lauritzen, and R. Ewers, Hardware and software modeling of initial conduit development in karst rocks. In: *Speleogenesis: evolution of karst aquifers*. 2000. National Speleological Society, Huntsville. pp. 175–183.
- [13] Li, G., *Laboratory simulation of solute transport and retention in a karst aquifer*. Ph.D dissertation, Florida State University, 2004.
- [14] Faulkner, J., et al., *Laboratory analog and numerical study of groundwater flow and solute transport in a karst aquifer with conduit and matrix domains*. Journal of Contaminant Hydrology, 2009. 110(1): pp. 34–44.
- [15] Bakalowicz, M., *Karst groundwater: a challenge for new resources*. Hydrogeology Journal, 2005. 13(1): pp. 148–160.
- [16] Dreybrodt, W., *Processes in karst systems, physics, chemistry, and geology*. 1988: Springer-Verlag, Berlin Heidelberg.
- [17] Lauritzen, S.-E., N. Odling, and J. Petersen. Modeling the evolution of channel networks in carbonate rocks. In: *ISRM Symposium: Eurock*. 1992: ISRM Symposium, Chester, UK, September 1992.
- [18] Groves, C.G. and A.D. Howard, *Early development of karst systems: 1. Preferential flow path enlargement under laminar flow*. Water Resources Research, 1994. 30(10): pp. 2837–2846.

- [19] Howard, A.D. and C.G. Groves, *Early development of karst systems: 2. Turbulent flow*. Water Resources Research, 1995. 31(1): pp. 19–26.
- [20] Kaufmann, G. and J. Braun, *Karst aquifer evolution in fractured, porous rocks*. Water Resources Research, 2000. 36(6): pp. 1381–1391.
- [21] Shoemaker, W.B., et al., *Documentation of a conduit flow process (CFP) for MODFLOW-2005*. 2008: USGS, Tallahassee, Florida.
- [22] Gallegos, J.J., B.X. Hu, and H. Davis, *Simulating flow in karst aquifers at laboratory and sub-regional scales using MODFLOW-CFP*. Hydrogeology Journal, 2013. 21(8): pp. 1749–1760.
- [23] Clemens, T., et al., *A combined continuum and discrete network reactive transport model for the simulation of karst development*. 1996: Golden, Colorado: IAHS publication. pp. 309–320.
- [24] Liedl, R., et al., *Simulation of the development of karst aquifers using a coupled continuum pipe flow model*. Water Resources Research, 2003. 39(3).
- [25] Reimann, T., et al., *Representation of water abstraction from a karst conduit with numerical discrete-continuum models*. Hydrology and Earth System Sciences, 2014. 18(1): pp. 227–241.
- [26] Reimann, T., et al. Addition and enhancement of flow and transport processes to the MODFLOW-2005 conduit flow process. In: *2013 NGWA Summit—the national and international conference on groundwater*. 2013: Ngwa.
- [27] Hill, M.E., M.T. Stewart, and A. Martin, *Evaluation of the MODFLOW-2005 conduit flow process*. Groundwater, 2010. 48(4): pp. 549–559.
- [28] Saller, S.P., M.J. Ronayne, and A.J. Long, *Comparison of a karst groundwater model with and without discrete conduit flow*. Hydrogeology Journal, 2013. 21(7): pp. 1555–1566.
- [29] Xu, Z., et al., *Simulating long term nitrate-N contamination processes in the Woodville Karst Plain using CFPv2 with UMT3D*. Journal of Hydrology, 2015. 524: pp. 72–88.
- [30] Xu, Z., et al., *Numerical study of groundwater flow cycling controlled by seawater/freshwater interaction in a coastal karst aquifer through conduit network using CFPv2*. Journal of Contaminant Hydrology, 2015. 182: pp. 131–145.
- [31] Zheng, C. and P.P. Wang, *MT3DMS: a modular three-dimensional multispecies transport model for simulation of advection, dispersion, and chemical reactions of contaminants in groundwater systems; documentation and user's guide*. 1999, DTIC Document, University of Alabama, Tuscaloosa, Alabama.
- [32] Spiessl, S.M., *Development and evaluation of a reactive hybrid transport model (RUMT3D)*. 2004, Ph. D. Thesis, Georg-August-University of Goettingen. <http://webdoc.sub.gwdg.de/diss/2004/spiessl/spiessl.pdf>.

- [33] Spiessl, S.M., et al., *A process-based reactive hybrid transport model for coupled discrete conduit–continuum systems*. *Journal of Hydrology*, 2007. 347(1): pp. 23–34.
- [34] Reimann, T., et al., *Effects of dynamically variable saturation and matrix-conduit coupling of flow in karst aquifers*. *Water Resources Research*, 2011. 47(11).
- [35] Davis, J.H., B.G. Katz, and D.W. Griffin, *Nitrate-N movement in groundwater from the land application of treated municipal wastewater and other sources in the Wakulla Springs Springshed, Leon and Wakulla counties, Florida, 1966–2018*. US Geol Surv Sci Invest Rep, 2010. 5099: p. 90.
- [36] Davis, J.H. and B.G. Katz, *Hydrogeologic investigation, water chemistry analysis, and model delineation of contributing areas for City of Tallahassee public-supply wells, Tallahassee, Florida*. 2007: Geological Survey (US), Tallahassee, Florida.
- [37] Harbaugh, A.W., et al., *MODFLOW-2000, the US Geological Survey modular ground-water model: user guide to modularization concepts and the ground-water flow process*. 2000: US Geological Survey, Reston, VA.
- [38] Kincaid, T.R. and C.L. Werner. Conduit flow paths and conduit/matrix interactions defined by quantitative groundwater tracing in the Floridan aquifer. In: *Sinkholes and the engineering and environmental impacts of karst: proceedings of the eleventh multidisciplinary conference, Am. Soc. of Civ. Eng. Geotech. Spec. Publ.* 2008.
- [39] Dyer, S.B., *Dye tracing confirms conduit connections from Lost Creek Swallet to Spring Creek Springs and the Leon Sinks – Wakulla cave system*. In: *Department of Earth, Ocean and Atmosphere*. Master Thesis, Department of Earth, Ocean and Atmosphere Science, Florida State University, 2015: Florida State University: Tallahassee, FL.
- [40] Bear, J., *Dynamics of fluids in porous media*. 2013: Courier Corporation. Reprint of the American Elsevier Publishing Company, INC., New York, 1972 edition.
- [41] Zheng, C. and G.D. Bennett, *Applied contaminant transport modeling*. Vol. 2. 2002: Wiley-Interscience, New York.

Modelling Water Dynamics, Transport Processes and Biogeochemical Reactions in Soil Vadose Zone

Vilim Filipović, Gabrijel Ondrašek and Lana Filipović

Additional information is available at the end of the chapter

<http://dx.doi.org/10.5772/63496>

Abstract

Large numbers of numerical models are nowadays available for the description of physical and chemical processes affecting water flow and solute transport in soil vadose zone. This chapter explains basic principles of water flow and solute transport modelling in soil vadose (variably saturated) zone and some of the most important processes present in it. First part deals with water dynamics in the soil, that is, soil water content, pressure head, soil porosity, and water flow. Also, some of the measurement techniques used to estimate water dynamics in soil are explained. Water retention curve and soil hydraulic properties needed for modelling are briefly discussed with the explanation of basic (i.e. most commonly used) hydraulic relationship in soil (van Genuchten equation) and water flow (Richards equation) approaches. Second part includes solute transport description in vadose zone, including processes such as advection, diffusion, dispersion, and adsorption. Basic advection-dispersion equation is explained and also the implementation of boundary and initial conditions in the numerical model. Preferential flow is shortly discussed with the basic principles behind its occurrence and modelling in the soil vadose zone. One real case one-dimensional (1D) example of modelling with HYDRUS software is presented in which water flow and nitrate transport is simulated on the lysimeter study. Short overview of the most widely used numerical models for simulating vadose zone processes is also presented, whereas the final part is focused on chemical speciation modelling in relatively homogeneous soil solutions using visual MINTEQ interface.

Keywords: vadose zone, water flow, solute transport, numerical modelling, biogeochemical reactions

1. Introduction

In the past few decades, more attention is devoted to environmental protection and pollution control in the soil-plant-atmosphere continuum. There are growing numbers of potentially harmful substances that are introduced in the environment, especially by agricultural practices and industry in arable and urban areas. Such substances can accumulate in the soil (and potentially get into food chain), surface water, or can be transported in a deeper soil zone and eventually reach groundwater. Intensive agriculture uses large amounts of fertilizer (organic and inorganic), plant protection products (pesticides), animal hormones, and include various other substances that may accumulate in environment (e.g. pathogens, bacteria, and trace metals). Although most of the substances applied in agricultural production are useful in the surface layer of the soil, due to their leaching into the deeper soil layers and groundwater and their bioaccumulation potential, they can also cause serious pollution and degrade natural resources.

Water flow and solute (pollutant) transport models can be used as tools for describing and predicting specific processes in variably saturated soil zone or vadose zone. For example, different models can be used for predicting and/or management of irrigation and drainage systems, crop growth, fertilizer application, and pesticide leaching to protect soil and water resources. Models are also equally necessary for the design of waste disposal sites (industrial, municipal) or long-term management of various harmful substances (e.g. radioactive waste). A large number of models were developed to simulate the numerous simple hydraulic or complex biogeochemical processes and may be used for different purposes. Vadose zone is in focus of many research topics due to its complex nature and also the possibility of elimination and remediation of present/introduced contaminants before leaching to underground water resources.

Transfer of solutes in the soil is closely linked with the flow of water through vadose zone, which largely affects the concentration and biochemical reactions of various substances. Solute transport in soil vadose zone is one of the most demanding problems that occur in numerical modelling. It includes the transport of water and solutes, chemical reactions and microbial transformations. With the development of new numerical models, it is possible to describe more complex processes that are occurring in the soil-plant-atmosphere continuum. In this chapter, basic soil physical concepts and numerical modelling procedures (with example) are explained. Trace metal behaviour in the ecosystems, their mobility in soil, and metal chemical forms (species) in the soil solution are shortly discussed with a chemical speciation modelling example presented.

2. Water dynamics

2.1. Soil water content

Soil system can be defined as a three-phase system that can be divided into solid, gas, and liquid phase. The fractions of liquid and gas are located in the voids between soil particles.

These voids are defined as pores and their quantification can be defined as ratio of pore volume to the total (bulk) volume of a soil. Soil porosity can be estimated using the following expression:

$$P = \frac{V_p}{V_s} \quad (1)$$

where V_p represents volume of pores [L^3] and V_s volume of the undisturbed soil sample [L^3].

Soil water content represents the quantity of water contained in soil and is expressed as a ratio, which can range from completely dry to the soil porosity value at the point of saturation. Volumetric soil water content is defined as θ_v [L^3L^{-3}]:

$$\theta_v = \frac{V_w}{V_s} \quad (2)$$

where V_w is the volume of water in soil pores [L^3], and V_s is the volume of the undisturbed soil sample [L^3]. Its expression is unitless; however, usually, it is expressed as cm^3/cm^3 (or m^3/m^3) to emphasize its volumetric origin. Soil water content can be also defined as a mass, thus named gravimetric water content θ_g [MM^{-1}]:

$$\theta_g = \frac{m_w}{m_s} \quad (3)$$

where m_w is the mass of water and m_s is the mass of soil [M]. It is also unitless but often expressed as gram per gram (or kg per kg), following the same rule as mentioned earlier. Both values can be multiplied by 100 to express it as a percentage.

2.1.1. Soil water content measurements

Measurement of the soil water content can be direct or indirect depending on the used method. Direct measurements include the estimation of water quantity by removal from soil through evaporation, leaching or by chemical procedure. They include destructive soil sampling, and hence, additional soil samples need to be taken in order to achieve more reliable results. Therefore, small undisturbed cores are usually taken to determine water content and bulk density. Indirect methods rely on monitoring soil properties that are directly affected by soil water content (e.g. electrical conductivity). These methods require instrumentation placed in the soil or sensors placed over the soil. For this approach, the calibration is needed in addition to precise installation. The advantage of the *in situ* water content measurements are repeated measuring at the same location during given time period (e.g. years) without disruption of the soil system. There are various methods used for soil water content determination; here, the

most common methods are shortly explained. More in depth explanation of a given methods could be found in Refs. [1, 2].

2.1.1.1. *Direct measurement*

The gravimetric method for the water content measurement represents simplest way to gather accurate soil water content. A soil sample of a known mass is placed in the container, dried in an oven, removed from the container, and allowed to cool in desiccator, then reweighted. The drying procedure is done by placing the sample in convection oven at 105°C for 24 h. From the measurement, gravimetric water content can be calculated and also converted into volumetric water content using soil bulk density.

2.1.1.2. *Indirect measurement*

Neutron probe uses radioactive material for measuring soil water content. A neutron meter is placed at the soil surface above the access tube in which probe is lowered into the soil to the desired measurement depth. The probe contains an americium 241/beryllium pellet that emits fast high-energy neutrons. These high-speed neutrons pass through the accesses tube and collide with hydrogen atoms in the surrounding soil and water. When neutrons hit H nuclei, they slow down and some are reflected back to the source tube and counted by the neutron detector. Because soil water is the primary source of hydrogen atoms, the count is directly related to the soil water content. This method can produce reliable results and can be used for measurements at multiple depths in few minutes. Its application might be questionable for shallow measurements (>15 cm), since the neutrons might escape from the soil instead of being detected. However, the main disadvantage is the use of radiative source that can be a potential health hazard for the device operator.

Time domain reflectometry (TDR) is a technique that involves measuring the travel time of an electromagnetic wave along a wave guide. The bulk soil properties affecting electromagnetic wave are electrical conductivity and dielectric permittivity. Electrical conductivity is a measure of the free electrons flow when exposed to an electric field. The dielectric permittivity is a measure of the displacement of constrained charges when exposed to an electric field. The speed of the electromagnetic wave in soil is dependent on the dielectric permittivity of soil matrix. The fact that water (80) has much larger dielectric constant than air (1), soil (3–7), or its organic components (2–5) is used to determine the volumetric water content of the soil. The TDR instrument consists of 2–3 parallel rods that are inserted into the soil and act as a waveguides. Electronics in the TDR instrument generate and sense the return of high-energy signal that travels through the soil along the waveguide, that is, stainless steel rods. The high-frequency signal is then converted to the volumetric water content. Readings can be affected by high clay content, high organic matter, or high soil salinity. The rods need to be inserted fully into the soil and have good contact with surrounding soil particles. The TDR probes are widely used due to its simplicity, accurate readings, and minimal soil disturbance.

Capacitance devices are used to determine the resonance frequency of a given soil. The capacitor is connected to an oscillator to form an electrical circuit; changes in soil moisture can

be detected by changes in the circuit operating frequency. Probes usually consist of two or more electrodes (e.g. plates, rods, or metal rings) that are inserted into the soil. With the ring configuration, the probe is introduced into an access tube installed in the field. When parallel rod configuration is used, the probes are buried at the required depth into the soil and the soil represents a medium between capacitor electrodes. Compared to TDR, frequency domain sensors are relatively inexpensive and have a faster response time. However, because of the complex electrical field around the probe, the sensor needs to be calibrated specifically for different soil types.

2.2. Soil water potential

While the knowledge of soil water content is important, it is also important to know its energy potential since water can be held by the force fields of soils particles differently depending on soil type, (soil texture). For example, two soils with identical water content may have different soil water potential, such that one will easily allow plant water uptake (e.g. sandy soil), while in the other type, soil water will be extracted much harder (e.g. clay soil). The total energy state of soil water is defined by its equivalent potential energy, as determined by the various forces acting on the water per unit quantity. In most cases the kinetic energy of water can be neglected, since the flow rates in soil are very slow. Therefore, the energy state of soil water is defined by its equivalent potential energy, which is derived from its position in a force field. Water in the soil will move from area with high soil water potential energy to area of lower potential energy. Driving force for the flow is the change in potential energy with distance (soil water potential gradient).

These driving forces determine the following:

- Direction and magnitude of water flow
- Plant water uptake
- Drainage amount
- Capillary rise
- Soil temperature changes
- Solute transport.

The potential energy of water in the soil is defined relative to its reference or standard state. Standard state water is pure (no solutes), free (no external forces other than gravity) water at a reference pressure (atmospheric), reference temperature, and reference elevation [3]. Soil water potential is defined as the difference in potential energy per unit of volume, mass, or weight of water compared to the standard (reference state). Depending on the choice of unit for quantity, three different systems can be used (**Table 1.**)

Name	Symbol	Definition	Dimensions	SI units
Chemical potential	μ_i	Energy per mass	L^2T^{-2}	$J\ kg^{-1}$
Soil water potential	ψ_i	Energy per volume	$ML^{-1}T^{-2}$	$N\ m^{-2}$
Soil water potential head	H	Energy per weight	L	m

Table 1. Different unit systems for expressing soil water potential (adapted with permission from [4]).

Total soil water potential is defined as the amount of work per unit quantity of pure water that must be completed by external forces to transfer reversibly and isothermally an infinitesimal amount of water from the standard state to the soil at the point under consideration [3]. The transformation of water from the reference states can be divided into the components caused by each force field acting on soil water. These components are forces caused by gravity, hydrostatic pressure, capillarity, solute, air pressure, and swelling [5].

Following are presented the definitions of the most important components of total soil water potential (ψ) which is represented by the sum of its active components:

$$\Psi = \Psi_z + \Psi_p + \Psi_s + \Psi_m + \Psi_a \quad (4)$$

Gravitational potential (ψ_z) is defined as the difference in energy per unit volume or weight between standard water and soil water due to gravity. This component quantifies the effect of the gravitational force field on the energy of soil water.

Hydrostatic pressure potential (ψ_p) is defined as the difference in energy per unit volume or weight between standard water and soil water due to the pressure exerted by overlying free water. This component quantifies the pressure effect from overlying water on the energy of water.

Osmotic (solute) potential (ψ_s) is defined as the difference in energy per unit of volume or weight between standard water and soil water due to the presence of solutes. This component quantifies the effect of solutes on the energy of soil water.

Matric potential (ψ_m) is defined as the difference in energy per unit volume or weight between standard water and soil water due to capillarity and adsorption. This component quantifies the effect of the capillarity and adsorption on the energy of soil water.

Air potential (ψ_a) is defined as the difference in energy per unit volume or weight between standard water and soil water due to effect of soil air pressure. This component quantifies the effect of the air pressure in soil porous system on the energy of soil water.

Some of the components of water potential can be neglected like osmotic pressure and also the effect of air pressure in most of the cases due to its low effect (and estimation difficulty) on the global soil water potential. Following these assumptions, total soil water potential head or hydraulic head is when expressed per unit weight:

$$H = h + z \quad (5)$$

Thus, hydrostatic pressure (h) and gravity (z) dominate the potential energy of water under unsaturated condition.

2.2.1. Measuring soil water potential components

Tensiometer is a measuring device used to determine matric water potential (ψ_m) in the vadose zone. The device consists of an airtight glass or plastic tube filled with water and connected to a porous cup at the bottom. Tensiometers are placed in the soil and the water inside the tube comes into equilibrium with the soil solution (i.e. it is at the same pressure potential as the water held in the soil matrix). Then, the reading is collected from the pressure gauge (water or mercury) at the top of the device. Typically, the measurement range is 0–80 centibars. These devices are easy to use and inexpensive. They require a close contact with surrounding soil around porous cup that might sometimes be hard to achieve, for example, on swelling or coarse soil types. More details about this method can be found in [6].

Piezometers are used to measure hydrostatic potential (ψ_p) and positive pressure head (h), since they are used below water table. A piezometer is a hollow plastic tube installed in the soil, which is open to the atmosphere at the top and located in the saturated soil at the bottom. The bottom of the tube has perforated screened section which allows water to enter the piezometer. Water rises in the tube until the hydrostatic pressure of the water inside the tube is the same as hydrostatic pressure of surrounding soil water. Hydrostatic pressure can be calculated from the water level readings in the piezometer.

Thermocouple psychrometers are used to measure soil matric potential based on the relative humidity of the water vapour in the soil [7]. At equilibrium, the vapour water potential is equal to the liquid water potential. Since the vapour and liquid are at the same elevation, the components of the soil water potential measured by the psychrometer are the sum of the matric and osmotic potential, assuming atmospheric air pressure. The unit consists of a measuring device and soil sensor, which is buried into the soil (ceramic cup) and connected via cable to a measuring device. Electrical circuit (thermocouple) is used to measure temperature. The output of the psychrometer is expressed in voltage, which represents the difference in temperature measured in the ceramic cup and the reference (constant) temperature. If the soil is dry, the output voltage will be greater. A calibration equation is used to convert readings to water potential.

Electrical resistance sensors measure the electrical resistance of a porous block that is in contact with surrounding soil. Electrical resistance between electrodes embedded in a porous medium (block) is proportional to its water content, which is related to the soil water matric potential of the surrounding soil. Electrical resistance decreases as the soil and the block lose water. The most common sensor is a gypsum block. The block is part of a simple DC circuit and buried in the soil. Cable is connecting the block and a voltage measuring device. These sensors are not very accurate [8] and are best suited to manage irrigation systems if precise measurements are not needed.

Soil water constants are used to describe water content across different water potential range in soil and are related to the energy required to extract water from soil (**Figure 1**).

Maximal water capacity (SWMAX) is the maximal water content of soil, that is, at (or near) saturation. The potential energy gradient is downward through the soil profile, mainly due to gravity forces and through macropores.

Field capacity (FC) is the amount of water that remains 2–3 days after the saturation of a soil with water after gravity movement of water has largely ceased. The water is held in the soil at tension of -0.33 bar (pF 2.0) by matric forces (in micro- and mesopores). Water held between saturation and field capacity is subject to free drainage over short time periods, and it is generally considered unavailable to plants.

Permanent wilting point (PWP) is the lowest amount of water in the soil at which matric forces hold water too tight for plant extraction (-15 bar or pF 4.2).

Available field capacity (aFC) or plant available water (PAW) is the difference between field capacity (FC) and wilting point of a soil. It is considered as water available for plants to extract from the soil moisture zone. Plant available water is mostly located in soil micro- and mesopores.

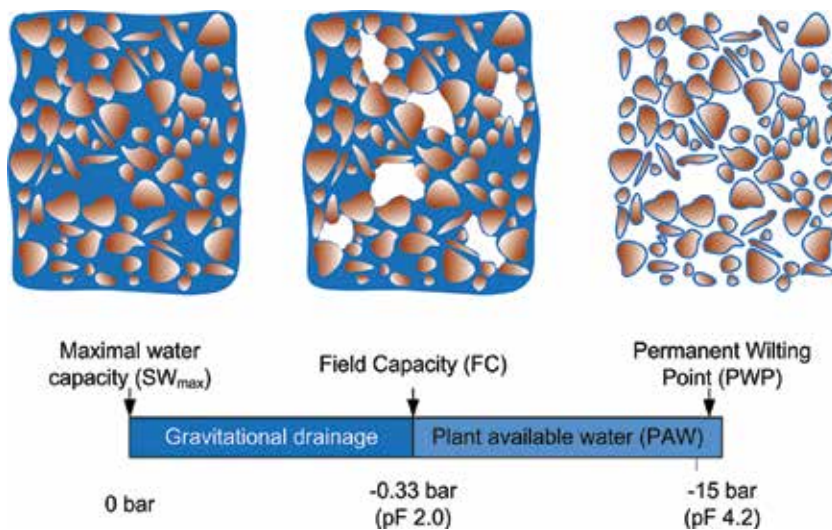


Figure 1. Scheme of the mayor soil water constants: maximal water capacity, field capacity, permanent wilting point and plant available water depending on the soil water potential range.

2.3. Soil water retention curve

Soil water retention curve represents the relationship between the water content (θ), and the soil water potential (h). In the literature, different names could be found such as soil water characteristic curve, capillary pressure saturation relationship, and/or pF curve. The water retention curve provides information on how tight water is held in soil porous system and

how much energy would need to extract it from the different pores. The main characteristics of soil water retention curves are visible from **Figure 2** where the x -axis shows the relative water content in the soil (θ), while the y -axis shows pressure head (h). If the pressure head values are close to 0, the soil is almost completely saturated, as θ decreases, the binding force is getting stronger (more energy is needed to extract water from the soil). At the low-pressure head values (close to the border wilting point pF 4.2 or -15,000 cm), the water that is retained in the soil is located in the smallest pores.

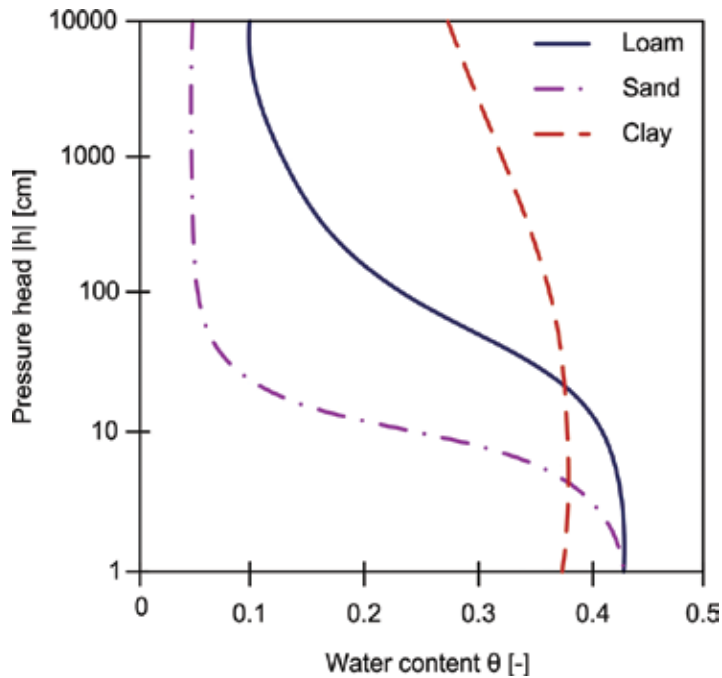


Figure 2. Water retention curve example for loam, sand, and clay texture soil based on soil hydraulic parameters taken from [9].

Coarser textured soils (sandy) lose water more quickly than fine textured soils (clay) as a direct reflection of the size distribution of pores in the soil. As most of the pores in the coarser soils have greater diameter, water will percolate during small negative soil water potential, while in the finer textured soils (clay, loam, silty loam), water drainage occurs at very high values of negative soil water potential.

Hysteresis in soil is defined as the difference in the relationship between the water content of the soil and the corresponding water potential obtained under wetting and drying process. Soil water retention curve is usually developed by going from high to low water content producing drying curve. However, if the measurements started from saturated conditions (e.g. pressure plate), this would produce wetting curve. It means that water content in the drying (or drainage) curve of water potential is larger than water content in the wetting curve for the same value of water potential.

Most common methods for soil water retention curve estimation are pressure plate and pressure cells, although there are other methods to determine its shape like hanging water column, suction tables, or soil freezing.

Pressure plate has a range for measuring water retention curve ($h=0$ to $-15,330$ cm) and usually can provide very accurate measurements in the wet range. The pressure plate was introduced in the 1930s by Richards [10]. Device is used to make indirect measurements of soil pressure head (matric potential) by imposing a known pressure potential on saturated soil samples until free water no longer flows from the system. When the sample comes to equilibrium, its water potential will be equivalent to the applied pressure.

Pressure chambers are usually used to estimate the dryer part of soil water retention curve. Pressure chambers that hold a single intact soil sample are called pressure (tempe) cells and are usually used for h range from 0 to -1000 or even -3000 cm. The cell consists of plastic housing, a porous ceramic plate at the bottom, a metal ring to secure the soil sample and a rubber sealing between the housing and the ring. The positive known pressure is applied to the sample to extract water and the sample is weighted at specific pressure values (when equilibrium is reached).

The shape of water retention curve can be explained using a wide range of mathematical expressions [11–13]. However, most common expression used is the van Genuchten-Mualem one [14]:

$$\theta(h) = \theta_r + \frac{\theta_s - \theta_r}{(1 + |\alpha h|^n)^m} \text{ for } h < 0 \quad (6)$$

$$\theta(h) = \theta_s \text{ for } h \geq 0 \quad (7)$$

$$K(h) = K_s S_e^l (1 - (1 - S_e^{\frac{1}{m}})^m)^2 \quad (8)$$

$$S_e = \frac{\theta - \theta_r}{\theta_s - \theta_r} \quad (9)$$

$$m = 1 - \frac{1}{n}; n > 1 \quad (10)$$

where θ_r and θ_s denote residual and saturated volumetric water content [L^3L^{-3}], respectively, K_s is the saturated hydraulic conductivity [LT^{-1}], S_e is the effective saturation, α [L^{-1}] and n [-] are the shape parameters, and l [-] is a pore connectivity parameter. The pore connectivity parameter value is usually taken from an average for many soils ($l=0.5$) [15].

The hydraulic conductivity characterizes the ability of a soil to transmit water and as such is inversely related to the resistance to water flow [16]. The hydraulic conductivity decreases as soil becomes unsaturated and smaller quantity of pore space is filled with water. The unsaturated hydraulic conductivity function shows the dependency of the hydraulic conductivity on the various ranges of water content or pressure head. Hydraulic conductivity of saturated soil is much higher in coarser texture soils (sand) compared with clay or loam texture soils.

The fitting of soil water retention curve data can be obtained by optimizing some of the parameters used in the equation. This requires non-linear optimization method. The RETC (REtention Curve) program [17] may be used to predict the hydraulic conductivity from observed soil water retention data assuming that one observed conductivity value (not necessarily at saturation) is available. The program also permits one to fit analytical functions simultaneously to observed water retention and hydraulic conductivity data.

2.4. Soil hydraulic properties estimation

Modelling of water flow and solute transport in soils is predefined with hydraulic properties of studied soil system. Soil hydraulic properties can be obtained directly by conducting laboratory or field measurements and experiments. However, these techniques can be costly and time-consuming which have resulted in different method for the estimation of soil hydraulic properties. It is possible to estimate these properties from soil information, which are widely available or easy to measure. Mathematical functions to estimate soil hydraulic parameters from basic soil information, such as soil texture, soil organic matter content, bulk density, etc. are called pedotransfer functions (PTFs). Large databases, including soil hydraulic properties and corresponding textures, bulk densities, organic matter content, field capacity, wilting point etc., are available for different soil types. One example is program ROSETTA [18] that predicts parameters of van Genuchten-Mualem functions. Soil hydraulic parameters are used in agricultural, environmental, and hydrological modelling in which the number of parameters needed depends on simulated processes and used model. Some models require knowledge of the shape of soil water retention curve (SWAP, HYDRUS). Other models, for example, the SWAT model, require water retention values at given matric potentials. Direct point predictions for given matric potentials can lead to more accurate estimations than if water retention values of these matric potentials are derived from predicted SWRC (parameter estimation). Therefore, it is important to have both point predictions and parameter estimations. It is also well known that the performance of prediction models is highly dependent on the quality of the data set (number and type of measured properties, sample size and its heterogeneity) used for their development.

3. Vadose zone modelling

3.1 Water flow modelling

Water flow modelling in the unsaturated zone is based on Richards equation [19]. It is a non-linear partial differential equation, which is often difficult to approximate since it does not

have a closed-form analytical solution. The expression of Richards equation for one-dimensional (1D) water flow can be written as:

$$\frac{\partial \theta}{\partial t} = \frac{\partial}{\partial z} \left(K(h) \frac{\partial h}{\partial z} \right) + \frac{\partial K(h)}{\partial z} - S(h) \tag{11}$$

where θ represents volumetric water content [$L^3 L^{-3}$], h is pressure head [L], z is vertical coordinate (positive upwards) [L], t is time [T], K is the unsaturated hydraulic conductivity [LT^{-1}], S represents a sink term (root water uptake) [$L^3L^{-3}T^{-1}$]. Richards equation is based on continuity equation and Darcy's law. The continuity equation in general states that the change in the water content (storage) in a given volume is due to spatial changes in the water flux. Darcy's law is a constitutive equation that describes the flow of a fluid through a porous medium. The Darcy-Buckingham equation is formally similar to the Darcy's equation, except that the proportionality constant (i.e. the unsaturated hydraulic conductivity) in the Darcy-Buckingham equation is a nonlinear function of the pressure head (or water saturation), while $K(h)$ in Darcy's equation is a constant equal to the saturated hydraulic conductivity, K_s . Root water uptake can be also considered through a sink term in the Richards equation. Sink term is usually modelled using Feddes equation [20]:

$$S(h) = \alpha(h)S_p \tag{12}$$

where $S(h)$ is the root uptake removed from a unit of soil in time [T^{-1}], $\alpha(h)$ is water stress response function, which varies between 0 and 1 [T^{-1}], and S_p is potential root water uptake rate [T^{-1}].

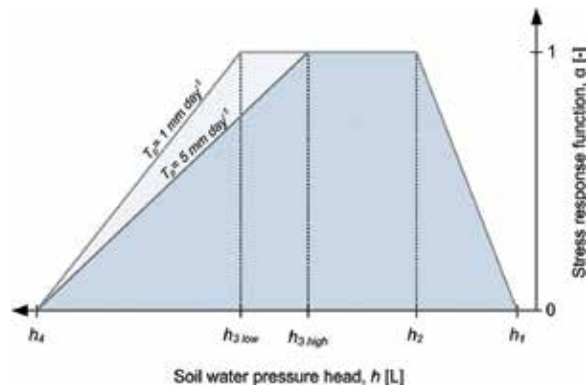


Figure 3. Plant water stress response function according to Feddes equation.

The stress response function is shown in **Figure 3**. Water uptake is assumed to be 0 close to saturation due to a lack of oxygen in the root zone (pressure head greater than h_1). For a

pressure head less than h_4 (the willing point pressure head), water uptake is also assumed to be zero. Water uptake is optimal between pressure heads of h_2 and h_3 . The pressure head h_3 may be adjusted depending on the transpiration rate so that it is more negative when transpiration rates are low (optimal root water uptake occurs over a wider range in pressure head at lower transpiration rates).

3.2. Solute transport modelling

Transport of various substances in soil is associated with water flow. Some of the substances present in a soil system dissolve in water and they are transported through the soil. On the other hand, some of the substances do not dissolve in water and they are transported simultaneously with water. Substances either do not react with surrounding soil system and do not change during time or react with soil and change due to chemical reactions, microbiological transformations, etc. Given the solute transport is either conservative (transported solute mass is constant) or non-conservative (transported solute mass is usually decreasing due to adsorption, nitrification, degradation, volatilization, etc.). Some of the main processes that affect solute transport in soil are explained in this section.

Advection represents transport of solute mass at the average rate caused by the water flux.

$$q_a = qc \tag{13}$$

where q_a is solute flux density due to advection [$\text{ML}^{-2}\text{T}^{-1}$], c is solute concentration [ML^{-3}], and q is water flux density [LT^{-1}]. If the solute transport in the soil would be controlled only by advection its transport velocity would be identical as the average water flow in soil.

Hydrodynamic dispersion includes solute spreading by mechanical dispersion and molecular diffusion in direction of the flow (longitudinal dispersion) and perpendicular to it (transverse dispersion). Mechanical dispersion occurs in the soil as a result of differences in the pore size, the difference in the flow path length and ongoing mixing between pores (due to arrangement of pores in the soil) and the difference in transport velocity within a pore [16]. This process happens in the micro (within the pores) and macro (preferential flow through cracks in the soil) scale. Molecular diffusion represents transfer of solutes due to concentration gradient. Hydrodynamic dispersion is the result of two processes $D = D_n + D_m$ where D is the hydrodynamic dispersion coefficient, D_n is mechanical dispersion, and D_m is molecular diffusion. This can be expressed by Fick's law:

$$q_d = -\theta D \frac{\partial c}{\partial z} \tag{14}$$

where q_d is solute flux density due to hydrodynamic dispersion [$\text{ML}^{-2}\text{T}^{-1}$], D is dispersion coefficient [L^2T^{-1}], c is solute concentration [ML^{-3}], θ is soil water content [L^3L^{-3}] and z represent spatial coordinate [L].

The *advection-dispersion equation* (ADE) is most common mathematical description used for solute transport in the soil. For numerical or analytical solution of ADE, it is necessary to know the value of the dispersion coefficient. Hydrodynamic dispersion coefficient can be estimated by field or laboratory experiments. The most commonly used method for estimating dispersion coefficient is the application of tracer (a non-reacting compound) to soil column and estimation of the dispersion coefficient from gathered data. From the experiment, a *breakthrough curve* is derived, which plots relative concentration of a given substance versus time, where relative concentration is defined as the ratio of the actual concentration to the source concentration.

The dispersion coefficient in one-dimensional (1D) system is proportional to the average water flow velocity in porous system where proportionality constant is referred to as the (longitudinal) dispersion [21]. Dispersion can be derived from Newton's law of viscosity which states that velocities within a single capillary tube follow a parabolic distribution, with the largest velocity in the middle of the pore and zero velocities at the walls (this can be applied on soil porous system, **Figure 4a**). Solute transport due to dispersion is the result of the unequal distribution of water flow rate in the pores of different sizes. Since soils consist of pores of different radii, solute fluxes will be significantly different, with some solutes again traveling faster than others (**Figure 4b**).

$$\theta D = D_L |q| + \theta D_m \tau \quad (15)$$

where D_L is longitudinal dispersivity [L], q is water flux [LT^{-1}], D_m is molecular diffusion [L^2T^{-1}], θ is soil water content [L^3L^{-3}], and τ is tortuosity factor [-].

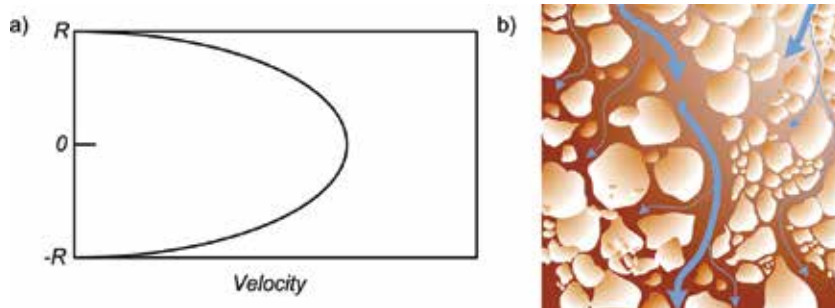


Figure 4. Distribution of single pore velocity (a), and distribution of velocities in a larger-complex pore system (b, adapted with the permission from [16]).

Continuity equation is used to calculate the mass balance of solute in soil, that is, it states the changes of total solute concentration in time per volume of soil:

$$\frac{\partial(\theta c)}{\partial t} = -\frac{\partial(q_d + q_a)}{\partial z} \quad (16)$$

where θ is soil water content [L^3L^{-3}], c is solute concentration [ML^{-3}], q_d is solute flux density due to hydrodynamic dispersion [$ML^{-2}T^{-1}$], q_a is solute flux density due to advection [$ML^{-2}T^{-1}$], and z is coordinate [L].

Adsorption dispersion equation is based on the continuity, advection and dispersion equation. The ADE for one-dimensional solute transport during transient water flow in a variably saturated medium:

$$\frac{\partial(\theta c)}{\partial t} + \frac{\partial(\rho s)}{\partial t} = \frac{\partial}{\partial z} \left(\theta D \frac{\partial c}{\partial z} - qc \right) - \emptyset \quad (17)$$

where c is solute concentration [ML^{-3}], s is adsorbed concentration [MM^{-1}], θ is soil water content [L^3L^{-3}], ρ is soil bulk density [ML^{-3}], D is dispersion coefficient [L^2T^{-1}], q is volumetric flux [LT^{-1}], and \emptyset is rate constant representing reactions [$ML^{-3} T^{-1}$].

3.2.1. Adsorption (linear, nonlinear)

For solving solute transport equation, additional information is needed to describe the relationships between various substances whose transport is modelled. Adsorption is a physical and chemical process in which one substance is bound to the surface of the other phase (in this case, the binding of substances occur mostly to the soil solid phase). The most widely used and simplest way of describing this process is to assume instantaneous sorption and to use adsorption isotherms. The most elementary form of the adsorption isotherm is the linear isotherm given by the following equation:

$$s = K_d c \quad (18)$$

where K_d is the distribution coefficient [L^3M^{-1}]. This assumption simplifies the mathematical description of solute transport; however, adsorption is generally nonlinear and often depends on the presence of various competing substances in the soil solution. The most commonly applied models used to describe the nonlinear adsorption are presented by [22] Freundlich and [23] Langmuir:

$$s = K_f c^\beta \quad (19)$$

$$s = \frac{K_d c}{1 + \eta c} \quad (20)$$

where K_f [$M^{-\beta}L^{-3\beta}$] and β [-] are coefficients used in the Freundlich isotherm, and η [L^3M^{-1}] is coefficient used for description of the Langmuir isotherm. Linear adsorption represents a case where the Freundlich equation has β equal to 1. For cases when $\beta < 1$, less solute mass is

adsorbed per unit increase in c at high concentrations compared with low concentrations (**Figure 5a**). This happens when the amount of solute added exceeds the ability of adsorption of a type of soil. In the Langmuir model with increasing η value, the isotherm becomes more non-linear and is approaching the maximum sorbed concentration (**Figure 5b**).

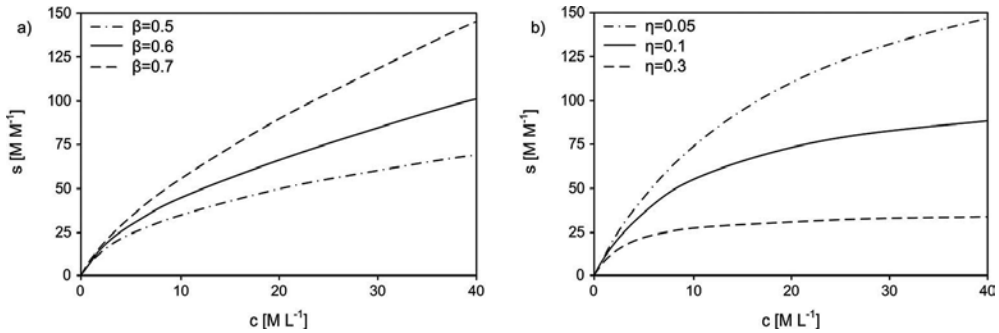


Figure 5. Examples of nonlinear adsorption isotherm using the Freundlich (a), and Langmuir (b) equations assuming different β and η values.

3.3. Initial and boundary conditions

Before starting the simulation process, it is necessary to determine the initial conditions of water flow (the potential distribution at $t=0$) and solute transport (distribution of solute concentration at $t=0$). This means that it is necessary to describe the initial state of the simulated soil system in terms of the relative amounts of water (pressure head or water content distribution) and concentration of simulated solute or solutes in the soil profile at the moment of the beginning of the simulation. Boundary conditions are the conditions specified at the edges of the transport model area and they define how the site specific model interacts with its environment. The water flow and transport equations can be solved analytically or numerically after determination of the initial and boundary conditions. Complex interactions between the transport domain and surrounding unsaturated zone should be considered carefully for any problem having in mind that this interaction determines the dynamics of water flow and solute transport (velocity and quantity) on the domain boundaries. To solve the solute transport equation, most numerical models used three types of boundary conditions. Dirichlet (first) type of boundary conditions is used when the concentration of the solute at the boundary of domain is known. In some cases, for example, when a boundary is impermeable ($q_0=0$) or when water flow is directed out of the region, Neumann (second) type of boundary conditions is used. Cauchy (third) type of boundary conditions can be used to describe solute transport on the domain boundaries (a combination of the first two types of boundary conditions). Since Cauchy boundary conditions define the solute flux across a boundary, the solute flux entering the transport domain will be known exactly. This specified solute flux is then divided into advective and dispersive components. On the other side, Dirichlet boundary condition controls only the concentration on the boundary, but not the solute flux because its advective and dispersive contributions will be larger than for the Cauchy boundary condition [4].

3.4. Preferential flow modelling

The term preferential flow combines all transport where water and solutes move along certain pathways, while bypassing other volume fractions of the porous soil matrix [24, 25]. In heterogeneous structured soils, which contains large interconnected voids (e.g. root channels, fissures, earthworm pathways) water and transported solutes bypass soil matrix creating non-equilibrium conditions in pressure heads and solute concentrations between preferential flow paths and the soil matrix-pore region. Large number of approaches has been developed to model preferential flow in soil vadose zone. Most of these models try to separately describe flow and solute transport in matrix and fracture pore regions, that is, dual porosity, dual permeability models and multiporosity or multipermeability models [26–29] (Figure 6). Dual-porosity and dual-permeability models both assume that the porous medium consists of two interacting regions, one associated with the interaggregate, macropore, or fracture system, and one comprising micropores (or intra-aggregate pores) inside soil matrix (soil aggregates). While dual-porosity models assume that water in the soil matrix is stagnant (immobile), dual-permeability models allow for water movement in the matrix domain as well. Dual-permeability models in which water can move in both the inter- and intra-aggregate pore regions are now also becoming more popular [27, 30]. The main difference between available dual permeability is the implementation of water flow in and between two pore regions (i.e. fracture and matrix). Different approaches are used to estimate water flow in fracture and matrix domains like the Poiseuille's equation [31], the Green and Ampt or Philip infiltration models [32], the kinematic wave equation [30, 33, 34], and the Richards equation [27]. Multiporosity and/or multipermeability models are based on the same concept as dual-porosity and dual-permeability models but include additional interacting pore regions [35, 36]. In these models, the transport of solute mass is determined with the transfer rate which describes the transport of solutes between the fracture and matrix domain by the sum of diffusive and convective fluxes. Straightforward descriptions of main preferential flow modelling approaches are given in reviews by [29] and [25].

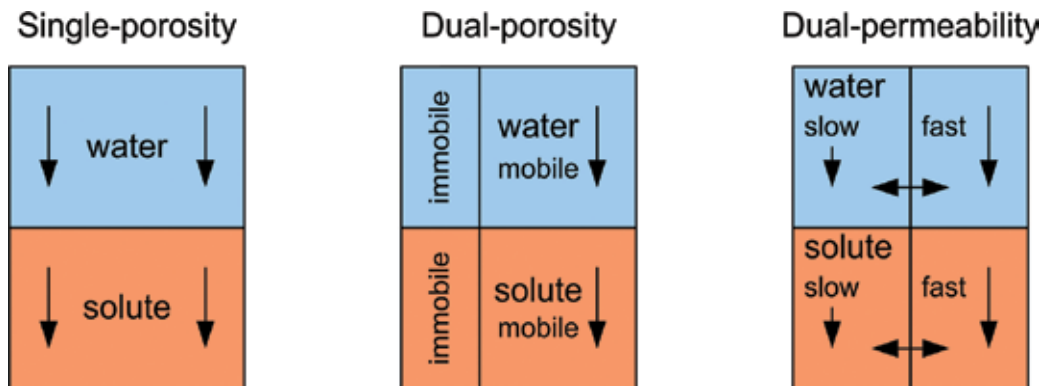


Figure 6. Scheme of transport processes assumptions in (from left to right) single-porosity, dual-porosity and dual-permeability models (adapted with the permission from [16]).

3.5. Available vadose zone models

A large number of programs are available for the description of water flow and solute transport in soil vadose zone. Below is the list and brief description of the most widely used software for modelling water flow and solute transport, which are applicable to unsaturated and partially saturated conditions.

HYDRUS-1D software includes one-dimensional finite-element model for simulating the movement of water, heat, and multiple solutes in variably saturated media [37].

HYDRUS (2D/3D) is a software package for simulating water, heat, and solute movement in two- and three-dimensional variably saturated media [38].

MACRO is a one-dimensional, process-oriented, dual-permeability model for water flow and reactive solute transport in soil [30].

TOUGH ('transport of unsaturated groundwater and heat') suite of software codes are multidimensional numerical models for simulating the coupled transport of water, vapour, non-condensable gas, and heat in porous and fractured media [39].

SWAP (soil, water, atmosphere, and plant) simulates transport of water, solutes and heat in unsaturated/saturated soils at field scale level, during growing seasons and for long-term time series [40].

The RZWQM is an integrated physical, biological, and chemical process model that simulates plant growth and movement of water, nutrients, and pesticides in run-off and percolate within agricultural management systems [41].

Animo is a detailed process-oriented simulation model for the evaluation of nitrate leaching to groundwater, N and P loads on surface waters and greenhouse gas emission [42].

LEACHM (the leaching estimation and chemistry model) refers to a suite of simulation models describing the water and chemical regime in unsaturated or partially saturated soil profiles [43].

Daisy is a dynamic model for the simulation of water and nitrogen dynamics and crop growth in agro-ecosystems [44].

4. Water and solute transport using HYDRUS software: case study in Croatia

The example will show the procedure of modelling water flow and nitrogen species transport in soil vadose zone. In this example, urea and NPK fertilizers were added to soil profile. The study site is located in the eastern Croatia in the intensive agricultural production area. The more information about the study can be found in [45]. The project main goal was to evaluate the influence of high fertilizer load, mostly nitrogen based, on the groundwater resources. Here, the results of modelling study on one selected site will be presented from year 2014.

HYDRUS-1D [37] was used to simulate water flow and nitrate transport and its ability to reproduce observed water and nitrate outflows (collected by lysimeters) was assessed. Simulations are carried out in one-dimensional domain using measured soil hydraulic parameters, climatic daily data, crop growth parameters, and fertilizer application rates as the input for model. Evapotranspiration rates were calculated using CROPWAT model [46] (based on the Penman-Monteith approach). The soil type at the site was classified as Haplic Gleysol Calcaric Eutric Siltic (Horizons: Ap-Bg-Cr-Cg), from which saturated hydraulic conductivity, retention curve (at different pressure head values), and saturated water content were measured. Optimization of necessary remaining hydraulic parameters (θ_r , α , and n) was performed using RETC software [17] by fitting the measured data. **Figure 7** shows the graph of the water retention curve data (circle) and the fitted water retention equation (line) for two upper soil layers. The fitting of the van Genuchten equation to data was confirmed by high R^2 values (>0.97).

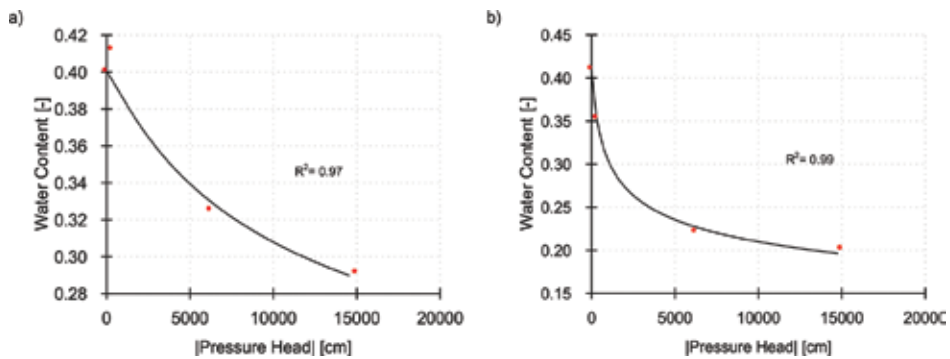


Figure 7. Soil water retention curves for (a) 0–25 soil layer, and (b) 25–50 cm soil layer derived from RETC software.

After acquiring all the necessary input data, we can proceed to modelling with HYDRUS. In the main processes window (**Figure 8** left), water flow and solute transport are selected with additional root water uptake and root growth option since Barley (*Hordeum vulgare* L.) was

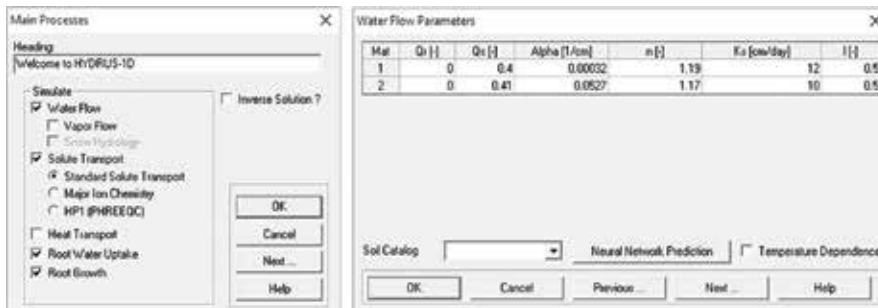


Figure 8. Main modelling process selection in HYDRUS-1D (left) and input of soil hydraulic parameters (right).

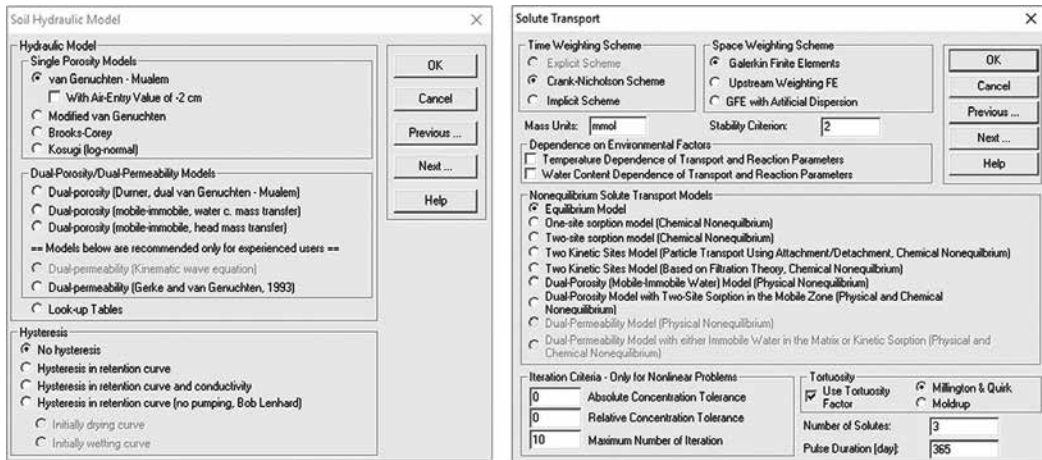


Figure 9. Snapshot of soil hydraulic (left) and solute transport (right) selection window in HYDRUS-1D.

grown at the site. After selecting geometry (length of the profile i.e. 50 cm) and time information (duration of the simulation, that is, 365 days) hydraulic parameters (θ_r , θ_s , α , n , K_s , l) for selected model are inserted (Figure 8 right).

In the soil hydraulic model window (Figure 9 left), there are multiple option to choose from, varying from single porosity to dual porosity/permeability model with different approaches. In this example, van Genuchten-Mualem equation was used without considering the effect of soil hysteresis. Initial and boundary conditions were chosen. Atmospheric boundary condition (which includes precipitation and evapotranspiration) was selected at the top and seepage face at the bottom boundary (to mimic lysimeter plate). Root water uptake was simulated using Feddes [20] model. As for water flow, it is necessary to select solute transport parameters (Figure 9 right). The number of solute are set to three since the simulation consider nitrification chain (urea > ammonium > nitrate). The first-order reaction term representing nitrification of urea to ammonium was 0.38 per day [47]. The first-order reaction term representing nitrification of ammonium to nitrate was 0.2 per day [47]. The first-order reaction term for the volatilization of ammonium to ammonia was 0.0552 per day [48]. The distribution coefficient for ammonium (K_d) is assumed to be $3.5 \text{ cm}^3 \text{ g}^{-1}$ [47]. The unrestricted passive root uptake of urea, ammonium and nitrate was assumed. For solute boundary condition, concentration flux and zero concentration gradient were selected for upper and lower boundary condition, respectively.

After inserting all the necessary data (derived from field observation and laboratory measurements of addition optimization) and running the model, pre-processing (input parameters, Figure 10 left) and post-processing (results, Figure 10 right) window are displayed in the HYDRUS.

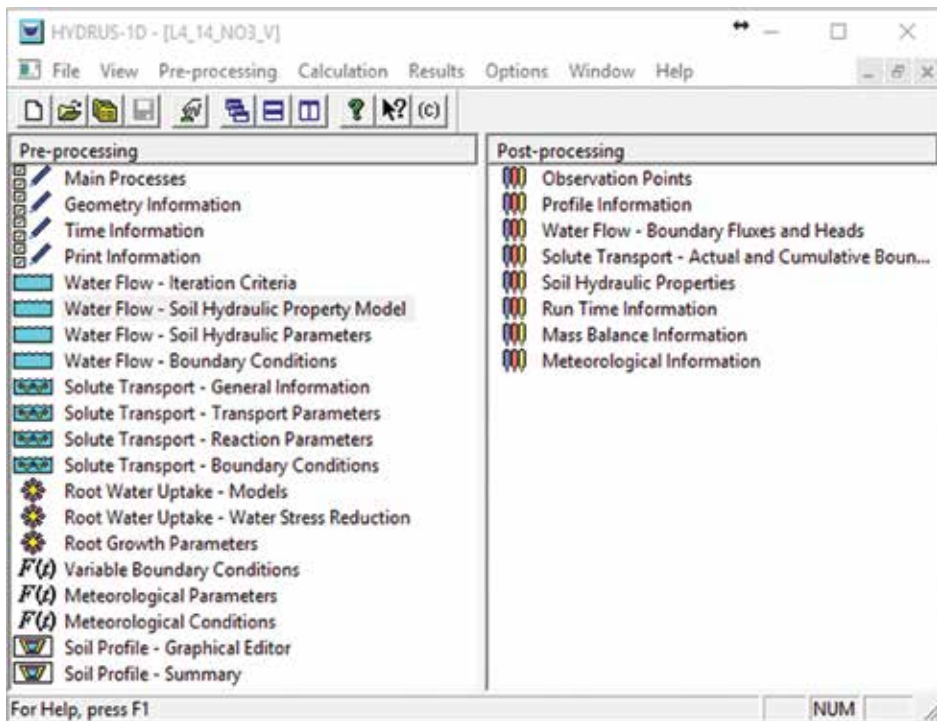


Figure 10. Snapshot of pre-processing (input data) and post-processing (results) window in HYDRUS-1D.

Cumulative water outflow, which was measured in lysimeter at site 4 during 2014 and simulated ones using HYDRUS-1D are presented on the **Figure 11**. The amount of water outflow from lysimeter was mainly the result of high precipitation events. The largest outflows were collected during wet part of the year, while during main crop vegetation season the outflows were very small due to large crop water demand (large transpiration intensity). Very high value of R^2 (0.96) between the measured and simulated values indicates that the HYDRUS model was capable to reproduce field data with high efficiency. Simulated values of nitrate outflow reflect the water flow pattern (**Figure 12**) which was measured in the same lysimeter (site 4) during 2014. Although the model derived larger cumulative nitrate outflows compared to the measured ones, the R^2 value of 0.72 indicate good model ability to simulate nitrogen transformation (from urea and ammonium to nitrate) and transport. The larger simulated nitrate values could be due to denitrification process that might occur in soil which was not considered in the modelling. From **Figure 12**, it can be seen that the main nitrate leaching occurs at the end of the simulation period after barley harvesting (day 164) and during wet period (autumn/winter). Our results indicate that numerical models can be very helpful for estimating water flow and nitrate dynamics under field conditions. From this example, it can be seen the possible negative influence of the nitrogen fertilizer application and their potential of leaching below root zone. One of the possible numerical models usages is their application in crop water demand (irrigation) and fertilization optimization or pesticide management in agriculture which can eventually lead to the protection of environment.

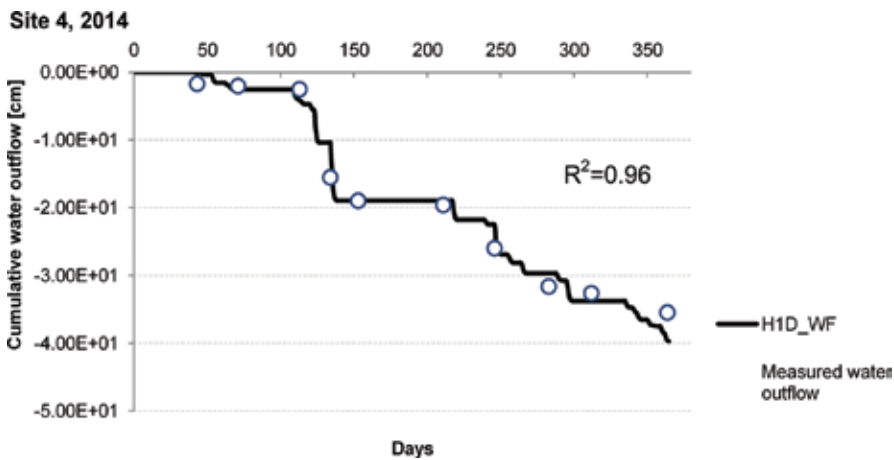


Figure 11. Observed cumulative water outflows from lysimeter (site 4) in 2014 and simulated ones using HYDRUS-1D.

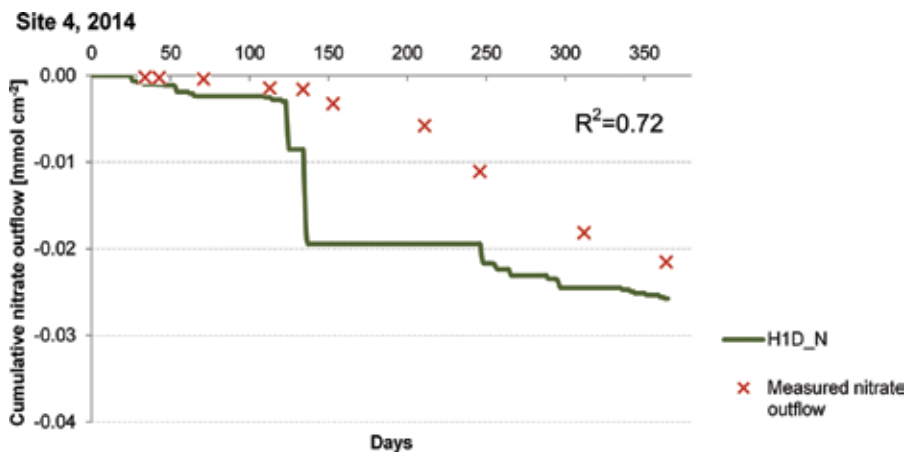


Figure 12. Observed cumulative nitrate outflows from lysimeter (site 4) in 2014 and simulated ones using HYDRUS-1D.

5. Trace metals mobility in soil-plant system

In some recent reports by European Commission [49], contamination by trace metal elements (Cd, Cu, Pb, Zn, Ni, Cr) and some nutrients (N, P) was defined as one of the main pressures to environmental resources in Europe. Contamination of arable soil resources by trace metal elements due to different anthropogenic activities is increasing rapidly and continuously in the last decades at the global level and often with detrimental ecological scenarios [50]. Trace metal elements represent relatively wide group of essential and some of the most toxic

elements for biota which occur generally at very low levels in the 'clean' pedospheres. For instance, the total contents of trace elements in non-contaminated mineral top soils range from 1 to 100 ppm [51], but in contaminated soils, their concentrations may be higher by up to several orders of magnitude.

Trace metal behaviour in the ecosystems, their chemical forms (species), mobility and risk of inclusion into the food chain, greatly depend on the environmental conditions. For example, the contamination of soil by trace metals is followed by a cascade of reactions with soil surfaces and the concentration of metals in the soil solution is controlled by a number of inter-related processes: oxidation/reduction, precipitation/dissolution, adsorption/desorption, inorganic and organic complex formation [52]. Which processes will predominate depends on the physical, chemical, and biological properties of the (non)contaminated soil, as well as the important environmental factors (e.g. moisture, temperature, aeration). The most dominant parameters controlling soil trace metals chemistry and availability to plants are pH and soil OM. At lower soil pH values, hydrogen ions are adsorbed to soil particles, which increases the positive charge on inorganic and organic soil components, resulting in weaker adsorption of metal cations and their increased mobility in soil. SOM has a two-sided role in metal mobility in soil: (i) particulate SOM is retaining trace metals through the formation of metal-SOM complexes, thus decreasing their mobility [53], and (ii) dissolved organic matter (DOM) can increase trace metal mobility due to formation of metal-DOM complexes [54] that are substantially less bounded to soil particles than a free metal ions.

Particular metal forms in soil fractions (soluble, solid, liquid) are possible to detect by adequate analytical technique [55] or predict by some of computational models (e.g. next section). However, inside the cultivated soil (vs. soil without plants), even at very small scales (up to several mm), the physically-chemical and/or biological characteristics may differ substantially, and thus consequently influence trace metal biogeochemistry. It is especially pronounced at the soil-root interface, or so-called rhizosphere microarea. From the biogeochemical perspective, the rhizosphere is very dynamic and heterogenic microarea dominantly controlled by plant roots and released different organic metabolites.

Inside of relatively numerous group of trace metals, during the last decades, copper (Cu) has been intensively studied from different scientific perspectives given on several next facts: it is essential phytonutrient at small concentrations but easily becomes phytotoxic at higher levels; its biochemistry is pH-dependent; it is one of the most reactive trace metal elements with soil OM and over the huge reactive (mostly negatively charged surface) interface of OM, Cu strongly competes with some other positively charged metals (e.g. Cd, Zn) and thus impacts on its bioavailability. In the next section, one of the most advanced biogeochemical modelling approaches elaborates the influence of particular soil OM substances on Cu chemical speciation in relatively homogenous and realistic rhizosphere conditions.

5.1. Visual Minteq example: copper chemical speciation

Chemical speciation modelling was recognized as a very useful tool for studying various types of elements (nutrients, trace metals) and their mobility in natural systems such as rhizosphere. In the next, modelling in Visual MINTEQ chemical equilibrium program [56]) was performed

for three levels of Cu (non-contaminated and contaminated system), at three pH levels (covering the most naturally-occurring pH reactions in different rhizosphere environments) and at three levels of soil dissolved OM (DOC; corresponds for mineral to organic soil types) (Table 2).

Species ^{1,2}	DOC ₁₀			DOC ₂₀			DOC ₃₀		
	Cu ₄₀	Cu ₂₅₀	Cu ₅₀₀	Cu ₄₀	Cu ₂₅₀	Cu ₅₀₀	Cu ₄₀	Cu ₂₅₀	Cu ₅₀₀
	% of total concentration			% of total concentration			% of total concentration		
pH 5 Cu ²⁺	4	18	28	1	6	11	0	3	5
CuNO ₃ ⁺	0	1	2	0	0	1	0	0	0
CuCO ₃ (aq)	0	0	0	0	0	0	0	0	0
Cu(OH) ₂ (aq)	0	0	0	0	0	0	0	0	0
Cu(CO ₃) ₂ ²⁻	0	0	0	0	0	0	0	0	0
HA1-Cu (6) (aq)	60	61	55	55	67	68	50	66	70
HA2-Cu (6) (aq)	36	20	14	44	27	21	49	31	25
pH 7 Cu ²⁺	0	1	2	0	0	0	0	0	0
CuNO ₃ ⁺	0	0	0	0	0	0	0	0	0
CuCO ₃ (aq)	0	1	4	0	0	1	0	0	0
Cu(OH) ₂ (aq)	0	0	0	0	0	0	0	0	0
Cu(CO ₃) ₂ ²⁻	0	0	0	0	0	0	0	0	0
HA1-Cu (6) (aq)	5	13	18	3	9	13	3	7	11
HA2-Cu (6) (aq)	95	85	75	97	91	85	97	93	89
pH 9 Cu ²⁺	0	0	0	0	0	0	0	0	0
CuNO ₃ ⁺	0	0	0	0	0	0	0	0	0
CuCO ₃ (aq)	0	1	4	0	0	0	0	0	0
Cu(OH) ₂ (aq)	0	0	1	0	0	0	0	0	0
Cu(CO ₃) ₂ ²⁻	0	0	2	0	0	0	0	0	0
HA1-Cu (6) (aq)	0	1	2	0	1	1	0	0	1
HA2-Cu (6) (aq)	100	97	91	100	99	98	100	99	99

¹HA-Cu: humic acid-complexed Cu via 1-carboxylic and 2-phenolic functional groups.

²Species with the < 0.5% of total concentration are not shown.

Table 2. Distribution (%) of Cu species in tested soil solution, estimated by Visual MINTEQ chemical equilibrium software (NICA-Donnan model) as affected by soil pH (5, 7, and 9), dissolved organic carbon (DOC; 10, 20, and 30 mgL⁻¹) and different soil Cu total concentration (40, 250, and 500 mg kg⁻¹).

Even though the total soil Cu content by itself is not an adequate measure to determine Cu mobility and phytoavailability, a strong positive correlation between total element concentra-

tion and its bioavailable fraction is often reported, especially in contaminated soils or in trials on soils spiked by metals [57]. In this model, chosen soil total Cu concentrations were (in mg kg⁻¹); 40 (correspond to most of non-contaminated soil conditions), 250 and 500 (corresponds from medium to highly contaminated soil conditions). The mobility of trace metals in soil depends ultimately on their chemical speciation, which is actually a function of pH and the presence of inorganic and organic ligands in the soil solution. The non-ideal competitive adsorption (NICA)-Donnan (sub)model for the adsorption of cations onto dissolved organic matter (DOC) and software database on equilibrium constants [58] was applied in this model. Cu concentrations used for Cu speciation here were average values obtained from experimental data from CaCl₂ extracts, and for other elements in soil solution from saturated soil water extracts [53]. Ionic strength was set to be calculated and temperature of 25°C for all the calculations. Other software default settings were not modified.

From the data presented in **Table 2**, it can be seen that the majority of Cu in the modelled solutions was founded as a Cu-DOC complex, suggesting that DOC might be the main factor affecting Cu ultimate fate after its release from the soil solid phase into the rhizosphere solution. Increase in total Cu concentration led to an increase in free Cu²⁺ ion in the modelled solutions, but only at lower concentrations of DOC and at acid pH (**Table 2**). Even though in every investigated scenario, the majority of Cu in the modelled solution was found to be complexed with DOC (**Table 2**), an increased soil pH caused the reduction of the percentage of free Cu ion in the solution. It is known that free metal ion is considered the most mobile species in the soil, thus data are implicating a decreased metal mobility in soil with an increase in soil pH. Furthermore, with an increase in soil pH Cu shifted from carboxylic groups in humic acids (HA1-Cu (6)) to phenolic functional groups (HA2-Cu (6)), which is in agreement with some previous models that phenolic groups might be more important for metal (e.g. Cd, Cu) binding under higher pH of surrounding media [55].

6. Conclusion

Located at the atmosphere, plant, soil, and water interface, vadose zone is represented by a variety of linked complex processes. For solving problems such as the transport of nutrients, pesticides, pharmaceuticals, colloids, bacteria, viruses, hormones, and toxic trace elements, carbon sequestration, and bioremediation of organic contaminants, a thorough understanding and coupling of multiple hydrogeological, geochemical, and microbiological processes is needed. Models should be considered as one of the most advanced and useful 'tools' which, when used properly, can predict different scenarios, with positive or negative outcome, that can occur in the natural systems. With development of numerical models, such complex problems can be solved more successfully using different mathematical expressions and approaches. The accuracy of model predictions rely largely upon a quality and quantity of input parameters required for a specific problems, mostly due to large heterogeneity of the soil. Thus, fundamental knowledge of basic soil physics is needed, which combined with new measurement techniques provides satisfactory foundation for performing modelling. In recent

years, scientists have been mostly engaged in the coupling of different numerical models, since no single model is yet available for describing such complex system as soil vadose zone [59]. Development of coupled numerical models capable of describing unstable preferential flow in soils, as well as models coupled with sophisticated geochemical models capable of describing complex kinetic chemical and biological reactions will remain a focus of research in the near future.

Author details

Vilim Filipović, Gabrijel Ondrašek and Lana Filipović

*Address all correspondence to: vfilipovic@agr.hr

Department of Soil Amelioration, Faculty of Agriculture, University of Zagreb, Svetošimunska, Zagreb, Croatia

References

- [1] Topp GC, Ferré PA. Thermogravimetric using convective oven-drying. In: Dane JH, Topp GC, editors. *Methods of Soil Analysis: Part 4, Physical Methods*. Madison: SSSA; 2002. p. 422–424.
- [2] Topp GC, Ferré PA. Water content. In: Dane JH, Topp GC, editors. *Methods of Soil Analysis: Part 4, Physical Methods*. Madison: SSSA; 2002. p. 417–422.
- [3] Bolt GH. Soil physics terminology. *Bulletin of International Society of Soil Science*. 1976;49:26–36.
- [4] Radcliffe D, Šimunek J. *Soil physics with HYDRUS: modeling and applications*. Boca Raton: CRC Press; 2010. 370 p.
- [5] Jury WA, Horton R. *Soil physics*. 6th ed. Hoboken: Wiley; 2004. 370 p.
- [6] Young MH, Sisson JB. Tensiometry. In: Dane JH, Topp GC, editors. *Methods of Soil Analysis: Part 4, Physical Methods*. Madison: SSSA; 2002. p. 575–608.
- [7] Andraski BJ, Scanlon BR. Thermocouple psychrometry. In: Dane JH, Topp GC, editors. *Methods of Soil Analysis: Part 4, Physical Methods*. Madison: SSSA; 2002. p. 609–642.
- [8] Scanlon BR, Andraski BJ, Bilskie J. Miscellaneous methods for measuring matric or water potential. In: Dane JH, Topp GC, editors. *Methods of Soil Analysis: Part 4, Physical Methods*. Madison: SSSA; 2002. p. 643–670.

- [9] Carsel RF, Parrish RS. Developing joint probability distributions of soil water retention characteristics. *Water Resources Research*. 1988;24:755–769. DOI: 10.1029/wr024i005p00755
- [10] Richards LA, Ogata G. Psychrometric measurements of soil samples equilibrated on pressure membranes. *Proceedings of Soil Science Society of America Journal*. 1961;25:456–459. DOI: 10.2136/sssaj1961.03615995002500060012x
- [11] Brooks RH, Corey AT. Hydraulic properties of porous media. *Hydrology Paper*. 3 ed. Fort Collins: Colorado State University; 1964. 24 p.
- [12] Leij FJ, Russell WB, Lesch SM. Closed-form expressions for water retention and conductivity data. *Ground Water*. 1997;35:848–858. DOI: 10.1111/j.1745-6584.1997.tb00153.x
- [13] Kosugi K. Lognormal distribution model for unsaturated soil hydraulic properties. *Water Resources Research*. 1996;32:2697–2703. DOI: 10.1029/96wr01776
- [14] van Genuchten MTh. A closed form equation for predicting the hydraulic conductivity of unsaturated soils. *Soil Science Society of America Journal*. 1980;44:892–1037. DOI: 10.2136/sssaj1980.03615995004400050002x
- [15] Mualem Y. A new model for predicting the hydraulic conductivity of unsaturated porous media. *Water Resources Research*. 1976;12:513–522. DOI: 10.1029/wr012i003p00513
- [16] Šimunek J, van Genuchten MTh. Contaminant transport in the unsaturated zone: theory and modeling. In: Delleur J, editor. *The Handbook of Groundwater Engineering*. 2nd ed. Boca Raton: CRC Press; 2006. p. 22.1–22.46.
- [17] Van Genuchten MTh, Leij FJ, Yates SR. *The RETC Code for Quantifying the Hydraulic Functions of Unsaturated Soils*. Version 1.0. EPA Report 600/2-91/065 ed. Riverside, California: U.S. Salinity Laboratory, USDA; 1991. 85 p.
- [18] Schaap MG, Leij FJ, van Genuchten MTh. ROSETTA: a computer model for estimating soil hydraulic parameters with hierarchical pedotransfer functions. *Journal of Hydrology*. 2001;251:163–176. DOI: 10.1016/s0022-1694(01)00466-8
- [19] Richards LA. Capillary conduction of liquids through porous mediums. *Physics*. 1931;1:318–333. DOI: 10.1063/1.1745010
- [20] Feddes RA, Kowalik PJ, Zaradny H. *Simulation of Field Water Use and Crop Yield*. New York: Wiley; 1978. 188 p.
- [21] Biggar JW, Nielsen DR. Miscible displacement and leaching phenomena. In: Hagen RM, editor. *Irrigation of agricultural lands*. Agronomy Monograph ed. American Society of Agronomy; Madison, 1967. p. 254–274. DOI: 10.2134/agronmonogr11.c15
- [22] Freundlich H. *Kapillarchemie; eine Darstellung der Chemie der Kolloide und verwandter Gebiete*. Leipzig, Germany: Akademische Verlagsgesellschaft; 1909.

- [23] Langmuir I. The adsorption of gases on plane surfaces of glass, mica, and platinum. *Journal of the American Chemical Society*. 1918;40:1361–1403. DOI: 10.1021/ja02242a004
- [24] Beven KJ, Germann PF. Macropores and water flow in soils. *Water Resources Research*. 1982;18:1311–1325. DOI: 10.1029/wr018i005p01311
- [25] Gerke HH. Preferential-flow descriptions for structured soils. *Journal of Plant Nutrition and Soil Science*. 2006;169:1–19. DOI: 10.1002/jpln.200521955
- [26] Pruess K, Wang JSY. Numerical modeling of isothermal and non-isothermal flow in unsaturated fractured rock—a review. In: Evans DD, Nicholson TJ, editors. *Flow and Transport through Unsaturated Fractured Rock*. Geophysics Monograph ed. Washington: American Geophysical Union; 1987. p. 11–22.
- [27] Gerke HH, van Genuchten MTh. A dual-porosity model for simulating the preferential movement of water and solutes in structured porous media. *Water Resources Research*. 1993;29:305–319. DOI: 10.1029/92wr02339
- [28] Jarvis NJ. Modeling the impact of preferential flow on nonpoint source pollution. In: Selim HM, Ma L, editors. *Physical Nonequilibrium in Soils: Modeling and Application*. Chelsea: Ann Arbor Press; 1998. p. 195–221.
- [29] Šimunek J, Jarvis NJ, van Genuchten MTh, Gärdenäs A. Review and comparison of models for describing non-equilibrium and preferential flow and transport in the vadose zone. *Journal of Hydrology*. 2003;272:14–35. DOI: 10.1016/s0022-1694(02)00252-4
- [30] Jarvis NJ. The MACRO Model (Version 3.1). Technical Description and Sample Simulations. Reports and Dissertations. 19 ed. Uppsala, Sweden: Swedish University of Agricultural Science; 1994. 51 p.
- [31] Ahuja LR, Hebson C. Root Zone Water Quality Model. GPSR Technical Report No. 2 ed. Fort Collins: USDA, ARS; 1992.
- [32] Chen C, Wagenet RJ. Simulation of water and chemicals in macropore soils. Part 1. Representation of the equivalent macropore influence and its effect on soil water flow. *Journal of Hydrology*. 1992;130:105–126. DOI: 10.1016/0022-1694(92)90106-6
- [33] Germann PF. Kinematic wave approach to infiltration and drainage into and from soil macropores. *Transactions of the ASAE*. 1985;28:745–749. DOI: 10.13031/2013.32331
- [34] Germann PF, Beven K. Kinematic wave approximation to infiltration into soils with sorbing macropores. *Water Resources Research*. 1985;21:990–996. DOI: 10.1029/wr021i007p00990
- [35] Gwo JP, Jardine PM, Wilson GV, Yeh GT. A multiple-pore-region concept to modeling mass transfer in subsurface media. *Journal of Hydrology*. 1995;164:217–237. DOI: 10.1016/0022-1694(94)02555-p

- [36] Hutson JL, Wagenet RJ. A multiregion model describing water flow and solute transport in heterogeneous soils. *Soil Science Society of America Journal*. 1995;59:743–751. DOI: 10.2136/sssaj1995.03615995005900030016x
- [37] Šimunek J, Šejna M, van Genuchten MTh. The HYDRUS-1D Software Package for Simulating the One-Dimensional Movement of Water, Heat, and Multiple Solutes in Variably-Saturated. Version 2.0, IGWMC – TPS-70 ed. Golden: International Ground Water Modeling Center, Colorado School of Mines; 1998. 202 p.
- [38] Šimunek J, van Genuchten MTh, Šejna M. Development and applications of the HYDRUS and STANMOD software packages and related codes. *Vadose Zone Journal*. 2008;7:587–600. DOI: 10.2136/vzj2007.0077
- [39] Finsterle S, Sonnenthal EL, Spycher N. Advances in subsurface modeling using the TOUGH suite of simulators. *Computers & Geosciences*. 2014;65:2–112. DOI: 10.1016/j.cageo.2013.06.009
- [40] van Dam JC, Huygen J, Wesseling JG, Feddes RA, Kabat P, van Walsum PEV, Groenendijk P, van Diepen CA. Theory of SWAP, Version 2.0. Simulation of Water Flow, Solute Transport and Plant Growth in the Soil- Water-Atmosphere- Plant Environment. Report 71, DLO Winand Staring Centre, Technical Document 45 ed. Wageningen: Department Water Resources, WAU; 1997. 165 p.
- [41] Ahuja LR, Rojas KW, Hanson JD, Shaffer MJ, editors. The Root Zone Water Quality Model: Modelling Management Effects on Water Quality and Crop Production. Highlands Ranch: Water Resources Publications LLC; 1999. 384 p.
- [42] Groenendijk P, Renaud LV, Roelsma J. Prediction of Nitrogen and Phosphorus Leaching to Groundwater and Surface Waters. Process Descriptions of the Animo 4.0 Model ed. Wageningen: Alterra–Report 983; 2005. 114 p.
- [43] Hutson JL, Wagenet RJ. LEACHM: Leaching estimation and chemistry model: a process-based model of water and solute movement, transformations, plant uptake and chemical reactions in the unsaturated zone. Version 3.0. Cornell University, Ithaca. 1992.
- [44] Abrahamsen P, Hansen S. Daisy: an open soil-crop-atmosphere system model. *Environmental Modelling & Software*. 2000;15:313–330. DOI: 10.1016/s1364-8152(00)00003-7
- [45] Filipović V, Kodešová R, Petošić D. Experimental and mathematical modeling of water regime and nitrate dynamics on zero tension plate lysimeters in soil influenced by high groundwater table. *Nutrient Cycling in Agroecosystems*. 2013;95:23–42. DOI: 10.1007/s10705-012-9546-5
- [46] Smith M. CROPWAT: Manual and Guidelines. Rome: FAO of UN; 1991.

- [47] Hanson BR, Šimunek J, Hopmans JW. Numerical modeling of urea-ammonium-nitrate fertigation under microirrigation. *Agricultural Water Management*. 2006;86:102–113. DOI: 10.1016/j.agwat.2006.06.013
- [48] Bolado-Rodríguez S, Alonso-Gaite A, Álvarez-Benedi J. Characterization of nitrogen transformations, sorption and volatilization processes in urea fertilized soils. *Vadose Zone Journal*. 2005;4:329–336. DOI: 10.2136/vzj2004.0102
- [49] European Commission. Communication from the Commission to the Council, the European Parliament, the European Economic and Social Committee and the Committee of the Regions. Thematic Strategy for Soil Protection. Brussels, COM (2006) 231.
- [50] Seshadri B, Bolan NS, Naidu R. Rhizosphere-induced heavy metal(loid) transformation in relation to bioavailability and remediation. *Journal of Soil Science and Plant Nutrition*. 2015;15:524–548. DOI: 10.4067/s0718-95162015005000043
- [51] Kabata-Pendias A. Soil–plant transfer of trace elements—an environmental issue. *Geoderma*. 2004;122:143–149. DOI: 10.1016/j.geoderma.2004.01.004
- [52] Romić M. Bioavailability of trace metals in terrestrial environment: methodological issues. *European Chemical Bulletin*. 2012;1:489–493.
- [53] Matijević L, Romić D, Romić M. Soil organic matter and salinity affect copper bioavailability in root zone and uptake by *Vicia faba* L. plants. *Environmental Geochemistry and Health*. 2014;36:883–896. DOI: 10.1007/s10653-014-9606-7
- [54] Kirchmann H, Eriksson J. Trace elements in crops: effects of soil physical and chemical properties. In: Gliński J, Horabik J, Lipiec J, editors. *Encyclopedia of Agrophysics*. Dordrecht: Springer; 2011. p. 910–912.
- [55] Ondrasek G, Rengel Z. The role of soil organic matter in trace element bioavailability and toxicity. In: Ahmad P, Prasad MNV, editors. *Abiotic Stress Responses in Plants: Metabolism, Productivity and Sustainability*. New York: Springer; 2012. p. 403–423.
- [56] Gustafsson JP. Arsenate adsorption to soils: modelling the competition from humic substances. *Geoderma*. 2006;136:320–330. DOI: 10.1016/j.geoderma.2006.03.046
- [57] Romić M, Romić D, Ondrašek, G. Heavy metals accumulation in topsoils from the wine-growing regions. Part 2. Relationships between soil properties and extractable copper contents. *Agriculturae Conspectus Scientificus*. 2004;69:35–41.
- [58] Kinniburgh DG, Milne CJ, Benedetti MF, Pinheiro JP, Filius J, Koopal LK. Metal ion binding by humic acid: application of the NICA-Donnan model. *Environmental Science and Technology*. 1996;30:1687–1698. DOI: 10.1021/es950695h
- [59] Šimunek J. Models of water flow and solute transport in the unsaturated zone. In: Anderson MG, editor. *Encyclopedia of Hydrological Sciences*. Wiley-Blackwell; Hoboken, 2005. p. 1171–1180. DOI: 10.1002/0470848944.hsa080

Study of Unsaturated Soils by Coupled Numerical Analyses of Water Flow-Slope Stability

Norma Patricia López-Acosta and
José Alfredo Mendoza-Promotor

Additional information is available at the end of the chapter

<http://dx.doi.org/10.5772/63903>

Abstract

The geotechnical engineering, among the problems related to water flow, is specifically interested in soil and water that it contains, and also on the movement of water through their pores, in addition to the laws governing this phenomenon. A very important subject is to quantify the retention and filtration of water within the soil structure; however, the emphasis should be not only on how much water flows through the soil but also on the state of pore water pressures because this pressure, either positive or negative, has a direct influence on the stress state and changes in volume of soil. Several publications address the issue of water flow in saturated state; however, only some of them consider the flow under unsaturated conditions. In this chapter, the main emphasis is focused on the study of water flow in unsaturated soils.

Initially, the basic concepts and the main equations applicable to the study of water flow in unsaturated media are defined. Then, fitting and estimation models of soil hydraulic functions (soil-water characteristic curve and hydraulic conductivity function) necessary to solve this type of problems are discussed. The importance of considering calculations in the unsaturated zone of the flow region is demonstrated by the analysis of a tailings dam. It is explained how to perform two-dimensional (2D) and three-dimensional (3D) numerical analysis of water flow by finite element method (FEM) under steady and transient-state conditions, whose results are evaluated and coupled to study the stability of the structure assuming the *phi-b* linear model for unsaturated soils. Special attention to the analysis of the variations obtained in 2D and 3D models constructed with extrusions and rough topography of the site is given. Finally, important recommendations for engineering practice according to the results obtained are issued.

Some concluding remarks and recommendations of the analyses presented in this chapter are as follows:

- The mathematical models for estimating soil-water characteristic curve and hydraulic conductivity function are an important tool when laboratory test results

are not available because of the high costs of these tests or the requirements of specialized equipment and personnel to perform them.

- 3D models have important advantages over 2D models because they can include irregular geometries of the structure under study, topographical configuration of soil, unsaturated flow conditions, more realistic boundary conditions representing the environment, among others.
- To get more representative numerical analyses, the unsaturated soil theory should be considered for all those situations where the material is in this state.
- In this chapter, it is demonstrated that the considerations exposed for modelling, estimation, and fitting of hydraulic functions of soil provide the necessary elements to carry out these analyses in a simple way.
- Computer programs facilitate the study of transient-state flow and unsaturated soil condition, whose analytical solutions are generally complicated and laborious.

Keywords: water flow, unsaturated soils, numerical analysis, coupled water flow-slope stability analysis, soil-water characteristic curve, hydraulic conductivity function

1. Introduction

Unsaturated soils are characterized by negative pore-water pressure. In practical terms, partially saturated and unsaturated are synonymous: both terms indicate a degree of saturation lower than one; however, in specific terms, unsaturated implies the introduction of a third phase (gaseous) to the two-phase system already present in the saturated soils (liquid and solid phases only) [1].

Currently, computer programs are helpful for solving problems of water flow and facilitate both the study of transient-state flow and the characterization of unsaturated soils, which, from an analytical standpoint, are complicated and laborious tasks [2].

To demonstrate the application of the theoretical foundations presented in this chapter, an analysis of a tailings dam is presented as a case study. These structures are generally found in an unsaturated state. Thus, the primary goals of this analysis are to describe the applied methodology and to establish criteria and recommendations that can be followed to solve related problem types.

2. General theoretical foundations of unsaturated soils

2.1. Soil suction

Several definitions exist that define soil suction and its significance [3–5]; however, for practical engineering applications, proposed definitions are either unsuitable or complex because they are largely based on thermodynamic concepts. In simpler terms, suction can be defined as a

state of negative water pressure in the soil, which is influenced by several factors [6], including temperature, gravity, capillary effects, salt content, and electrical charge (van der Waals forces), among others.

Total suction, or simply suction, is composed of two variables: (a) matric suction and (b) osmotic suction. Matric suction describes the difference between air pressure and water pressure [6], whereas osmotic suction is defined as the negative pressure resulting from the effect of the dissolved salts in the water of the soil matrix. Osmotic suction is commonly disregarded due to its lesser influence on total suction in addition to the difficulty of separating these two variables.

2.2. Water storage function or SWCC

The storage function, which is also defined by the soil-water characteristic curve (SWCC), describes the relationship between the water content of the soil (degree of saturation, gravimetric, or volumetric water content) and the soil suction. The nature of the SWCC is directly associated with grain-size distribution and soil structure. Therefore, the water content-suction ratio varies as a function of the material type (Figure 1).

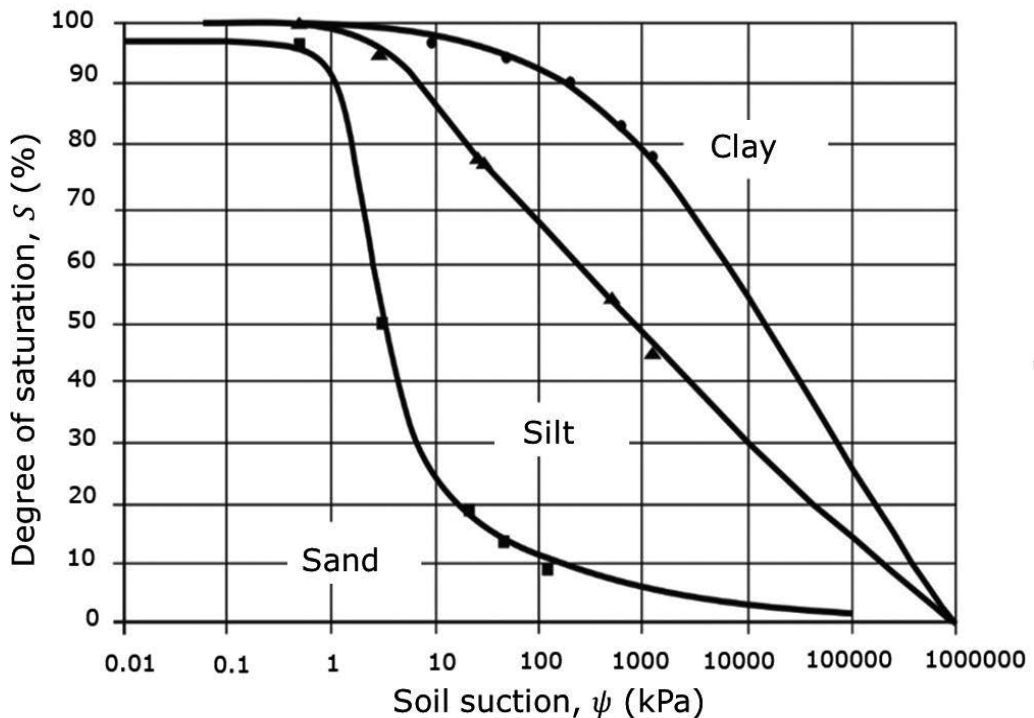


Figure 1. Soil-water characteristic curve (SWCC) for different soil types [7].

The SWCC represents a fundamental relationship that can be used to describe the behaviour of unsaturated soils [8]. Similarly, the SWCC can be used to determine other properties, such as the permeability and shear strength of soil and the volumetric changes of soil [9].

Several methods and empirical relationships have been proposed to describe the SWCC. Several of these models use relationships that depend on the air entry value, the residual water content, or the slope of the curve [10, 11]. Other procedures are based on the grain-size distribution curve in addition to other soil properties (volume-mass properties) or the use of statistical correlations between soil data and soil water content [9, 12, 13]. The reliability of the models depends on the quality and quantity of data used for the statistical correlations [14]. Other methods consider the pore-size distribution within the soil, which, in certain cases, can be determined from the grain-size distribution curve of the material [15–17].

2.2.1. Interpretation of the SWCC

The SWCC can be associated with three zones that describe the desaturation process of a soil (**Figure 2**). In addition, the SWCC allows for the saturated and residual water content to be determined, as well as their respective suction values, which are the main parameters that represent the SWCC as an input into one of the fitting methods mentioned in this chapter:

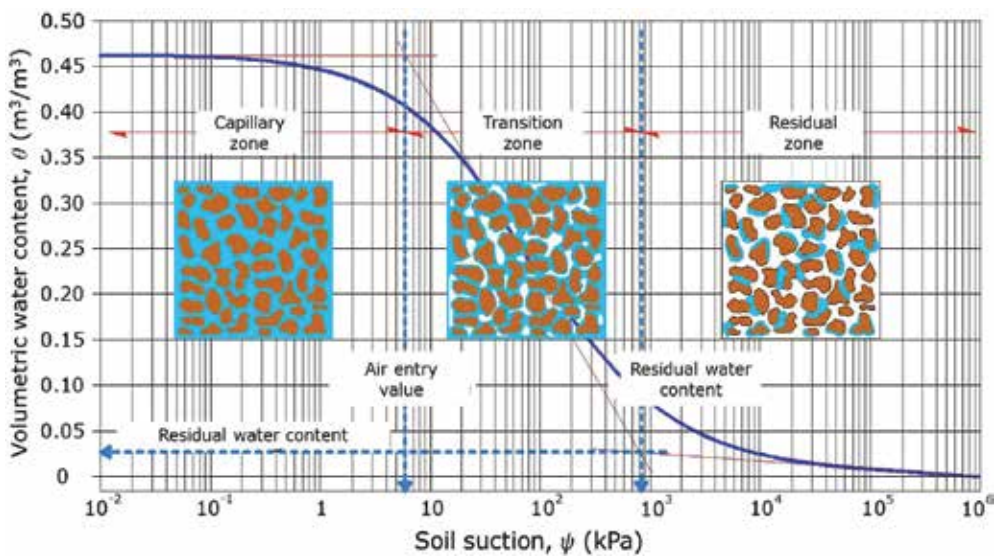


Figure 2. Zones corresponding to the soil-water characteristic curve (SWCC).

- *Saturated capillary zone.* The soil zone that is maintained in a saturated state, whose defining limit coincides with the air-entry value [18], which can be described as the value that the matric suction must exceed before air enters into the soil macropores.

- *Desaturation zone.* The zone where water is displaced due to the air entry in the pores. The defining limit of this zone is determined by the residual water content or where water in the pores becomes discontinuous and permeability considerably decreases.
- *Residual zone.* This section of the curve represents the zone where increases in suction do not produce significant changes in water content. As water is so scarce, it does not flow between pores, and its removal only occurs by evaporation [19]. This region is characterized by extremely high suction values.
- *Air-entry value.* Represents the suction value at which air begins to displace water in pores, which begins with those of greatest size.
- *Residual value.* Represents the suction value at which the liquid phase of the soil becomes discontinuous and surrounds soil particles as a thin film.
- *Residual water content.* The content of water at which high suction values are required to remove any additional water from the soil mass.
- *Saturated water content.* The water content in soil in a saturated state.

2.2.2. Estimation methods of SWCC

When laboratory data on the relationship between suction and water content are unavailable or insufficient, estimation models are one method used to determine the SWCC as a function of the index properties of soil (volume-mass and grain-size distribution relationships). Currently, there are several models that allow for the SWCC to be determined, including the following:

- Fredlund and Wilson method [9]
- Scheinost, Sinowski, and Auerswald method [20]
- Aubertin, Mbonimpa, Bussi re, and Chapuis method (modified from Kovacs) [21]
- Zapata's correlations [22]
- Arya and Paris method [15]

2.2.3. Fitting methods of SWCC

Fitting methods are based on experimental or empirical equations that aim to define the SWCC according to data obtained from laboratory tests. Fitting methods are used when laboratory data are available, yet given the dispersion of the values, it is necessary to apply models to adjust or define the data trend to generate a representative curve for the material considered in the study.

Several models have been developed to define the SWCC [23], which consider fitting parameters that provide a range of flexibility to represent distinct materials. In **Table 1**, several of the most common fitting methods for SWCC are listed. These equations consider gravimetric water content as the primary variable; however, the equations can also use volumetric water content or the degree of soil saturation as inputs [24].

Model	Equation
Van Genuchten (1980)	$w_w = w_r + (w_s - w_r) \left\{ \frac{1}{1 + (a_{vb}\psi)^{n_{vb}}} \right\}$
Gardner (1958)	$w_w = w_r + (w_s - w_r) \left\{ \frac{1}{a_g \psi^{n_g}} \right\}$
Brooks and Corey (1964)	$w_w = w_r + (w_s - w_r) \left[\frac{a_c}{\psi} \right]^{n_c}$
Van Genuchten and Mualem (1976)	$w_w = w_r + (w_s - w_r) \left\{ \frac{1}{1 + (a_{vm}\psi)^{n_{vm}}} \right\}^{m_{vm}}$
Van Genuchten (1980)	$w_w = w_r + (w_s - w_r) \left\{ \frac{1}{1 + (a_{vg}\psi)^{n_{vg}}} \right\}$
Fredlund and Xing (1994)	$w_w = w_s \left[1 - \frac{\ln(1 + \psi/\psi_r)}{\ln(1 + 10^6/\psi_r)} \right] \left\{ \frac{1}{[\ln(e + (\psi/\psi_r)^{n_f})]^{m_f}} \right\}$
where	
w_s	saturated gravimetric water content
w_r	residual gravimetric water content
ψ	soil suction
a_{vb}	adjustment parameter that depends on the air-entry value of the soil
n_{vb}	adjustment parameter that depends on the desaturation velocity of the soil once the air-entry value has been exceeded
m_{vm}	adjustment parameter related to the residual water content of soil, which is considered to be $m_{vm}=1-2/n_{vb}$
a_g	adjustment parameter derived from the air-entry value of the soil
n_g	adjustment parameter that depends on the desaturation velocity of the soil once the air-entry value has been exceeded
a_c	air pressure
n_c	soil pore size index
a_{vm}	adjustment parameter that depends on the air-entry value of the soil
n_{vm}	adjustment parameter that depends on the desaturation velocity of the soil once the air-entry value has been exceeded
m_{vm}	adjustment parameter related to the residual water content of soil, which is considered to be $m_{vm}=1-1/n_{vm}$
a_{vg}	adjustment parameter that depends on the air-entry value of the soil

Model	Equation
n_{vg}	adjustment parameter that depends on the desaturation velocity of the soil once the air-entry value has been exceeded
m_{vb}	adjustment parameter related to the residual water content of soil, is considered to be $m_{vg}=1-1/n$ or $m_{vb}=1-1/2n$
a_f	adjustment parameter that depends on the air-entry value of the soil
n_f	adjustment parameter that depends on the desaturation velocity of the soil once the air-entry value has been exceeded
m_f	adjustment parameter related to the residual water content of soil
ψ_r	residual suction
e	irrational number

Table 1. Experimental fitting models of the SWCC.

2.3. Hydraulic conductivity function

The hydraulic conductivity function represents the relationship between hydraulic conductivity and soil suction and can be expressed as a function of the degree of saturation or volumetric water content of soil.

Several estimation methods are based on the SWCC and the saturated hydraulic conductivity at distinct suction intervals. These techniques can be classified into the following categories:

- *Empirical or experimental equations.* These equations outline the relationship between the SWCC and a hydraulic conductivity function, including the models of Brooks and Corey [25] and Gardner [26].
- *Statistical equations.* These equations consist of a physical model that represents the trajectories of water flow through soil pores of different sizes. Examples of these include the models of Van Genuchten and Burdine [27] and Van Genuchten and Mualem [28].
- *Correlation equations.* These models are based on a proposed relationship between the SWCC and the hydraulic conductivity function, for example, the model of Leong and Rahardjo [29].
- *Regression equations.* These models use values of hydraulic conductivity obtained from laboratory testing or other estimation method, for example, the model of Fredlund and Xing [30].

A summary of the main estimation methods expressed as a function of hydraulic conductivity is presented in **Table 2**.

Model	Equation
Van Genuchten and Burdine (1953)	$k(\psi) = k_s \frac{\{1 - (a_{vb}\psi)^{n_{vb}} - 2[1 + (a_{vb}\psi)^{n_{vb}}]^{m_{vb}}\}^2}{[1 + (a_{vb}\psi)^{n_{vb}}]^{2m_{vb}}}$
Gardner (1958)	$k(\psi) = \frac{k_s}{1 + a_g \left(\frac{\psi}{\rho_w g}\right)^{n_g}}$
Brooks and Corey (1964)	$k(\psi) = \begin{cases} k_s & \psi \leq \psi_{aev} \\ k_s \left(\frac{\psi_{aev}}{\psi}\right)^{2+3\lambda} & \psi \geq \psi_{aev} \end{cases}$
Van Genuchten and Mualem (1976)	$k(\psi) = k_s \frac{\{1 - (a_{vm}\psi)^{n_{vm}} - 2[1 + (a_{vm}\psi)^{n_{vm}}]^{m_{vm}}\}^2}{[1 + (a_{vm}\psi)^{n_{vm}}]^{2m_{vm}/2}}$
Fredlund and Xing (1994)	$k(\psi) = k_s \frac{\int_{\ln(\psi)}^b \frac{\theta(e^y) - \theta(\psi)}{e^y} \theta'(e^y) dy}{\int_{\ln(\psi_{aev})}^b \frac{\theta(e^y) - \theta_s}{e^y} \theta'(e^y) dy}$
Leong and Rahardjo (1997)	$k(\psi) = k_s [\Theta_d(\psi)]^q$
where	
$k(\psi)$	hydraulic conductivity function
k_s	saturated hydraulic conductivity coefficient
ψ	soil suction
ψ_{aev}	soil suction at the air-entry value
λ	pore size distribution index
ρ_w	water density
g	acceleration of gravity
a_g	adjustment parameter related to the air-entry value
a_{vb} or a_{vm}	adjustment parameter related to the inverse of the air-entry value
n_g	soil parameter that depends on the desaturation process once the air-entry value is exceeded
n_{vb} or n_{vm}	adjustment parameter of the characteristic curve obtained from Van Genuchten's model (1980)
m_{vb}	adjustment parameter $(1-2/n_{vb})$; value oscillates between zero and one
m_{vm}	adjustment parameter $(1-1/n_{vm})$; value oscillates between zero and one
b	upper integration limit (1,000,000 kPa)
y	fictitious variable that describes soil suction (logarithm scale)
θ'	variable derived from the function of soil storage capacity (characteristic curve)

Table 2. Estimation models for determining hydraulic conductivity function.

3. Unsaturated seepage theory

In geotechnical engineering, water flow through soil can be categorized in several ways: laminar or turbulent flow (determined by the Reynolds number); one-dimensional (1D), two-dimensional (2D), or three-dimensional (3D) flows (depending on the number of planes); steady-state and transient seepage (constant and variable across time, respectively); and confined and unconfined flows (depending on the limits defining them).

3.1. Steady-state seepage

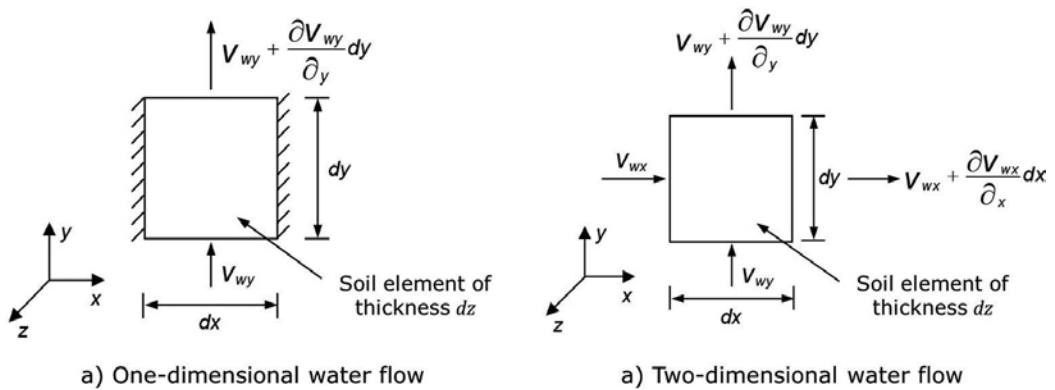


Figure 3. One- and two-dimensional water flow through an unsaturated element [24].

Considering that **Figure 3(a)** represents a soil sample subject to an upward flow and taking into consideration the law of continuity, the following can be proposed:

$$\left(v_{wy} + \frac{dv_{wy}}{dy} dy \right) dx dz - v_{wy} dx dz = 0 \quad (1)$$

After applying Darcy's law [31], the one-dimensional water flow through an unsaturated soil can be expressed as

$$k_{wy} \frac{d^2 h_w}{dy^2} + \frac{dk_{wy}}{dy} \frac{dh_w}{dy} = 0 \quad (2)$$

where

dh_w/dy is the hydraulic gradient

dh_w is the hydraulic head

For the example of **Figure 3(b)**, which demonstrates a two-directional water flow, the following expression can be deduced from the continuity equation:

$$\left(v_{wx} + \frac{\partial v_{wx}}{\partial x} dx - v_{wx} \right) dydz + \left(v_{wy} + \frac{\partial v_{wy}}{\partial y} dy - v_{wy} \right) dx dz = 0 \tag{3}$$

After applying Darcy’s law [31], the following equation can be proposed to describe steady-state seepage in two directions for an unsaturated anisotropic soil:

$$k_{wx} \frac{\partial^2 h_w}{\partial x^2} + k_{wy} \frac{\partial^2 h_w}{\partial y^2} + \frac{\partial k_{wx}}{\partial x} \frac{\partial h_w}{\partial x} + \frac{\partial k_{wy}}{\partial y} \frac{\partial h_w}{\partial y} = 0 \tag{4}$$

Under isotropic conditions, the previous equation can be expressed as follows:

$$k_w \left(\frac{\partial^2 h_w}{\partial x^2} + \frac{\partial^2 h_w}{\partial y^2} \right) + \frac{\partial k_w}{\partial x} \frac{\partial h_w}{\partial x} + \frac{\partial k_w}{\partial y} \frac{\partial h_w}{\partial y} = 0 \tag{5}$$

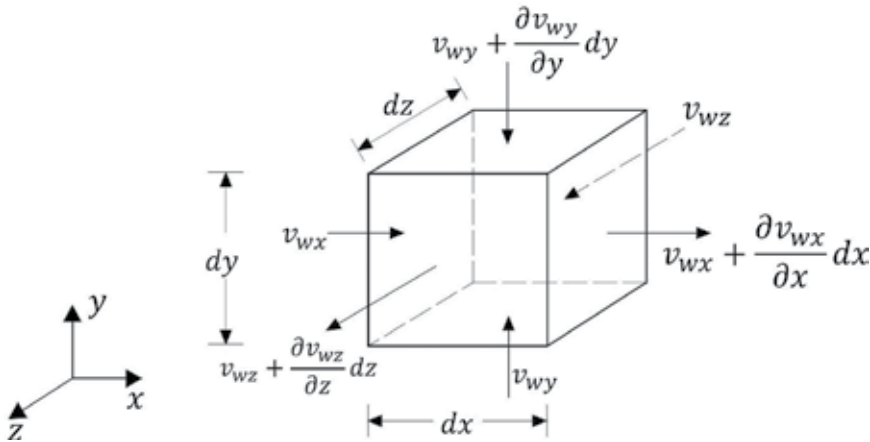


Figure 4. Three-dimensional water flow through an unsaturated element [24].

For three-directional water flow, considering the unsaturated soil sample subjected to the water flow conditions indicated in **Figure 4**, where the hydraulic conductivities vary in all directions, the following expression can be deduced based on flow continuity:

$$\left(v_{wx} + \frac{\partial v_{wx}}{\partial x} dx - v_{wx} \right) dydz + \left(v_{wy} + \frac{\partial v_{wy}}{\partial y} dy - v_{wy} \right) dx dz + \left(v_{wz} + \frac{\partial v_{wz}}{\partial z} dz - v_{wz} \right) dx dy = 0 \tag{6}$$

Once again, after applying Darcy's law, the equation that describes the steady-state seepage in three directions in anisotropic conditions is detailed as follows:

$$k_{wx} \frac{\partial^2 h_w}{\partial x^2} + k_{wy} \frac{\partial^2 h_w}{\partial y^2} + k_{wz} \frac{\partial^2 h_w}{\partial z^2} + \frac{\partial k_{wx}}{\partial x} \frac{\partial h_w}{\partial x} + \frac{\partial k_{wy}}{\partial y} \frac{\partial h_w}{\partial y} + \frac{\partial k_{wz}}{\partial z} \frac{\partial h_w}{\partial z} = 0 \quad (7)$$

For isotropic soils, the previous equation can be simplified to

$$k_w \left(\frac{\partial^2 h_w}{\partial x^2} + \frac{\partial^2 h_w}{\partial y^2} + \frac{\partial^2 h_w}{\partial z^2} \right) + \frac{\partial k_w}{\partial x} \frac{\partial h_w}{\partial x} + \frac{\partial k_w}{\partial y} \frac{\partial h_w}{\partial y} + \frac{\partial k_w}{\partial z} \frac{\partial h_w}{\partial z} = 0 \quad (8)$$

3.2. Transient seepage (the Richards equation)

In the transient seepage analysis and in contrast to steady state seepage, a variable hydraulic head exists over time. Variation occurs due to the changes in the boundaries of the system (due to variation in water levels over time).

For practical applications, Darcy's law [31] can be generalized to unsaturated water flow problems by considering hydraulic conductivity to be a function of the soil suction or suction head [32, 33]:

$$q_x = -k_x(h_m) \frac{\partial h}{\partial x} ; q_y = -k_y(h_m) \frac{\partial h}{\partial y} ; q_z = -k_z(h_m) \frac{\partial h}{\partial z} \quad (9)$$

where

h_m is the suction head

$k(h_m)$ is the hydraulic conductivity function.

If the osmotic pressure head is disregarded, then the total head of an unsaturated soil can be expressed as the sum of the matric suction head and the elevation head ($h = h_m + z$). Thus, if this consideration is substituted in the equation of the law of conservation of matter and a constant water density is assumed, then the following expression can be obtained:

$$\frac{\partial}{\partial x} \left[k_x(h_m) \frac{\partial h_m}{\partial x} \right] + \frac{\partial}{\partial y} \left[k_y(h_m) \frac{\partial h_m}{\partial y} \right] + \frac{\partial}{\partial z} \left[k_z(h_m) \left(\frac{\partial h_m}{\partial z} + 1 \right) \right] = \frac{\partial \theta}{\partial t} \quad (10)$$

where the additional term in the direction of the z-axis is due to the elevation head.

The term on the right side of Eq. (10) can also be expressed as a function of the matric suction head:

$$\frac{\partial \theta}{\partial t} = \frac{\partial \theta}{\partial h_m} \frac{\partial h_m}{\partial t} \quad (11)$$

where $\partial \theta / \partial h_m$ is the slope of the relationship between the volumetric water content and the suction head, which can be directly determined from the SWCC. The slope denotes the specific moisture capacity, which is typically denoted as C . As the soil storage function is not linear, it is necessary to describe the specific moisture capacity as a function of the suction or suction head:

$$C(h_m) = \frac{\partial \theta}{\partial h_m} \quad (12)$$

If Eqs. (11) and (12) are substituted in Eq. 10, the expression that describes transient seepage in unsaturated soils can be expressed as follows:

$$\frac{\partial}{\partial x} \left[k_x(h_m) \frac{\partial h_m}{\partial x} \right] + \frac{\partial}{\partial y} \left[k_y(h_m) \frac{\partial h_m}{\partial y} \right] + \frac{\partial}{\partial z} \left[k_z(h_m) \left(\frac{\partial h_m}{\partial z} + 1 \right) \right] = C(h_m) \frac{\partial \theta}{\partial t} \quad (13)$$

Eq. (13) is known as the Richards [33] equation, where given the boundary limits and initial conditions specific to a system, the equation provides the values for suction across space and time. It is highlighted that in using this equation, it is necessary to have data on the SWCC and the hydraulic conductivity function that are specific to the material being studied.

4. Slope stability analyses

One of the most common methods for evaluating slope stability is the general limit equilibrium (GLE) method. A series of equations has been proposed by several authors, who agree in dividing the slide zone into slices. The primary differences are related to the equations that these seek to satisfy and to the differential forces influencing each slice, including the existing relationship between shear and normal forces. The foundation of this method is based on two equations that determine the factor of safety and evaluate the relationship between normal and shear forces [34, 35]. Thus, one equation provides the factor of safety with respect to the equilibrium of moments (F_m) and the other with respect to horizontal forces (F_f).

For the GLE, shear forces are determined according to the equation proposed by Morgenstern and Price [36]:

$$X = E\lambda f(x) \quad (14)$$

where

X is the shear force between slices

E is the normal force

λ percentage (in decimal form) of the expressed function

$f(x)$ is the function used for study.

For the GLE, the factor of safety is determined with respect to the method of moments and is determined by

$$F_m = \frac{\sum [c' \beta R + (N - u \beta) R \tan \varphi']}{\sum Wx - \sum Nf - Dd} \quad (15)$$

However, the factor of safety with respect to the balance of forces is determined by

$$F_f = \frac{\sum [c' \beta \cos \alpha + (N - u \beta) \tan \varphi' \cos \alpha]}{\sum N \sin \alpha - \sum D \cos \omega} \quad (16)$$

where

c' is the effective cohesion

φ' is the effective friction angle

u is the pore pressure

N is the normal force at base of slice

W is the weight of slice

D is the load line

$\beta, R, x, f, d, \omega$ are the geometric parameters

α is the slope.

One important factor that is relevant for the previous equations is the normal force N , which is a term defined as

$$N = \frac{W = X_R - X_L - \frac{c' \beta \sin \alpha + u \beta \sin \alpha \tan \varphi'}{F}}{\cos \alpha + \frac{\sin \alpha \tan \varphi'}{F}} \quad (17)$$

5. Practical application: coupled water flow-slope stability analyses of a tailings dam

5.1. Introduction

Mining waste (tailings) is disposed of in structures called tailings dams. The most important difference between a tailings dam and a typical water storage dam in the conventional water-retaining sense is that tailings dams do not contain an engineered water barrier and they are built and used simultaneously. For this reason, it is common for the originally conceived project to undergo constant modifications. Current technological advances allow for the numerical modelling of steady and transient state flow analyses for these structures, and along with adequate monitoring, their stability can be verified with coupled water flow-slope stability analyses before the occurrence of any potential errors. In the following sections, a cross section of a tailings dam is analysed (Figure 5), and the importance and benefits that result from the numerical model are highlighted; in addition, further recommendations are given for this type of analysis.

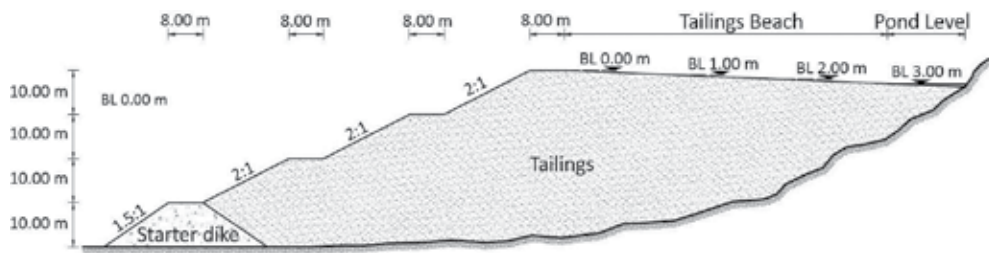


Figure 5. Maximum tailings dam cross section for two-dimensional model.

5.2. Material properties

The properties of tailings dams are variable because they depend largely on the origin of the materials used for their construction. Several authors have performed tests with different materials and have specified typical values for these [37–40]. Based on these references, in Table 3, the properties of the materials from the case study considered in the numerical model of this section are provided.

Material	USCS classification		k (m/s)	c' (kPa)	φ' (°)
	Name	Symbol			
Fine material	Silt with sand	ML	1.582×10^{-8}	0	25
Coarse material	Silty sand	SM	1.000×10^{-6}	0	35

Table 3. Tailings properties for the tailings dam considered.

Assuming that the materials of the tailings dam are found in unsaturated state, for this analysis, the SWCC and hydraulic conductivity functions must be determined. If laboratory data are unavailable, it is possible to use estimates with the aid of material index properties, such as grain-size distribution curves, which are considered in the calculations performed here (Figure 6).

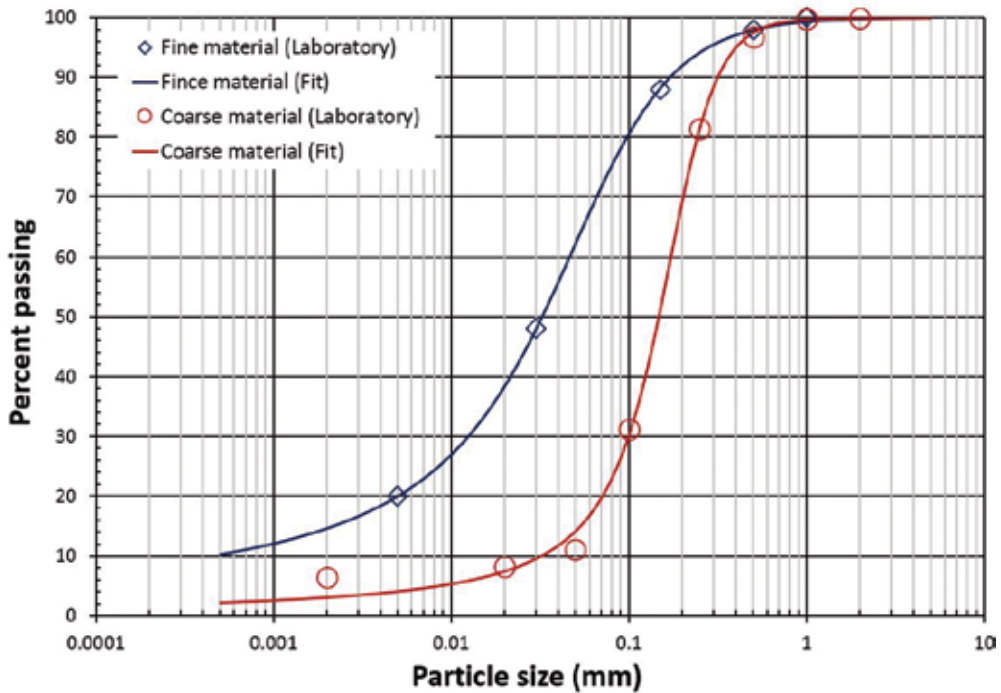


Figure 6. Grain-size distribution curves for tailings considered in the numerical model.

5.3. Unsaturated soil properties functions

For the dam materials analysed in the present case study, the SWCC (that represent the relationship between water content and soil suction) of Figure 7 were determined by the following method:

- For coarse material, based on data generated from a laboratory experiment with a pressure plate, the fitting Fredlund and Xing [30] SWCC equation was applied.
- For fine material, the estimation method of Fredlund and Wilson [9] was initially used, and afterwards, the fitting Fredlund and Xing [30] SWCC equation was applied.

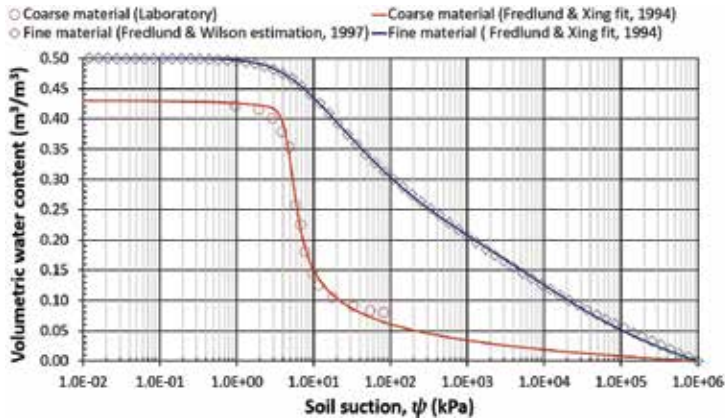


Figure 7. Soil-water characteristic curves of tailings dam materials.

In Figure 8, the hydraulic conductivity functions considered in the present dam case study are presented. A great similarity between the laboratory data and the estimated data can be observed. Thus, the use of estimation methods when laboratory data are unavailable represents a feasible solution and potential advantage; however, such models should be used with caution and rationality.

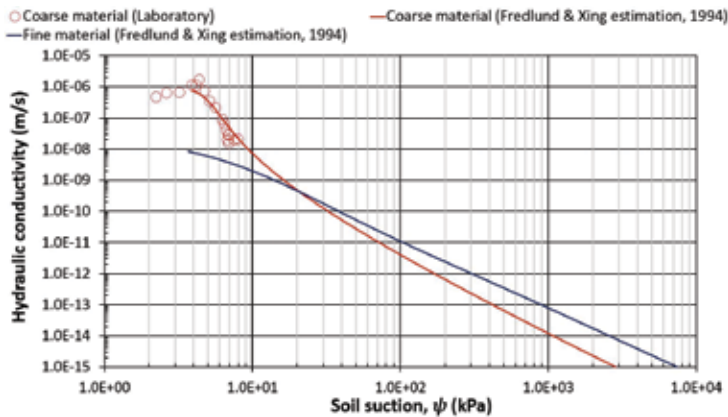


Figure 8. Hydraulic conductivity functions of the tailings dam materials.

5.4. Two-dimensional modelling for steady-state seepage conditions

A steady-state seepage analysis was performed with Eq. (5), which can be solved numerically by the finite element method using the Seep/W algorithm [41]. For two-dimensional models, boundary conditions should be adequately defined in addition to discretizing the flow regions the best possible. Greater emphasis must be placed on areas that require greater detail in the expression of results, where numerical difficulties may be presented, or for areas with high

contrast in the permeability of materials by orders of magnitude. In **Figure 9**, the boundary conditions and the discretization of the flow regions are detailed.

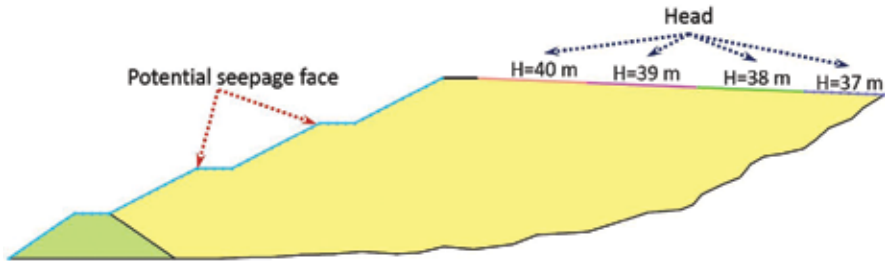


Figure 9. Boundary conditions and discretization model for the tailings dam with Seep/W [41].

Based on the steady-state seepage analysis, it is possible to estimate the position of the phreatic surface of the tailings dam and for the different pond levels (**Figure 10**).

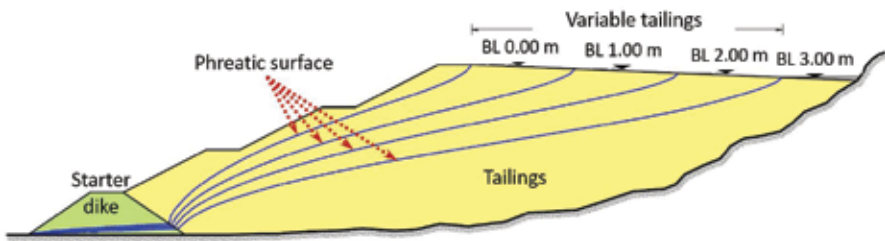


Figure 10. Variation in the phreatic surface due to reduction of the freeboard with Seep/W [41].

Based on the previous results, the stability of the structures of the tailings dam can be evaluated by a GLE method, such as the Morgenstern-Price method, to define the slip surface for each level of the pond. In **Figure 11**, the slip surfaces are indicated, which were obtained from the Slope/W algorithm [42] and from considering the results of the steady-state groundwater flow analyses.

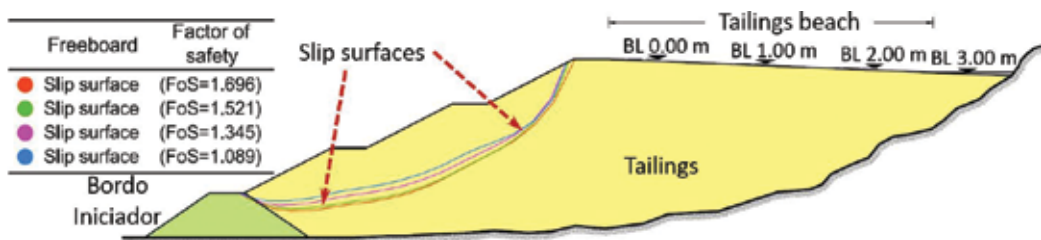


Figure 11. Slip surfaces due to phreatic surfaces for different pond levels with Slope/W [42].

5.5. Two-dimensional modelling for transient conditions

A transient model (variable over time) was performed to evaluate the influence of rainfall on the tailings dam defined in **Figure 5** by the numerical solution of Eq. 13. In addition, the behaviour of the pond levels is studied when the level varies 3.00 m with respect to the crest. In this case, the boundary conditions are modified to be a time-dependent function while the discretization of the model was maintained without modifications with respect to the mesh used for the steady-state analysis.

The aforementioned model allows for the distinct stages of the analysis to be defined. The first set of calculations corresponds to the period of 0–48 h, after which, a storm would cause an immediate increase in water level of the pond (**Figure 12**). An evaluation of the infiltration due to rainfall during this period is also shown in **Figure 13**.

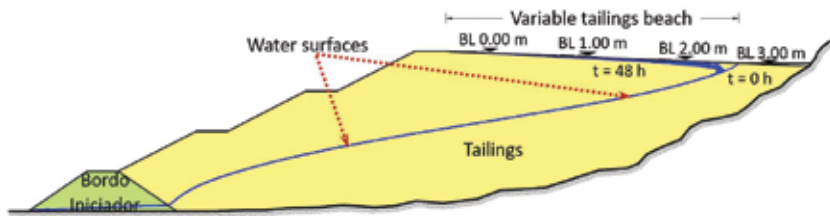


Figure 12. Variation in the water surface within the tailings structure due to rainfall and loss of freeboard for 48-h period with Seep/W [41].

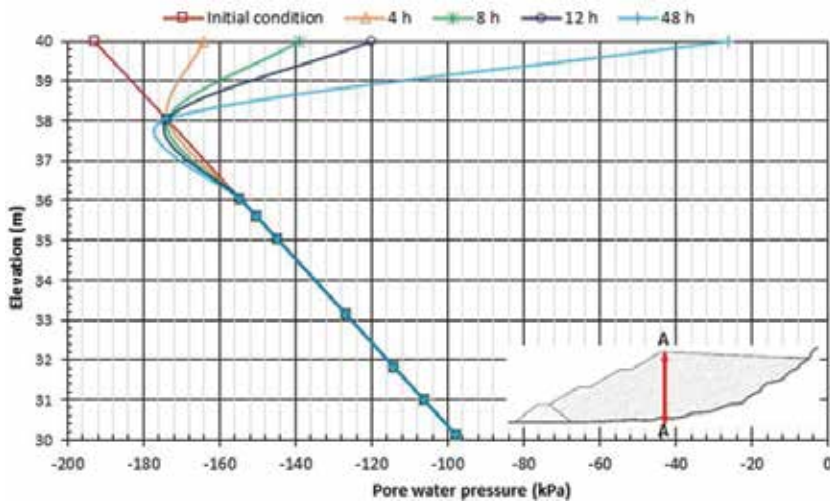


Figure 13. Behaviour of the pore-water pressure near the ground surface due to rainfall and loss of freeboard.

Short analysis periods for materials of low permeability are often inadequate because they might not be able to clearly determine the influence of water. For example, in the previous

analysis during the water filling of pond, the water surfaces variation was unable to be clearly distinguished. Similarly, rainfall was shown to have low significance because it was unable to infiltrate to a considerable enough depth to affect the slope stability.

Therefore, long-term analyses for these types of materials are more representative because they allow remark the water surfaces variation over a longer period of time. Thus, the results of these analyses are shown in **Figure 14**.

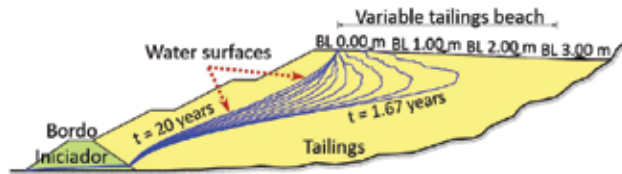


Figure 14. Water surfaces variation within the tailings structure for a transient analysis of 20 years with Seep/W algorithm [41].

Following the previous procedure and considering the pond levels indicated in **Figure 12**, the slip surfaces were defined by the Morgenstern-Price method with the Slope/W algorithm [42]. It is worth mentioning that a stability analysis for a period of 48 h did not provide significant results because during this time, the structure was not considerably influenced by the water. However, for long-term conditions, such stability analyses could play an important role in the study.

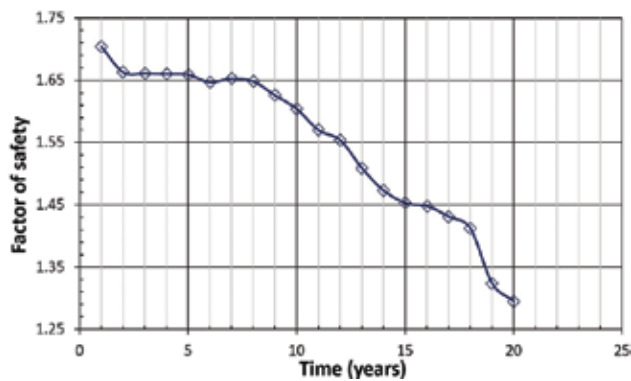


Figure 15. Variation in the factor of safety in the tailings dam over a period of 20 years.

In **Figure 15**, the variation of factor of safety over time is presented, wherein the variation in the position of water surface over time is considered (**Figure 14**). A decrease in stability over time is also observed. For this type of evaluations, numerical difficulties may be presented that are subsequently reflected in the result, which leads to erroneous behaviour. Therefore, it is recommended to manipulate the variables that may affect the model, such as the calculated time intervals (smaller time increments may lead to a more detailed response), the finite

elements mesh, and the convergence parameters. An adequate manipulation of these variables can significantly improve the results of the numerical model [43].

5.6. Three-dimensional numerical modelling

5.6.1. Model geometry

In current numerical modelling, it is common for 3D domains to be extruded, or in other words, two-dimensional sections are assigned a certain thickness. Then, the model is extended along a horizontal axis, resulting in a continuous, three-dimensional model.

Extrusions are recommended depending on the type of problem to be solved. For example, extrusions are suitable for analyses of protection levees or embankments with regular geometries that extend over long distances. In the case of structures with irregular geometries, such as dams, it is more suitable that calculations consider the specific topography of the site for these to be more representative. This latter method requires a greater amount and detail of information for the numerical model to be successfully resolved. However, it is convenient in this case to standardize certain surface areas of the model to avoid an excessive discretization of each region. In **Figure 16**, the geometries assumed for both cases performed here are shown.

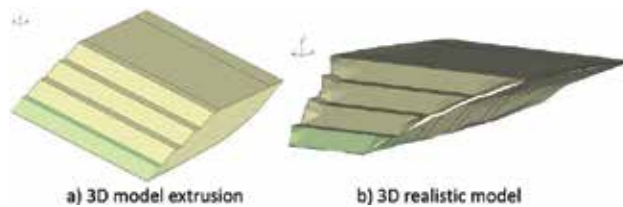


Figure 16. Geometries: (a) 3D model extrusion and (b) 3D realistic model.

5.6.2. Boundary conditions

In assigning boundary conditions, sufficient regions must be created to allow the site-specific conditions to be adequately represented and well defined, which thus leads to optimum modelling results. In **Figure 17**, the conditions assigned in both scenarios of the case study analysis are shown.

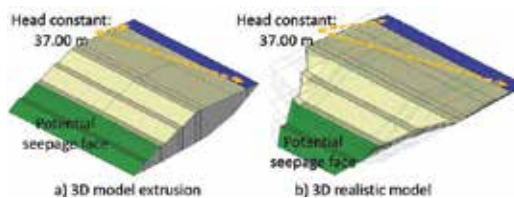


Figure 17. Boundary conditions of the 3D models considered in the calculations with SVFlux algorithm [44].

5.6.3. Discretization of the model

The mesh generation for 3D models is perhaps the most complicated part of this process and even more so when considering site-specific topographic conditions. During these processes, the benefits of the extruded 2D models are evident because the generation of the mesh, as well as its distribution, is more regular. Moreover, 3D models of realistic topographies make mesh generation more difficult; in addition, 3D models require a greater number of elements to adapt to the model. In **Figure 18**, the distribution of the meshes obtained with the SVFlux algorithm is shown [44], and in **Table 4**, a comparison is made of the number of elements required for each model.

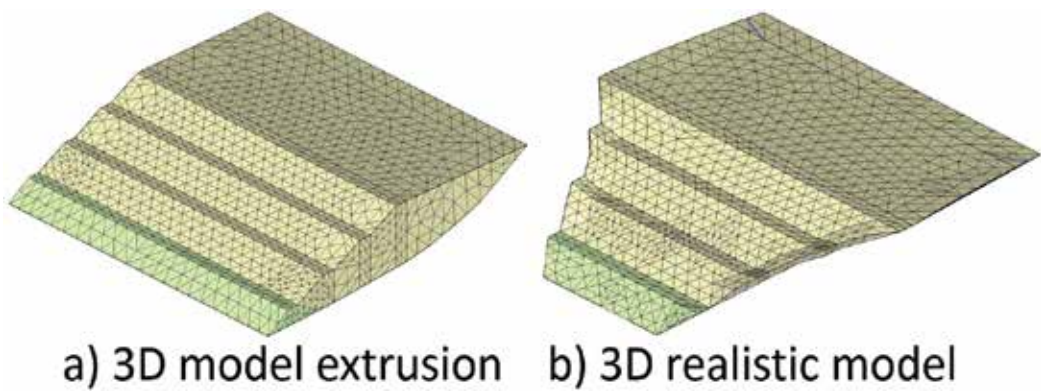


Figure 18. Finite element mesh used for calculation of the 3D models with SVFlux algorithm [44].

Model	Nodes	Elements
2D	220	91
3D extruded	1342	758
3D realistic topography	2889	1580

Table 4. Comparison of the number of finite elements for different analysis conditions.

5.6.4. Water flow analyses

Important differences are found when 3D model extrusions are compared to 3D models that consider site-specific topography. In **Figure 19**, it can be observed that the distribution of the hydraulic heads tends to vary in both cases. The 3D model extrusion shows a constant dissipation in the hydraulic head; however, this is not very representative of this type of structure. On the other hand, the 3D realistic model that considers site-specific topography shows a more variable behaviour in the distribution of the hydraulic head, which can be considered to be more representative of the analysed case study.

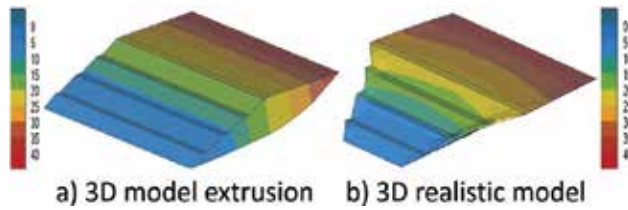


Figure 19. Distribution of hydraulic heads (m) with SVFlux algorithm [44].

The previous results can be verified by comparing the distributions of the hydraulic heads at the maximum cross section of the structure. Theoretically, the distributions of the 2D model, 3D model extrusion, and 3D realistic model with site-specific topography should be nearly identical or extremely similar considering the similar conditions and inputs for the analysis. In **Figure 20**, this comparison is shown.

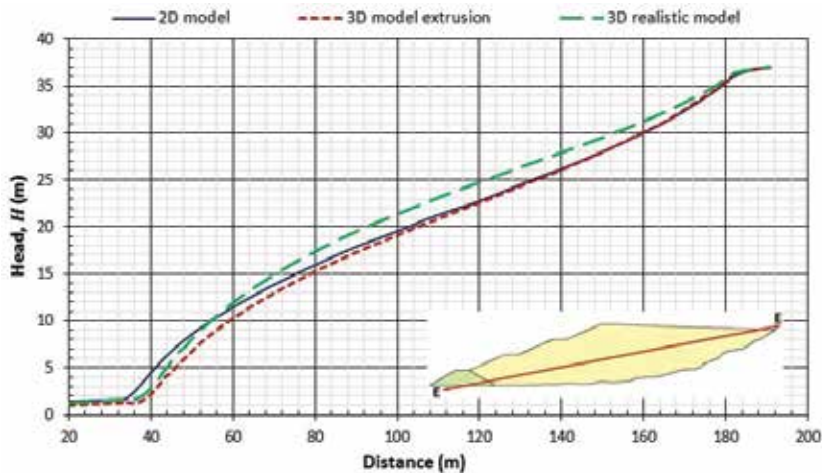


Figure 20. Variation in the hydraulic heads (m) for different analysis criteria.

5.6.5. Three-dimensional slope stability analysis

Several studies have demonstrated the importance of defining the relationship between the two-dimensional and three-dimensional models. The majority of studies agree in that the values for the factors of safety obtained from the 2D slope stability analyses are conservative, and these values tend to increase upon considering 3D models, which occurs because these calculations consider steady-state water conditions and disregard the filtration forces generated within the structure [45, 46]. This phenomenon is observed in **Figure 21**, where the results of a slope stability analysis during dry conditions are shown. In this case, the 3D model extrusion and 3D realistic model (considering site-specific topography) did not present significant differences.

On the contrary, in **Figure 22**, the safety factors obtained for each scenario from a slope stability analysis with the linear *phi-b* model are shown, which consider water flow in the tailings structure. For these cases, the differences between each of the analyses and their criteria are distinguishable. According to the previous results, it is important to consider the water flow through the specific medium under study because it can significantly affect the stability of the earth structures. In this case, the 2D and 3D model extrusions show a high value for the factor of safety in comparison with the 3D realistic model. These differences can be attributed to the irregular topography, which causes the distribution of the hydraulic head to exhibit non-linear behaviour.

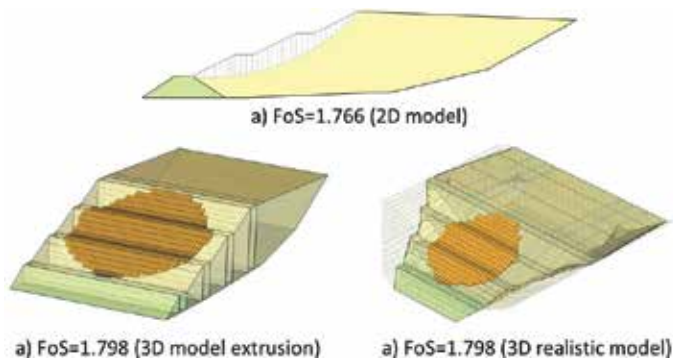


Figure 21. Factor of safety for distinct slope stability analyses in dry conditions (without water flow) with SVSlope algorithm [47].

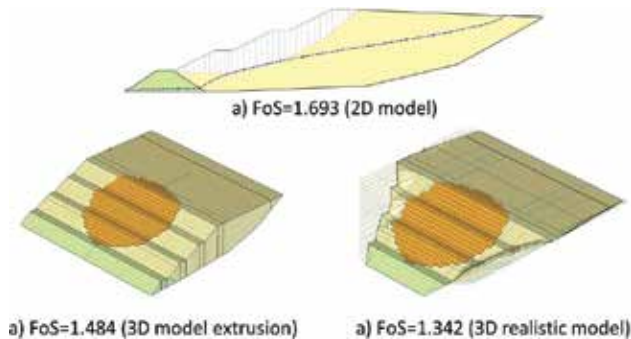


Figure 22. Factor of safety for distinct slope stability analyses considering water flow through the tailings structure with SVSlope algorithm [47].

It is important to highlight that this type of analysis requires more exhaustive evaluations. In this case, only the importance of these calculations is reinforced, and methodological suggestions are proposed. However, additional numerical analyses and their respective validation in the field are imperative to adequately define the behaviour of these types of numerical models.

6. Conclusions

The primary focus of this study was unsaturated soils. The most important specific concepts related to this subject were detailed with the goal of enabling their application with the aid of specialized computer programs based on the finite element method.

Several of the concluding comments and recommendations derived from the analysis of the case study in this chapter are detailed as follows:

- When specialized laboratory results are unavailable (to describe variations in water content and permeability with respect to suction), the unsaturated soil property functions required for the analysis can be determined by estimation methods.
- For the correct estimation of unsaturated soil property functions (soil-water characteristic curve and hydraulic conductivity function), a large amount of laboratory data can be required, specifically, results from different index properties, grain-size distribution curve, and soil permeability experiments.
- To determine the appropriate unsaturated soil property functions (soil-water characteristic curve and hydraulic conductivity function) for the calculations in analyses performed here, the form and tendency of the soil curves were considered. However, it is possible to use statistical methods to define these functions. Certain programs will perform these calculations (such as SoilVision Database).
- For numerical modelling that considers materials with high contrast in permeability by orders of magnitude, for example, it is common for numerical difficulties to be presented. To resolve this type of problems, highly permeable materials that do not contribute to the dissipation of the hydraulic head can be omitted; however, as a consequence, these will not have an effect in the final resolution of the model. If the material must be considered in calculations, then it can be substituted by gravel to facilitate the convergence of the model. To obtain satisfactory results, an adequate definition of the SWCC is necessary in addition to the hydraulic conductivity functions, which will be necessary to obtain representative solutions. Despite this, numerical complications may be present, which can only be reduced with convergence parameters, or in this case, by step-by-step analysis until an optimal solution is achieved.
- Depending on the problem to be analysed and its complexity, more detailed discretizations may be required to decrease the numerical error of calculations. This approach should not be confused with the automatic generation of a dense finite element mesh because for many water flow models, the use of such discretizations is not justified and will only affect calculation times without leading to improvements in the solution of the problem.
- Water infiltration plays an important role in the stability of deposits of mining wastes (tailing dams), and it is appropriate to consider water movement in these calculations to better understand its behaviour. Therefore, the benefits of numerical modelling are numerous because these methods allow for diverse situations, given relatively short periods of analysis, to be considered, thereby informing and enabling appropriate decision-making.

- Currently, 3D models have wide advantages over 2D models because the latter do not consider all the variables that influence the behaviour of structures. Some of the main features that can be included in three-dimensional models are irregular geometry of the structure under study, topographic configuration of soil, unsaturated flow that represent more realistically the physical conditions of the problem, among others.
- In 3D analysis, extrusions are recommended depending on the type of problem to be solved. For example, protection levees or embankments with regular geometries extending in great lengths are suitable extrusions. In the case of structures with irregular geometries, such as dams, it agrees that calculations are performed considering the topography of the site, to give greater representation to them.

Finally, for more representative numerical analyses, it is recommended to apply the theory of unsaturated soils in all those situations where the material is in this state. This chapter demonstrated that the considerations for modelling, estimating, and fitting methods of the soil properties functions provide the necessary elements to carry out these analyses in a simple way. Illustrated examples also evaluated the potential of numerical methods to increase the degree of realism in unsaturated soils analysis. Computer programs facilitate the study of transient flow and unsaturated soil conditions, cases that attempt to analytically solve are complicated and laborious. However, it should be recognized that the computer programs now replaces the judgement of an engineer.

Author details

Norma Patricia López-Acosta* and José Alfredo Mendoza-Promotor

*Address all correspondence to: nlopeza@iingen.unam.mx

Institute of Engineering, Nacional University of Mexico (UNAM), Mexico City, Mexico

References

- [1] Lu N, Likos W. Unsaturated soil mechanics. 1st ed. Hoboken, New Jersey: John Wiley and Sons; 2004.
- [2] López-Acosta N P. Numerical modelling of water flow problems. In: Proceedings of the 27th National Meeting on Geotechnical Engineering. SMIG (November 20–21, 2014), Puerto Vallarta, Jalisco, Mexico; 2014. (in Spanish)
- [3] Aitchison G D, Richards B G. A broadscale study of moisture conditions in pavements subgrade throughout Australia. In: Moisture Equilibria and Moisture Changes in Soils Beneath Covered Areas, A Symposium in Print; Butterworths, Sydney, Australia. pp. 184–232.

- [4] Aslyng H C et al. Soil physics terminology, draft report. Int. Soc. of Soil Sci. 1962; Bull. 23. pp. 7.
- [5] Lee H C, Wray W K. Techniques to evaluate soil suction—a vital unsaturated soil water variable. In: Proceedings of the First International Conference on Unsaturated Soils; Paris, France: A.A. Balkema/Presses de l' Ecole Nationale des Ponts et Chaussées; 1995.
- [6] Zepeda-Garrido J A, editor. Unsaturated soil mechanics. 1st ed. México D.F.: Mexican Society for Soil Mechanics, Autonomous University of Queretaro; 2004. 322 p. (in Spanish)
- [7] Pérez-García N, Determination of Soil-Water Characteristic Curve with pressure plate test. Safandila, Querétaro, México: Secretaria de Comunicaciones y Transportes, Mexican Transportation Institute; 2008. 54 p. Publicación Técnica No. 313 (in Spanish)
- [8] Fredlund D G, Rahardjo H. Soil mechanics for unsaturated soils. 1st ed. New York: John Wiley and Sons; 1993. 521 p. DOI: 10.1002/9780470172759
- [9] Fredlund M D, Fredlund D G, Wilson G W. Prediction of the soil-water characteristic curve from grain-size distribution and volume-mass properties. In: 3rd Brazilian Symposium on Unsaturated Soils; April 22–25; Rio de Janeiro, Brazil; 1997.
- [10] Van Genuchten M T. A closed form-equation for predicting the hydraulic conductivity of unsaturated soils. Soil Sci. Soc. Am. J. 1980;44:892–898.
- [11] Fredlund D G, Xing A, Fredlund M D, Barbour S L. The relationship of the unsaturated soil shear to the soil-water characteristic curve. Can. Geotech. J. 1996;33(3):440–448. DOI: 10.1139/t96-065
- [12] Aubertin M, Ricard J F, Chapuis R P. A predictive model for the water retention curve: application to tailings from hard-rock mines. Can. Geotech. J. 1998;35(1):55–69. DOI: 10.1139/t97-080
- [13] Mbagwu J S C, Mbah C N. Estimating water retention and availability in Nigerian soils from their saturation percentage. Comm. Soil Sci. Plant Anal. 1998;29(7–8):913–922.
- [14] Rojas E. Towards a Unified Soil Mechanics Theory. The Use of Effective Stresses in Unsaturated Soils. 1st ed. Sharjah, United Arab Emirates: Bentham eBooks; 2013. 190 p.
- [15] Arya L M, Paris J F. Physicoempirical model to predict the soil moisture characteristic from particle-size distribution and bulk density data. Soil Sci. Soc. Am. J. 1981;45:1023–1030.
- [16] Arya L M, Dierolf T S. Predicting soil moisture characteristics from particle-size distributions: And improved method to calculate pore radii from particle radii. In: van Genuchten M.Th., Leij F.J., Lund L.J., editors. Indirect methods for estimating the hydraulic properties of unsaturated soils; University of California, Riverside, CA. 1992. p. 115–124.

- [17] Basile A, D'Urso G. Experimental corrections of simplified methods for predicting water retention curves in clay-loamy soils from particle-size determination. *Soil Technol., Elsevier*. 1997;10(3):261–272. DOI: 10.1016/S0933-3630(96)00020-7
- [18] Fredlund M D. The role of unsaturated soil property functions in the practice of unsaturated soil mechanics [thesis]. Saskatoon, Saskatchewan, Canada: Department of Civil Engineering, University of Saskatchewan; 1999. 292 p.
- [19] Hosagasi-Fuselier T. Evaluation of soil water characteristic curves and permeability functions for modelling of seepage in unsaturated soils [thesis]. Somerville/Medford, Massachusetts, USA: Tufts University; 2006.
- [20] Scheinost A C, Sinowski W, Auerswald K. Regionalization of soil water retention curves in a highly variable soilscape, I. Developing a new pedotransfer function. *Munich, Germany: Geoderma*, 78, Elsevier Science B. V. 1997. p 129–143.
- [21] Aubertin M, Mbonimpa M, Bussière B, Chapuis R P. A model to predict the water retention curve from basic geotechnical properties. *Can. Geotech. J.* 2003;40(6):1104–1122. DOI: 10.1139/t03-054
- [22] Zapata C E. Uncertainty in soil-water characteristic curve and impacts on unsaturated shear strength predictions [thesis]. Tempe, Arizona: Arizona State University; 1999.
- [23] Siller W S. The mathematical representation of the soil-water characteristic curve [thesis]. Saskatoon, Saskatchewan, Canada: University of Saskatchewan; 1997.
- [24] Fredlund D G, Rahardjo H, Fredlund M D. *Unsaturated soil mechanics in engineering practice*. 1st ed. Hoboken, New Jersey: John Wiley and Sons; 2012. 857 p.
- [25] Brooks R H, Corey A T. Hydraulic properties of porous media. *Fort Collins, Colorado: Colorado State University Hydrology Papers*. 1964;(3):27.
- [26] Gardner W R. Some steady state solutions of the unsaturated moisture flow equation with application to evaporation from a water-table. *Soil Sci. J.* 1958;85(4):228–232.
- [27] Burdine N T. Relative permeability calculations from pore size distribution data. *Trans. Metall. Soc. AIME*. 1953;198:71–78.
- [28] Mualem Y. A new model for predicting the hydraulic conductivity of unsaturated porous media. *Water Resour. Res.* 1976;12:513–522.
- [29] Leong E C, Rahardjo H. Permeability functions for unsaturated soils. *J Geotech. Geoenviron. Eng.* 1997;123(12):1118–1126.
- [30] Fredlund D G, Xing A. Equations for the soil-water characteristic curve. *Can. Geotech. J.* 1994;31(4):521–532. DOI: 10.1139/t94-061
- [31] Darcy H. *Histoire des Fontaines Publiques de Dijon*. Paris: Dalmont; 1856. pp. 590–594.

- [32] Buckingham, E. Studies of the movement of soil moisture. Washington, DC: U.S. Department of Agriculture, Bureau of Soils; 1907. Bulletin No.: 38.
- [33] Richards L A. Capillary conduction of liquids in porous medium. *Physics*. 1931;1:318–333.
- [34] Fredlund D G, Krahn J. Comparison of slope stability methods of analysis. In: 29th Canadian Geotechnical Conference; Vancouver, British Columbia; 1976. pp. 56–74.
- [35] Fredlund D G, Krahn J, Pufahl D E. The relationship between limit equilibrium slope stability methods. In: Proceedings of the International Conference on Soil Mechanics and Foundation Engineering; Stockholm, Sweden; 1981. Vol. 40: pp. 409–416.
- [36] Morgenstern N R, Price V E. The analysis of the stability of general slip. *Geotechnique*. 1965;15(1):77–93.
- [37] Manual tailings dams and reservoirs (In Spanish). Mexico D.F.: Association of Mining Engineers, Metallurgists and Geologist of Mexico; 1993. 80 p. (in Spanish)
- [38] Mining waste storage. 1st ed. México D.F.: Mexican Society for Soil Mechanics; 2001. 137 p. (in Spanish)
- [39] Flores Castrellón O. Dynamic properties of tailings [thesis] (In Spanish). México D.F.: National Autonomous University of Mexico, Faculty of Engineering; 1996. (in Spanish)
- [40] Flores Castrellón O. Modulus and Poisson's ratio dynamic measurements obtained on the fringe of the middle third in granular soil specimens [thesis]. México D.F.: National Autonomous University of Mexico, Faculty of Engineering; 2008. 123 p. (in Spanish). Available from: <http://132.248.9.195/ptd2009/enero/0638478/Index.html>
- [41] GeoSlope International. Geostudio suite, Seep/W groundwater seepage analysis. Calgary, Alberta, Canada: 2007. Version: V7.23.
- [42] GeoSlope International. Geostudio suite, Slope/W slope stability analyses. Calgary, Alberta, Canada: 2007. Version: V7.23.
- [43] López-Acosta N P, Mendoza-Promotor J A. Water flow in partially saturated soils and its application in geotechnical engineering. 1st ed. Mexico City: Engineering Institute of the UNAM; 2016. 125 p. (In Spanish)
- [44] SoilVision Systems LTD. SVFlux 1D/2D/3D Saturated/Unsaturated finite element groundwater seepage modelling. Saskatoon, Saskatchewan, Canada 2009. Version: 2.4.26
- [45] Escobedo Rodríguez B. Stability analyses of the tailings dam No. 5, "La Negra" mining unit, Querétaro [thesis]. Mexico D.F.: Universidad Nacional Autónoma de México, Facultad de Ingeniería; 2011. 210 p. (in Spanish). Available from: <http://132.248.9.195/ptb2011/octubre/0674273/Index.html>

- [46] Zhang L, Fredlund M D, Fredlund D G, Haihua L. Comparison of 2-D and 3-D slope stability analyses for unsaturated soil slopes. Geo Regina; 2014.
- [47] SoilVision Systems LTD. SVSlope 2D/3D Limit equilibrium slope stability analysis; 2009. Version: 2.4.26.



Edited by Muhammad Salik Javaid

Water inside the earth, the groundwater and the invisible resource is the most important source of survival of mankind on this globe. Part of the hydrological cycle between entry (percolation and recharge) and exit (natural or forced extraction and discharge), the groundwater fascinates all: engineers, hydrogeologists, agriculturists, environmentalists, scientists, academia, resource managers and domestic and industrial users.

This book is the outcome of efforts of those eminent authors who despite their fascination were able to write upon some important facet of groundwater flow and the transport of pollutants with it. The dimensions covered range from simple descriptive narratives; to expose of analytical methods; to complex mathematical treatment; to numerical simulations and computer modeling. All areas have been touched upon for the sake of general readers, students, professional engineers and scientists.

Photo by szefei / CanStockPhoto

IntechOpen

